AN ABSTRACT OF A DISSERTATION

INDEX-BASED REACTIVE POWER COMPENSATION SCHEME FOR VOLTAGE REGULATION

Damian Obioma Dike

Doctor of Philosophy in Engineering

Increasing demand for electrical power arising from deregulation and the restrictions posed to the construction of new transmission lines by environment, socio-economic, and political issues had led to higher grid loading. Consequently, voltage instability has become a major concern, and reactive power support is vital to enhance transmission grid performance. Improved reactive power support to distressed grid is possible through the application of relatively unfamiliar emerging technologies of "Flexible AC Transmission Systems (FACTS)" devices and "Distributed Energy Resources (DERS)." In addition to these infrastructure issues, a lack of situational awareness by system operators can cause major power outages as evidenced by the August 14, 2003 widespread North American blackout. This and many other recent major outages have highlighted the inadequacies of existing power system indexes.

In this work, a novel "Index-based reactive compensation scheme" appropriate for both on-line and off-line computation of grid status has been developed. A new voltage stability index (Ls-index) suitable for long transmission lines was developed, simulated, and compared to the existing two-machine modeled L-index. This showed the effect of long distance power wheeling amongst regional transmission organizations. The dissertation further provided models for index modulated voltage source converters (VSC) and index-based load flow analysis of both FACTS and microgrid interconnected power systems using the Newton-Raphson's load flow model incorporated with multi-FACTS devices. The developed package has been made user-friendly through the embodiment of interactive graphical user interface and implemented on the IEEE 14, 30, and 300 bus systems. The results showed reactive compensation has system wide-effect, provided readily accessible system status indicators, ensured seamless DERs interconnection through new islanding modes and enhanced VSC utilization. These outcomes may contribute to optimal utilization of compensation devices and available transfer capability as well as reduce system outages through better regulation of power operating voltages.

INDEX-BASED REACTIVE POWER COMPENSATION SCHEME FOR VOLTAGE REGULATION

A Dissertation

Presented to

The Faculty of the Graduate School

Tennessee Technological University

Damian Obioma Dike

In Partial Fulfillment

of the Requirements for the Degree

DOCTOR OF PHILOSOPHY

Engineering

August, 2008

CERTIFICATE OF APPROVAL OF DISSERTATION

INDEX-BASED REACTIVE POWER COMPENSATION SCHEME FOR VOLTAGE REGULATION

Damian Obioma Dike

Graduate Advisory Committee:

Satish Mahajan — 7-25-2008

Satish M. Mahajan, Chairperson — Date

Ghadir Radman — 7-25-2008

Ghadir Radman — Date

Wenzhong Gao — 7-25-2008

David Wenzhong Gao — Date

S Munukutla — 7-25-08

Sastry Munukutla — Date

Brian M. O'Connor — 7/25/08

Brian O'Connor — Date

Approved for the Faculty:

Francis Otuonye

Associate Vice President for

Research and Graduate Studies

7/25/08

Date

DEDICATION

This dissertation is dedicated to my wife, Blessing Chinemerem Dike, and our children (Ijeoma and Obioma) who have endured the long years of separation from me; and to our Almighty God who had kept His promise to sustain me in all situations.

PUBLICATION DISSERTATION OPTION

This dissertation has been prepared in the form of five papers for publication. To give the readers a complete view of the dissertation, Chapters one and seven contain introduction and conclusions for the complete dissertation. Thereafter, Chapters two through six contain the five papers arranged in the order of development of model, its structure, and schematically stepwise implementation of the applications in major areas closely related to the subject of its theme.

The first paper consisting of pages 21 through 45 was presented at the IEEE Electrical Power Conference 2007, Montreal Canada, QC, Canada, October 24-26, 2007. The second paper consisting of pages 46 to 68 presented at the IEEE Power Engineering Society General Meeting, July 20-24, Pittsburg, PA, USA. The third paper covering pages 69 to 107 has been submitted for publication in the *International Journal of Emerging Electric Power Systems*. Fourth paper contained in pages 108 to 154 was submitted to *IEEE Transactions on Power Delivery*. The fifth paper consisting of pages 155 to 185 is about to be submitted to *IEEE Transactions on Power Delivery.*

ACKNOWLEDGMENTS

I wish to express my deep sense of gratitude and indebtedness to my major Professor and chair of the advisory committee, Dr. Satish M. Mahajan, for his supervision, skilled guidance, unfailing support, and constant encouragement throughout the duration of my study. I would like to express deep appreciation to my committee members, Dr. G. Radman, Dr. W. Gao, Dr. S. Munukutla, and Dr. B. O'Connor, for their valuable directions and encouragements. Dr. Radman was very willing to join Dr Mahajan in meeting with me daily during the conception stages of this dissertation.

I am verily grateful to the Chair of ECE Department, Dr. Stephen Parke, the Associate Dean of Engineering and Coordinator of PhD program, Dr. S. Deivanayagam for their support and friendly encouragements. I thank specially, the Associate Vice President, Graduate Studies and Research, Prof. Francis Otuonye for his mentorship and encouragement to me during most of the trying periods of my studies in TTU. I am grateful to all the staff in the Office of Graduate Studies and Research as well as those in ECE department for their readiness to assist. I appreciate in its totality the Minority Fellowship awarded to me by Tennessee Technological University to undertake this Ph.D. study; and to my home University, the Federal University of Technology Owerri (FUTO), Nigeria, for approving the four year paid study fellowship which reduced the pains of staying away from my family.

To my cousin and his wife, Jude and Uche, brothers and In-laws, the Advisors and members of both the African Students Union and National Society of Black Engineers TTU Chapter, numerous friends and colleagues, I thank you all for your prayers as we match into the next stage of helping to improve our society with this great opportunity our Almighty God is about granting us. Finally, I return all thanks to our Almighty God for His infinite mercies and keeping His promise.

TABLE OF CONTENTS

Chapter Page

LIST OF FIGURES

Figure Page

LIST OF TABLES

Table Page

CHAPTER 1

INTRODUCTION

1.1 General Introduction

Reactive power compensation has long been recognized as a veritable mechanism for improving the performance of power system under both normal and stressed conditions. In the earliest form, it was employed as a static capacitor bank to inject reactive power on a long transmission line to increase the transmission line transfer capability and voltage control. However, this was drastically altered in the late nineties with the emergence of fast acting electronic AC transmission line compensators in the form of Flexible AC Transmission Systems (FACTS). With the increasing number of wide scale blackouts recorded after the nineties, there is a need to develop tools to assess the impact of FACTS and other compensation devices on the electrical power system network and optimize their usage.

In this Chapter, an overview of a traditional power system, power system stability categorization, justification of the present research effort, and the organization framework for the dissertation will be presented.

1.1.1 Overview of Electric Power System

An electric power system is an interconnection of generating sources and loads via a transmission system, transformers, and other ancillary equipment. In the primordial form, it used to be a radial supplying power from a generator to a defined load. However, the

modern transmission system is a complex network of transmission lines interconnecting all generator stations and all major loading points, carrying large blocks of power which can be routed via any desired direction to achieve desired economic benefits and performance objectives. The power system has a meshed distribution system near the densely populated residential and industrial centers, longitudinal systems connecting utilities, groups of utilities under an Independent System Operators (ISOs), and/or group of ISOs under a given Regional Transmission Organization (RTOs), forming a giant continental grid like that of North America and Europe. Other continents of Asia, Africa, and Middle East are also forming larger sub-regional networks to tap the seemingly benefits of global power village. Hence, the direction of power flow is not specified but depends on operating conditions at the nodes.

In its present form, an AC transmission line is composed of a series resistance and inductance, shunt conductance and capacitance, forming distributed circuit parameters. However, the deterministic parameters of the transmission line behavior are the reactive elements - series inductance '*l*'and shunt capacitance '*c*'. The 'two machine model' of a lumped-element representation of a transmission line is represented in Fig. 1.

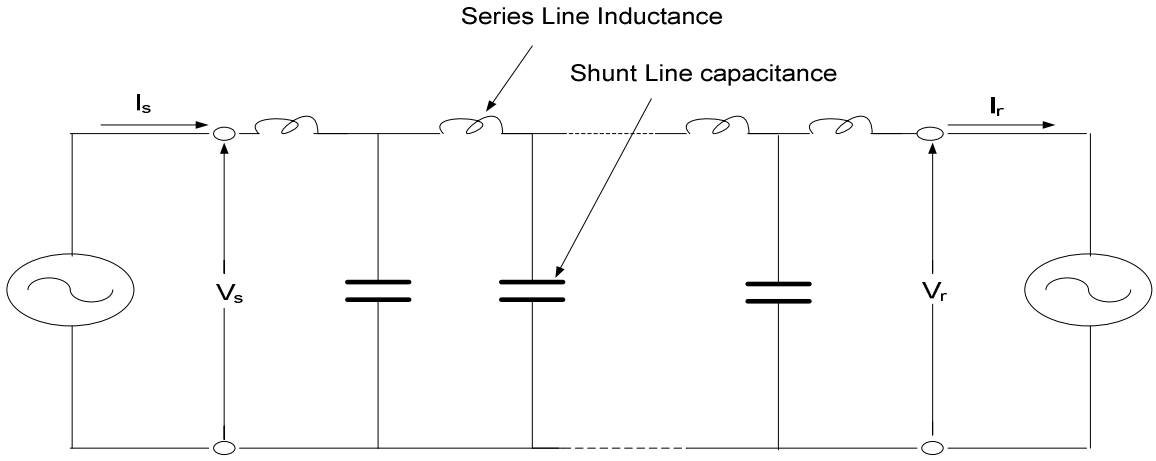

Fig. 1.1: Lumped element representation of lossless transmission line [1].

From Fig. (1.1), given that the phase angle between sending end voltage V_s and receiving end voltage V_r is δ, the generalized expression characterizing the power transmission over a lossless line is given by [1] as

$$P = \frac{V_s V_r}{Z_o \sin\theta} \sin\delta \qquad (1$$

where θ the power factor angle and the surge impedance of the line is given by:

$$Z_o = \sqrt{\frac{l}{c}} \qquad (2)$$

An ideal transmission characteristic is exhibited by the lossless line at surge impedance loading given the maximum transmitted power which is independent of line length as:

$$P_o = \frac{V_o^2}{Z_o} \qquad (3)$$

At surge impedance loading, the shunt and series reactive power balance is at dynamic equilibrium and the current and voltage stays in phase with each other along the transmission line. This is the optimal state which system ought to be was it that generation, transmission, and load capacities are balanced. However, the present power system state varies between two extremes of light and heavy loading; more often heavy loading is the case unless there is an abrupt loss of load.

During light loads, the transmission line is overcompensated by the shunt capacitor reactive power generation, and the voltage increase across the series line reactance is greater than the voltage drop by the load current. This causes the transmission line voltage to increase reaching a maximum value at the midpoint, and the surplus charging current also flows at the terminal generators forcing them to absorb reactive power. Above surge impedance loading, the transmission line is under-compensated and the

voltage increase resulting from shunt line capacitance is unable to cancel the voltage drop across the series line reactance due to the load current, hence the voltage along the line decreases reaching a minimum at the midpoint.

Therefore, the reactive power demand of the line (inductive) must be supplied by the sending end and receiving end generators. If these terminal generators cannot supply the required reactive power compensation, the voltage will continue to decrease until a point where it could provide the requisite will voltage to sustain the interconnected loads and transmission line stability; hence it will lead to voltage collapse.

For an electrically short transmission line, $\sin\theta \cong \theta$

With this approximation, θ is now defined as the electrical length of the line in radians and is given as

$$\theta = \omega a\sqrt{lc} \tag{4}$$

Therefore $Z_o\theta = \omega al = \omega L = X$ (5)

Hence, the simplified transferable electric power can now be given as

$$P = \frac{V_s V_r}{X}\sin\delta \tag{6}$$

In Equation (6), the shunt capacitance is neglected, and since the line is lossless, V_s and V_r are equal, which implies that Equation (5) can be written as

$$P = \frac{V^2}{X}\sin\delta \tag{7}$$

The reactive power provided at each end for this lossless case is given as

$$Q_s = -Q_r = VI\sin\frac{\delta}{2} = \frac{V^2}{X}(1-\cos\delta) \tag{8}$$

At constant voltage magnitude and fixed line reactance, real power, reactive power and voltage angle are coupled as can be seen from equations (7) and above. So increasing one parameter leads to increase on the other up until the midpoint where maximum power is reached.

The above analysis shows that power flow is largely dependent on transmission line impedance, voltage magnitude, and angle difference at the transmission terminals. Therefore, the increasing distances of both regional and continental longitudinal interconnections impose a lot of constraints on the power system. This is more so as power is generated at remote locations and transmitted over long distances which gives rise to large I^2R losses necessitating the need to transfer bulk power at high voltages. At a certain temperature, the physical characteristics of the conductor would irreversibly change leading to deformation. The steady state active power transmission limit for short transmission line is set by the resistance, while the reactance sets the limit for long line. A transmission line reactance to resistance ratio of less than five may impose practical limitation on the active power transmission before the thermal limit is set by increasing the reactive power flow of the line [1].

To improving the system power factor, provide requisite reactive power consumed by nonlinear loads, sustain desirable transmission lines, and bus voltage magnitudes, and angles, there is need for introduction of reactive power compensation. Series capacitor banks served the need of the various transmission networks until the late nineties when the power system of North America and Europe was unbundled and commercialized [2]. This brought in competition among the now privatized utilities and larger numbers of

customers were then connected without commensurate growth in generation and transmission capacity to meet the growth in demand [3 -11].

The need to make better use of the existing transmission facilities and ensure delivery of quality power to consumers led to embrace the newly developed Flexible AC Transmission System (FACTS) devices. FACTS devices can be effectively utilized for power flow control, loop-flow control, load sharing among parallel corridors, voltage regulation, and enhancement of transient stability and mitigation of oscillations [1]. It is pertinent to mention here that the prohibitive cost of most FACTS devices played a key role in slowing down the expected wide spread application. Despite these positive contributions of FACTS devices to power system improvement, there have been more incidents of large scale system outages leading to blackouts in significant parts of the grids [11], which underscore the need to develop tools for realistic power system status monitoring.

1.1.2 Power System Stability Issues

Evaluating power system status involves accessing its Reliability and Stability. For an interconnected bulk power system, the North American Electric Reliability Corporation defines reliability in terms of two basic and functional aspects as [12]

Adequacy – "the ability of the bulk power system to supply the aggregate electrical demand and energy requirements of the customers at all times, taking into account scheduled and reasonably expected unscheduled outages of system elements."

Security –"the ability of the bulk power system to withstand sudden disturbances such as electric short circuits or unanticipated loss of system element from creditable

contingencies." Stability is the ability of an electric power system to regain a state of operating equilibrium after being subjected to a physical disturbance from its initial operating conditions and with most of its variables bounded so that the entire system remains intact [13]. While reliability is the overall objective of power system design and operation, it is guaranteed by system stability. Therefore, a measure of stability of the power system gives a good indication of how reliable it will be. Power system stability encompasses rotor angle stability, frequency stability, and voltage stability. Rotor angle stability is the ability of the power system synchronous machines to maintain equilibrium between each other and with other components of the system after being subjected to a disturbance. It is further grouped into small signal and large signal stability problems depending on the strength of the causative phenomena.

Frequency stability refers to the ability of the power system to maintain steady frequency following severe disturbance in the system which results in significant imbalance between generation and load. To what extent the equilibrium can be restored with minimal load loss after a noticeable perturbation in the system is the focus of frequency stability. The present huge size of the grid is of great concern, particularly when islands are formed after splitting of sections of the interconnected system.

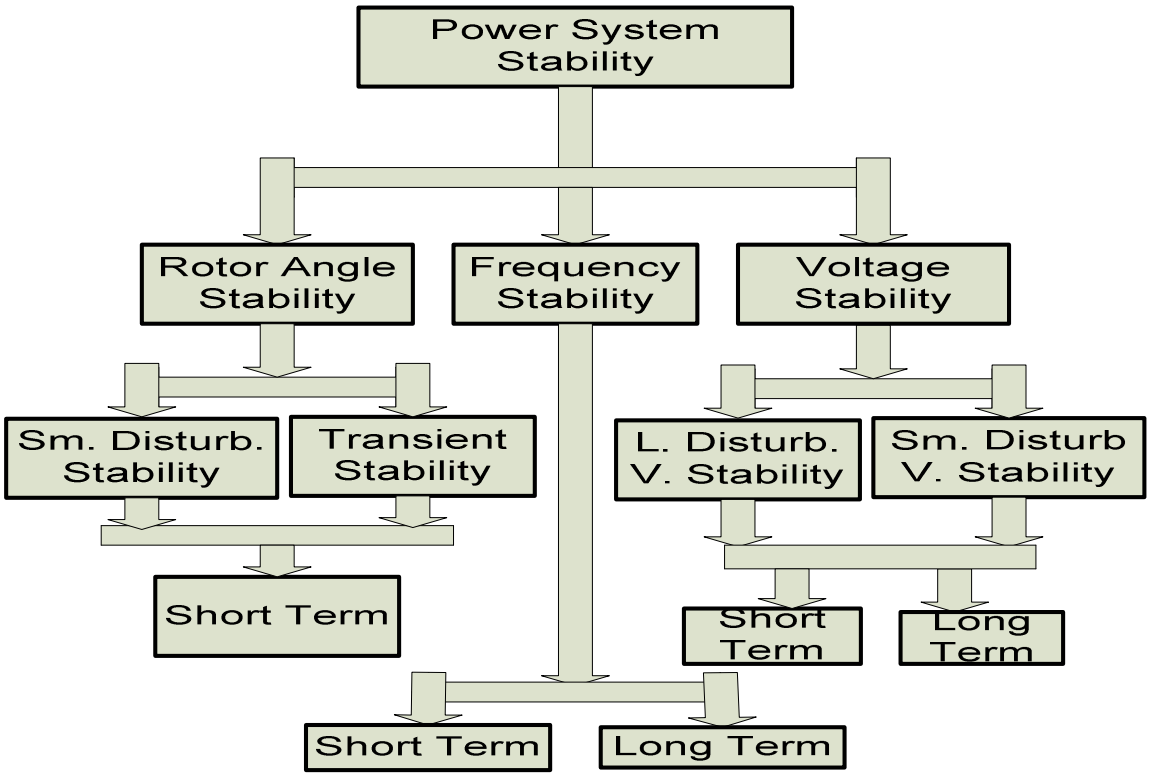

Fig. 1.2: Power system stability classification [14].

Voltage stability involves the ability of the power system to maintain steady state voltage supply at all buses after a disturbance given an initial operating condition. Like frequency stability, it is concerned with equilibrium between generation and load in the event of a disturbance. However, it defers in the same that voltage stability looks at the voltage rise or fall occasioned by the disturbance while frequency stability considers the fluctuation in system frequency due to the imbalance between supply and demand. The general classification of power system stability is shown in Fig. 2.

The focus of power stability studies for decades has been on rotor angle instability as it was considered the major cause of system disturbances with less emphasis on frequency and voltage stabilities. However, with continued growth in power system interconnections, use of new technologies and controls as well as the increased operation

of power system under stressed conditions, the role of voltage, frequency, and inter-area instabilities in power system large scale disturbances have become very significant[14].

This new development has led to the emergence of fast dynamic reactive power compensators in the form of Flexible AC Transmission Systems (FACTS) in the last three decades in view of the direct contribution of reactive power towards the system voltage and frequency regulation.

1.2 Problem Statement

In the current deregulated power system condition, with competition and profit maximization among utilities and private system operators, power transmission system is being operated under heavy loading and with less reactive power generation by utilities due to disinterest in reactive power generation investment occasioned by poor pricing. There is a great difficulty in meeting up with the operational equilibrium between the aggregate reactive power demand and reactive power supplied to the transmission system network. The direct consequences of the above situation are the non-optimal power transfer to meet demand and voltage degradation due to insufficient reactive power. Worst still, the available reactive capability are applied arbitrarily without recourse to the changing nature of the grid status. There exist therefore, the problem of reactive power compensational need quantification – what is required, where, when, and how?

Then the next question is: how does the reactive power affect the voltage stability status of the interconnected power system grid? Available literatures point to the fact that system operators are very often unaware of the operating status of their network [15-18]. These are the problems that this research work is focused on solving, and lead to the

motivation as statement next. An effort has been made in this work to develop an index that will help monitor the 'voltage stability health' of the system.

1.3 Motivation for the Work

This work is motivated by the reports of the various committee setup to consider the immediate causes of the August 14th 2003 North American blackout that affected eight states in United States and two Provinces of Canada leaving over 50 million people without power and the attendant loss of millions of dollars [15-19]. These reports clearly stated four factors that contributed to this and other previous blackouts which have not been addressed, namely:

1.3.1 Improper Visualization of Power System Conditions

There was no effective tool to monitor the status of the different largely interconnected grids by both North American Reliability Council (NERC), Regional Transmitting Organizations (RTOs), and Independent System Operators (ISOs). Relays only have localized actions and as such could not control the blackouts. Worst still, First Energy (FE), and Midwest Independent System Operator (MISO) did not inform the adjoining ISOs, RTOs, nor the NERC of the impending emergency situations in their networks and this made the early control of the blackout difficult.

1.3.2 Insufficient Static and Dynamic Reactive Power Supply

The Northeast American grid had FACTS devices which were installed but not monitored to determine if they were providing sufficient compensation since present power system contain dynamic loads. FE was importing 1800 MW from South Ohio while selling reactive power without knowing it had low reactive power supply itself; hence very abnormal low voltage was noticed minutes later which helped in triggering off the collapse situation [8].

1.3.3 Improper Reactive Power and Voltage Control Practices

Adequate control of reactive power will lead to improved voltage control and since the reactive power provided by the FACTS devices had no effective monitoring mechanism, there was no control of both reactive power and voltage levels.

1.3.4 Poor Analysis Tools

First Energy (FE) where the incidents that led to the outage started at 15.00 EDT had no effective power system analysis tool. Therefore, the operators at its control room could not understand the unfolding scenario at their system and therefore watched helplessly for minutes as an outage of a single transmission line led to series of events that spread to other networks.

1.4 Research Objectives

To address the above and similar situations, this research is being carried out with the following objectives

1.4.1 Assess Status of Power System Buses and Transmission Lines

Most of the transmission grids in USA are old and built to carry limited electrical power to nearby load centers. However, with unbundling and privatization of the power industry, it has become necessary to bulk-wheel power over long distances with transmission lines loaded close to their stability limits. Therefore, an index which will determine when these transmission line loadings may are exceed limits and how reactive power could be injected into or absorbed from the transmission line to increase its transmission capacity is required.

1.4.2 Determine the Amount and Location of Compensation Required

The emergence of FACTS devices came at a time when there was immediate need to improve the ability of power system to transmit more power due to pressure on utilities to meet the demand for improved, efficient, and reliable power by consumers. With this pressure and the seemingly satisfactory performances of the various FATCS devices, there was no effort to determine the type and amount of reactive power required and where. The consequence was the emergence of uncharacterized power system phenomena which was previously unknown and therefore the power system operators could not determine what is happening to their system until voltage collapse scenes sent

in and eventual loss of large parts of the grid. Therefore, this work will help to indicate the type of compensation (series or shunt) and where it is required. Monitoring the progress of the compensation will also help to inform the system operator when the required level of compensation has been met instead of infinite supply of reactive power.

1.4.3 Monitor the Effect of Reactive Compensation on the Over-all System

With the inclusion of multi-FACTS devices in the Newton's power flow model and simulation of the system, we hope to monitor the effect of the reactive power on the entire interconnected network since the injection or absorption of reactive power at a particular location on the grid affects the entire system. This will help to operate the power system optimally and adjust to meet specific conditions that may arise from the reactive power compensation schemes to be adopted.

1.4.4 Make Optimal Utilization of Reactive Sources

Lack of optimal utilization of reactive sources has resulted in system blackouts since reactive power is directed related to system stability [9]. Developing an index which will give a measure the reactive sources utilization will help in effective pricing and payment for reactive power supplies. Currently, only few utilities invest in the generation of reactive power, but if improved rewards are given to the providers of reactive power, system operators will invest in reactive power generations. This is expected lead towards system stability improvement.

1.4.5 Provide Alternative Mechanisms to Save Power System from Collapse

The model to be developed in this work will consider alternative mechanisms to save power system from collapse since reactive power is not always available to meet all power system operating conditions. This scheme is achieved by providing seamless incorporation of microgrids to the power system and improved load shedding by effectively detaching the microgrid loads from the main grid during adverse periods.

1.4.6 Provide System Operators Mechanisms for Appropriate Voltage Stability Index Selection

There are different voltage stability indices which are modeled to take into cognizance specific system conditions like transmission line length, reactive power demand, and maximization of transmission line active power transfer. The scheme will develop selection criteria to determine which index will be applied given the actual condition of the power system.

1.5 Research Methodology

Since this research is focused on the development of improved “power system vulnerability computation index” applicable to voltage regulation, the research approach will be as follows:

1.5.1 Review Voltage Stability Index Models and Compensation Schemes

This will enable the identification of possible weaknesses when operated in a deregulated power system environment and with compensation devices application affecting the overall network dynamics. Based on these reviews, the determination of factors affecting index performances will be made.

1.5.2 Development of Selection Criteria

Appropriate selection criteria will be evolved to guide the development of improved index model taken into account the issues involved in a restructured power system, like long distance power wheeling and operation close to voltage stability limits.

1.5.3 Development of a Novel Voltage Stability Index Model

Based on the present status of power system operation, a new index model will be developed.

1.5.4 Algorithm and MATLAB Load Flow Program Development

A MATLAB-based load flow program will be developed using Fast-decoupled load flow model to establish a base case scenario and then extending the development to full Newton Raphson's load flow model with the voltage stability index model incorporated. The load flow program will be tested on both IEEE 14 and 30 bus systems to enable the comparison of the developed model with the results from existing index models. The simulation will also reveal weak buses and transmission lines that require compensation.

1.5.5 Application of Model in Voltage Regulation Concepts

In view of the voltage support role that microgrids are presently utilized for particularly with sub-transmission and distribution network and the problem of instability the results from its islanding operation and voltage violations that its incorporation to the utility grid is causing, the modeled voltage stability index will be applied to develop a new operational set of transition mode for microgrids.

A scheme that will enable the direct utilization of voltage stability index values to modulate multi-level voltage source converter (VSC) will be developed since this serves as the hub of both shunt and series devices. The simulation of the VSC dynamic model will be made to see the effect of variation in operating conditions of power systems on the actual converter switching function modulation.

Multi-FACTS devices model will be included in the Newton Raphson's load flow model and this will used to separately regulate and monitor the operation of both shunt and series compensation devices. These last set of models will be implemented on the IEEE 300 bus system with zoning to facilitate fast determination of vulnerable buses and transmission lines.

The concept of line voltage stability index will be extended to a new horizon by applying it to compute available transmission capacity since line overloading is currently a major source of voltage instability. This is of great concern to system operators and regulatory bodies.

1.6 Organization f Dissertation

The remaining Chapters of this work comprise of the various papers developed. Paper one, “Development of a Versatile Voltage Stability Index Algorithm” is presented in Chapter 2. This paper provides the framework for this dissertation. Apart from giving an overview of available voltage stability index models and reactive power compensation devices, it contains the modeling for a novel bus voltage stability index appropriate for present power system long distance power-wheeling.

In Chapter 3 is presented the second paper, “Utilization of L-Index in Microgrid Interconnected Power System Network.” This paper came as an alternative mechanism to provide further reactive (back-up) support to the power system, provide smooth load shedding during peak loading and insufficient reactive support periods, and also play special role in protecting sensitive installation when outage is unavoidable.

“L-index Modulated Voltage Source Converter (VSC),” which is the subject of paper three is presented in Chapter 4. Having an improved VSC working with actual power system operating status is significant since most FACTS devices presently developed use it as the main engine. The dynamic modeling of a three-level Neutral Point Clamped Converter using L-index as a control parameter and its simulation under different conditions form the main foci of this particular paper.

Chapter 5 contains the fourth paper, “L-index Regulated Shunt Compensation Scheme.” Fast-decoupled load flow model is used as a quick process of determining the load buses that require compensation. Then Multi-STATCOM power and constraint equations are incorporated into more reliable Newton Raphson’s load flow model with the developed L-index models utilized to compute the status of the entire system which

will indicate the effect of the interconnected FACTS devices under different loading conditions.

Chapter 6 will discuss “Line Voltage Stability-index Based Series Compensation Scheme for Optimal ATC Computation.” This uses the best available line voltage stability index model to simplify the computation of available transmission capacity for each line, and gives the improvement in series compensated lines to increase the amount of power that may be wheeled across such a line.

The general conclusions to the entire work will be presented in Chapter 7.

1.7 References

[1] Y. H. Song and A. T. Johns, "Flexible AC transmission Systems (FACTS)," Published by the *Institute of Electrical Engineers*, London, UK, pp xv, 1999.

[2] W. S. Read, "Electrical utility restructuring in North America," *IEEE Power Engineering Review*, pp 6-9, May 2001.

[3] International Energy Outlook 2007, published by Energy Information Administration, Office of Integration Analysis, Department of Energy, Washington, DC 20585, May 2007.

[4] *Fact book* – Generation Capacity in Europe, pp 1 – 30, June 2007.

[5] South Africa Country Analysis Briefs, *Energy Information administration*, Official Energy Statistics from the U.S. Government, Country Analysis Briefs, www.eia.doe.gov

[6] Electric Power Annual, *Energy Information administration*, Official Energy Statistics for the U.S. Government, October 22, 2007.

[7] M. Amin, "North American's electricity infrastructure: Are we ready for more perfect storms?" *IEEE Security and Privacy*, published by the IEEE Computer Society, pp.19, September/October 2003.

[8] North American Electric Demand Continues to Outpace Resource Growth; Reliability Concern Remains, *Transmission and Distribution World*, October 2007.

[9] M. Begovic, D. Novosel and M. Milisavljevic, "Trends in power system protection and control," Proceedings of the 32nd Hawaii International Conference on System Sciences – 1999.

[10] E. Hirst, "U.S. transmission capacity, present status and future prospects," prepared for Edison Electric Institute and Office of Electric Transmission and Distribution, U.S. Department of Energy, August 2004.

[11] 2007 Long-Term Reliability Assessment (2007-2016) by North American Electric Reliability Corporation (NERC incorporated in 2006, instead of Council), October 2007.

[12] G. Anderson, P. Donalek, R. Farmer, N. Hatziargyriou, I. Kamwa, P. Kundur, N. Martins, J. Paserba, P. Pourbaik, J. Sanchez-Gasca, R. Schulz, A. Stankovic, C. Taylor and V. Vittal, "Causes of 2003 major grid blackouts in North America and Europe, and recommended means to improve system dynamic performance," *IEEE Transactions on Power Systems*, vol. 20, no. 4, pp 1922-1928, November 2005.

[13] *2007 Long-Term Reliability Assessment* (2007-2016) by North American Electric Reliability Corporation (NERC incorporated in 2006, instead of Council), October 2007.

[14] P. Kundur et'l, "Definition and classification of power system stability," IEEE/CIGRE Joint Task Force on Stability Terms and Definition, *IEEE Transactions on Power Delivery,* vol. 19, no. 2, pp 1387-1401, May 2004.

[15] August 14, 2003 Blackout NERC Final Report, pp 1-5 July 13, 2004.

[16] U.S.-Canada Power System Outage Task Force, August 14 2003 Blackout: Causes and recommendation, Appendix D "NERC actions to prevent and mitigate the impacts of future cascading blackouts," pp. 193-202, February 10, 2004. [Online] Available: http://www.nerc.com.

[17] U.S-Canada Power System Outage Task Force, "Final report on the implementation of the Task Force Recommendations," September 2006, pp. 103-106.

[18] D. J. Ray, "Blackout 2003: "Description and responses," Power System Engineering Research Center (PSERC), November 7, 2007. [Online] http://www.pserc.org/cgi-pserc/getbig/generalinf/presentati/presentati/blacoutpr/ray_blackout_sep03.pdf.

[19] "Principles of efficient and reliable reactive power supply and consumption," Federal Energy Regulatory Commission Staff Report, February 10, 2004.

CHAPTER 2

PAPER 1: DEVELOPMENT OF A VERSATILE VOLTAGE STABILITY INDEX ALGORITHM[†]

D. O. Dike, S. M. Mahajan and G. Radman

Department of Electrical and Computer Engineering

Tennessee Technological University, Cookeville, TN 38505, USA.

ABSTRACT— Power system experts have shown interest in the development of methods for predicting system status in the form of voltage stability indices. These indices performed well because they were primarily used for system planning as utilities then were either highly localized and regulated by the state or owned and operated by big electricity consumers. However, the situation changed drastically with the advent of unbundling, privatization/competition, and power pooling in the last two decades. Consequently, incidents of power outages have become a common occurrence worldwide because of increasing load demand without proportionate increase in electrical power supply due to difficulties posed to the building of new generation centers and transmission lines by residents and environment. This paper develops a versatile index algorithm that incorporates robust features so as to guarantee the optimal utilization of the various voltage collapse indices to adequately predict, monitor, and detect the status of power system both online and offline. It reviews existing voltage stability indices, and for the first time outlines index selection criteria to guide system operators and planners in their optimal usage to reduce outages and operational cost. The work, also, presents a new index computation scheme utilizing the complex pi-model of the medium and long transmission line. This new index will be used to effectively determine the status of power systems to prevent system overloading during power pooling and long distance wheeling of power, which has become a common phenomena among independent system operators (ISOs), and regional transmission organizations (RTOs) during peak and emergency periods. The simulation results show a favorable performance of this new index on both IEEE 14 and 30 bus systems with respect to existing indices.

[†] Published on the proceedings of IEEE Electrical Power Conference 2007, Montreal QC, Canada, October 24-26, 2007.

2.1 Introduction

With increased loading of power system occasioned by astronomical rise in demand for electrical power resulting from high level of industrialization and urbanization as well as the unbundling and commercialization of the power industry [1], the incidents of power outages and blackouts have become a frequent occurrence [2 -5]. This is being worsened by the opposition to the building and construction of new generation and transmission facilities by environment, right-of-way, and cost concerns to match increasing demand [6].

Power outages and blackouts are direct consequences of voltage instability and collapse. Operating power systems close to their voltage and thermal stability limits have led to voltage collapse taking place in systems and sub-systems quite abruptly which requires improved continuous monitoring of the system. These disturbing and unreliable nature of electrical utilities may be attributed to a large extent on the failure of power system planning, operation, monitoring, and control experts to maximize the utilization of system stability indices to accurately determine in a timely manner, the status of a given power system at any point in time. This failure on the part of the voltage stability index models was as a result of power systems becoming more complex and heavily loaded, in addition to economic and environmental constraints, thereby making voltage instability an increasingly serious problem.

A comparison of voltage stability indices was provided in [7], but no attempt was made to provide operators the criteria that were utilized in the comparison, and which will guarantee large scale application of these indices to specific system need. Since an

accurate knowledge of how close the actual system's operating point is from the voltage collapse margin is very important to system operators, it becomes imperative to develop a model which will guarantee the optimal utilization of the various voltage collapse indices to adequately predict, monitor, and detect the status of power system both online and offline.

This present effort entails a review of existing indices and their performance in the present power system structure, defining of criteria for index selection(s), development of models to determine index relevance in each application area, development of algorithm to combine two or more of the index models to solve current multifaceted power system problems, and simulation of typical cases using IEEE 14 and 30 bus systems. The authors have also provided a model for the computation of bus voltage stability index based on the medium and long transmission line pi-model. It is our hope that in this era of power wheeling over long distances between independent system operators (ISOs), and regional transmission operators (RTOs), there is a dire need to provide an index that will appropriately give the status of power systems at each location.

The results obtained in this present attempt gave a direct indication of the status of each of the buses and lines which were not reflected in the earlier work**.** This new index (Ls-index) developed could also be applied in the unfolding microgrid networks in large cities to compute the voltage stability condition of the interconnected load buses. This is possible since such a scheme could operate in both grid-connected mode and the islanded mode where microgrid is interfaced to the main power grid [8]. Such an application, which is part of ongoing research by the authors, when concluded will prevent the

occurrence of fast voltage dynamics which develop immediately after an outage. This could not be addressed by traditional control methods as reported in [9].

2.2 Review of Existing Indices

The study of voltage stability index had been performed under dynamic and static analysis. The dynamic analysis uses a model of the power system characterized by nonlinear differential and algebraic equations in which transient stability simulations reflect tap changing transformers and generator dynamics. Most voltage stability analysis and models have been based on static analysis which depends on the steady state or dynamic model described by the steady state operation of power systems because of their ease of computation and existing load flow models. Therefore, this present work is based on the static index which may be grouped under (i) bus voltage computation indices presented in 1 – 4, and (ii) line stability indices stated in 5 - 8.

2.2.1. L-index

In [10], a quantitative measure for the estimation of the distance of the actual state of the system to the stability limit was developed. It described the stability of the complete system and has direct application towards the determination of the status of the load buses condition. Represented as

$$L = \max_{j \in \alpha_L} \left(L_j \right) = \max \left| 1 - \frac{\sum_{i \in \alpha_G} F_{ji} \bar{V}_i}{\bar{V}_j} \right| \tag{1}$$

$$F_{ji} = -\left[Y_{jj} \right]^{-1} \left[Y_{ij} \right] \tag{2}$$

where L_j is the local indicator of bus bars from where collapse may originate.

2.2.2. Voltage Ratio

The load voltage to no-load voltage ratio (V/Vo) at each load bus yields a voltage stability map of the system which allows for the immediate detection of the weak buses.

2.2.3. P-V and Q-V curves

These curves are used to determine power system loading margins, and provided the oldest form of voltage stability indices where power flows are recomputed after each incremental loading until the nose of the P-V or Q-V curve is reached. The distance of the operating point at any particular loading to the nose of the curve gives an indication as to the closeness of the system to collapse. The point where $\frac{\partial Q}{\partial V} = 0$ gives the voltage stability limit.

2.2.4. Modal Analysis

Here, the smallest eigenvalue and its associated eigenvectors of the reduced Jacobean matrix of the power system are computed. Positive eigenvalue implies stability, while if one eigenvalue is found to be negative indicates instability of voltage. The magnitude of each minimum eigenvalue shows how close the system is to voltage collapse. The weakest bus is determined using participation factor.

2.2.5. Lmn Line Stability Index

This index was derived based on a two machine model of the power system connected by a single transmission. In the derivation that followed, the discriminant of the voltage quadratic equation is set to be greater than or equal to zero to achieve stability. This is represented mathematically as

$$Lmn = \frac{4XQ_j}{\left[V_i(\theta - \delta)\right]^2} \tag{3}$$

for $0 \le Lmn \le 1$

Lines that represents Lmn close to 1 are reaching their stability limits.

2.2.6. FVSI Line Stability Index

This is developed based on the single line concept as well, but the emphasis here is placed on the transmission line impedance, reactance supply voltage, and consumed reactive power. As such line presenting values close to one are reaching their stability limit. Represented as

$$FVSI_{ij} = \frac{4Z^2 Q_j}{V_i^2 X_{ij}} \tag{4}.$$

2.2.7. LQP Line Stability Index

Using same concepts as earlier, we define this as

$$LQP_{ij} = 4\left(\frac{X_{ij}^2}{V_i^4} P_i^2 + \frac{X_{ij}}{V_i^2} Q_j \right) \tag{5}$$

In this formulation, the effect of the generated real power and consumed reactive power are taking into consideration in arriving at the final line index.

2.2.8. VCP and VCQ Line Stability Indices

The line stability indices here are derived by utilizing the concept of maximum real and reactive power carrying capacity. Then the ratio of the real and reactive line flows computed from the load flow to their respective maximum line transfer capability is used to compute the real and reactive power stability index for the line.

These are given as

$$VCP = \frac{P_r}{P_{r(\max)}} \tag{6}$$

$$VCQ = \frac{Q_r}{Q_{r(\max)}} \tag{7}$$

2.3 Development of Novel Bus Voltage Stability Index

Most of the bus voltage and line stability indices reviewed above were derived using a single line model of the power system and then applied to multiple lines. However, in power pooling where many different utilities are linked using medium and long lines forming intertie network, the simple single line two machine model may not be a good representation of the whole network. This, therefore, calls for utilization of the medium and long transmission line representation shown in Figure 1 in the development of the required index.

From Fig. (2.1), the voltage stability index could be modeled as follows

$$S_2 = S_{21} = \frac{Y'^*}{2}|V_2|^2 + \frac{|V_2|^2}{Z'^*} - \frac{V_2 V_1}{Z'^*} \tag{8}$$

$$S_1 = S_{12} = \frac{Y'^*}{2}|V_1|^2 + \frac{|V_1|^2}{Z'^*} - \frac{V_1 V_2}{Z'^*} \tag{9}$$

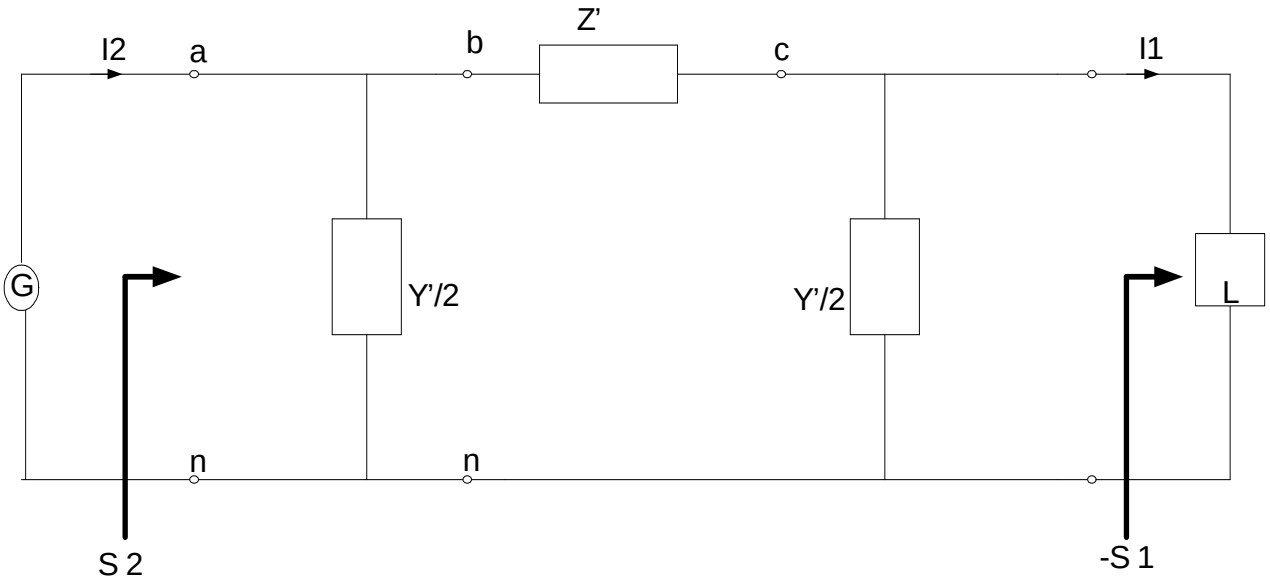

Fig.2.1: Pi-model of complex power transmission line [12].

$$\frac{S_1}{V_1} = \frac{Y'^*}{2}\frac{|V_1|^2 V_1^*}{V_1 V_1^*} + \frac{|V_1|^2 V_1^*}{Z'^* V_1 V_1^*} - \frac{V_2}{Z'^*} \tag{10}$$

$$\frac{S_1}{V_1} = V_1^*\left(\frac{Y'^*}{2} + \frac{1}{Z'^*}\right) - \frac{V_2}{Z'^*} \tag{11}$$

Letting $$M_{11} = \frac{Y'^*}{2} + \frac{1}{Z'^*} \tag{12}$$

$$M_{12} = \frac{1}{Z'^*} \tag{13}$$

$$I_1 = \frac{S_1}{M_{11}} = V_1^* V_1 - \frac{M_{12} V_2}{M_{11}} V_1^* = a_1 + jb_1 \tag{14}$$

$$|V_1|^2 + V_{01} V_1^* + = I_1 = \frac{S_1}{M_{11}} = a_1 + jb_1 \tag{15}$$

where $$V_{01} = -\frac{M_{12}}{M_{11}} V_2 \tag{16}$$

Solving Equation (15) gives

$$|V_1| = \pm\sqrt{\frac{|V_{01}|^2}{2} + a_1^2 \pm \sqrt{\left(\frac{|V_{01}^4|}{4} + a_1 |V_{01}|^2 - b_1^2\right)}} \tag{17}$$

From (1), it was it was deduced that the stability limit of the two-node system which we are considering here lies at the border line satisfying the discriminant of Equation (17) given as

$$\pm\sqrt{\left(\frac{|V_{01}^4|}{4} + a_1 |V_{01}|^2 - b_1^2\right)} = 0 \tag{18}$$

Continuing the voltage stability limit for the 2-bus medium and long transmission line model derived as

$$L = \left| 1 + \frac{V_{01}}{V_1} \right| \tag{19}$$

The major difference between the index from the pi-model and that from the single line model as used in [10] is that in the single machine model equation (16) is given as

$$V_{01} = -\frac{Y_{12}}{Y_{11}} V_2 \tag{20}$$

The multi-machine model of the index is

$$L_s = \sum_{l \in \alpha_L} \max \left| 1 - \frac{\sum_{k \in \alpha_G} \frac{M_{lk}}{M_{ll}} V_k}{V_l} \right| \tag{21}$$

2.4 Index Selection Criteria

To obtain an accurate status of the power system given varying operating conditions, a predefined set of criteria to select the most optimal index to be applied in each case must be made. From the study of various static indices and the present nature of the power system, the following may be considered by a utility or system operator in the choice of which index to apply in the determination of how close its system is to the stability limit.

2.4.1 Organizational Interest

This is the most important point for selection of index to be used. Interest area of application may be focused on: (i) bus voltage stability, (ii) line stability, (iii) maximum active power transfer, (iv) optimal reactive power usage, (v) optimal reactive power location, or (vi) a combination of two or more of the interest areas. In this criterion, index models (1-4) are used primarily to compute bus voltages, while index models (5 – 8) are for line stability indices, though there have been cases where some of the bus indices have been used to predict line overloading, and the line indices used to predict weak buses. Index models of equations (3), (4), and (7) are for reactive power transfer status determination, while index model (6) is for active power. Index model (5) combines both. Since voltage instability and collapse result from insufficient reactive power supply to meet consumption, those index computation schemes related to reactive power give better indication of the closeness to collapse.

A local company or a utility may be interested in ensuring adequate compensation of its loads to avoid bus voltage collapse, so invest in number one. On the other hand, an independent system operator (ISO) may be interest in both the load bus status as well as that of the transmission network interconnecting its customers or group of utilities it is servicing, hence will require a combination of both bus and line stability indices measurement. On the other extreme, regional transmission organization (RTO) will be interested in ensuring adequate power transfer between one ISO and another within its jurisdiction, and therefore will opt for an appropriate line stability index.

2.4.2. Level of Response Required

Typically, there is need for compromise on fastness and accuracy. When speed of computation of the closeness of the system to its stability limit is the major focus, the full Newton-Raphson's load flow method may be sacrificed to the used of Fast-decoupled. So there is always the need for compromise.

2.4.3. Online and Offline Requirements

Many index models used for purely planning purposes are used offline to predict the status of the system given some anticipated future conditions. However, with the present state of power systems now, such offline schemes are now supported by online devices since to detect fast changes in loading and system topology. The algorithm developed here is an online one given that it continues to read the latest system data and compute the status, and is designed to be incorporated into FACTS devices.

2.4.4. Expected Contingencies

The type of contingencies anticipated for a given system is also a factor considered in the selection of indices. Where line outages, generator loss, and large non-linear load variations are expected, the use of multiple indices may be advisable, with some acting as backup. In large industrial centers with nonlinear loads, we expect to use more of the bus voltage indices and less of the line indices. However, between utilities, ISOs, and RTOs where there are often large wheeling of power over long distances during peak and emergency periods, we will need the line stability indices.

2.4.5. System Size

The size of the network and the transmission line length are critical factors to be considered in the selection indices. The type of index used for a single utility may not be suitable for a power pool where many utilities are connected using tie-lines and where the indices need to be zoned and controlled by hierarchical automated system.

2.4.6. Level of Loading

In [13] it was reported that at heavy loading conditions, the active/reactive power decoupling characteristics are lost. So for an accurate result at heavy system loading, a different index needs to be used.

2.4.7. Cost and Time

As in every engineering endeavor, the cost and time required in the use of a given index play significant role in the selection of an index to be applied.

2.4.8. Reliability

It is important to consider how reliable an index will be when applied in a given condition before it is selected.

2.5 Optimal Index Utilization Algorithm

To ensure the selection of the most suitable index computation scheme to give an improved computation of the bus voltage and line stability status of a given network the optimal flowchart shown in Fig. (2) was developed.

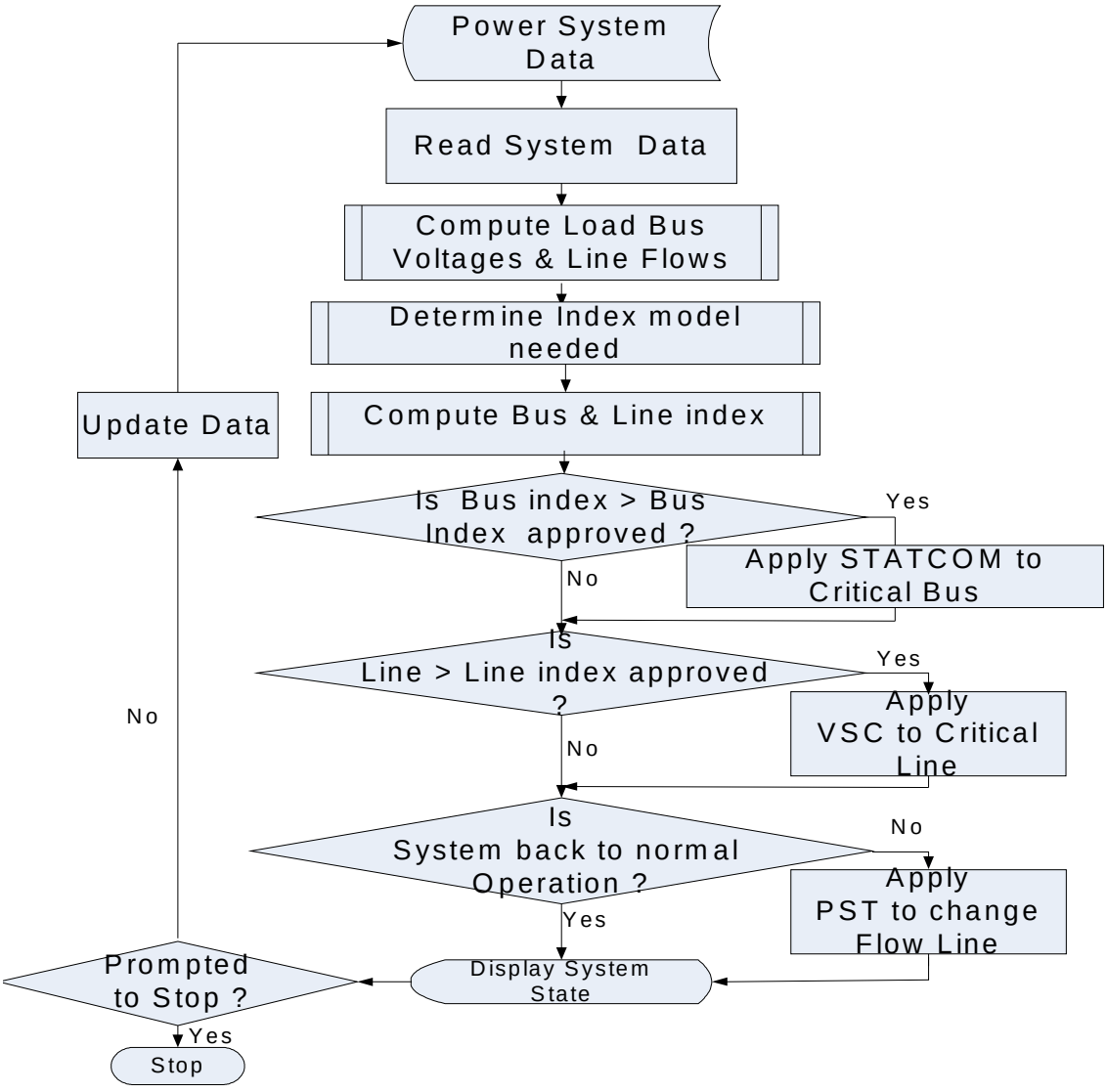

Fig.2.2: Stability index optimal utilization flowchart

The algorithm as depicted in the flowchart involved an online reading of the power system data and running of the base load flow to determine load bus voltages and line flows. From the load flow results, the program will check whether the problem area is on the bus voltage or line stability to choose which scheme to adopt. Also, the inputs data will contain information on other criteria stated earlier and the preferred interest of the client to enable a narrowing of choice to a specific scheme or combination of the schemes. This will be followed by the computation of the stability indices for all the load buses and interconnected lines. With these indices, the program determines the best FACTS device to apply.

2.6 Results and Discussion

The results obtained by using the above flowchart on IEEE 14 and 30 bus systems are presented in Figures (2.3) to (2.7). In the 14 bus system, the generator buses are 1, 2, 3, 6, and 8, while in the modified IEEE 30 bus system, the generator buses are 2, 13, 22, 23, and 27, respectively. In the L-index, the voltage stability increases from 0 – 1(i.e. from stable - collapse point). L1 indicates the base loading condition for the IEEE 14 bus system while L2 is the voltage stability index for each of the buses with 0.01p.u increased loading.

It can see that bus 14 is the most critical bus followed by 12, with bus 5 as the most stable. The generator buses have zero values indicating stability. This agrees with the result published in [7] and [10]. Then, the pi-model is applied to lines 6, and 12 connecting buses 3 to 4, and 6 to 12, respectively. The results as presented in Fig. (4) shows that effect of medium and long lines in the stability of interconnected buses. L3

and L4 represent the based and 0.01 p.u. increased loading for the IEEE 14 bus system. Due to attenuation and increases losses across the longer transmission line, there were increases in the voltage stability indices of the affected load buses.

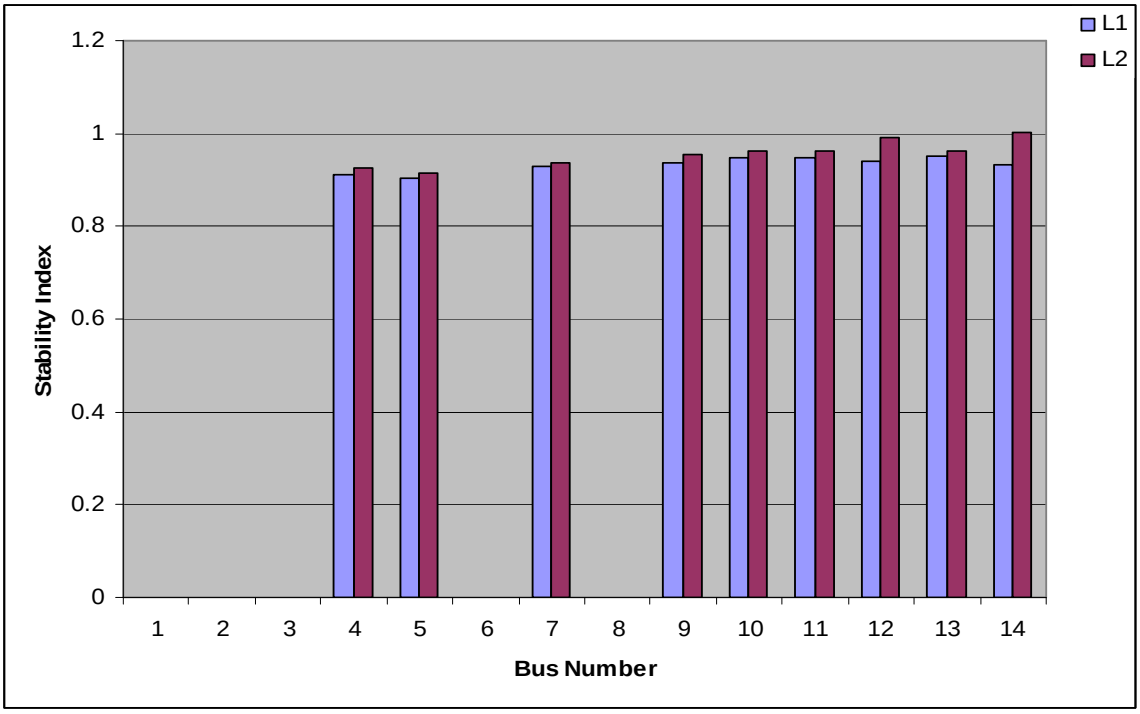

Fig. 2.3: L-index for IEEE 14 bus system

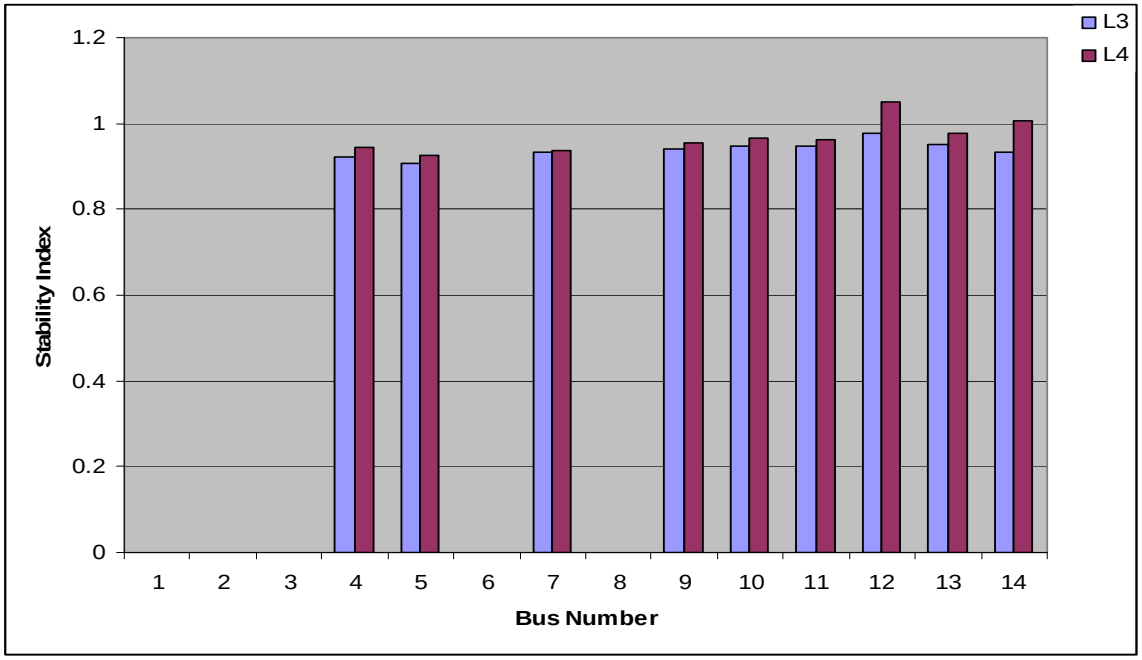

Fig. 2.4: Ls-index for IEEE 14 bus system

Based on the values indexes obtained in Fig. (2.4), it can be seen that bus 12 will collapse if the line feeding it falls within the medium or long transmission line margin and its load demand is increased by 0.01p.u which was not the case when the two machine short line model was applied.

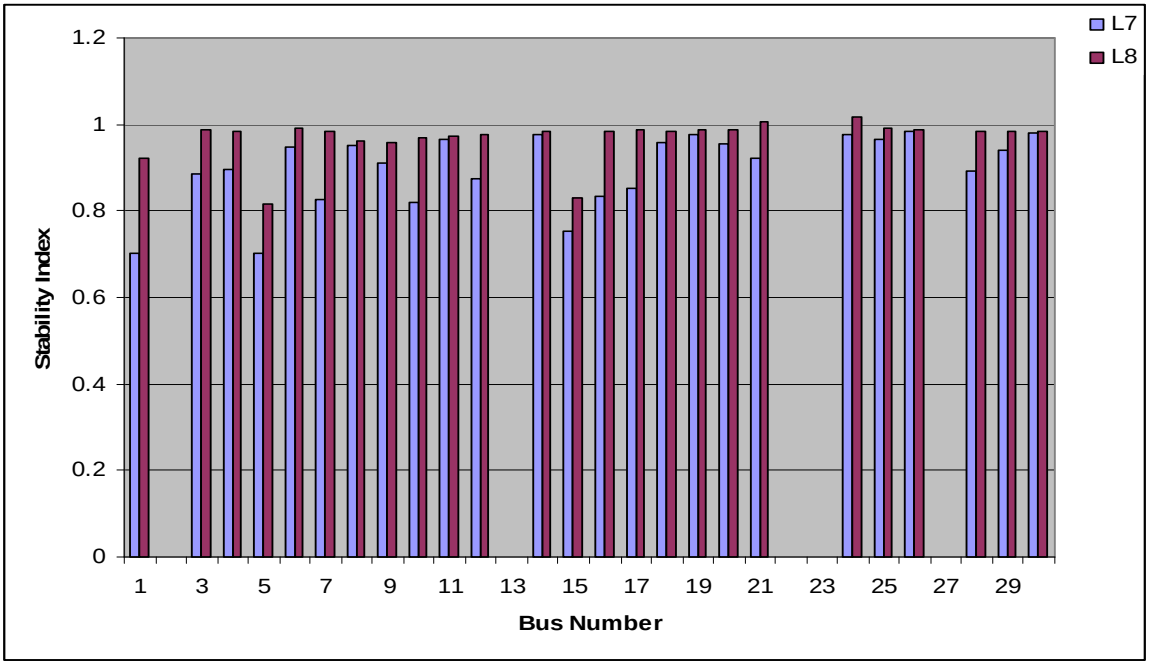

Fig. 2.5: L-index for modified IEEE 30 bus system

Performing the same operations in IEEE 30 bus system gave identical effects as shown in Figures (2.5) and (2.6). Here the pi-model was applied to lines 6 and 31 connecting bus 2 to 6 and 22 to 24, respectively. Expectedly, bus 24 collapsed when its index value increased from 0.989603 in the two machine model of L-index to 1.017560 in the Ls-index of pi-model which implied a collapse situation. On the other hand, that of bus 6 index changed from 0.980746 with L-index computation to 0.990052 with the Ls-index.

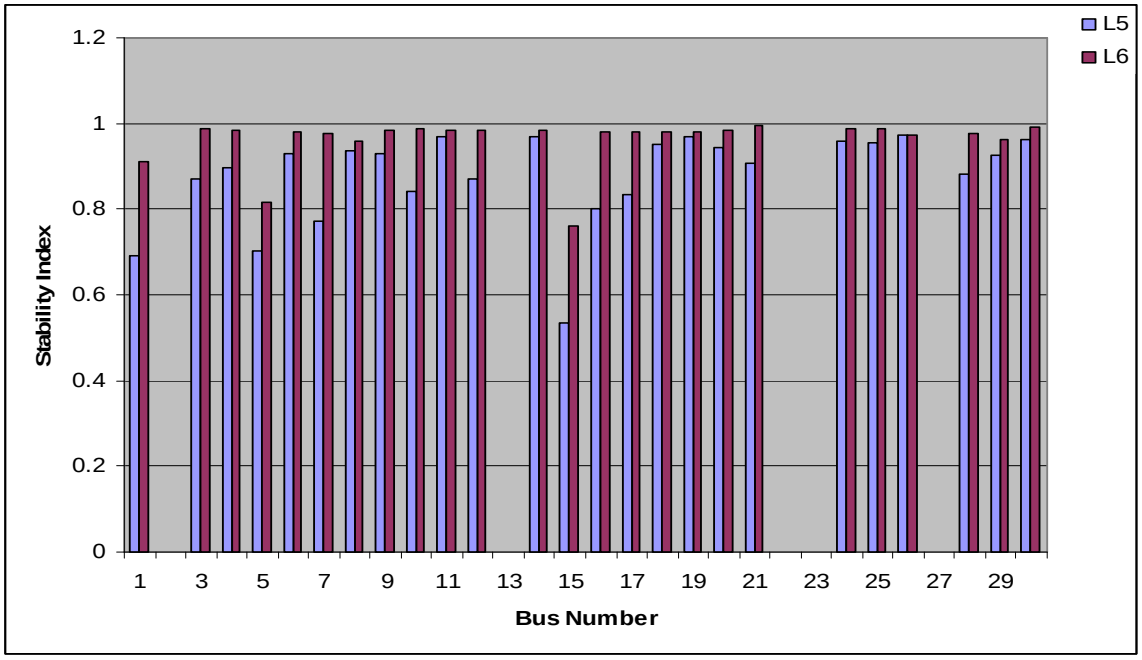

Fig. 2.6: Ls-index for modified IEEE 30 bus system

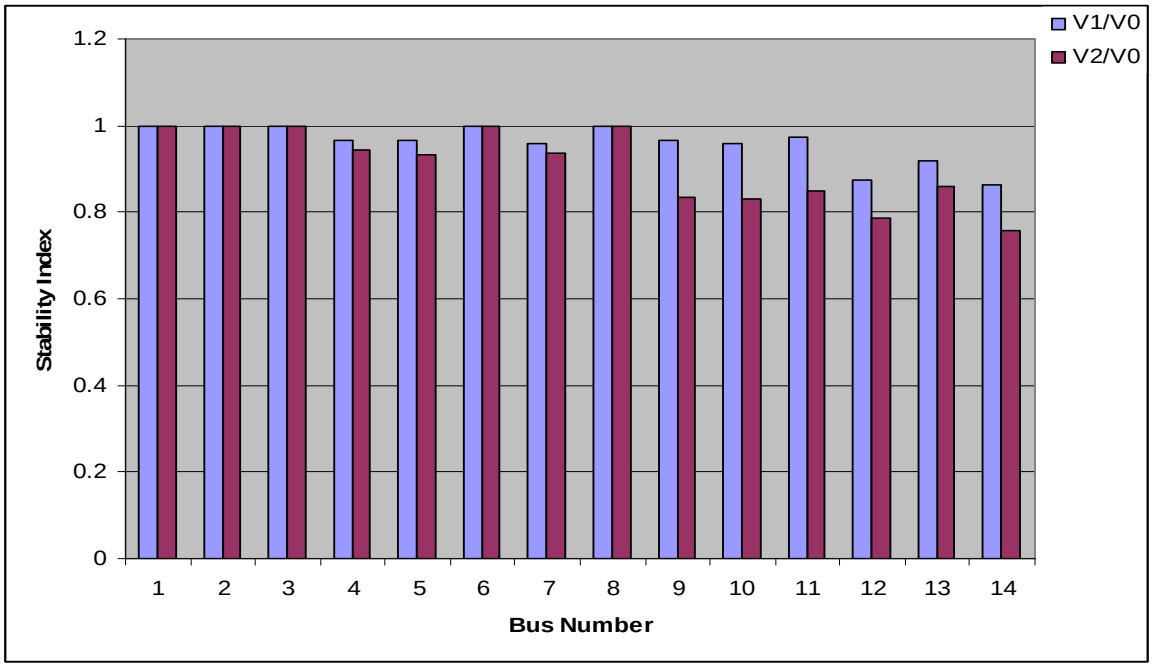

Fig. 2.7: Voltage ratio index for IEEE 14 bus system

Generally speaking, the results obtained by applying the medium/long transmission line pi-model to selected lines in either the IEEE 14 bus or IEEE modified 30 bus system reveals an increase in the stability indices showing that systems are prone to collapse when the interconnecting transmission lines between some of the buses are longer than the short transmission line distance of 50 miles. In Fig. (2.7) is displayed the result obtained when the ratio of base loading voltage and no-load voltage as well as that of 0.01p.u increased loading to the no-load voltage is plotted.

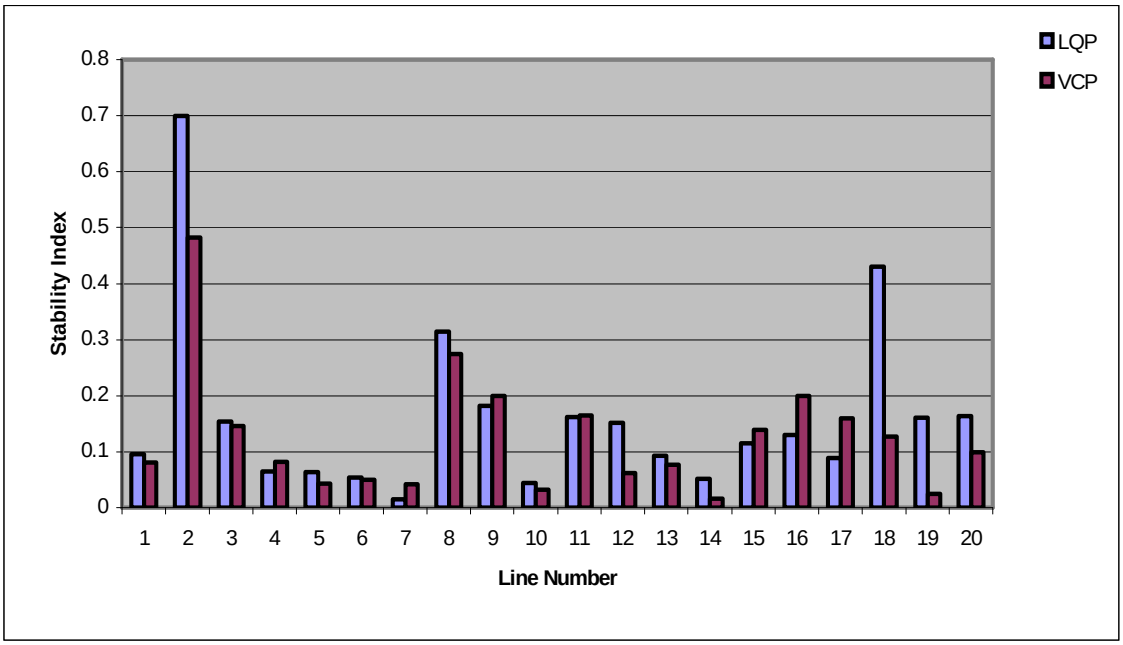

Fig. 2.8: LQP and VCP line stability index for IEEE 14 bus system

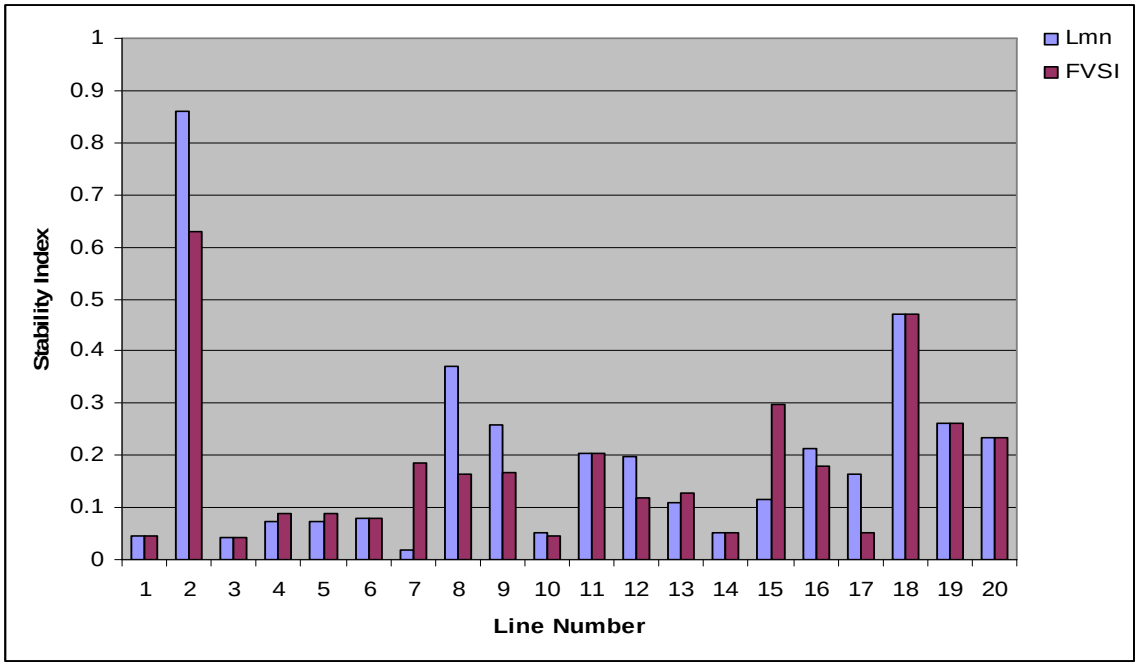

Fig. 2.9: Lmn and FVSI line stability indices for IEEE 14 bus system

This is an approximate and simple method of showing the voltage stability condition of buses. The generator buses have index values of 1.0 indicating stability, while proximity to zero reflects tendency to collapse. While the result obtained here agreed with the earlier results in showing that bus 14 is the weakest followed by 12, none of the values got close to zero to show nearness to collapse margin.

In Figure 8 is displayed LQP and VCP line stability index. As in other cases, both reflected same lines as been weak and strong. However, the degrees of variation in most of the lines are appreciable. These are due to the fact that while LQP depends on both the real and reactive power components, VCP depends on the real power transfer ratio only. VCQ also showed the same pattern of result hence is not included here. Lmn and FVSI line stability indices results are presented in Fig. (9) for the 14 bus IEEE system.

The Lmn and FVSI line indices showed corresponding lines as been the weakest, but with slight variation in the stability indices values. These differences in value could be accounted for by the effects of sending end bus and transmission angle as well as the direct reactance relationship to the Lmn index. FVSI depends more on the square of the line impedance. The same pattern of results for the line indices were obtained for the IEEE 30 bus system, hence not included here.

2.7 Conclusion

This paper prescribed a set of criteria which will guide power system operators and planners on how best to select an appropriate index for particular power system application based on a study of major voltage stability indices available. It also presented novel voltage stability index (Ls-index) computation model based on the pi-equivalent structure of medium and long transmission lines. Results obtained using this new Ls-index model compared favorably with those of the other indices in the IEEE 14 and 30 bus systems.

This new model will improve the computational accuracy of power system status over medium and long transmission lines connecting large load centers under different ISOs and RTOs to guarantee reliable bulk wheeling of power. It will improve power quality and reduce the incidents of power outage which is critically needed in this era of power system privatization and commercialization. Areas of improvement will be in the incorporation of alternate sources of energy and smart systems [14], as well as the inclusion of the lumped transmission line parameters into the new model. The authors are

presently working on the online implementing of the reactive power compensation aspects of the developed algorithm and microgrid application.

2.8 References

[1] W. S. Read, "Electrical utility restructuring in North America," IEEE Power Engineering Review, May 2001, pp 6-9.

[2] U.S-Canada Power System Outage Task Force, "Final report on the implementation of the Task Force Recommendations," September 2006, pp. 103-106.

[3] August 14, 2003 Blackout NERC Final Report, July 13, 2004, pp 1-5.

[4] K. Takahashi and Y. Nomura "The Power System Failure on July 23rd 1987 in Tokyo" CIGRE SC-37 Meeting 37.87 (JP) 07 (E) 1987.

[5] M. Amin, "2003 Blackout – North American power grid vulnerabilities," IEEE Security and Privacy, published by the IEEE Computer Society, September/October, 2003, pp 20.

[6] H. Rahman and B. H. Khan, "Power upgrading of transmission line by combining ac-dc transmission," IEEE Trans. on Power Systems, vol. 22, no. 1, February 2007, pp 459-466.

[7] C. Reis and F. P. Maciel Barbosa, "A comparism of voltage stability indices," IEEE Melecon 2006, May 16-19, Benalmadena Spain.

[8] H. Nikkhajoei and R. Lasseter, "Microgrid Protection," IEEE PES General Meeting, Tampa Florida, 24-28 June 2007, pp 1-6.

[9] R. J. Koessler, W. Qiu, M. Patel and H. K. Clark, "Voltage stability study of the PJM system following extreme disturbances," IEEE Trans. on Power Systems, vol. 22, no. 1, February 2007, pp 285-293.

[10] P Kessel and H. Glavitsch, "Estimating the voltage stability of a power system," IEEE Trans. on Power Delivery, vol. 1. PWRD-1, no.3, July 1986.

[11] Editor/Coordinator: C. Canizares, "Voltage stability assessment concepts, practices and tolls," IEEE/PES Power System Stability Subcommittee Special Publication, August 2002.

[12] A.R. Bergen and V. Vittal, Power System Analysis, 2nd ed., Prentice-Hall, Inc. New Jersey 07458, 2000, pp 112.

[13] F. W. Mohn and A. C. Zambroni de Souza, "Tracing PV and QV curves with the help of a CRIC continuation method," IEEE Transactions on Power Systems, vol. 21, no. 3, August 2006.

[14] D.O. Dike and O. D. Momoh, “An integrated AC/DC supergrid system – a mechanism to solving the North American power crisis,” 39th Southeastern Symposium on System Theory, Mercer University, Macon, GA 31207, March 4-6, 2007, pp 204-209.

CHAPTER 3

PAPER 2: UTILIZATION OF L-INDEX IN MICROGRID INTERCONNECTED POWER SYSTEM NETWORK[†]

D. O. Dike and S. M. Mahajan

Department of Electrical and Computer Engineering

Tennessee Technological University, Cookeville, TN 38505, USA

ABSTRACT-This paper proposes the application of a novel voltage stability index computation scheme to microgrid interconnected power systems. The L-index provides an online mechanism for computing and rating the status of the interconnected system into the Utility-supplied, pre-microgrid, microgrid-supplied, and island operational modes for improved operation. It may also provide a triggering signal to control the point of common coupling (PCC) converter to reduce network voltage violations in situations where the microgrid system has the capability to inject reactive power to the grid during periods of emergency or peak loads. Simulation results obtained with IEEE 14 bus system with microgrid later connected to load bus twelve as a PCC to the microgrid system, showed the suitability of the developed model towards providing smooth operation under both normal and distressed conditions.

[†] Accepted for publication on the proceedings of IEEE Power Engineering Society General Meeting, July 20-24 2008, Pittsburg, PA, USA.

3.1 Introduction

As a means of securing sensitive installations in the wake of market meltdown in major cities and its associated reliability problems, terrorist threats, and continued widespread power disruptions in North America and many parts of Europe [1-8], as well as environmental friendliness [9-10] and saving in cost of building new giant generation centers and transmission lines, prominence is now being given to the building of microgrid power networks. This has resulted in a phenomenal increase in the use of distributed generations (DGs) of various types [11]. Due to the satisfactory results obtained in its use in ensuring non-disruption of power supply to military and other sensitive installations and its self-healing capability, microgrid is now being referred to as intelligent grid network [12].

With the privatization and commercialization of electrical power industries, consumers of electrical power are now paying heavily for the services; therefore the agitation for regular, reliable, and quality power is no more an exclusive preserve of military installations and governmental institutions. This has called for a wider application of microgrids in view of its ability to serve as an affordable back-up in event of disruption of supply from the utility.

However, the anticipated widespread application of this new revolution is hampered by the fact that connection of this assembly of DGs fundamentally alters distribution network operation and creates variety of well-documented impacts with voltage rise being the dominant effect [13-15]. It is also faced with the major problem of smooth incorporation to existing power networks due to the difficulty of accurate

determination of operational modes and transitional time for the different constituents of the distributed energy resources (DERs), based on present power system operating constraints.

In view of the realization of this obvious arising situation, the development of a scheme that will guarantee the computation of the status of the microgrid interconnected power systems is highly needed. The authors have come up with a new scheme that will enable the application of their earlier developed voltage stability index (L-index) computation algorithm to microgrid interconnected power system [16].

The scheme presented in this paper will provide four modes of operation for the microgrid system, instead of the two modes utilized presently [17-19]. Such a novel introduction will enhance the transition from grid connected to islanded settings and enable the DERs to reach stable status before the microgrid is called to supply the back-up power required in either the microgrid-supplied or the island mode. In the event of general or local blackout, this mechanism may further reduce customer interruption times by providing a fast black start recovery in the low voltage (LV) grid [20], in addition to supplying its immediate customers through an islanded operation. The proposed scheme may also provide appropriate location points for new distributed generation units within the interconnected power pool to prevent grid voltage violations. This particular problem had compelled distribution network operators (DNOs) to introduce bottlenecks in the connection of DGs to distribution systems. It will further serve as an input for the expert control system of the DG converters. In Native American communities that depend mostly on DERs and other rural communities in the developing countries, the new

scheme will very well help in providing regular power supply during periods of non-availability of sustainable electric power [21].

The paper is arranged in the following manner. In section II, a review of generalized basic features and operational principles of existing and earlier proposed microgrid setups, as well as outline of their significant merits and areas requiring further improvement are covered. The operational principles and algorithm of the new scheme are dealt with in section III. Section IV exhibits simulated results for the test system and accompanying discussions. Finally, conclusions are given in section V.

3.2 Review of Generalized Features of Microgrids

Generally, microgrid network is composed of an assembly of small modular DERs – fuel cells (FC), photovoltaic cells (PV), small wind generators (WG), internal combustion engines (ICE), gas turbines (GT), microturbines (MT), energy storage devices (ESD) and one or more load(s) with a low voltage distribution system connecting it to a point of common coupling (PCC), with dual operational capability – main grid interconnected or autonomous operation modes. In most cases, microgrid involves combined heat and power technologies producing electricity and steam from a single fuel facility located near the consumer [12, 22, 23].

3.2.1 Basic Constituents of Microgrid System

A schematic illustration of a fairly generalized representation of microgrid network with its accompanying control devices is illustrated in Fig. (1). Here, all the major energy sources are represented; there are loads and then the LV grid inter-linking them to the

medium voltage (MV) network of the utility grid. However, in actual installations, only one or two energy source types will be connected based on special needs and availability of requisite climatic conditions, technology, and cost.

Most emerging DER technologies, such as PV, FC, and gas ICE require DC/AC voltage source inverter (VSI) to interface them with the LV distribution network (Fig. 1). The VSI is needed since the characteristics of the electric power produced from these sources are not suitable for direct connection to the LV grid. In microgrids, there is an absence of fully controllable synchronous generators responsible for frequency, generation, and load balancing; hence each VSI is equipped with special control capabilities to take care of this role [22, 24].

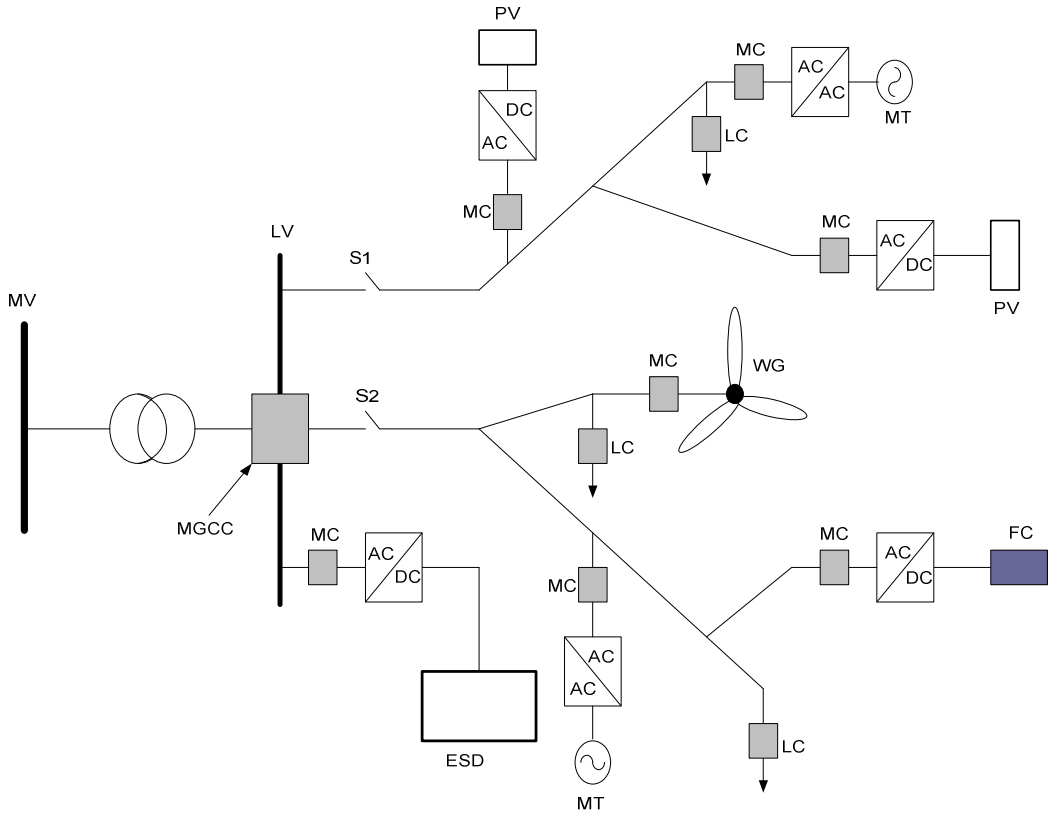

Fig.3.1: Microgrid architecture with control devices [22].

3.2.2 Operational Principles of Existing Microgrid Systems

From the features presented for the microgrid (Fig. 3.1), a critical factor is the presence of DERs with fast-acting power electronic interfaces provided by the voltage source inverter (VSI). This is used to regulate voltage and frequency, and to ensure proper load sharing among the various sources when operating in island mode. This happens when the disturbances in the main grid are much more than the microgrid (MG) compensatory capacity, or if the MG does not have enough resources to inject reactive power to the main grid and at same time supplies its load demand. When this happens, the microgrid central controller (MGCC) decouples the MG from the main grid at the PCC, and the MG now operates autonomously.

In an interconnected mode, the load controllers (LCs), microgrid controllers (MCs), and MGCC regulate the power exchange with the grid, monitor grid conditions, and ensure microgrid's proper separation from the utility grid when the need arises. The MG is connected to the main MV network for the supply of its power requirement, or to inject power into the grid where it has such capability. Injection of power into the grid happens during peak load, reduced grid power supply, and black start operation periods. During these periods, the static switches S1 and S2 are utilized to shed nonessential loads in the MG LV network while the ESD are actuated to supply additional back-up power.

3.3 Justification of Microgrid Utilization in Power System Networks

The major factors influencing the increasing emergence of microgrids could succinctly be stated as

3.3.1. Microgrid's Autonomous Operation Capability

By having the capability for separate existence, microgrids can now be employed in military on-shore and off-shore facilities due to its self-healing and survivability capacities.

3.3.2. Stressed Operating Conditions of Power System

Since unbundling and commercialization of utilities, the power system is now operating in stressed conditions due to increasing load demand not matched by generation and transmission growth and the fact that Independent Power Producers (IPPs) are mostly interested in generating active power and pushing them into the network with commensurate investment in reactive power. Due to the coupled nature of active and reactive power in transmission network, an increase in active power requires same increase in reactive power before it could be delivered, hence microgrids have now emerged to fill this gap to ensure quality power delivery.

3.3.3. Ageing of Power System Facilities

Most of the generation, transmission, and distribution facilities were built many years ago, and therefore are not adequate to carry the profit-induced increased bulk power transfer over long transmission distances. Hence, microgrid has to come in to provide backup supply in the event of power blackouts.

3.3.4. Strict Power Quality Requirements in Manufacturing Establishments

In these environments, very small power dips and spikes could cause disruption of production and loss of resources. Therefore, such establishments have resorted to ‘in house’ power generation to meet critical load requirements.

3.3.5. Emerging Technologies in Power Electronics Have Made the Conversion of Various Forms of Energy Fast and Cheap Converters

Many of the DERs that produced DC energy sources are now relevant in the generation of electricity by utilizing VSI.

3.3.6. Saving in Energy through Combined Heat and Power (CHP)

In the CERTS model of MG, CHP has been used as a big energy saving process that reduces cost of energy consumed by the establishments [11].

3.3.7. Environmental Concerns and Governmental Regulations

Microgrids do not contribute to significant environmental degradation when compared with other sources of electrical power. Therefore, in many industrialized cities with large population, governmental grants offer incentives to the populace to encourage utilization of microgrid in private and commercial buildings. This has led to an increase in MG investments.

Despite these overwhelming favorable considerations, general acceptability of MG by key power system operators is hampered by

(i) Difficulties in operational mode transition.

(ii) Non-predictable and irregular supply of power by DERs.

(iii) Difficulties in grid status and vulnerability monitoring.

(iv) Improperly developed MG protection system.

(v) No generalized standard for microgrid operation.

(vi) Perceived negative effects of DERs in distribution system such as voltage violation by IPPs selling power to the grids.

To address some of these shortcomings, the authors have introduced the index computation scheme into the microgrid operation and in the control system.

3.4 Algorithm for Index Utilization in Microgrid Connected Power System Networks

Voltage stability indices define a scalar magnitude which can be monitored as the system parameters changes. In particular, the L-index is a linear indicator of the voltage

stability state of interconnected power system network, with emphasis on showing the critical load buses of the system. L-index value is affected by change in transmission line parameters, loading levels, and proportional supply from the generator buses. The purpose of applying the voltage stability index computation scheme to the microgrid system is to provide a mechanism for an improved grid interconnection and disconnection operation without loss of normal operation of either the islanded microgrid or the utility grid. To do this, an algorithm was developed to detect the period of system instability initiation and growth so as to automatically switch the microgrid from one mode to another via a programmable intelligent electronic device (IED). From the simulation result obtained by the authors in [16] which corresponds to the results depict in [25] and [26], the stable load buses had L-index values between 0.9 and 0.95.

During the present work, it became reasonable to provide a range for the normal (i.e. utility supplied) mode and a pre-microgrid mode (microgrid start-up mode) within the stable limits. Then, the microgrid supplied and the island modes are provided for in the ranges which require restorative action.

The four proposed modes of operation are

(i) Utility supplied mode: $0 < L_i < 0.90$

(ii) Pre-microgrid mode: $0.90 \leq L_i < 0.95$

(iii) Microgrid supplied mode: $0.95 \leq L_i < 0.99$

(iv) Island mode: $0.99 \leq L_i < 1.0$

where i represent the load bus number at which the MG is connected to the utility grid, and there can be more than one system of microgrid connected to a given network. The flowchart for the implementation of the algorithm is shown in Fig. 2.

During grid-supplied mode, the microgrid system is seen at the point of common coupling by the utility MV grid as a single load and treated as such by the MGCC. At the pre-microgrid connected mode, it is still considered as a single load but the IED contained in the MGCC will send signals to the MC controlling the slow starting DERs to automatically start them up just like reserved players are warmed up during soccer matches by their team coach. If the situation worsens leading to the microgrid supplied mode, the rest of the DERs are started and the MG now injects reactive power to help salvage the situation. If this attempt does not solve the problem and the stability index continue rising up to island mode, then the MGCC will using the static switches disconnect the MG from the rest of the utility grid to save it from the eminent failure of the main grid. The range of values for each mode as stated above can be determined and fixed by each Regional Transmission Organization (RTO) and/or Independent System Operator (ISO) based on its required security margin.

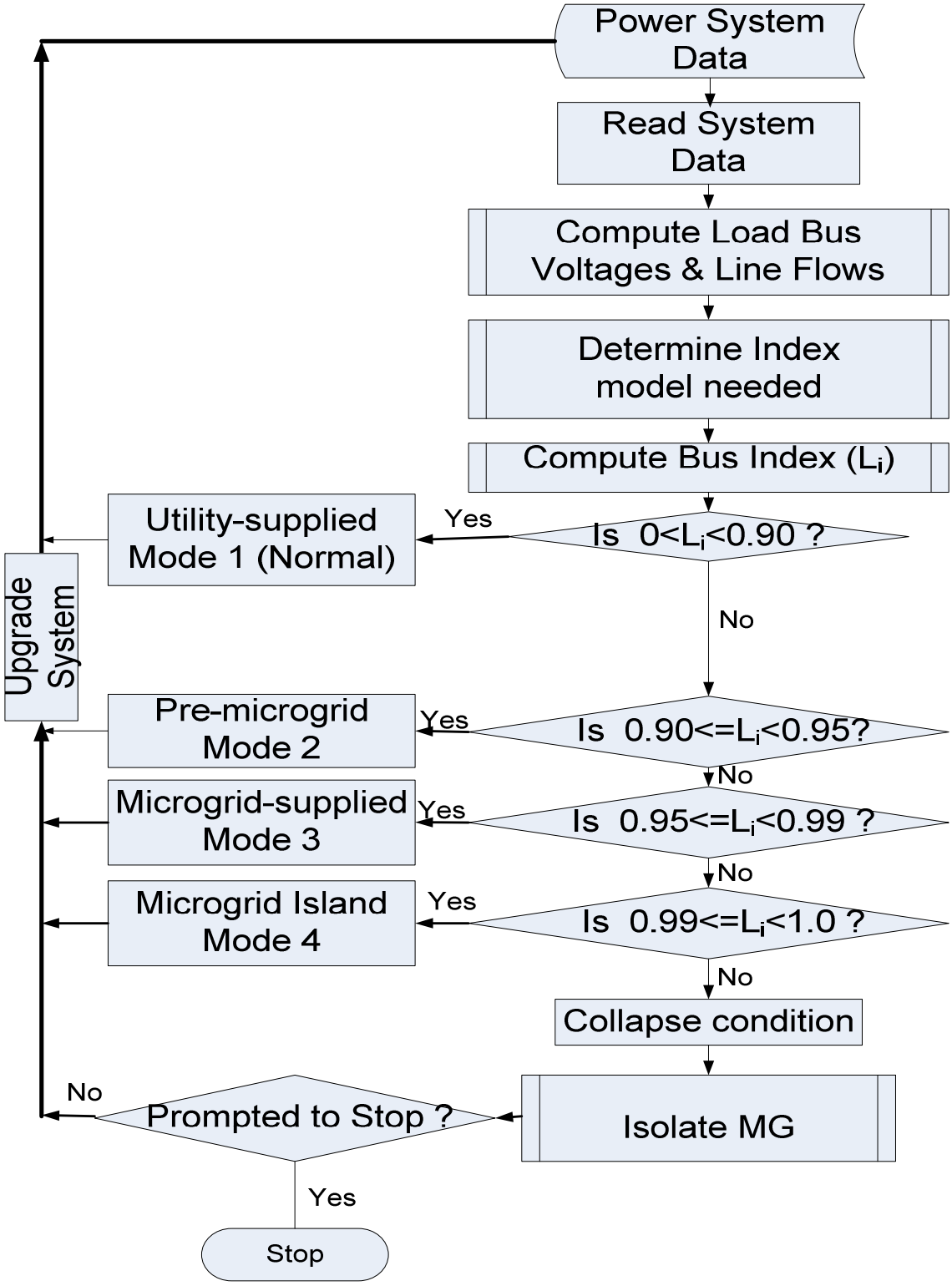

Fig. 3.2: Microgrid system L-index application flowchart

3.5 Simulation Results and Discussions

The IEEE 14 bus test system interconnection is depicted in Fig. 3. Buses one and two are the main generator buses, while buses three, six, and eight have voltage sources. Bus seven is a transformer bus with no load or voltage source connected to it and the remaining buses are load buses. The L-index developed in [26] is used here considering that the transmission lines linking the various buses of the IEEE 14 bus test system are within the short line length of less than 50 miles [27].

If in any system there is a transmission line connecting two buses with length longer than 50 miles, the Ls-index developed in [16] should apply. Using Ls-index will enable the effect of long transmission line to be included in the computation. Longer lines suffer from higher losses and the series reactance effects are more noticeable while the shunt capacitive reactance voltage contributions are minimal. Therefore, longer lines need more compensation than shorter network branches. Both L-index and Ls-index models have linear scale with values ranging from zero for voltages source buses and one at the collapse point. The reactive sources and generator buses are considered stable; therefore, their voltage stability indices are zero as reflected in the simulation results. Three different scenarios were considered.

CASE 1**:** IEEE 14 bus test system with increased reactive power demand, and the result is as shown in Fig. (4). Here, L1 represents the base loading condition, while L2, L3, and L4 represent increasing reactive power demand of 10, 20, and 30 percent p.u. of the base load, respectively. With operation mode ranges specified in section III, buses four and five appear in normal operation mode in all the four loading conditions, seven,

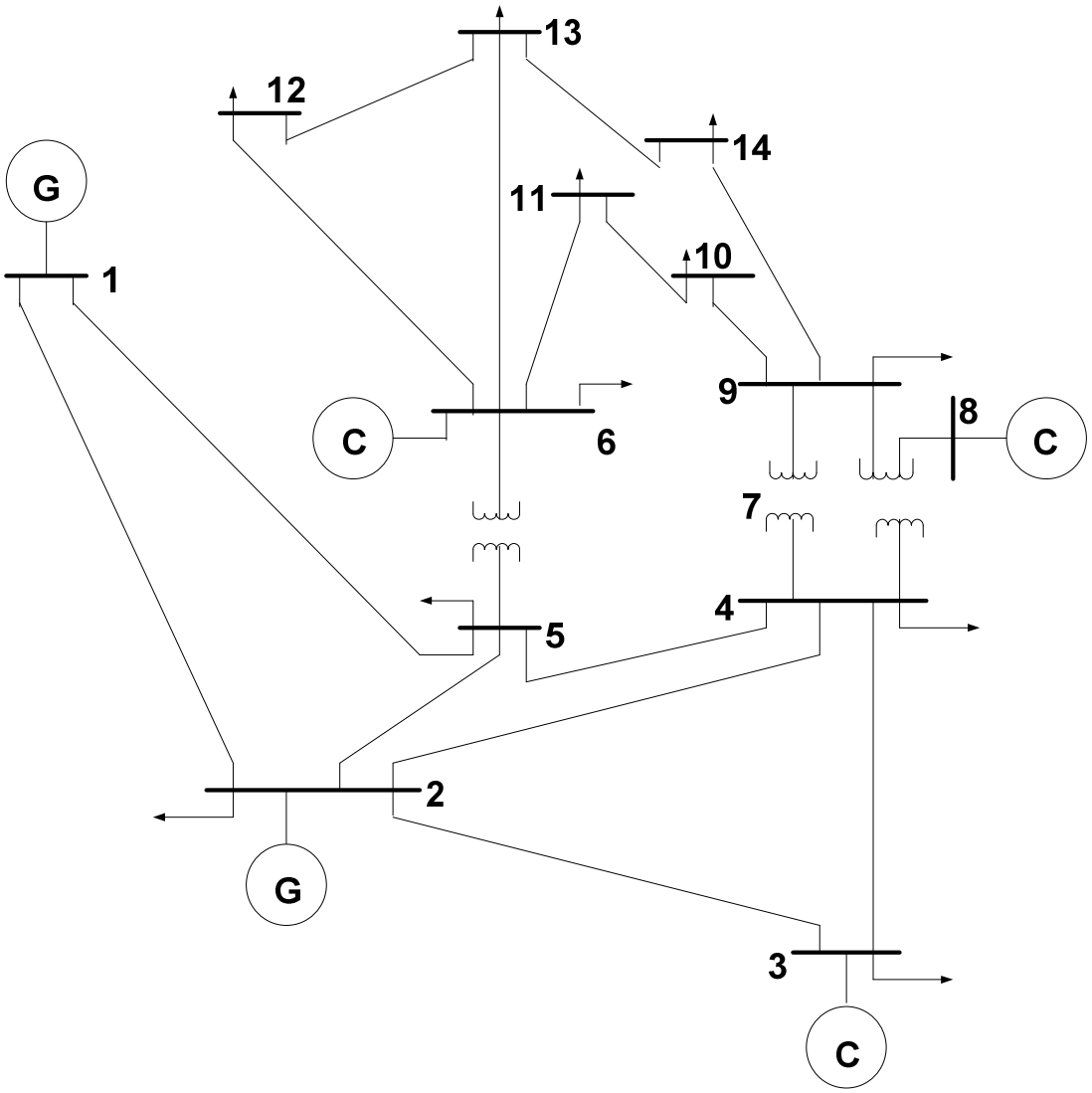

Fig. 3.3: IEEE 14 bus test system

and ten appear in the pre-microgrid mode while bus ten entered the microgrid supplied mode at L4. The remaining load buses are in the microgrid supplied mode for the first two loading conditions. Twelve and fourteen entered the islanded mode from the 20 percent increased loading while bus twelve reached the collapsed point at the 30 percent increased loading.

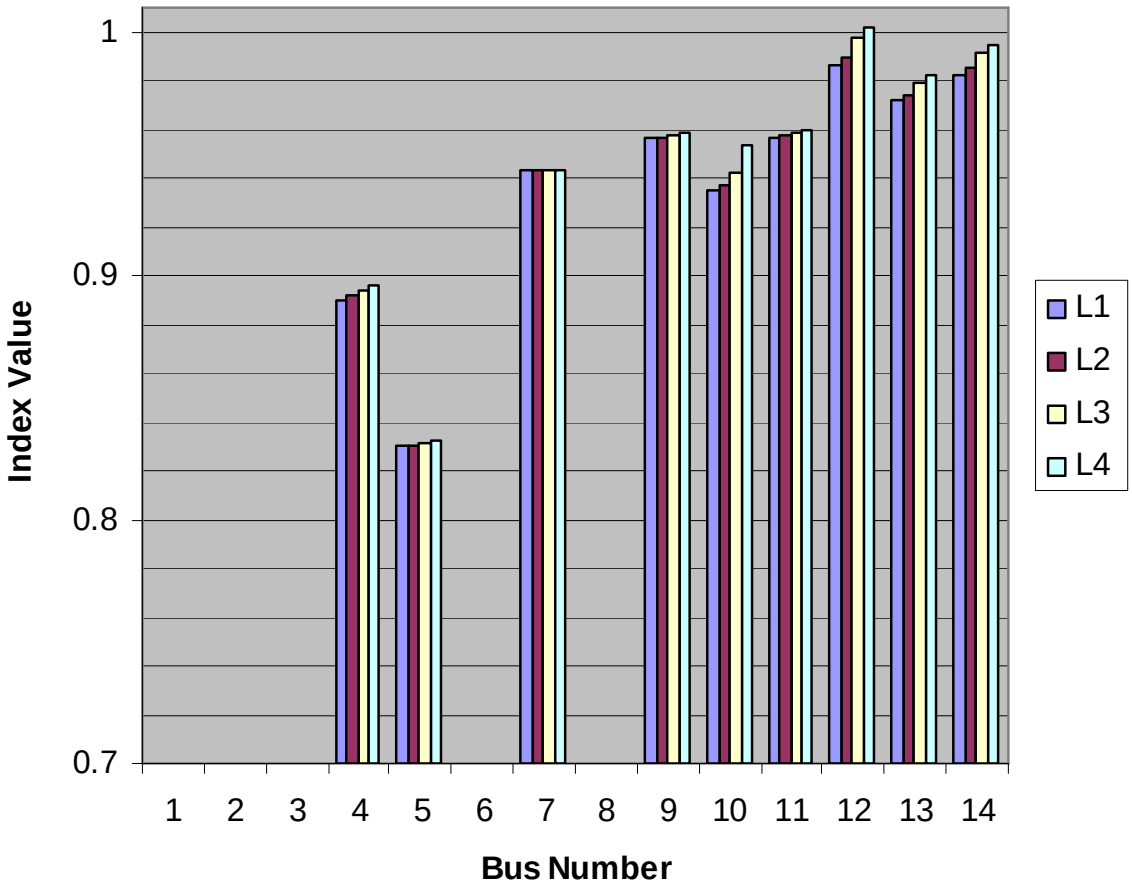

Fig. 3.4: IEEE 14 bus system L-index result for normal utility supplied mode with increasing reactive power demand

This implied that bus twelve is the weakest followed by fourteen. However, bus five proved to be the most stable load bus followed by four. This result agreed with previous work on the stability rating of the IEEE 14 bus system [16, 25].

From the ranges provided for the four proposed modes for microgrid interconnection to utility grid, buses four, five, seven, and ten are stable at the normal IEEE 14 bus test loading level. If buses nine, eleven, and thirteen have microgrid facilities, these should be connected to support the grid. The condition at buses twelve

and fourteen are critical such that the microgrid system available at these buses should isolate and operate its local network as island while the main grid is being improved upon. Similar inferences could be made for other loading conditions.

The range for each microgrid operation should be decided upon by each facility owner based on its required reliability level and operational constraints. The ranges used here are purely to explain the concept and not a standard to be adopted generally.

CASE 2: This is the IEEE 14 bus system with MG compensation at bus twelve, and the same loading conditions as in case 1. L5, L6, L7, and L8 correspond to the same conditions as L1, L2 L3, and L4, respectively, but with bus twelve connected to a microgrid network to inject reactive power into the main grid. From the result shown in Fig. 5, the injection of 0.02 MVAR into the system by the microgrid connected at bus twelve stabilized the entire grid, with improved stability index values at all the buses and greater impact on the adjoining buses to twelve. The stressed load buses were relieved.

Also, there was appreciable recovery of bus twelve where the microgrid is connected which moved from the isolated mode to microgrid supplied mode and stayed in this range for all the four loading conditions. The operational mode of bus fourteen also moved from the islanded mode in case one to microgrid supplied mode for all the four loading conditions when microgrid compensation is utilized. Hence, there was no need for island formation with just a single microgrid connected to entire system via bus twelve. Such application will be much valuable during periods of peak demand and loss of any major generation unit. If a large scale load is to be added to the grid, the microgrid can be used to provide additional support to the Utility till adequate generation capacity to accommodate the new load is available.

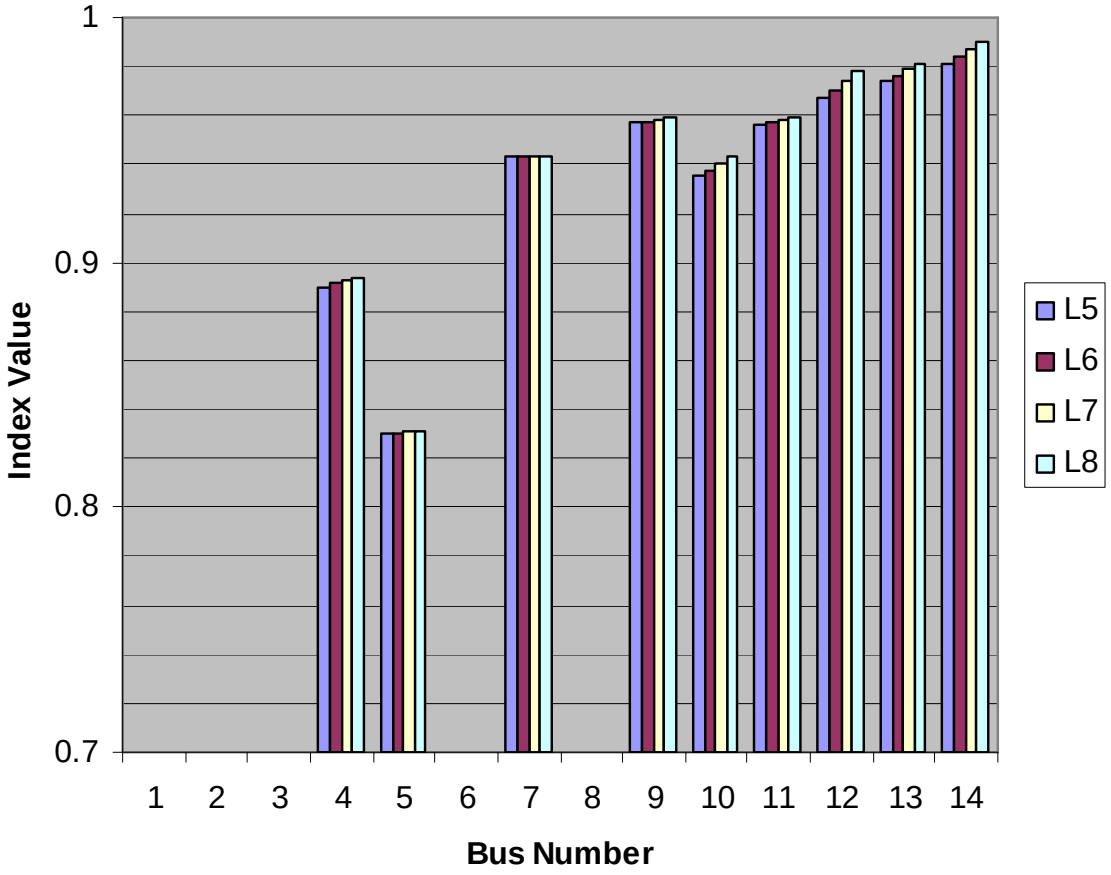

Fig. 3.5: IEEE 14 bus system L- index result for microgrid supplied mode

CASE 3**:** This is the IEEE 14 bus test system with MG connected at bus twelve in the island mode**,** and similar loading conditions as in previous cases. In this case the microgrid connected at bus twelve is used to isolate its local network. With this condition, the burden of supplying the aggregate load of the microgrid network which is seen previously as a single unit load by the main utility is now removed from the rest of the main grid.

The situation at bus twelve is closely related to that of bus seven in that neither its load nor its reactive power unit is available to the main grid, though bus seven is a transformer bus. L9, L10, L11, and L12 correspond to the increased reactive power demand as in cases one and two. The results obtained in the simulation of the IEEE 14 bus system in this condition (Fig. 6), show that with isolation of the critical load bus, there is improvement in the remaining system.

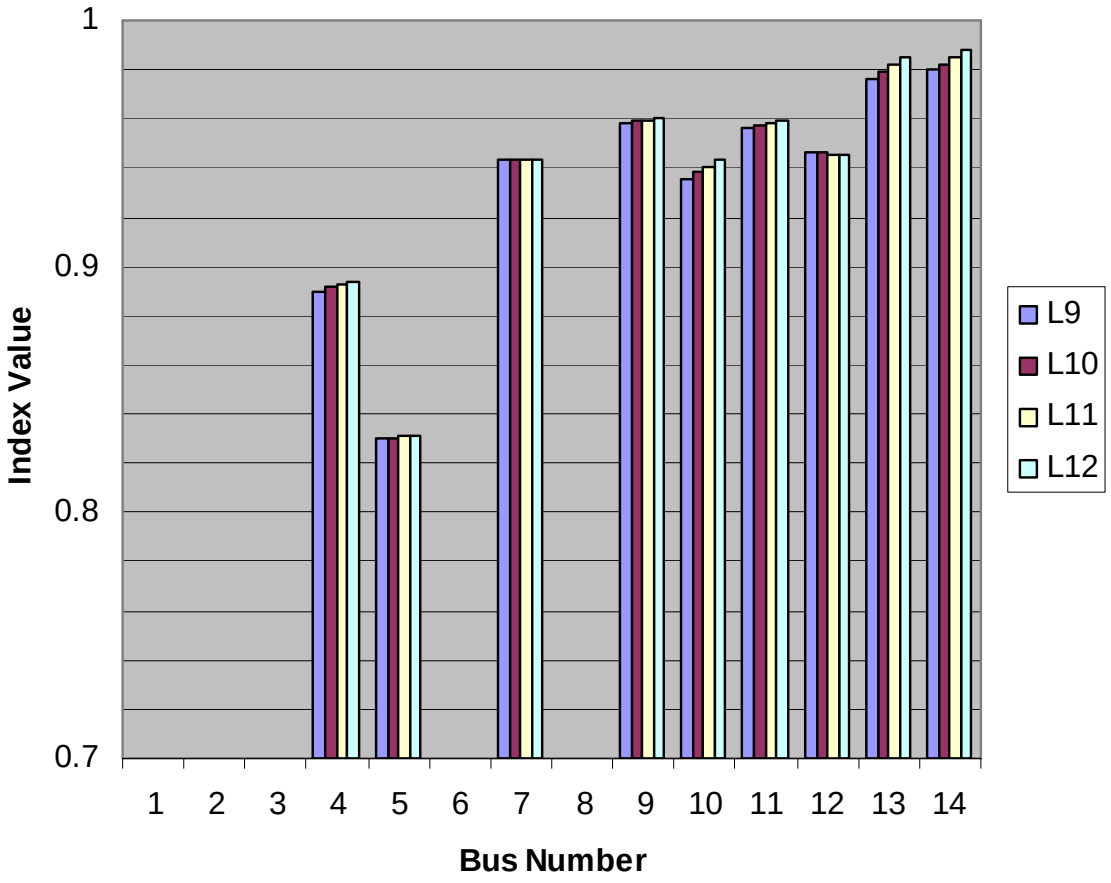

Fig. 3.6: IEEE 14 bus system L-index simulation for Island mode

This agrees with the general concept of load shedding during stressed conditions. Even load bus fourteen that was critical with a near collapse index value of 0.994374 in case one before isolation of bus twelve as a mini-grid, now recovered to a fairly stable value of 0.987810. Complete comparison of the results obtained bus by bus for cases one and three show a redistribution of the entire stability indices of all the buses. Buses four, five, ten, and eleven had improvement in their stability values while buses seven and nine had slight increase in their index values. Overall, the entire system became more stable as none of the buses reached the island mode lower limit of 0.99.

However, there is need to access the ability of the microgrid to adequately supply its local load demand periodically. Inability to do this may lead to further loss of synchronous operation of the various DERs supplying the MG LV network, and disruption of services to the supposedly sensitive loads due to the occurrence of frequency instability. This happens when there is mismatch between local power demand and that provided by the DERs. It may be necessary to isolate some non-sensitive loads using the localized micro-source controllers (MCs) till the slow starting sources build up.

3.6 Conclusions

An algorithm for the incorporation of voltage stability index in the emerging microgrid technology with improved operational modes has been presented. The results obtained by using the developed algorithm in the IEEE 14 bus system for three cases of increased loading, microgrid reactive power compensation, and full islanded conditions showed the effectiveness of utilizing such a model to monitor the status of microgrid

connected to a utility network. The work also showed the effectiveness of microgrid in mitigating local voltage collapse scenario which can spread to the larger network.

The proposed scheme may reduce problems faced by distribution network operators in regulating interconnection of microgrids to power system networks due to their effects on system voltages and appropriate determination of operation modes. It may also aid in appropriate network reactive power compensation and load shedding by microgrids during emergency and peak load demand periods**.**

Further research work will be required to determine practical operational ranges for each of the modes. It is the view of the researchers that modeling the various distributed energy resources and loads of the microgrid system and incorporating such into this model will be an interesting area for further studies as it will improve the effectiveness of the model.

3.7 References

[1] U.S.-Canada Task Force on 14 August 2003 Blackout, "The August 14 blackout compared with previous major North America outages," Final Report on the August 14th 2003 Blackouts in the United States and Canada, pp. 103-106, April 2004.

[2] "Storms knock out power to over 600,000 customers in U.S. Northeastern Coast," U.S. DOE Energy Assurance Daily, Wednesday, July 19, 2006.

[3] "Biggest blackout in U.S. history," CBS News, pp. 1-3, August 15, 2003.

[4] M. Amin, (2005, March). Powering the 21st century, we can – and must – modernize the grid, IEEE-U.S.A. Today's Engineer online at http://www.todaysengineer.org/2006/Apr/backscatter.asp, March 2005.

[5] R. Siegel, "Massive power outages cripples Los Angeles," NPR October 14, 2006. National Energy Supergrid Workshop 2 Final Report, University of Illinois at Urban-Champaign (UIUC), pp. 5, October 25-27, 2004.

[6] "Principles for a restructured electricity industry," IEEE-U.S.A. position, approved by the IEEE-U.S.A. Board of Directors, June 17, 2004.

[7] M. Amin, "North America's Electricity Infrastructure: Are we ready for more storms?" IEEE Security & Privacy, published by the IEEE Computer Society pp. 19-25, September 2003.

[8] S. Brown, "Motown microgrid – life-cycle analysis rates energy and environmental performance," Cogeneration and On-site Power Production, pp. 75, November-December 2004.

[9] Y. Shimazaki, "Model analysis of microgrid cogeneration system zero emission industrial park," UPE7 – The 7th International Conference on Urban Planning and Environment, Bangkok, Thailand, 3-5 January, 2007.

[10] R. Lasseter, A. Akhil, C. Marnay, J. Stevens, J. Dagle, R. Guttromson, A. S. Meliopoulous, R. Yinger and J. Eto, (2002, April). The MicroGrid Concept, CERTS White Paper on Integration of Distributed Energy Resources, Available [Online] at http://eetd.lbl.gov/CERTS/pdf/50829-app.pdf.

[11] J. Lynch (2004, May). Microgrid power networks, Cogeneration and On-site Power Production.

[12] N. Panagis, A. E. Kiprakis, W. A. Robin, and G.P. Harrison, "Centralized and distributed voltage control: Impact on distributed generation penetration," IEEE Trans. on Power Systems, vol. 22, no. 1, February 2007.

[13] J. A. Silva, H.B. Funmilayo and K. L. Butler-Purry, "Impact of distributed generation on the IEEE 34 node radial test feeder with overcurrent protection," Proceedings of the 2007 39th North American Power Symposium, 30 September – 2 October 2007, New Mexico State University, Las Cruces, new Mexico. pp. 49.

[14] L.M. Cipcigan, P. C. Taylor and P. Trichakis, "The impact of small scale wind generation on low voltage distribution systems voltage," May 21-23, 2007 International Conference on Clean Electrical Power, Italy, pp. 9

[15] D. O. Dike, S. M. Mahajan and G. Radman, "Development of versatile voltage stability index algorithm, IEEE Electrical Power Conference 2007, Montreal QC, Canada, 25-26 October 2007.

[16] Z. Ye, R. Walling, N. Miller, P. Du and K. Nelson, "Facility microgrids, Executive Summary," NREL Innovation for our Energy future, Subcontract Report NREL/SR-560-38019, pp. iii, May 2005.

[17] D. E. Feero, D. C. Dawson and J. Stevens, (2002, May). Protection issues of the microgrid concept, CERTS, Transmission Reliability Program, Office of Power technologies, Assistant Secretary for Energy Efficiency and Renewable Energy, U.S. DOE, pp. 4-9.

[18] R. Firestone and C. Marnay, (2005, May). Energy manager design for microgrids, Consultant Report by CERTS for the California Energy Commission, pp. 1, CE500-2005-05.

[19] J. A. Pecas Lopes, C. L. Moreira and F.O. Resende, "Microgrids black start and islanded operation," 15th PSCC, Liege, 22-26 August 2005, session 27, paper 4.

[20] C. Billy, G. Heydt, P. Langness, A. Laughter, B. Mann, M. Rice and L. Winslow, "Sustainable electric power options with attention to native American communities," Proc. of the 39th North American Power Symposium, New Mexico State University, 30 September – 2 October 2007, pp 177,

[21] C. L. Moreira and J. A. Pecas Lopes, "Microgrids dynamic security assessment," International Conference on clean Electrical Power, Capri Italy, , May 21st-23rd, 2007, pp. 26.

[22] J. A. Pecas Lopes, C. L. Moreira and A. G. Madureira, "Defining control strategies for microgrids islanded operation," IEEE Trans. on Power Systems, vol. 21, no. 2, pp. 916-924, May 2006.

[23] R.H. Lasseter, "Microgrids and distributed generation," Journal of Energy Engineering, American Society of Civil Engineers, Sept. 2007.

[24] C. Reis and F. P. Maciel Barbosa, “A comparison of voltage stability indices,” IEEE Melecon Benalmadena Spain, May 16-19, 2006.

[25] P. Kessel and H. Glavitsch, “Estimating the voltage stability of a power system,” IEEE Trans. on Power Del., vol. 1. PWRD-1, no. 3, July 1986.

[26] A. R. Bergen and V. Vittal, *Power system analysis*, second edition. New Jersey: Prentice-Hall, Inc. 2000, pp 101-110.

CHAPTER 4

PAPER 3: L-INDEX MODULATED VOLTAGE SOURCE CONVERTER[†]

D. O. Dike and S. M. Mahajan

Department of Electrical and Computer Engineering

Tennessee Technological University, Cookeville, TN 38505, USA

ABSTRACT— A strategy is presented for self-tuning of voltage source converter (VSC) based Flexible AC Transmission Systems (FACTS) according to the prevailing system condition. L-index, which is a power system voltage stability status indicator, and its associated parameters are used to automatically regulate the modulation signal of the VSC. This will lead to a proportionate adjusting of the magnitude of the current injected into, or absorbed from, the interconnected load bus by the FACTS device. This regulating scheme will enhance seamless and optimal reactive power compensation by utilizing the dynamic operational nature of present day distressed power system networks. Results obtained using this method when applied to selected load buses of the IEEE 14 bus system under varying practical scenarios showed its capability to appropriately control FACTS devices operation to accommodate system changing conditions. The outcome of this work will provide efficient tools for the determination of power system status ensure optimal utilization of reactive power compensation devices and reduce system outages.

[†] Submitted for publication in the International Journal of Emerging Electric Power Systems,

4.1 Introduction

The advent of power system unbundling and privatization in the nineties created competition in wholesale (generation) and retail (distribution) levels in the power industry [1]. This opened up channels for mass participation in the generation and distribution of electrical power leading to significant increases, while there was no commensurate growth in transmission grid, as government maintained monopoly in this sector for security reasons. Furthermore, the restriction imposed on the building of new transmission systems by environmental and socio-economic constraints worsened the dwindling performance of present day power system.

In view of this situation, a faster, more robust, and advanced technology of VSC-based FACTS devices composed of Insulated Gate Bipolar Transistors (IGBT) or Insulated Gate Commutated Thyristors (IGCT) were developed and applied to provide free controllable voltage magnitude and phase [2, 3]. This replaced the earlier thyristor valve devices and their forerunners conventional forms such as switched shunt compensators, switched series compensators, and phase shifting transformers which were applied semi-crudely at load bus locations with presumably voltage deficiencies or reactive power imbalances. With the need to reduce increasing losses arising from higher switching frequencies of the VSC-based FACTS devices, increased equipment rating and reduced cost, multilevel design topologies and special modulation control methods have been implemented for these devices [4-6].

Though these designs have worked very well in low and medium power requirements, such as in industrial motor applications [7], their utilization in high level

power system transmission may have resulted in increased large scale power outages as reported in [10-14], since VSC-based FACTS device application has been the major technological introduction into the power grid within the last two decades. This position is supported by the fact that VSC semiconductors have led to increased harmonic contamination present in line currents which end up distorting voltage waveforms, poor power factor under light load conditions, and produce a series of problems in equipments related to active power filter usage when operated at high frequencies, such as circulating currents, dielectric stress, overvoltage, and corona discharges [5, 15]. Therefore, one may infer that the evolution of various dynamic reactive power compensation mechanisms in form of FACTS (Flexible AC Transmission System) to support the distressed grid without a robust tool to measure their impact on the status of interconnected power system exacerbated the situation.

This development has opened up interest in efficient reactive power utilization in the grid and raised such questions as: how reactive power could be generated sufficiently for a given grid condition? Who will degenerate it? What quantity is required? At which buses and transmission lines is it required? What will be the impact on the rest of the grid if injected at a particular bus or transmission line? And what is the best method to pay for it? In an attempt to answer some of these questions and contribute to the mitigation of increased power outages associated with current deregulated power system, this research work has focused attention on the development of a voltage stability index regulated VSC. This scheme will enable system operators to continually monitor the conditions of all load buses and transmission lines. It will also provide automated regulation of the degree and the direction of compensation. This can be achieved by introducing the power

flow program computed L-index and bus voltage values as input and control parameters for the dynamic simulation and modeling of the VSC.

The paper is arranged in the following manner. In section II, a review of topologies, applications, and modulations schemes of multilevel VSCs utilized in medium and high voltage applications are covered. Section III provides the structure and modeling of diode-clamped neutral point center-node voltage source inverter with the voltage stability index introduced as the modulation index. The implementation algorithm is developed in section IV. Section V exhibits simulated results for the test system and accompanying discussions. Finally, conclusions are given in section VI.

4.2 Review of Multilevel VSCs Used in Medium and High Voltage Applications

In view of the limitations imposed by the maximum ratings of gate turn-off (GTO) thyristors, IGCTs, IGBTs, and other emerging power semiconductors when contrasted to the need to transfer power at high voltages over long transmission lines, multilevel VSCs are becoming increasingly popular. This is due to the fact that multilevel VSC's has the following unique attributes: (i) reduced dv/dt per each device, (ii) provides almost perfect output waveforms due to removal of undesirable harmonics, (iii) utilizes low switching frequencies and speed semiconductors, (iv) low switching losses, (v) high power density, (vi) excellent performance and high reliability, (vii) ease of modularity into cascaded structures, and (viii) consequent reduction in component size, fabrication complexity and cost [4-9] .

4.2.1. Topologies and Applications of VSC

Some of the most viable multilevel VSCs and their possible areas of application are depicted in Fig. (4.1), as discussed variously in [2-9, 16-30]. The detailed descriptions of each of these topologies have been carried out in [2]-[9]. In typical power system applications, the numbers of levels for the diode-clamped and cascaded multilevel converters have same separate dc sources for each level needed to enable active power conversion.

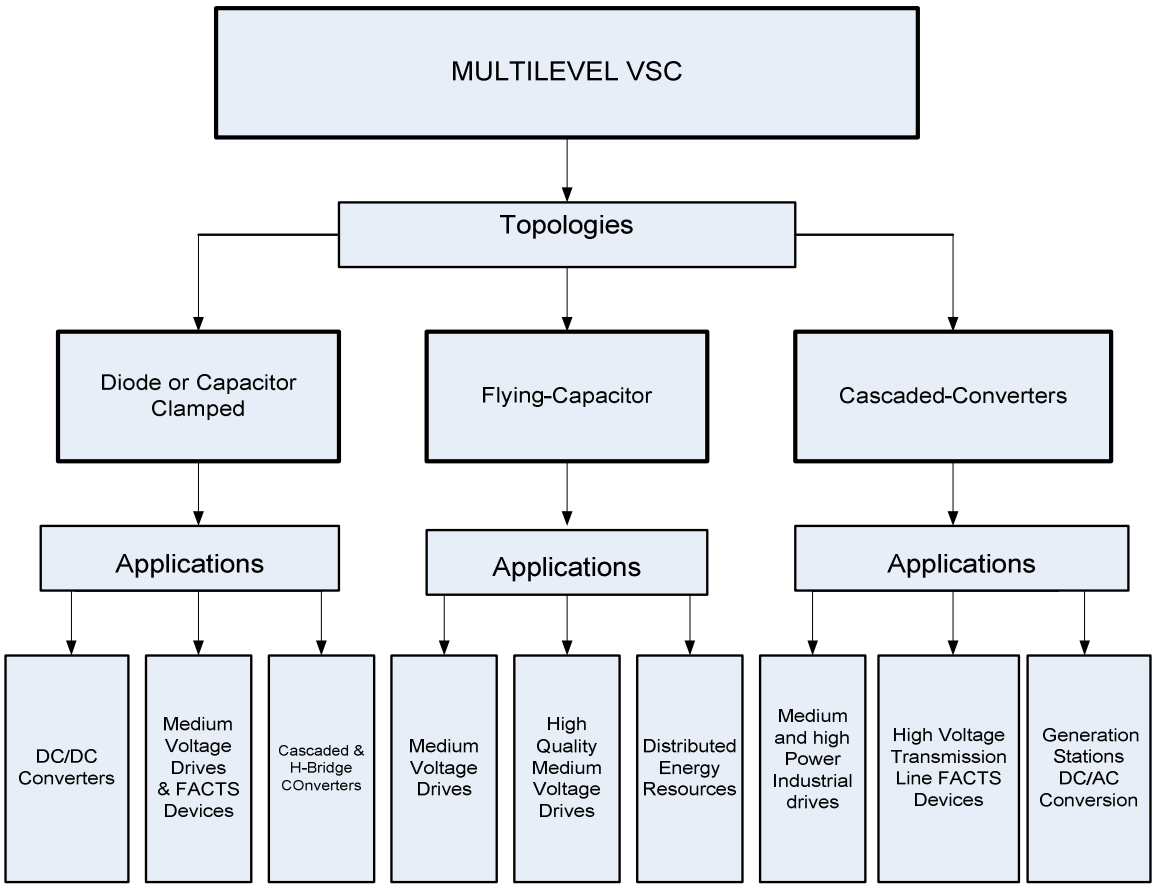

Fig. 4.1: Multilevel VSC topologies and applications

One other distinctive characteristic of diode-clamped and cascaded converters is that both have a perfect niche in harmonic and reactive power compensation. The capacitor-clamped converter, unlike diode-clamped and cascaded forms, cannot be used for reactive power compensation as this does not have balanced voltage for power conversion involving only reactive power [4]. However, since the three-level neutral-point-clamped (NPC) converter was the first practical and most popular form of the multilevel VSCs [5, 8] till, and is still the main building block for cascaded multilevel converters which are currently being used in VSC-based FACTS devices, we have utilized it in performing the modeling of index regulated VSC which will be presented in section III.

4..2.2 Multilevel VSC Modulation Scheme

In an effort to improve the performance of VSCs aimed at solving various challenging problems that emanated since the deregulation of power system in Europe, America, and some Asian countries, various modulation schemes have been developed and implemented. A schematic illustration of a fairly good classification of these modulation methods is presented in Fig. (4.2).

The low switching frequency schemes generally perform very few commutations of the semiconductor per cycle of output voltages. These are mainly utilized in space-vector control, which delivers to the load a voltage vector that minimizes the space error to the desired vector, and the selective harmonic elimination, which minimizes the harmonic distortion and achieve adjustable amplitude of the fundamental component by removing significant harmonic constituent from the voltage waveform. Low frequency

schemes are used to easily produce high level signals, thereby reducing equipment size and cost. Applications of these are in low and medium level industrial setups, where robustness and high signal quality are required. High switching frequency schemes arise from many semiconductor commutations per fundamental output voltage which are characteristics of pulse width modulation (PWM) controls. These methods which include the space vector PWM (SVPWM) and the sinusoidal PWM (SPWM) are applied in high-voltage, high-power applications due to their low current ripples, good use of the dc-link voltage, and ease of adaptability to digital microprocessors.

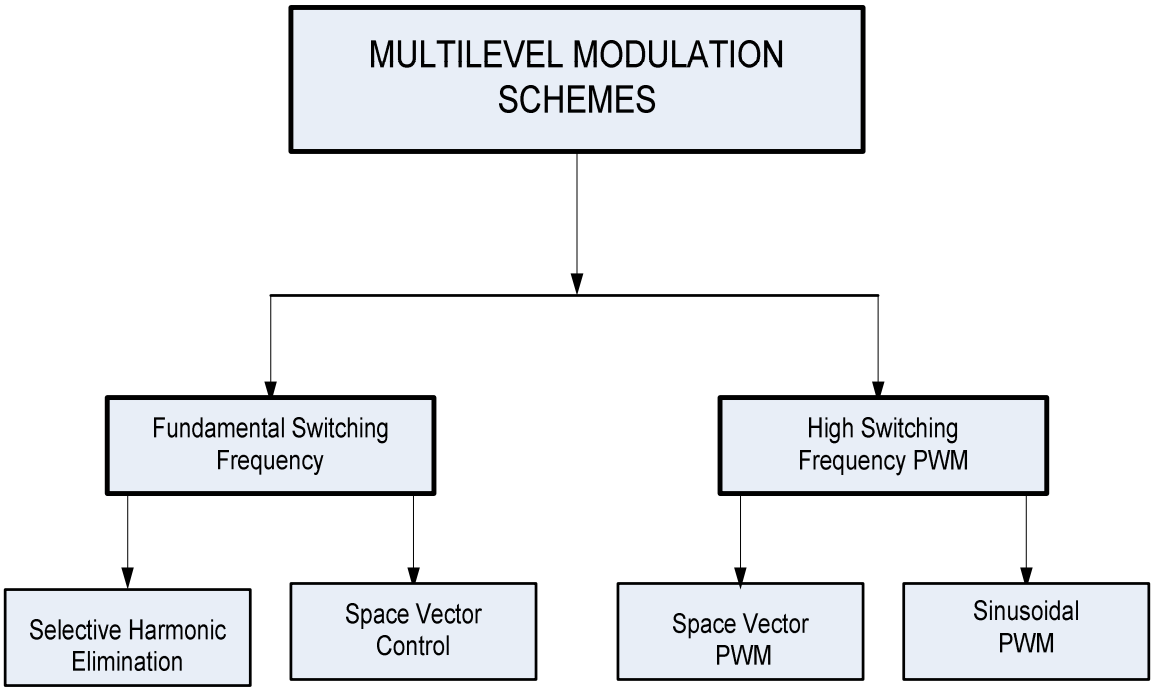

Fig. 4.2: Main classification of multilevel modulation schemes [4].

The generalized discontinuous PWM (GDPWM) which had been applied in [31] for the three-phase voltage source inverter and in [32] for multilevel high voltage rectifier is now applied in this work for the voltage source inverter.

4.3 **Structure and Modeling of NPC VSI**

4..3.1 Operation of Neutral Point Clamped VSI

The power circuit of three level neutral-point clamped (NPC) (also referred to as center-node diode-clamped inverter) for the modeling of L-index regulated VSC is depicted in Fig. 3. Its essential parts include: (i) a dc source for internal converter active power exchange and catering for losses; (ii) two equally sized dc capacitors C_1 and C_2 for reactive power stabilization; (iii) the switching devices, S_{ijk} which may be composed of any of the semiconductors mentioned earlier depending on design requirement; (iv) freewheeling diodes, d_{ijk}, for rectification via voltage reversal if external circuit conditions require such; (v) clamping diodes, d_{jk}, for voltage balancing and limiting dynamic and static over voltages from switching devices [9, 33]; (vi) resistances, r_j , and inductances, L_j , representing the net resistances and inductances of the VSI coupling devices to the network; and (vii) V_{jbus} represent the bus phase voltages where i=1 or 2, j=phase, and k=p for top and n for bottom devices.

In conventional voltage source inverters, the dc source is not included and therefore the active power required to compensate for losses is supplied by the interconnected transmission system.

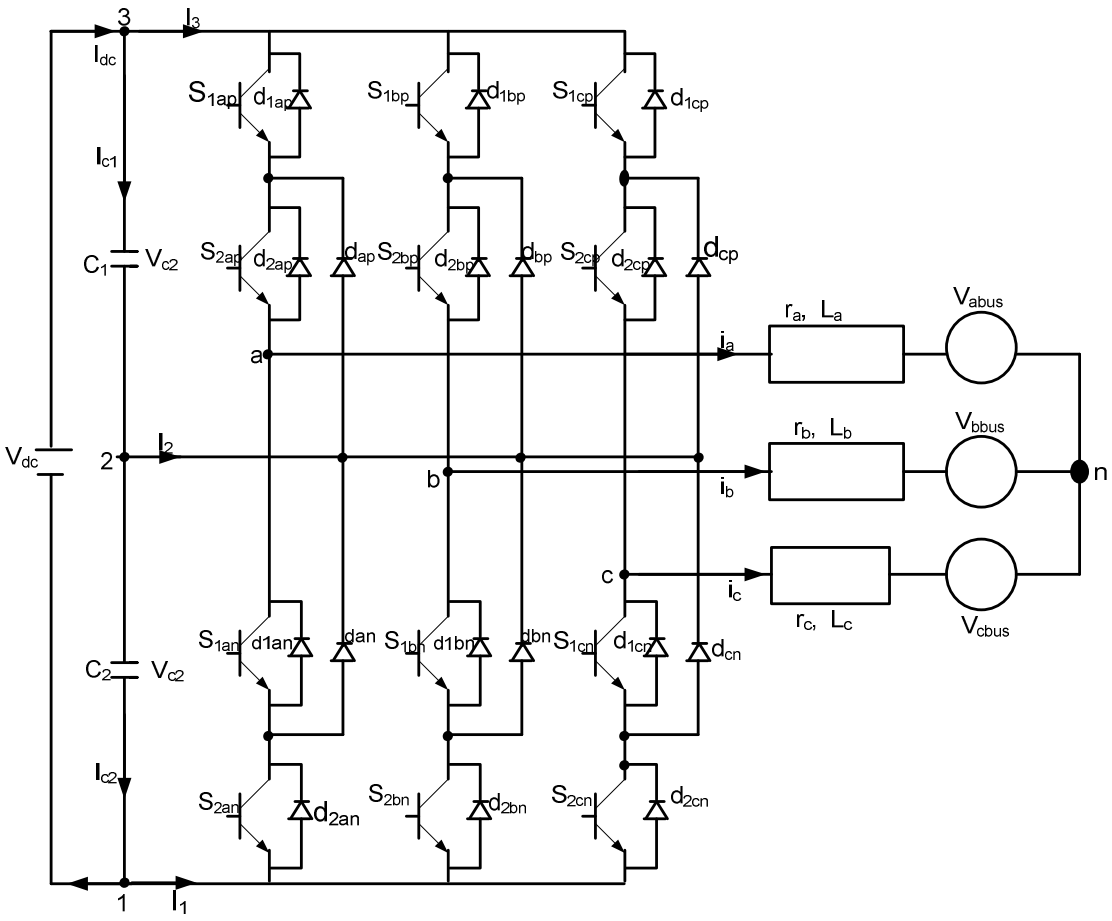

Fig. 4.3: Three-level neutral-point clamped VSI

Due to the constraints imposed by the current operation of power systems close to their transfer limit, to meet the increasing demand, the transmission network cannot afford to supply this extra active power, hence the inclusion of dc source.

The Multi-level NPC converters have the following advantages:

(i) Natural balancing mechanisms [34]

(ii) Simple power part

(iii) Low component count

(iv) Straight forward protection and modulation schemes

(v) Low total harmonic distortion

(vi) Off-line optimization of switching angles, and

(vii) Diminished *dv/dt* stress (capacitor stress) due to the modulation schemes adopted.

The major draw backs of VSI include [33, 34]:

(i) Low-frequency ripple at high modulation indexes occurs on neutral-point voltage.

(ii) Steady-state unbalance in the neutral-point voltage.

(iii) High switching losses and poor harmonic spectrum caused by hard-switching transients of the power semiconductor devices at high commutation voltages.

(iv) DC capacitor stress.

(v) Injection of harmonic signals into the system.

Fig. (4.3) presents a distinguishing feature which is aimed at addressing the problems of dc voltage balancing and capacitor stress - clamping diodes. The natural balancing capability of the three-level NPC inverter under vector modulation was ably presented in [33]. Here, the authors used the fundamental concept of NPC converter, where the sum of the dc capacitor voltages is equal to the constant dc source voltage. Further analysis involved including the net capacitor offshoot voltage (i.e. difference between the two dc capacitor voltages) to inverter output voltage equations.

These analyses are similar to the model equations presented in this work. The neutral voltage injection is used as a form of dc offshoot injection to balance the voltages. Additionally, zero sequence voltage and hysteresis control have been applied to ensure improved operation during unbalanced operations. Depending on system requirement,

various modulations and control schemes have been adopted to eliminate each of the other problems outlined [4-9, 30-34].

4.3.2 Modeling of L-index Modulated VSI

From [29], the modulation signals are given as

$$\begin{aligned} M_a &= m\cos(\ thrad\ \ (k)) \\ M_b &= m\cos(\ thrad\ \ (k) + \beta) \\ M_c &= m\cos(\ thrad\ \ (k) - \beta) \end{aligned} \tag{1}$$

Where $thrad(k) = i\pi/180$, $\beta =$ phase shift and i is an integer.

The modulation index 'm' which has always been fixed for a given VSC as a ratio of the dc voltage and assumed inverter reference voltage, is here replaced with an actual system status indicator, L-index value, obtained from actual load bus prevailing condition with a Fast-decoupled load flow program. L-index is computed for short and Ls-index for medium and long transmission lines [35-37] as

$$L = \sum_{l \in \alpha_L} \max \left| 1 - \frac{\sum_{k \in \alpha_G} F_{ji} V_k}{V_l} \right| \tag{2}$$

where $F_{ji} = -\left[Y_{jj}\right]^{-1} Y$

$$Ls = \max_{j \in \alpha_L} \{L_j\} = \max_{j \in \alpha_L} \left| 1 - \frac{\sum_{i \in \alpha_G} F_{ji}^1 V_k}{V_l} \right| \tag{3}$$

where $F_{ji}^1 = -\left[B_{jj}\right]^{-1} Y_{ji}$

The new phase modulation signals to be incorporated into the generalized averaged neutral voltage to obtain modified modulation signal are given by

$$\begin{aligned} M_{aa}^{*} &= L\cos(thrad(k))) + V_0 \\ M_{bb}^{*} &= L\cos(thrad(k) + \beta) + V_0 \\ M_{cc}^{*} &= L\cos(thrad(k) - \beta) + V_0 \end{aligned} \tag{4}$$

where $V_0 = 0.5V_{dc}(1-2\alpha)V_{\max} - \alpha V_{\min}$ (5)

The null state parameter 'α' is defined as $\alpha = \frac{1}{2}\{1 + Sgn[(\cos 3(\omega t + \delta))]\}$ (6)

δ = Modulation angle, and Sgn(X) =1, 0 and -1 for positive, zero, and negative sequence, respectively.

The modified modulation signals are obtained from power system load flow MATLAB ® program and stored in m-file as variables and then compared with two triangular signal, T_1 been the upper signal varying from 1 to 0, T_2 the lower varying from 0 to -1, to obtain the existence functions as

$$\begin{aligned} H_{i3} &= [S_{1ip}, S_{2ip}] \\ H_{i2} &= [S_{2ip}, S_{1in}] \\ H_{i1} &= [S_{1in,} S_{2in}] \end{aligned} \tag{7}$$

It can be seen from Equation (7) that the switching devices shown in Fig. 5 operate in pairs for each switching function and the logic governing their operation is same as that of the rectifier explained in [32]. For the analysis of the above converter, the dc voltage is shared according to the operation of the existence functions as follows:

When H_{i3} is operating, the voltage $V_3 = \frac{V_{dc}}{2}$, H_{i2} gives $V_2 = 0$ and H_{i1} gives $V_1 = -\frac{V_{dc}}{2}$ for balanced capacitor voltages. Unbalanced capacitor voltages give rise to offshoot

(i.e. $V_2 \neq 0$) which is accommodated in the program as this is fed back. The output voltage of this inverter is then given by

$$\begin{aligned} \nu_{an} &= H_{a3}V_3 + H_{a2}V_2 + H_{a1}V_1 \\ \nu_{bn} &= H_{b3}V_3 + H_{b2}V_2 + H_{b1}V_1 \\ \nu_{cn} &= H_{c3}V_3 + H_{c2}V_2 + H_{c1}V_1 \end{aligned} \tag{8}$$

To avoid short circuiting the voltage source, only one existence function will operate at a time in one leg, hence

$$\begin{aligned} H_{a3} + H_{a2} + H_{a1} &= 1 \\ H_{b3} + H_{b2} + H_{b1} &= 1 \\ H_{c3} + H_{c2} + H_{c1} &= 1 \end{aligned} \tag{9}$$

Eliminating the H_{i2} terms in Equation (9), substitute in Equation (8) and bringing in the capacitor voltages in place of the voltage drops V_3 and V_1 gives

$$\begin{aligned} \nu_{an} &= H_{a3}V_{c1} - H_{a1}V_{c2} + V_2 \\ \nu_{bn} &= H_{b3}V_{c1} - H_{b1}V_{c2} + V_2 \\ \nu_{cn} &= H_{c3}V_{c1} - H_{c1}V_{c2} + V_2 \end{aligned} \tag{10}$$

From Equation (10),

$$V_2 = \tfrac{1}{3}\{(\nu_{an} + \nu_{bn} + \nu_{cn}) + V_Z \tag{11}$$

where $V_Z = (H_{a1} + H_{b1} + H_{c1})V_{c2} - (H_{a3} + H_{b3} + H_{c3})V_{c1}$

For an unbalanced system, Equation 11 is used to compute the neutral voltage. If the system is balanced,

$$\nu_{an} + \nu_{bn} + \nu_{cn} = 0$$

$$\Rightarrow V_2 = \tfrac{1}{3}\{(H_{a1} + H_{b1} + H_{c1})V_{c2} - (H_{a3} + H_{b3} + H_{c3})V_{c1}\} \cong 0 \tag{12}$$

To accommodate any unforeseen system disturbances, the neutral voltage of Equation (11) is substituted back into Equations (9) to give

$$\begin{aligned} v_{an} &= \tfrac{1}{3}\{2(H_{a3}V_{c1} - H_{a1}V_{c2}) - (H_{b3}V_{c1} - H_{b1}V_{c2}) - (H_{c3}V_{c1} - H_{c1}V_{c2})\} \\ v_{bn} &= \tfrac{1}{3}\{-(H_{a3}V_{c1} - H_{a1}V_{c2}) + 2(H_{b3}V_{c1} - H_{b1}V_{c2}) - (H_{c3}V_{c1} - H_{c1}V_{c2})\} \\ v_{cn} &= \tfrac{1}{3}\{-(H_{a3}V_{c1} - H_{a1}V_{c2}) - (H_{b3}V_{c1} - H_{b1}V_{c2}) + 2(H_{c3}V_{c1} - H_{c1}V_{c2})\} \end{aligned} \quad (13)$$

The current Equations are given as

$$\begin{aligned} I_3 &= H_{a3}i_{an} + H_{b3}i_{bn} + H_{c3}i_{cn} \\ I_2 &= H_{a2}i_{an} + H_{b2}i_{bn} + H_{c2}i_{cn} \\ I_1 &= H_{a1}i_{an} + H_{b1}i_{bn} + H_{c1}i_{cn} \end{aligned} \quad (14)$$

The sum of voltage drop across the equivalent impedances (net resistance and inductance) of the interconnecting transformer and line, as well as the prevailing load bus voltages as depicted in Fig. (4.3) are equated to the inverter output voltage to determine the injected phase currents.

$$\begin{aligned} v_{an} &= r_a i_a + L_a p i_a + v_{aref} \\ v_{bn} &= r_b i_b + L_b p i_b + v_{bref} \\ v_{cn} &= r_c i_c + L_c p i_c + v_{cref} \end{aligned} \quad (15)$$

$$\begin{aligned} p i_a &= \tfrac{1}{L_a}(v_{an} - r_a i_a - v_{aref}) \\ p i_b &= \tfrac{1}{L_b}(v_{bn} - r_b i_b - v_{bref}) \\ p i_c &= \tfrac{1}{L_c}(v_{cn} - r_c i_c - v_{cref}) \end{aligned} \quad (16)$$

The capacitor equations are given by

$$\begin{aligned} C_1 p V_{c1} &= I_{dc} - I_3 \\ C_2 p V_{c2} &= I_{dc} + I_1 \end{aligned} \quad (17)$$

If C_1=C_2 and C_1+C_2=C, then adding Equation (17) gives

$$Cp(V_{c1} + V_{c2}) = 2I_{dc} + I_1 - I_3 \quad (18)$$

Since $V_{c1} + V_{c2} = V_{dc}$

Then $p(V_{c1} + V_{c2}) = 0$

Hence $I_{dc} = \frac{1}{2}(I_3 - I_1)$ (19)

Equations (10) to (19) are then used to perform the dynamic simulation of the three level neutral point clamped inverter. A series and parallel cascading of this converter provides the needed high voltage and current rating required in transmission line converters.

4.4 **Scheme Implementation Algorithm**

The implementation process involves development of the power system Newton-Raphson's load flow model equations with both the load bus voltage stability indexes and FACTS devices (shunt and series) incorporated. Then an associated MATLAB®-based program is developed and run to determine the stability status of the required load bus using L or Ls stability index depending on the transmission line distance [37, 38]. This status and the prevailing bus voltage are then used as the FACTS voltage source converter's modulation index and reference bus reference voltage in the modulation and control schemes of the NPC inverter to compensate the weak bus using the dynamic MATLAB ® Simulink tools.

Then the program checks if there is any variation in system parameters and uses this new updated data as well as the effect of reactive power compensation to determine the new stability status of the whole system to determine which load buses need further

compensation. The program continues until it is prompted to stop. The summarized algorithm is shown in Fig. (4.4).

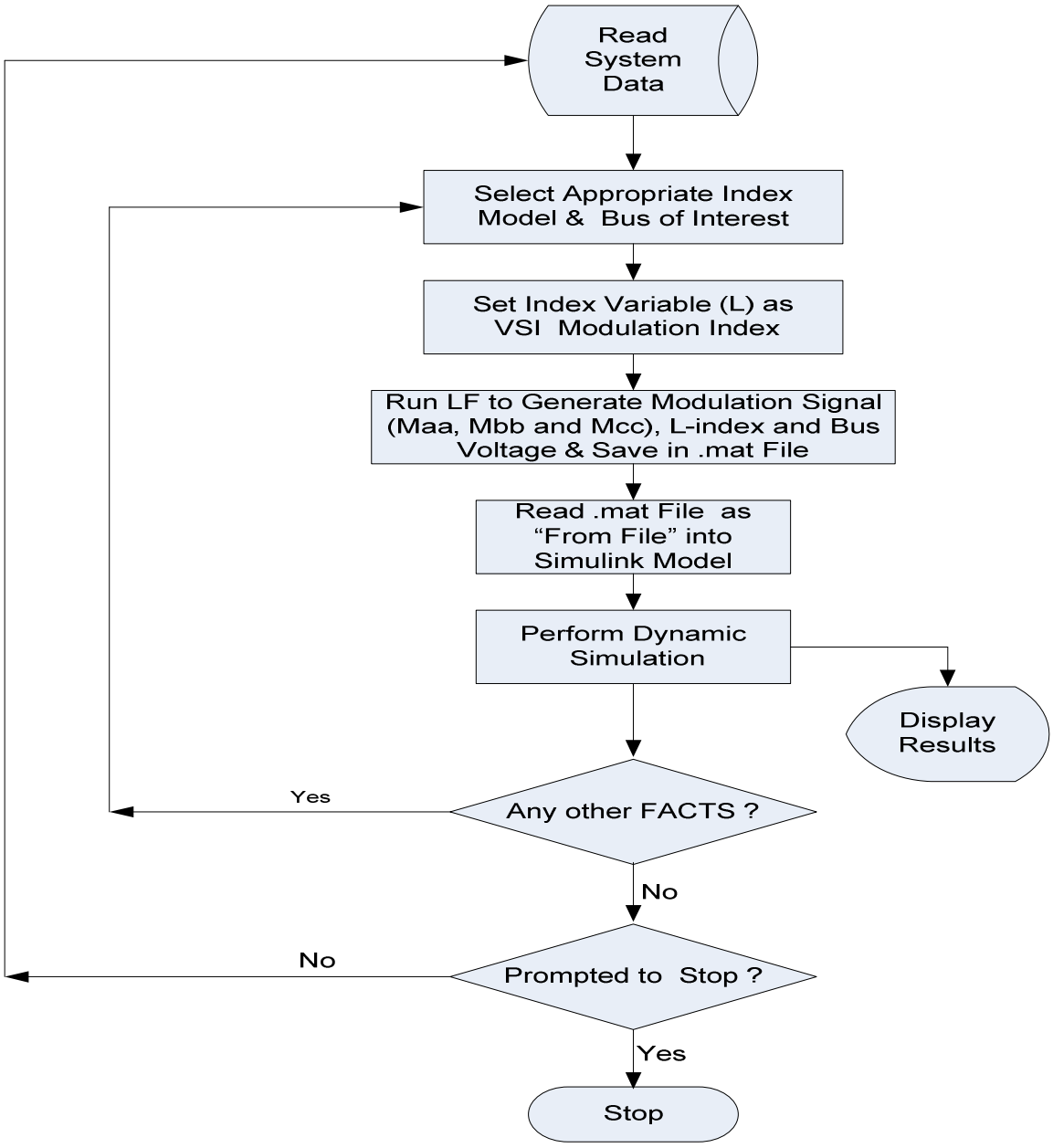

Fig. 4.4: L-index regulated VSI implementation algorithm

4.5 Simulated Results and Discussions

The voltage stability values of buses 5 and 12 which are respectively the most stable and weakest buses in the IEEE 14 bus test system are represented as L-5 and L-12 in the results displayed. With the Newton Raphson's load flow simulation performed on IEEE 14 and using the models of load bus voltage stability indices presented in Equations (2) and (3), L-5 and L-12 have values of 0.83 and 0.99, respectively. Then L-5 and L-12 are separately used as the modulation index and with their corresponding bus voltages used to compute the reference voltage which served as control parameters, the dynamic simulation of VSCs connected to these two load buses are performed at their normal loading using the model Equations (10) through (19). Figures (4.5) and (4.6) present the obtained generalized modulation and triangular signals for these two cases.

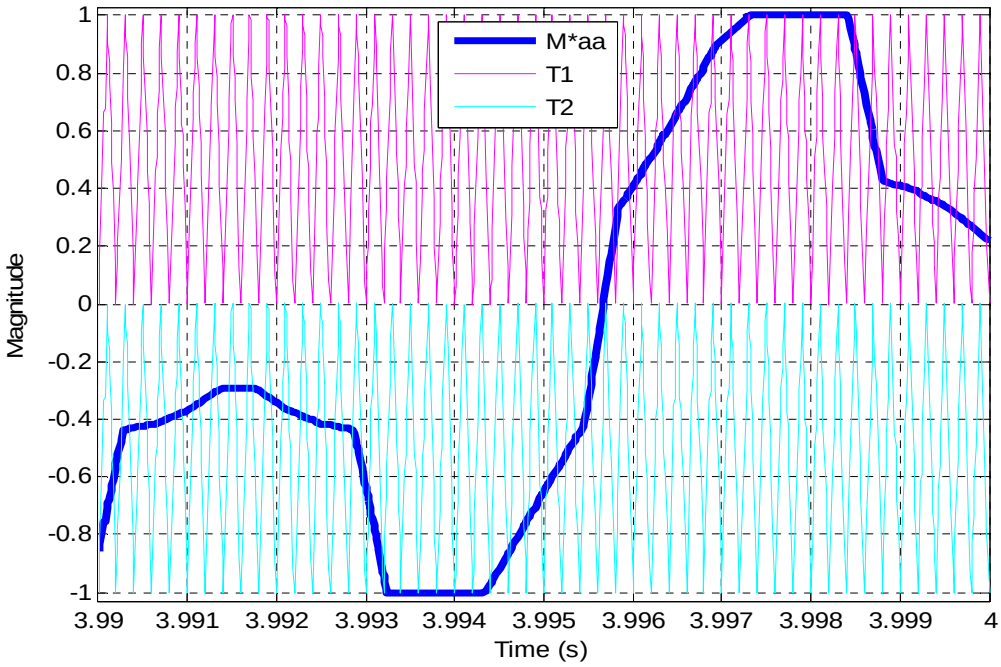

Fig. 4.5: Generalized modulation and triangular signals T1 & T2 with L-5

The comparison of these two signals generates VSI existence functions (switching pulses).

The most significant results were reflected in the variations of the inverter's output voltage and injected phase currents magnitudes given in Figures (4.7) through (4.17) and (4.19) through (4.28). The differences arose due to variations in the generalized modulation signals which compared with same triangular signals. With increased amplitude in the modulation index of bus 12 which corresponds to the index value of L-12 as modeled in this work, there was commensurate increase in the switching pulses of the existence functions. This was responsible for increased magnitude of the inverter output voltage and hence the injected phase currents.

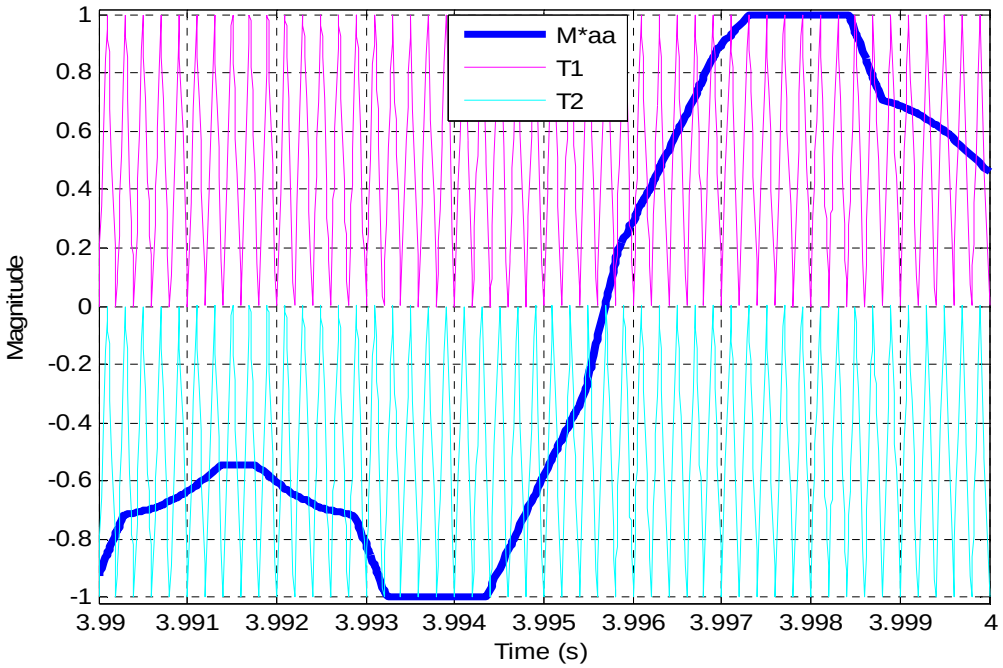

Fig. 4.6: Generalized modulation and triangular signals T1 & T2 with L-12

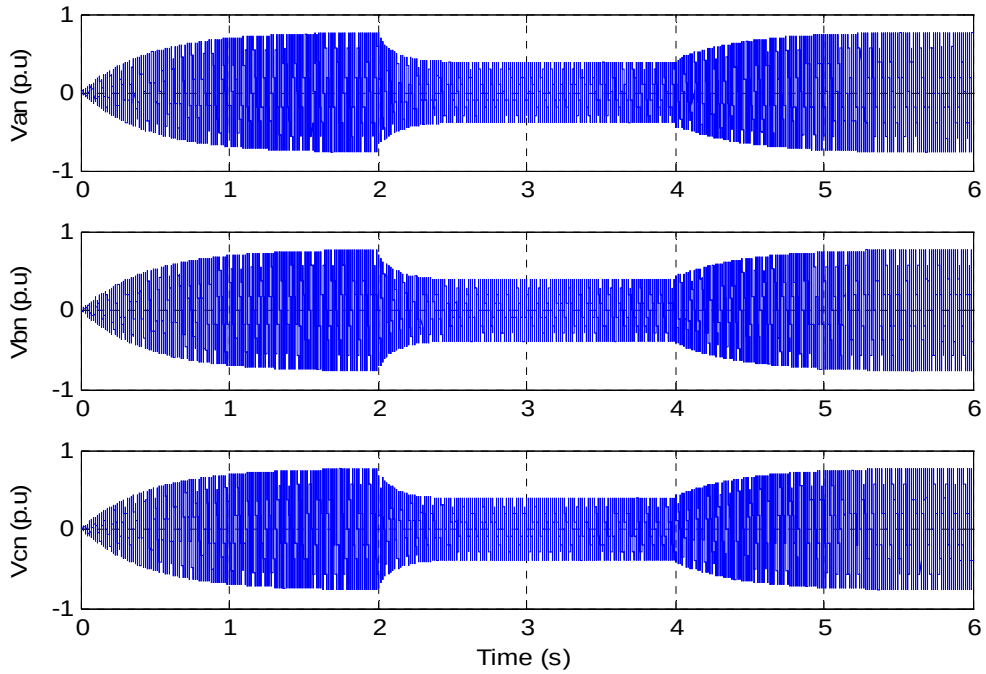

Fig. 4.7: Three-level NPC VSI output phase voltages showing changes in net line inductance at 2.0s and back to 0.003p.u at 4.0s (L-5 case)

To highlight the robustness of the scheme, we had introduced a variation in the interconnecting line net inductance which incorporates both coupling transformer and line inductances using Simulink step input function. The starting net inductance of 0.003p.u was stepped down to 0.0015p.u at 2.0 seconds simulation time, and then stepped up back to 0.003p.u at 4.0 seconds to check if the system was able to restore stability after disturbance was removed.

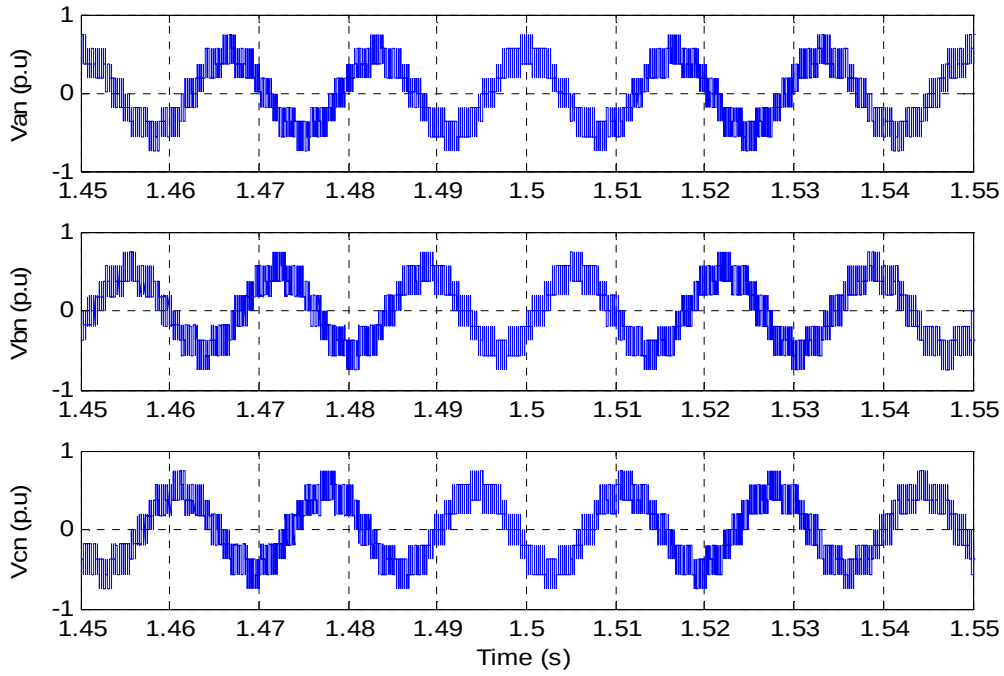

Fig. 4.8: Three-level NPC VSI output phase voltages with net line inductance of 0.003p.u (L-5 case).

These results showed the increased output for load bus twelve which was the weakest and needed much more compensation. At the current base loading, the final bus twelve voltage from the load flow program is 0.93p.u while the output voltage of the inverter connected at this bus with modulation index replaced with L-12 is 1.15p.u. Since the inverter output voltage is greater than the prevailing voltage at load bus twelve, the inverter will inject reactive power to support bus twelve voltage. The same situation repeated in many of the other load buses in the system though with decreasing level of compensation required apart from buses four, five, and seven.

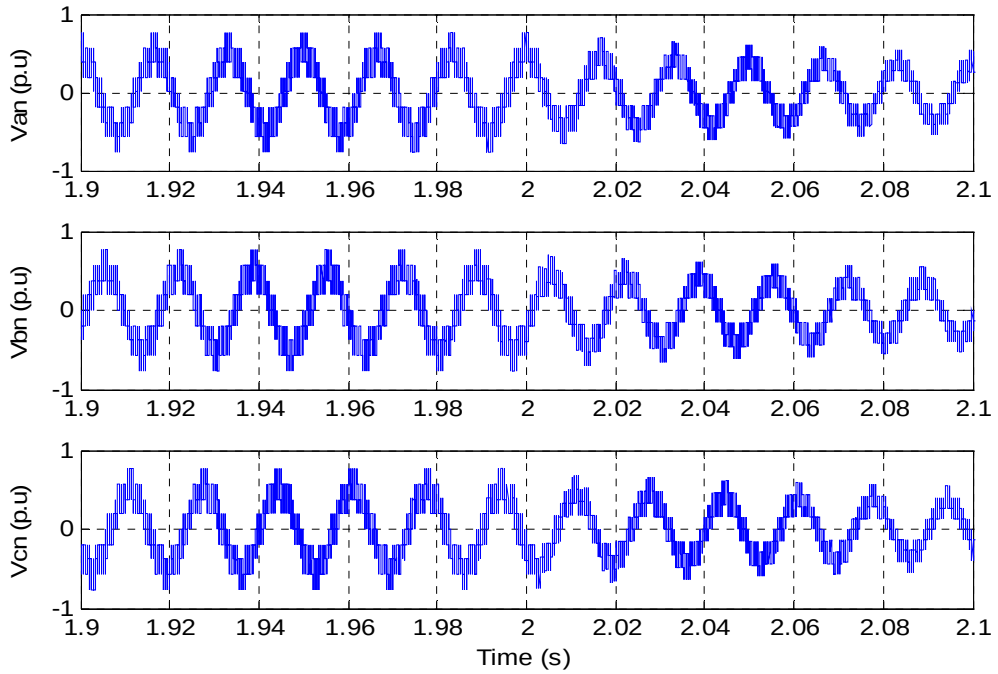

Fig. 4.9: Three-level NPC VSI output phase voltages with net line inductance changed from 0.003p.u to 0.0015p.u at 2.0s (L-5 case)

The resulting load flow voltage for bus five at this base loading is 1.03p.u. This was slightly above the base voltage of 1.0 p.u used for the load flow. This showed that there was enough reactive support already existing at bus five. When compared with the simulated inverter output voltage of 0.78p.u with L-5 utilized modulation index, it could be seen from the operational concept of STATCOM or any other shunt connected FACTS which uses VSC that the device now absorbs reactive power from bus five instead of injecting. The same scenario occurred in load bus four while at transformer bus seven (where there is neither load nor generation) there is no net exchange.

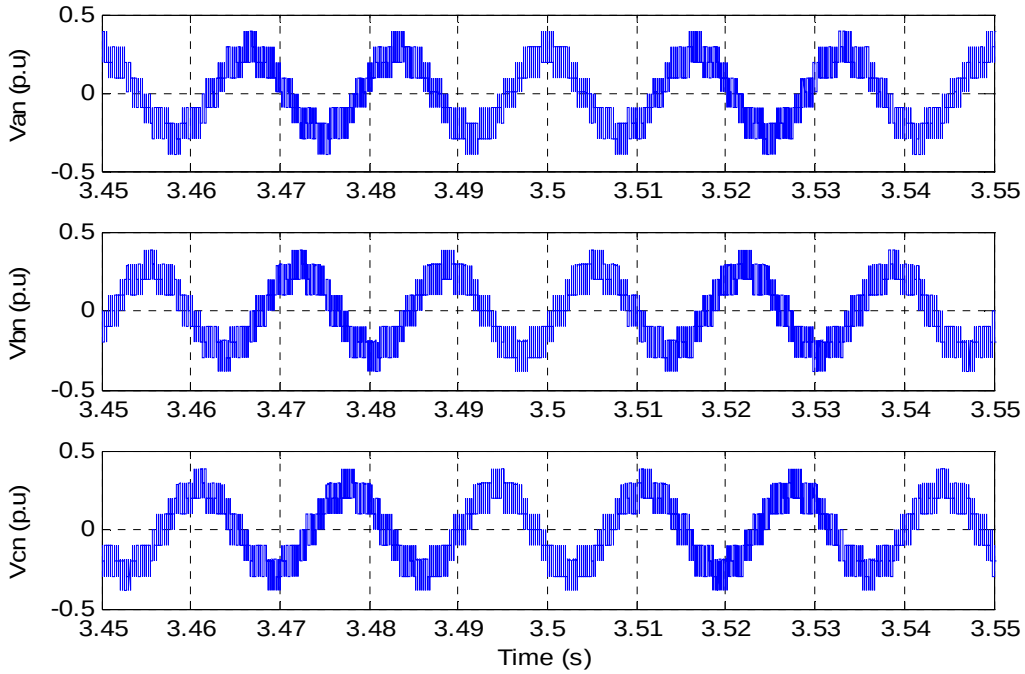

Fig. 4.10: Three-level NPC VSI output phase voltages with net line inductance of 0.0015p.u. (L-5 case)

From the results displayed the effect of step changing the VSC net coupling inductance from 0.003p.u to 0.0015p.u at 2.0 seconds and after 2.0 seconds stepping it back to 0.003p.u at 4.0s clearly showed the restorative power of the NPC multilevel inverter. The 0.005s transients noted in the results, particularly in the injected phase currents pictured the limitations in the use of STATCOM as faulted circuit device.

However, it is normally utilized as a three-phase balanced ac bus compensator to meet changing loading situations and not faulted transmission lines. However, due to recent developments in faster fault clearing using digital techniques, STATCOM could be as well utilized in such situations.

One other important milestone gained from the results depicted is the fact that with controlled step change in coupling line inductance and dc capacitor values, the VSC will be able to respond to changes in power system transmission line and bus conditions to restore normalcy.

From the results displayed the effect of step changing the VSC net coupling inductance from 0.003p.u to 0.0015p.u at 2.0 seconds and after 2.0 seconds stepping it back to 0.003p.u at 4.0s clearly showed the restorative power of the NPC multilevel inverter. The 0.005s transients noted in the results, particularly in the injected phase currents pictured the limitations in the use of STATCOM as faulted circuit device.

However, it is normally utilized as a three-phase balanced ac bus compensator to meet changing loading situations and not faulted transmission lines.

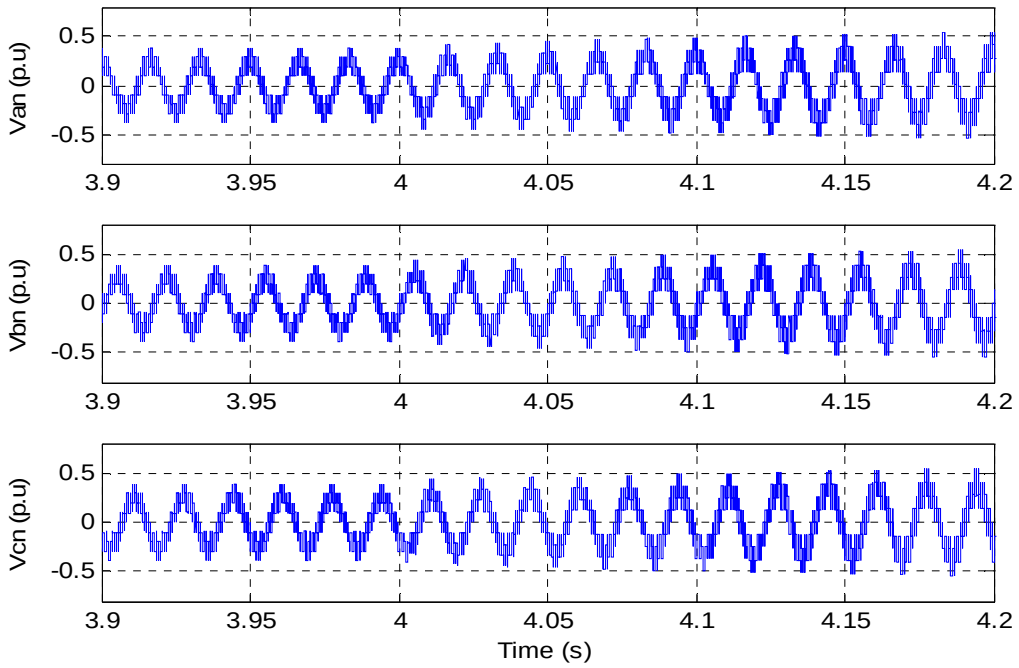

Fig. 4.11: Three-level NPC VSI output phase voltages with net line inductance changed from 0.0015p.u to 0.003p.u at 4.0s (L-5 case)

However, due to recent developments in faster fault clearing using digital techniques, STATCOM could be as well utilized in such situations. One other important milestone gained from the results depicted is the fact that with controlled step change in coupling line inductance and dc capacitor values, the VSC will be able to respond to changes in power system transmission line and bus conditions to restore normalcy.

These results when viewed from another perspective showed that the VSC output can be regulated using the bus voltage index (L-index), dc capacitors capacitance variation, and the coupling transformer/line inductance and even resistance.

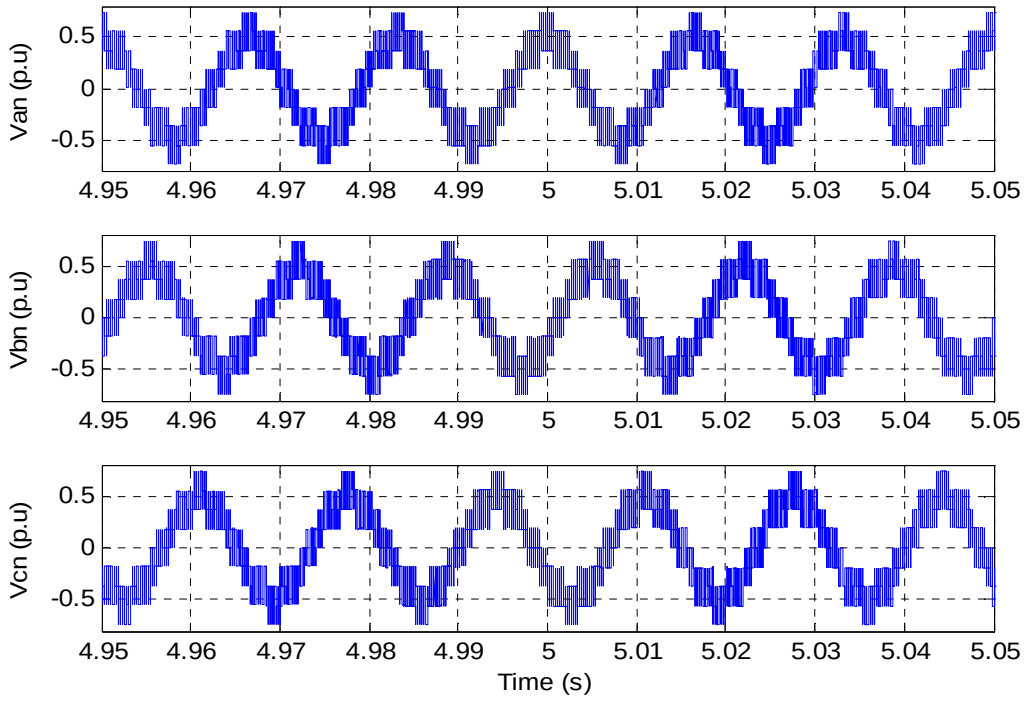

Fig. 4.12: Three-level NPC VSI output phase voltages with net line inductance of 0.003p.u. (L-5 case)

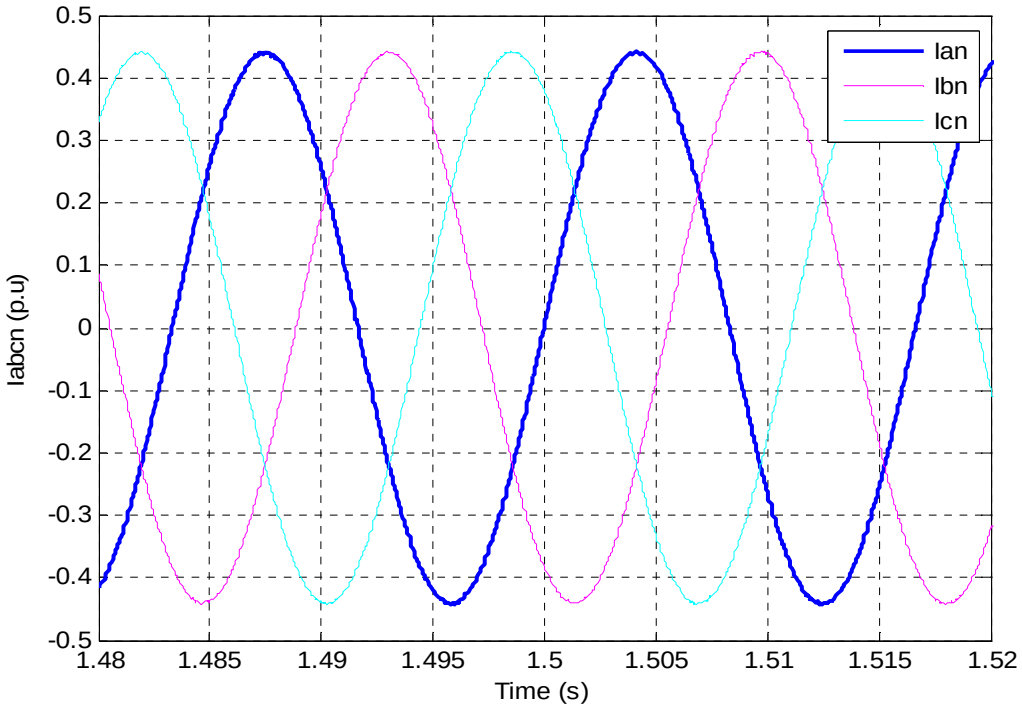

Fig. 4.13: Three-level NPC VSI injected phase currents with line inductance of 0.003p.u (L-5 case)

This could easily be seen from the displayed full simulation (0-6 seconds) for each of the variables considered. It is important to note that within one-twentieth of second of each transience, the system stabilizes for both the VSI output voltages and injected phase currents.

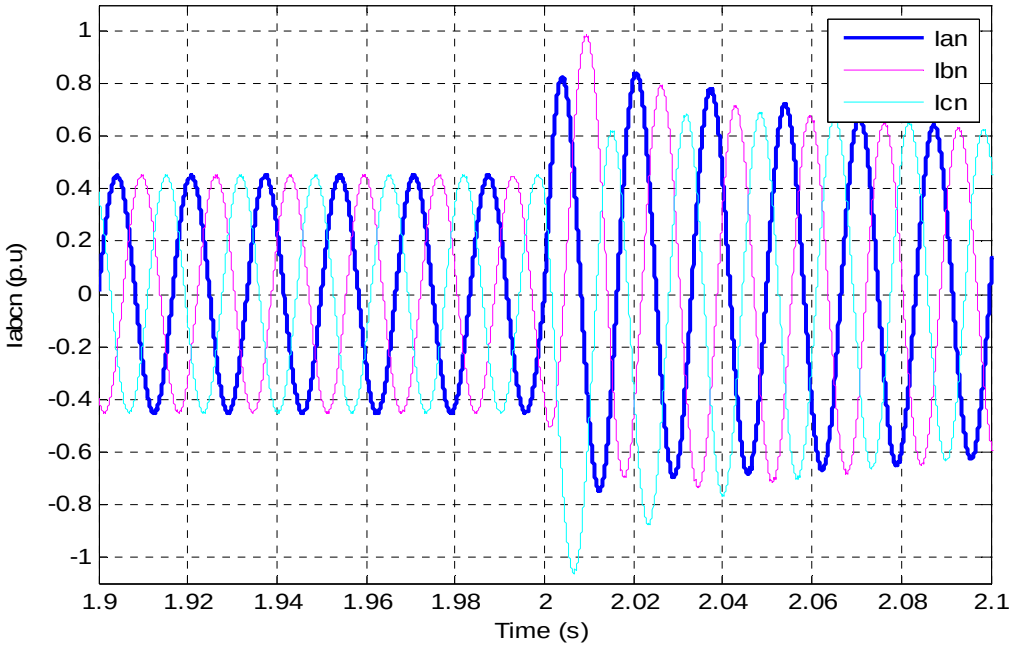

Fig. 4.14: Three-level NPC VSI injected phase currents with line inductance changing at 2.0s from of 0.003p.u to 0.0015p.u (L-5 case).

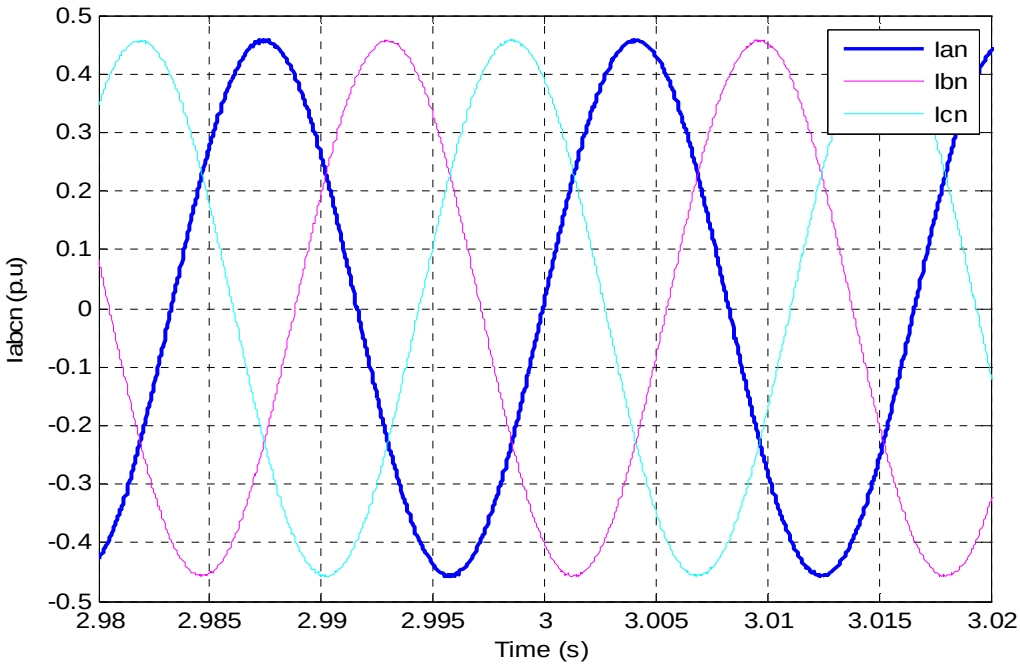

Fig. 4.15: Three-level NPC VSI injected phase currents with line inductance of 0.0015p.u (L-5 case)

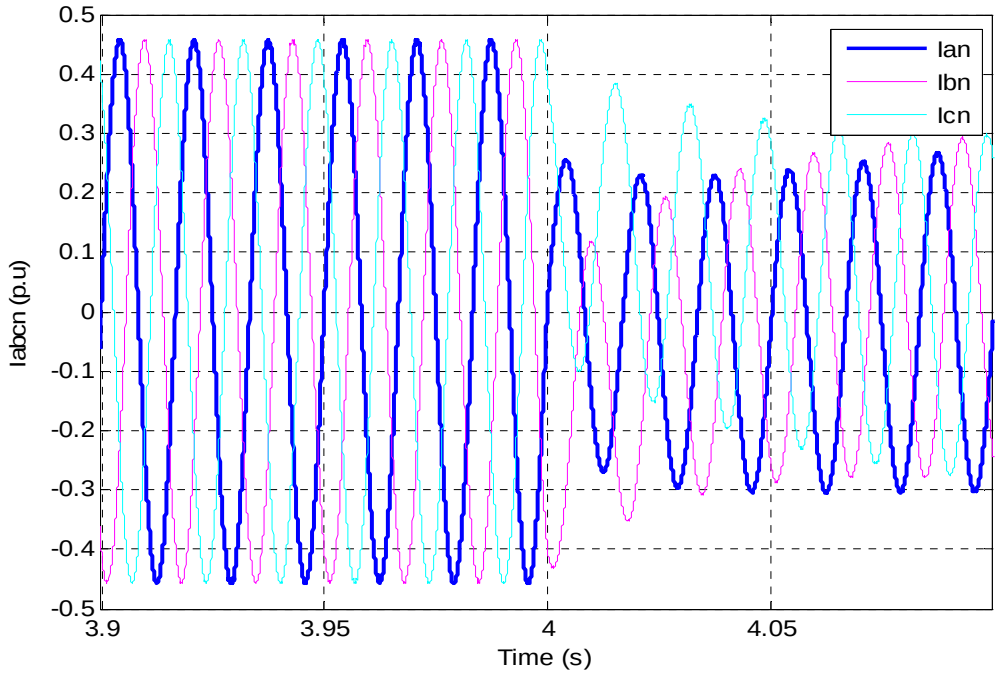

Fig. 4.16: Three-level NPC VSI injected phase currents with line inductance changing at 4.0s from of 0.0015p.u to 0.003p.u (L-5 case).

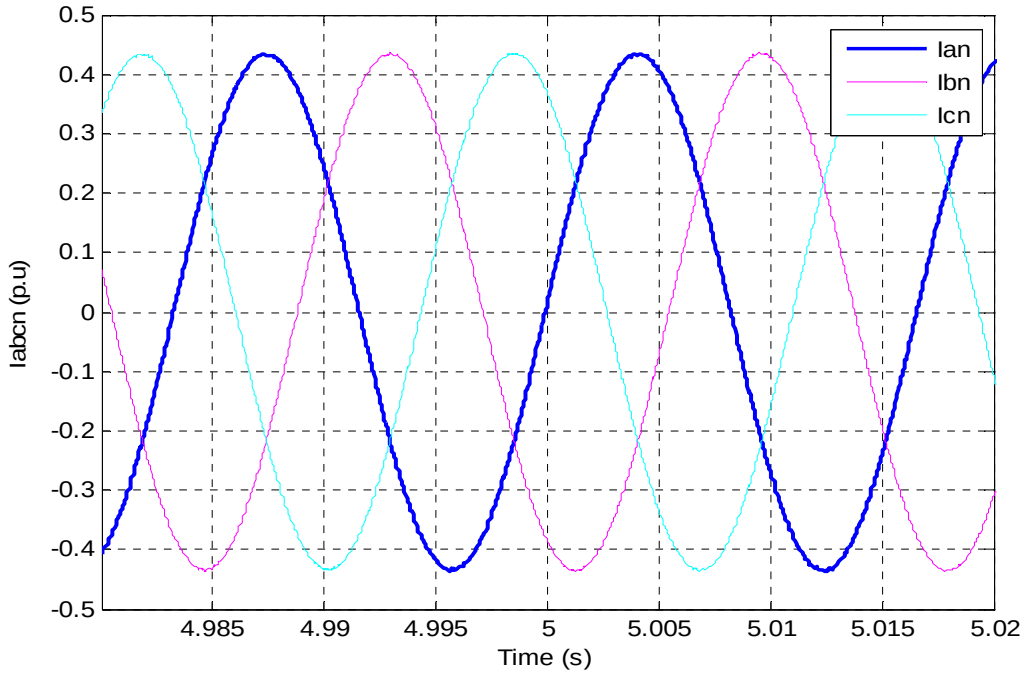

Fig. 4.17: Three-level NPC VSI injected phase currents with line inductance of 0.003p.u (L-5 case).

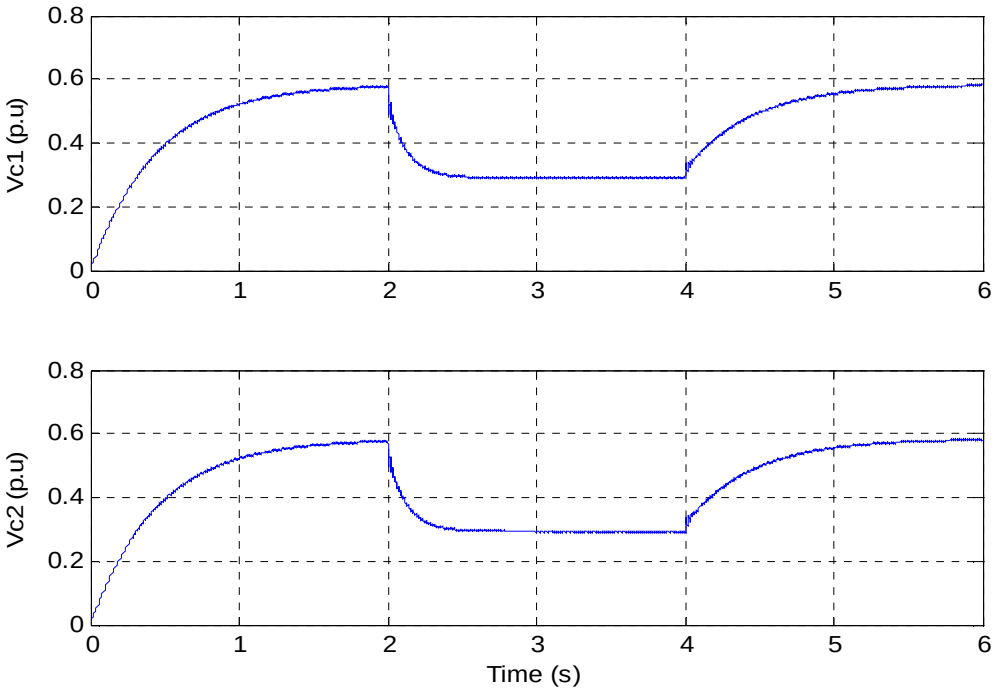

Fig. 4.18: Three-level NPC VSI dc capacitor voltages showing line changes in impedance and balancing features (L-12 case)

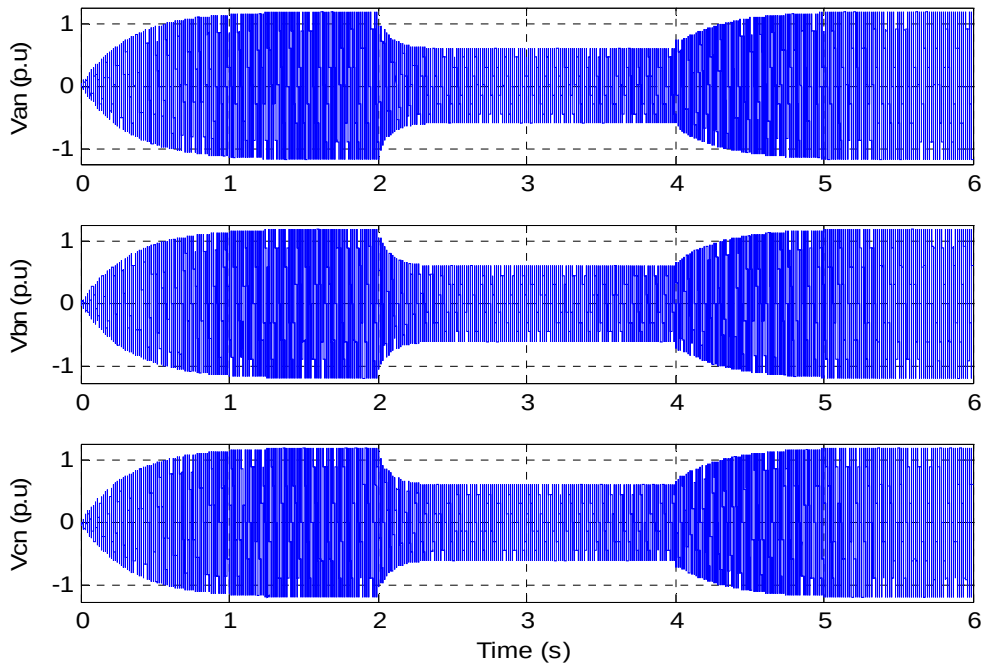

Fig. 4.19: Three-level NPC VSI output phase voltages with L-12 showing changes in effective coupling line reactance.

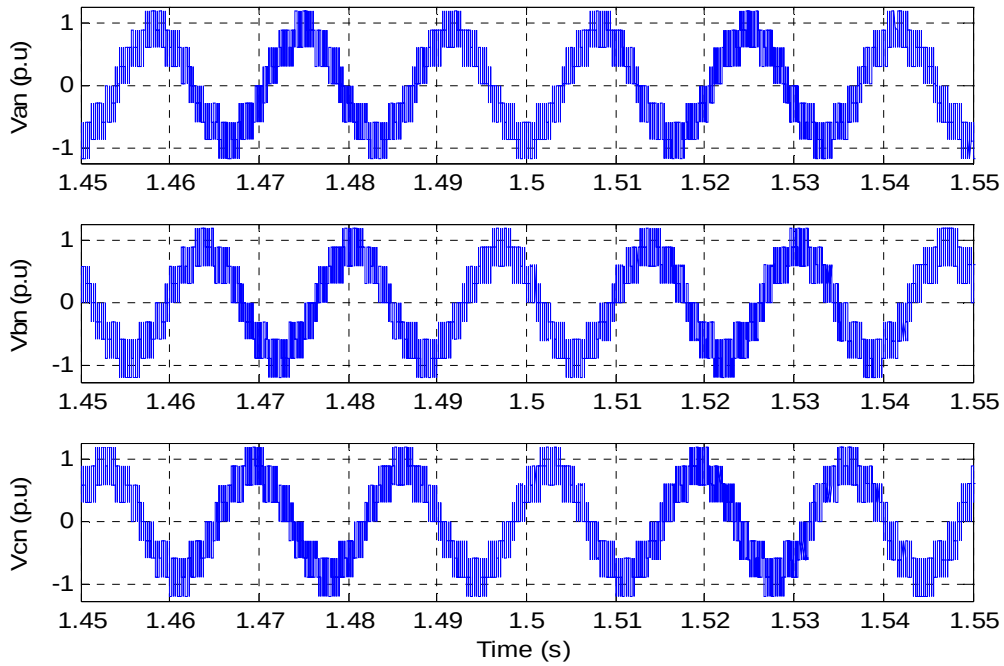

Fig. 4.20: Three-level NPC VSI output phase voltages with net line inductance of 0.003p.u.for L-12.

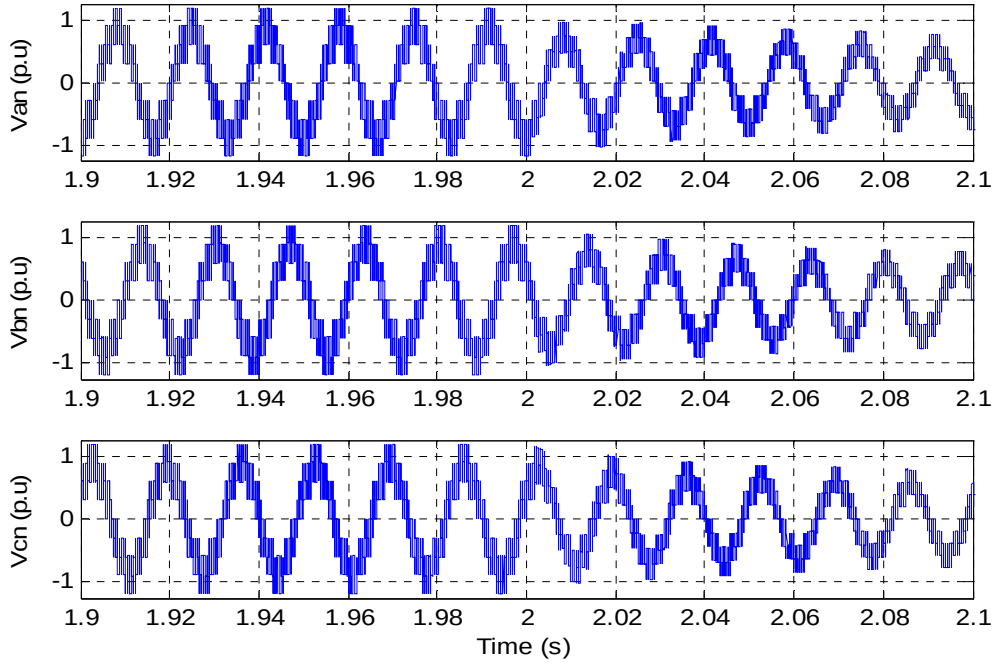

Fig. 4.21: Three-level NPC VSI output phase voltages with net coupling line inductance changed at 2.0 seconds from 0.003p.u to 0.0015p.u for L-12

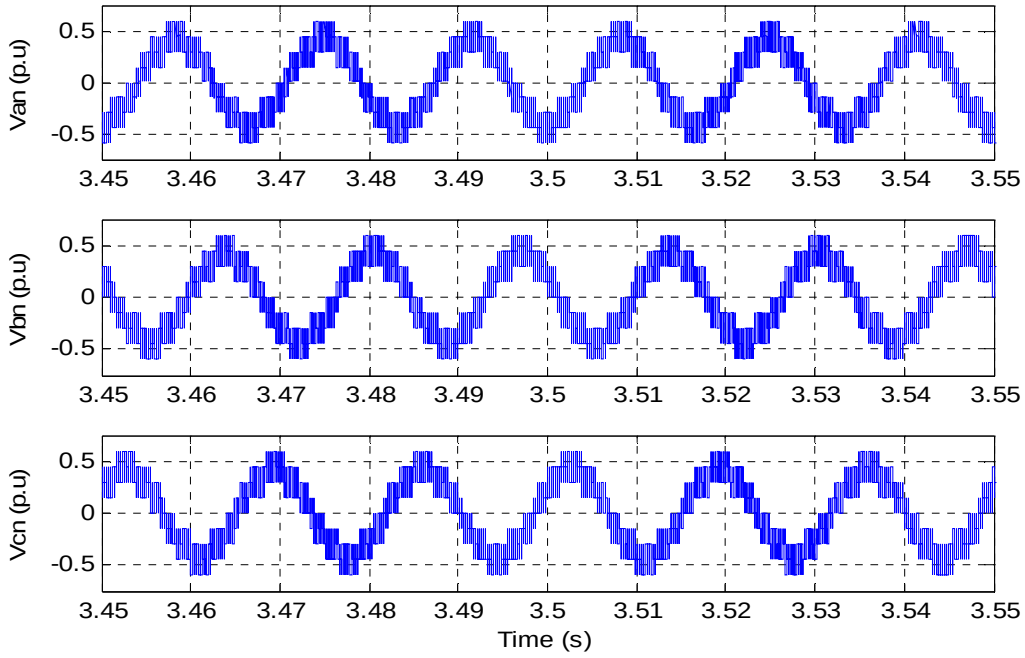

Fig. 4.22: Three-level NPC output phase voltages with net coupling line inductance of 0.0015p.u for L-12

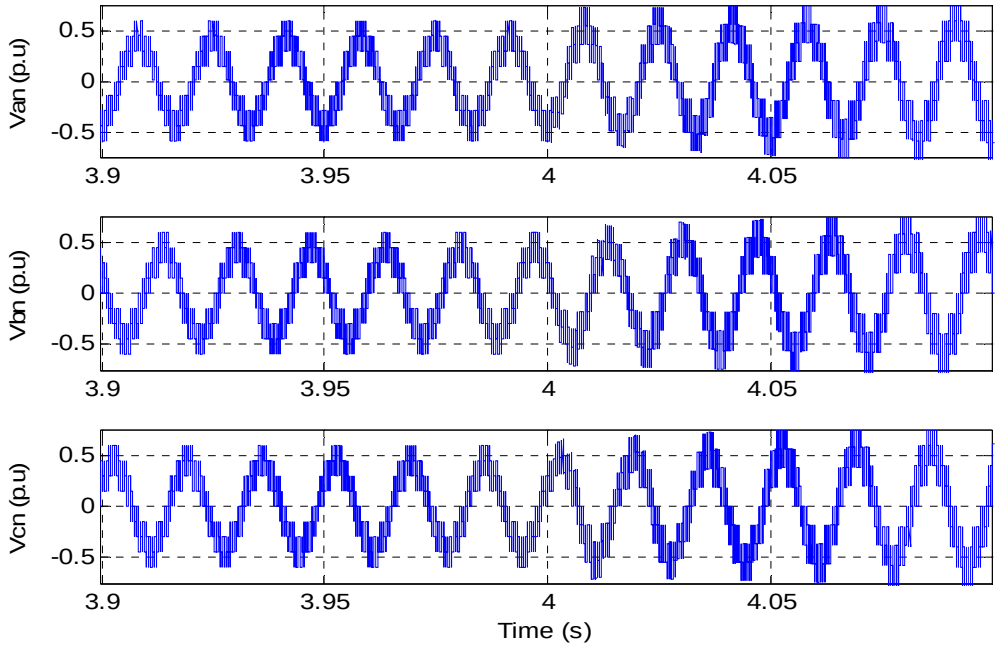

Fig. 4.23: Three-level NPC VSI output phase voltages with net coupling line inductance changed at 4.0 seconds from 0.0015p.u to 0.003p.u for L-12

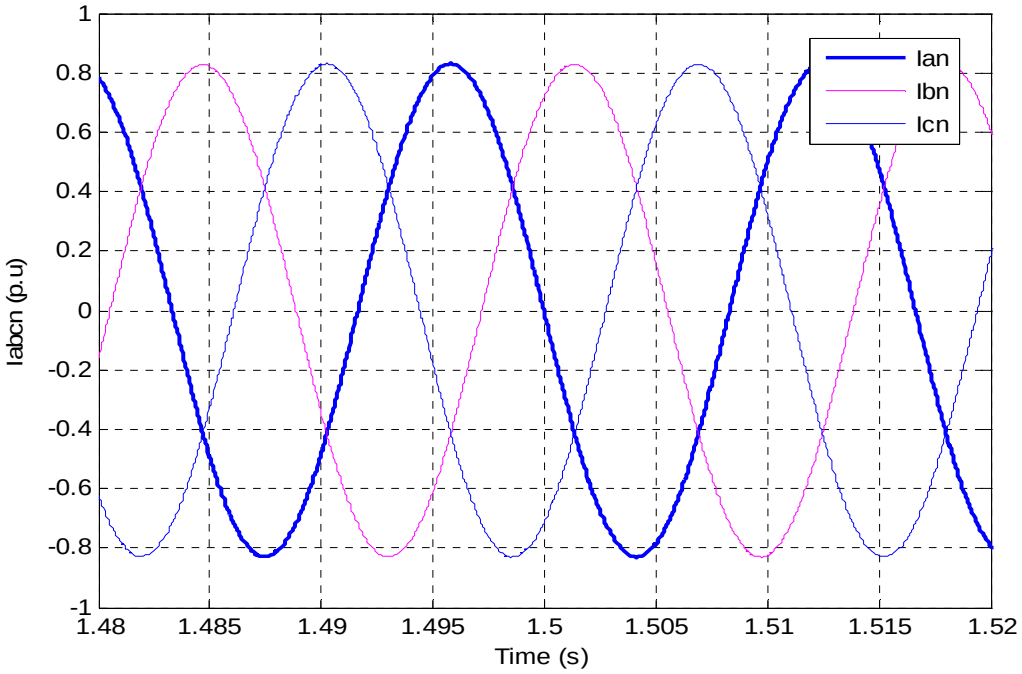

Fig. 4.24: Three-level NPC VSI injected phase currents with line inductance of 0.003p.u. for L-12.

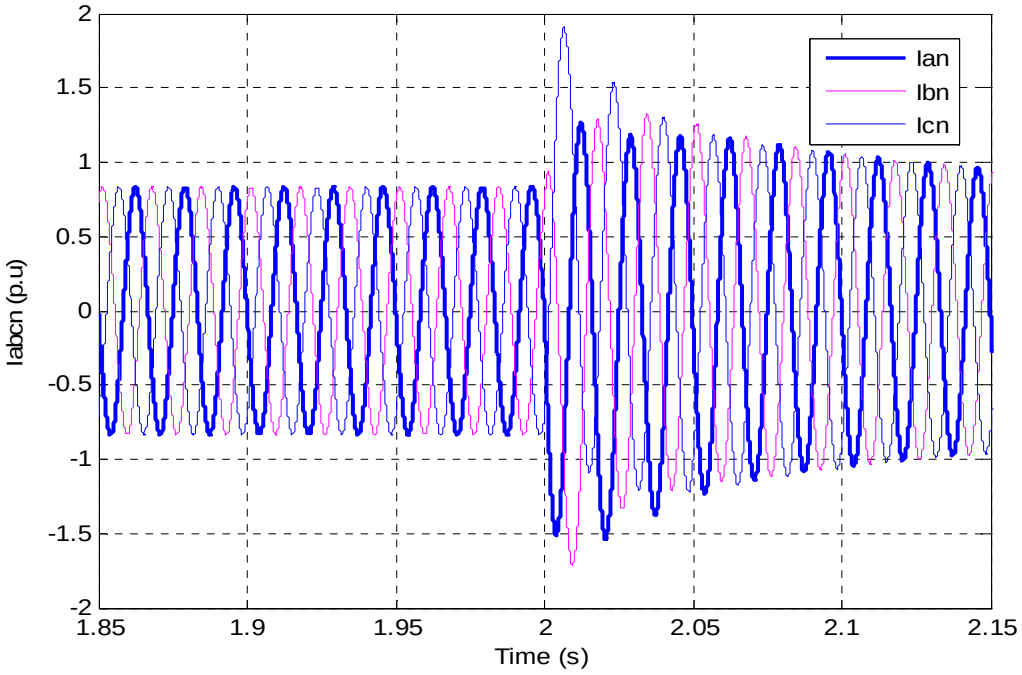

Fig. 4.25: Three-level NPC VSI injected phase currents with line inductance changing at 2.0s from of 0.003p.u to 0.0015p.u (L-12 case).

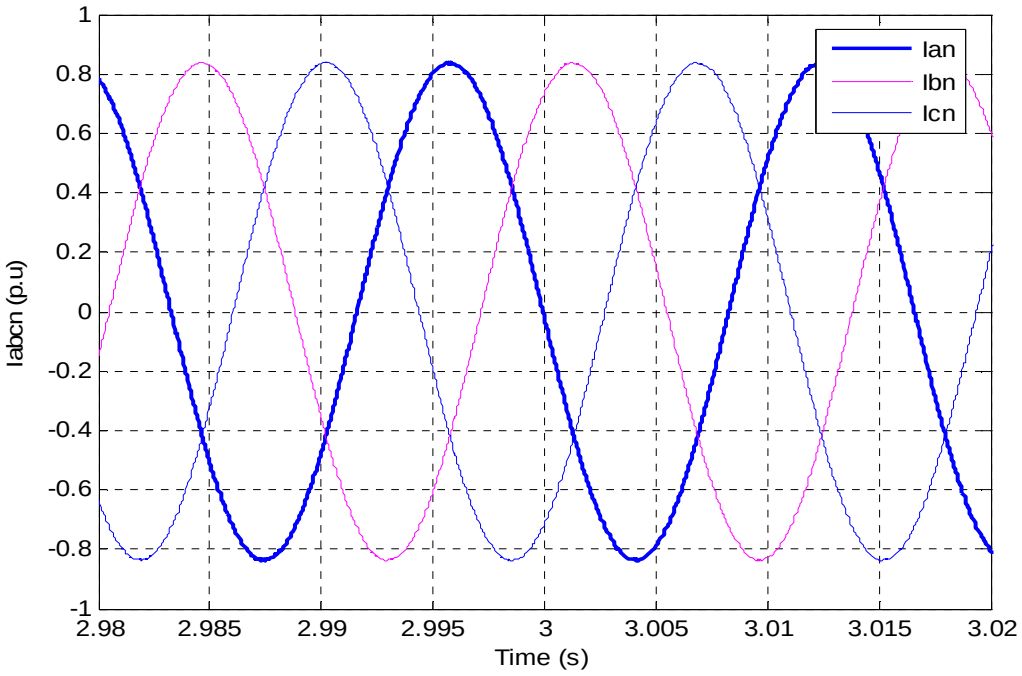

Fig. 4.26: Three-level NPC VSI injected phase currents showing recovery back to 0.82p.u despite the disturbance introduced at 2.0s (L-12 case).

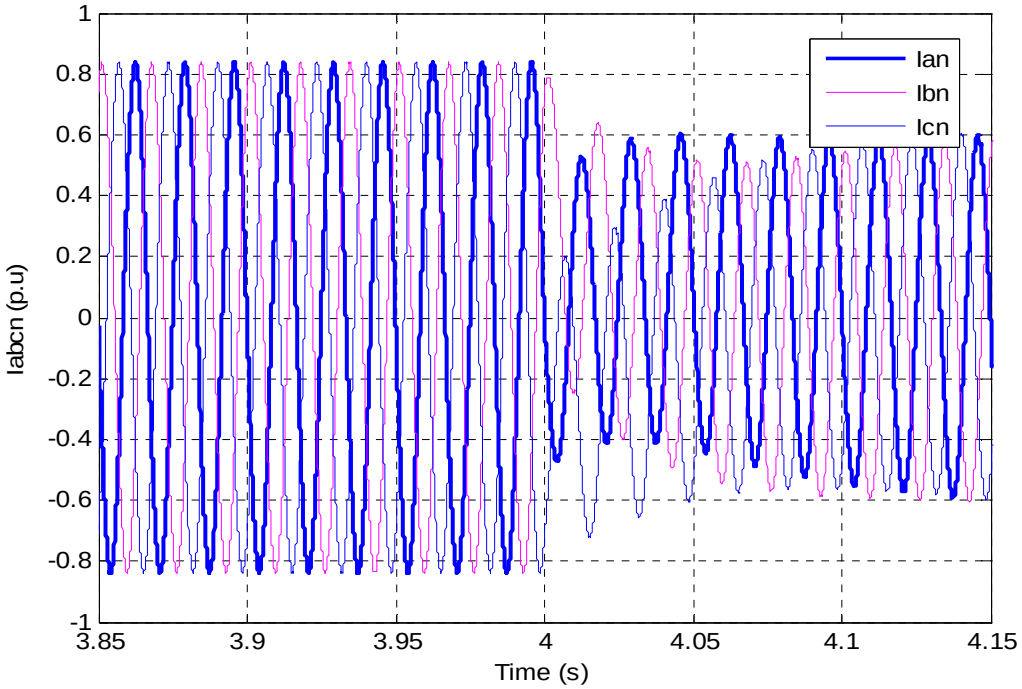

Fig. 4.27: Three-level NPC VSI injected phase currents with line inductance changing at 4.0s from of 0.0015p.u to 0.003p.u (L-12 case).

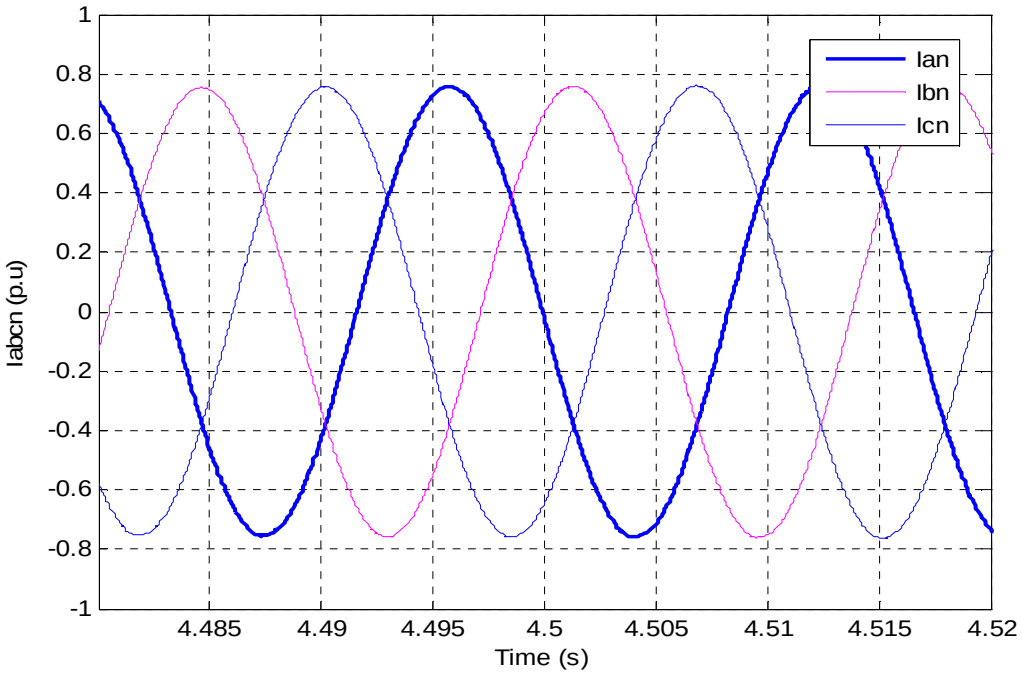

Fig. 4.28: Three-level NPC VSI injected phase currents showing recovery back to 0.82p.u despite the disturbance introduced at 4.0s (L-12 case).

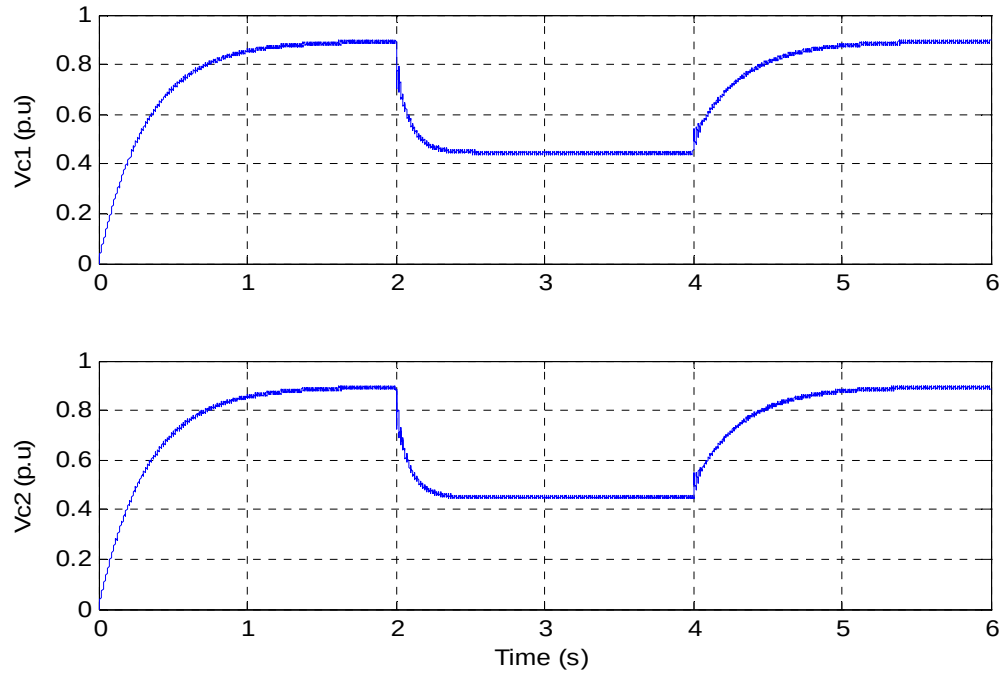

Fig. 4.29: Three-level NPC VSI dc capacitor voltages with L-12 showing line changes in impedance and balancing features.

To check for the dc bus voltage stabilization, we decided to plot the values of the two dc bus capacitor voltages for both the L-5 and L-12 cases. The results depicted in Figures (4.18) and (4.29) showed that the model produced balanced dc capacitor voltages. The balancing in the dc capacitor voltages was obtained through feeding back of the neutral (offshoot) voltage in the main model equations.

4.6 Conclusion

An algorithm for the incorporation of voltage stability index in the improved regulation of voltage source converter has been developed and implemented using IEEE 14 bus system. The developed scheme uses the power system stability status indicator as a regulatory input parameter to make VSC-based FACTS devices robust and self-adjustable to changing system condition. From the dynamic simulation results obtained, any malfunctioning of the interconnected power system sector could be easily detected by operators and the VSC could appropriately adjust its operation to reduce the incidents of outages.

The proposed scheme may reduce problems faced by network operators in regulating interconnection of FACTS devices and various distributed energy resources to power system networks due to their effects on system voltages. It will also be a good relieve for many industrial processes which rely on VSC based drives for power quality enhancement.

Further research work will be required to implement this scheme in a parallel computer simulation system where each program segment will be performed by different

processors with a master controller co-coordinating the over all decision-making process of the VSC. The simulation should also be performed under diverse power system operating conditions to reaffirm its robustness.

4.7 References

[1] L. Philipson and H. L. Willis [1998], "Understanding Electric Utilities and De-Regulation," Marcel Dekker, Inc. NY 10016, pp. 2.

[2] X. P. Zhang, C. Rehtanz and B. Pal [2006], "Flexible AC Transmission Systems: Modeling and Control," Springer-Verlag Berlin Heidelberg Germany, pp 2-3.

[3] V. Blasko and B. Lukaszewski [1997], "On the loading of power modules in a three phase voltage source converter," IEEE Ind. Applications Society Annual Meeting, New Orleans, Louisiana.

[4] J. Rodríguez, J. Lai and F. Z. Peng [2002], "Multilevel Inverters: A survey of topologies, controls and applications," IEEE Trans. Ind. Electronics, vol. 49, no. 4, pp. 724-738.

[5] E. Babaei, S. Hosseini and G. B. Gharehpetian, "A new topology for multilevel current source converters," ECTI Trans. Electrical Eng., Electronics and Communications, vol. 4, no. pp. 2-12, 2006.

[6] M. E. Ortúzar, R. E. Carmi, J. W. Dixon and L. Morán, "Voltage-source active power filter based on multilevel converter and ultracapacitor dc link," IEEE Trans. Ind. Electronics, vol. 53, no. 2, pp 477-485, 2006.

[7] J. Rodríguez, S. Bernet, B. Wu, J. O. Pontt and S. Kouro, "Multilevel voltage-source converter topologies for industrial medium –voltage drives," IEEE Trans. Ind. Electronics, vol. 54, no. 6, pp. 2930-2945, 2007.

[8] S. B. Monge, S. Somavilla, J. Bordonau and D. Boroyevuch, "Capacitor voltage balance for neutral-point-clamped converter using virtual space vector concepts with optimized special performance," IEEE Transactions on Power Electronics, vol. 22, no. 4, pp. 1128-1134, 2007.

[9] P. Purkait and R. S. Sriramakavacham [2006], "A new generalized space vector modulation algorithm for neutral-point-clamped multilevel converters," Progress in Electromagnetics Research Symposium, Cambridge, USA, pp.330-335.

[10] U.S.-Canada Task Force on 14 August 2003 Blackout [2003], "The August 14 blackout compared with previous major North America outages," Final Report on the August 14th 2003 Blackouts in the United States and Canada, pp. 103-106.

[11] "Storms knock out power to over 600,000 customers in U.S. Northeastern Coast," U.S. DOE Energy Assurance Daily, Wednesday, July 19, 2006.

[12] "Biggest blackout in U.S. history," CBS News, pp. 1-3, August 15, 2003.

[13] M. Amin, Powering the 21st century, we can – and must – modernize the grid, IEEE-U.S.A. Today's Engineer, 2005. Available online at http://www.todaysengineer.org/2006/Apr/backscatter.asp.

[14] R. Siegel [2006], "Massive power outages cripples Los Angeles," NPR October 14, 2006.

[15] M. Amin, "North America's Electricity Infrastructure: Are we ready for more storms?" IEEE Security & Privacy, published by the IEEE Computer Society, pp. 19-25, 2003.

[16] S. Brown, "Motown microgrid – life-cycle analysis rates energy and environmental performance," Cogeneration and On-site Power Production, pp. 75, 2004.

[17] Y. Shimazaki , "Model analysis of microgrid cogeneration system zero emission industrial park," UPE7 – The 7th International Conference on Urban Planning and Environment, Bangkok, Thailand, 2007.

[18] R. Lasseter, A. Akhil, C. Marnay, J. Stevens, J. Dagle, R. Guttromson, A. S. Meliopoulous, R. Yinger and J. Eto, "The MicroGrid Concept," CERTS White Paper on Integration of Distributed Energy Resources, Available [Online] at http://eetd.lbl.gov/CERTS/pdf/50829-app.pdf, 2002.

[19] J. Lynch Microgrid power networks, Cogeneration and On-site Power Production, 2004.

[20] N. Panagis, A. E. Kiprakis, W. A. Robin, and G.P. Harrison, "Centralized and distributed voltage control: Impact on distributed generation penetration," IEEE Trans. on Power Systems, vol. 22, no. 1, 2007.

[21] J. A. Silva, H.B. Funmilayo and K. L. Butler-, "Impact of distributed generation on the IEEE 34 node radial test feeder with overcurrent protection," Proceedings of the 2007 39th North American Power Symposium, New Mexico State University, Las Cruces, New México. pp. 49, 2007.

[22] L.M. Cipcigan, P. C. Taylor and P. Trichakis, "The impact of small scale wind generation on low voltage distribution systems voltage," International Conf. on Clean Electrical Power, Italy, pp. 9, 2007.

[23] Z. Ye, R. Walling, N. Miller, P. Du and K. Nelson], "Facility microgrids, Executive Summary," NREL Innovation for our Energy future, Subcontract Report NREL/SR-560-38019, pp. iii, 2005.

[24] D. E. Feero, D. C. Dawson and J. Stevens, "Protection issues of the microgrid concept, CERTS," Transmission Reliability Program, Office of Power Technologies, Assistant Secretary for Energy Efficiency and Renewable Energy, U.S. DOE, pp.4-9, 2002.

[25] R. Firestone and C. Marnay, "Energy manager design for microgrids," Consultant Report by CERTS for the California Energy Commission, pp. 1. 2005.

[26] J. A. Pecas Lopes, C. L. Moreira and F.O. Resende, "Microgrids black start and islanded operation," 15th PSCC, Liege, session 27, paper 4, page 2., 2005.

[27] C. Billy, G. Heydt, P. Langness, A. Laughter, B. Mann, M. Rice and L. Winslow, "Sustainable electric power options with attention to native American communities," Proc. of the 39th North American Power Symposium, New Mexico State University. pp 177, 2007.

[28] C. L. Moreira and J. A. Pecas Lopes, "Microgrids dynamic security assessment," International Conference on clean Electrical Power, Capri Italy, May 21st-23rd, pp. 26. 2007.

[29] J. A. Pecas Lopes, C. L. Moreira and A. G. Madureira, "Defining control strategies for microgrids islanded operation," IEEE Trans. on Power Systems, vol. 21, no. 2, pp. 916-924, 2006.

[30]R.H. Lasseter, "Microgrids and distributed generation," Journal of Energy Engineering, American Society of Civil Engineers, 2007.

[31] O. Ojo and P. Kshirsagar, "The generalized discontinuous PWM modulation scheme for three-phase voltage source inverters," ECE Department, TTU, Cookeville, TN, 2007.

[32] D. O. Dike and O. D. Momoh, "An integrated ac/dc super-grid system – a mechanism to solving the North American power crisis," 39th SSST Mercer University, Macon, GA 31207, pp 204-209, 2007.

[33] H. du Toit Mouton, "Natural balancing of three-level neutral-point-clamped PWM inverters," IEEE Trans on Industrial Electronics, vol. 49, no. 5, pp. 1017-1025, 2002.

[34] S. Kincic and A. Chandra, "Multilevel inverter and its limitations when applied as STATCOM," IEEE Trans on Industrial Applications, vol. 32, no. 3, pp. 509-517, 1996.

[35] P. Kessel and H. Glavitsch, "Estimating the voltage stability of a power system," IEEE Trans. on Power Delivery., vol. 1. PWRD-1, no. 3, 1986.

[36] C. Reis and F. P. Maciel Barbosa, “A comparison of voltage stability indices,” IEEE Melecon Benalmadena Spain, 2006.

[37] D. O. Dike, S. M. Mahajan and G. Radman , “Development of versatile voltage stability index algorithm,” IEEE Electrical Power Conference 2007, Montreal QC, Canada., October 25-26, 2007.

[38] A. R. Bergen and V. Vittal, Power System Analysis 2nd Edition Prentice-Hall Inc. Upper Saddle River, New Jersey 07458, 2000, pp 101 and 112., 2000.

CHAPTER 5

PAPER 4: BVS INDEX BASED SHUNT COMPENSATION SCHEME[†]

D. O. Dike and S. M. Mahajan

Department of Electrical and Computer Engineering

Tennessee Technological University, Cookeville, TN 38505, USA

ABSTRACT— Despite the large scale introduction of Flexible AC Transmission System (FACTS) devices to support the distressed grid, the number of notable power system outages has continued to increase. Reports of various committees setup to review these outages, pointed out that a major exacerbating factor has been lack of situational awareness by power system operators. To improved reactive power compensation and contribute to the mitigation of power outages associated with present near-limit operated commercialized grid, a bus voltage stability (BVS) index based reactive power compensation scheme has been developed. BVS index is a hybrid voltage stability computation model involving the two machine modeled L-index and a complex power $\pi-$transmission line structure modeled Ls-index developed by the authors. The current regional wheeling of power across transmission distance far beyond the two machine model has necessitated the development of a novel Ls-index model suitable for long line. The composite scheme is then incorporated into multi-shunt Newton-Raphson's (N-R) power flow. The results obtained from applying the developed models and schemes in the IEEE 300 bus system with zoning and under varying operating conditions, showed the system's capability to providing improved system monitoring and optimal compensation based on availability.

[†] Submitted to IEEE Transactions on Power Delivery.

5.1 Introduction

With growing concern for voltage instability and need to improve power system performances to meet load demand occasioned by deregulation, the industry has focused much attention on providing greater reactive support to the distressed grid [1-3]. Consequently, Flexible AC Transmission Systems (FACTS), and lately distributed energy resources (DERS) in the form of microgrids have been applied as two modern forms of dynamic reactive power supports [4-15]. The basic categories of precipitating events or causes of the August 14th 2003 North American blackout were:
(i) "inadequate situational awareness" on the part of FirstEnergy; (ii) FirstEnergy's failure to "manage adequately tree growth in its transmission right-of-way"; and (iii) failure of the interconnected grid's reliability organizations to provide effective diagnostic support" [16].

In view of the report and that of other large scale power system outages [17-22], which started occurring since this period of deregulation and inception of modern reactive compensation schemes there is the utmost need to develop an improved power system status indicator. The status indicators could be in the form of thermal stability or voltage stability. However, since this research is focused primarily on reactive power compensation which is directly related to the power system voltage, this work will dwell on voltage stability based index. Existing voltage stability index models have been presented in [23, 24].

Considering the medium and long distance wheeling of bulk between various independent system operators (ISOs), regional transmitting organizations (RTOs), and over international boundaries, a novel bus VSI (Ls-index) suitable for medium and long

transmission line application using the pi-complex transmission line model has been developed [25-27]. The results obtained from applying Ls-index had been compared with L-index developed using two-machine transmission line model [24, 26]. The results showed the effect of interconnecting transmission line distances on power system stability status [24]. In this paper, a hybrid voltage stability index scheme will be presented after combining the applications of L-index and Ls-index since most power system networks are composed of a mix of short, medium, and long transmission lines.

This hybrid scheme will be applied with the Newton Raphson's (N-R) power flow model to determine the weak buses that require compensation. Thereafter, shunt FACTS device will be included in the N-R power flow model. With this new model, a new load flow result will be obtained and used to compute the hybrid voltage stability index. This will give an independent indication of power system status which can be read to determine the impact of the reactive compensation on the entire network. The compensation device can be set appropriate and if it is not given the desired support, it may be replaced.

The same model may be applied to the transmission line voltage stability index models [26] and used to determine which lines need compensation, level of compensation required and effects on a selected portion of, or the whole interconnected network. Some of the formulations and selection criteria as discussed by the authors earlier [24, 27] with IEEE 14 and 30 bus system will be modified and incorporated in the IEEE 300 bus system. The algorithm developed here also includes a feature to subdivide large networks into groups to enhance faster operation and closer monitoring. It is hoped that the outcome of this work will provide efficient tools for the determination of power system

status, ensure optimal utilization of the dynamic reactive power compensation devices, reduce system outages through improved system monitoring.

The remaining sections of the paper is arranged in the following manner. Section 5.2 presents review of shunt compensation devices. In section 5.3 is contained a justification of BVS used in shunt compensation application in power system. Section, 5.4 treats modeling a BVS index suitable for long transmission line utilization, and the inclusion of multi-shunt compensation devices into the N-R power flow model is treated in section 5.5. The implementation algorithm is developed in this section 5.6 and 5.7 exhibits simulated results for the test system and accompanying discussions. Finally, conclusions are given in section 5.8.

5.2 Review of Currently Used Shunt Compensation Devices

FACTS application in power systems may be classified under three major groupings – shunt, series, and combined devices. Shunt devices in use today are shunt static VAR compensator (SVC) and static synchronous shunt compensator (STATCOM). Series devices include thyristor controlled series capacitor (TCSC) and a voltage source inverter based static synchronous series compensator (SSSC). A combination of shunt-series converters forms unified power flow controller (UPFC), two or more series – series connected converters gives interline power flow controller (IPFC) and a shunt-series-series composite of three or more converters gives the generalized unified power flow controller (GUPFC) [28]. There are other emerging forms of FACTS devices aimed at addressing recent power system problems and reduction of cost. These include the

various brands of Dynamic VAR system (D-VAR) which is been championed by the American Superconductor team [29].

5.2.1 SVC Utilization in Present Power Systems

As a result of variation in power system loadings, reactive power balance in the grid has been difficult to achieve. This can result in unpredictable variations in voltage amplitude. Therefore, the utilization of a rapid operating SVC which dynamically injects or absorbs reactive power at its point of connection is desirable. SVC usage improves the voltage stability, line stability, and voltage collapse limits of interconnected power system [30]. SVC is the most acceptable form of a FACTS device. It is primarily composed of a stack of series connected anti-parallel thyristors for control, air core reactors, and AC capacitors for reactive actions and a step transformer to connect to the grid (Fig. 5.1). It works on the principles of thyristor switched capacitors and thyristor switched or controlled reactors [28, 30].

The ability of SVC to adequately take care of power system fluctuation is limited by the fact that its reactive power provision is dependent on the actual voltage at the point of connection and the cost considerations. The presence of banks of reactors and capacitors pose some operational problems.

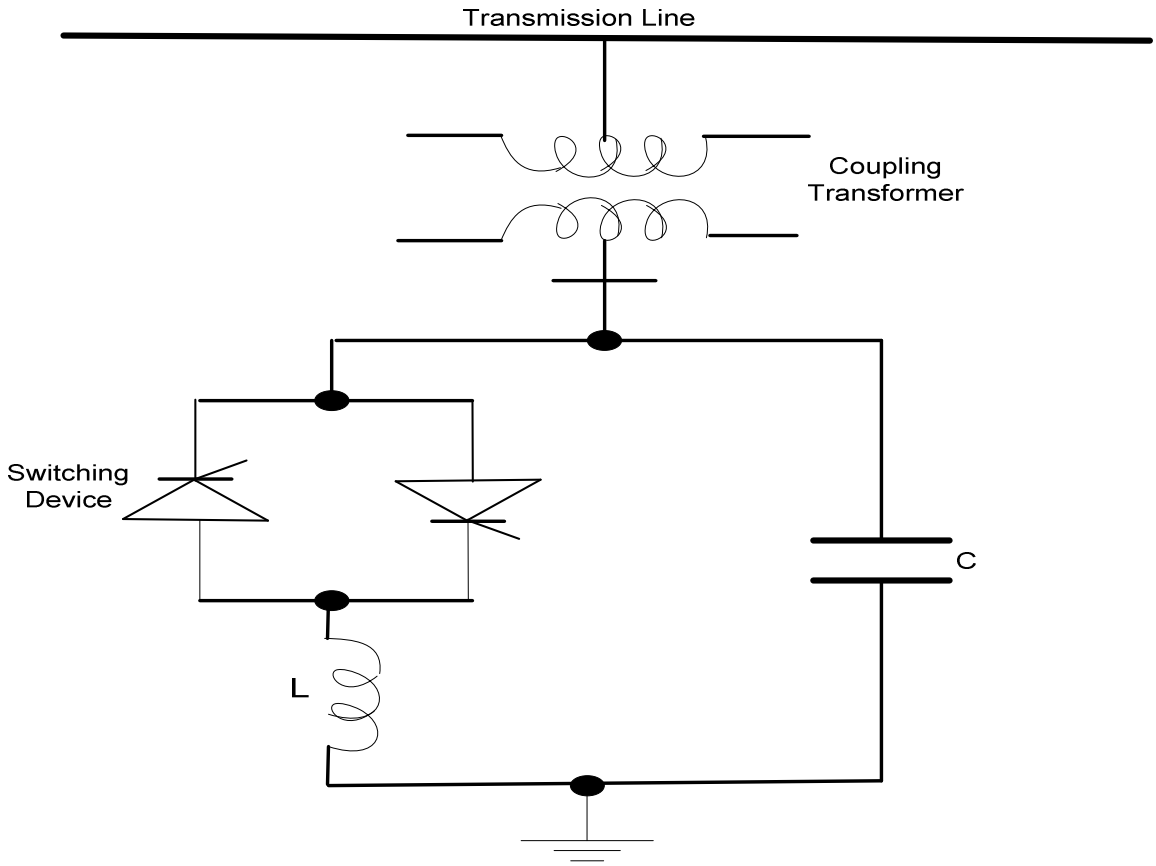

Fig. 5.1: SVC interconnection to a power transmission line

5.2.2 STATCOM Utilization in Power Systems

STATCOM (Fig. 5.2) is a class of SVC based on DC to AC solid state converter where the converter is controlled to behave like an idealized rotating machine. It is a member of the DC voltage source converter (VSC) based FACTS devices, which has become the most acceptable form of compensation devices. The DC voltage source may be a capacitor whose output voltage may be varied using the inverter semiconductor switching sequences or a battery with constant voltage supply. Earliest semiconductors utilized were the gate turn-off (GTO) thyristors and very recently integrated gate bipolar

transistor (IGBT), magnetic oxide semiconductor controlled thyristors (MCT), and integrated gate commutated thyristors (IGCT) have also been applied.

Similar to its precursor - the synchronous compensator - the STATCOM injects reactive power when its voltage output is in phase but greater than the voltage of the interconnected node (capacitive mode) and absorbs reactive power when its voltage is in phase but less than the voltage of the interconnected node (inductive mode). To increase the output of voltage source converter based STATCOM to meet transmission voltage of most power system networks; various multilevel converter based configurations and controls have been developed [31-37].

However like SVC, smooth operation of STATCOM is only achievable during normal operation when its voltage is in phase with the prevailing system voltage and the variation in load (reactive power demand) is within the operational limits of the STATCOM [38-40]. Therefore, in anticipation of unbalanced voltages resulting from unbalanced loads and system faults, an independent voltage stability index is required.

Similarly, series and combined FACTS devices provide reactive power compensation. Each configuration has its own merits and limitations. Details related to series and combined FACTS devices can be found in [28-30, 40-43]. From Table (5.1), shunt compensation accounts for 45% of number of installed FACTS devices and contributes to approximately 20% MVA capacity of FACTS devices worldwide.

Table 5.1: Estimated number & capacity of FACTS devices installed worldwide [28].

Type of Device	Number	Total Installed Power (MVA)
SVC	600	90,000
STATCOM	15	1,200
Series Compensation	700	350,000
TCSC	10	2,000
HVDC B2B	41	14,000
HVDC VSC B2B	8	900

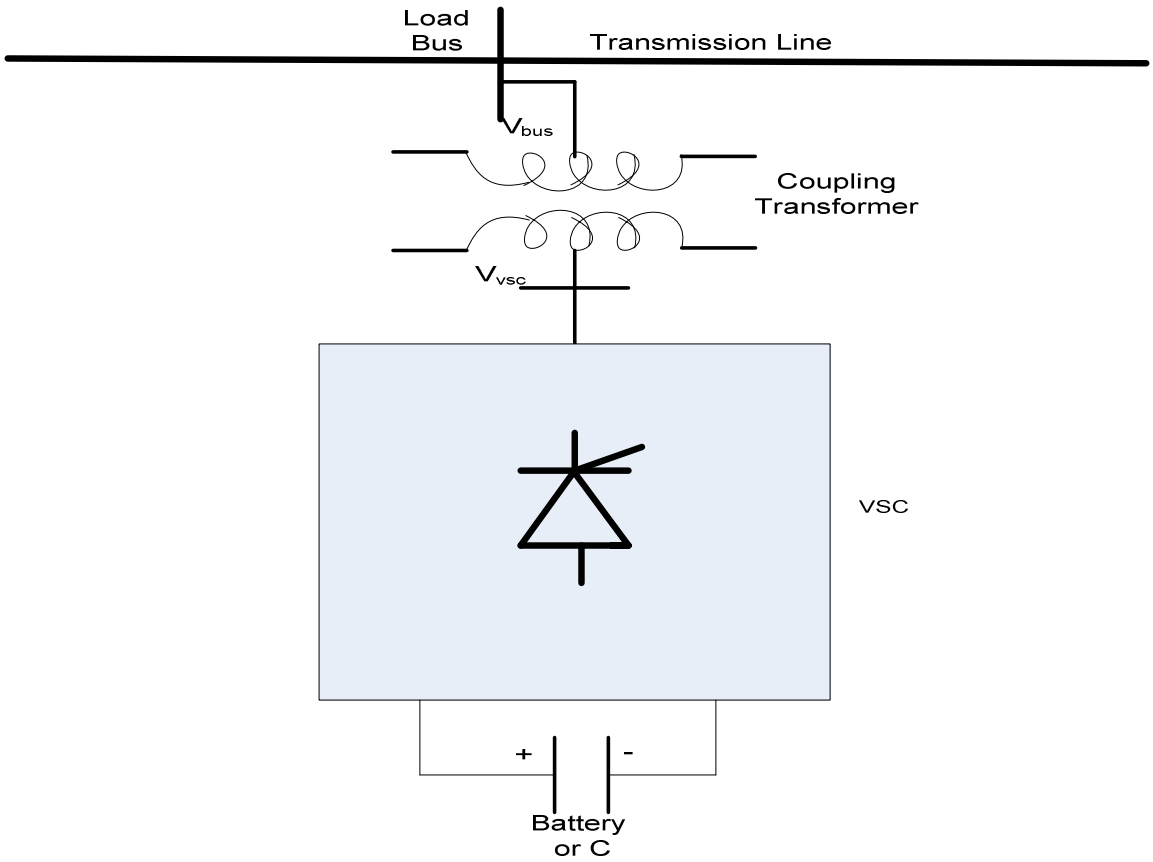

Fig. 5.2: STATCOM interconnection to a power transmission line

5.3 Justification for Use of BVS Index in Shunt Compensation Schemes

To be able to address the two critical issues stated as the major causes for the 2003 blackout – "inadequate situational awareness" and "failure of the interconnected grid's reliability organizations to provide effective diagnostic support," it is important to examine further the operational limitations of reactive power compensation devices as applied to present power system.

5.3.1 Cost of the FACTS Devices

The cost of procurement, installation, and maintenance of some of the FACTS devices reviewed are very exorbitant and economically non-viable from the commercial view point. Though SSSC, UPFC, IPFC, and GUPFC have been tested in pilot projects and considered very robust for the deregulated present day power industry, we saw from Table (5.1) that cases of practical installation are very insignificant. This has left system operators to continue making use of the simple, cheaper, and not too suitable compensation devices. Therefore, there is need to incorporate a status monitoring devices which will also guide in the appropriate setting the devices.

5.3.2 Problems of Developed Parallel and Series Circuit Resonances

In many of the devices reviewed, banks of capacitors and inductors were utilized which may lead to system resonance. The effect of this is considerably higher than normal, is primarily due to the fact that reactance of capacitor banks decreases with higher frequencies which make it to behave as a sink for higher harmonics currents. This

increases heating and dielectric stress of insulation materials. Parallel resonance circuits (Fig. 5.3) formed by the capacitance of capacitor banks and network inductances produce 10-15 times harmonic currents [44], while series resonance circuits (Fig. 4) lead to high voltage distortion levels at low voltage side of transformer. Presently due to cost considerations, reactive power required for compensation are either generated or absorbed by capacitor banks in Static VAR Compensators (SVCs) for voltage compensation, and in thyristor controlled series capacitors (TCSC) or reactor banks in thyristor controlled reactor for transmission impedance control. This leads to resonance in power system which is affected by dynamic nature of mostly nonlinear loads. The effective reactance of these loads interact with the capacitive reactance of the capacitor banks leading to mostly unpredictable resonances. This therefore calls for the need to introduce independent power system status indicators.

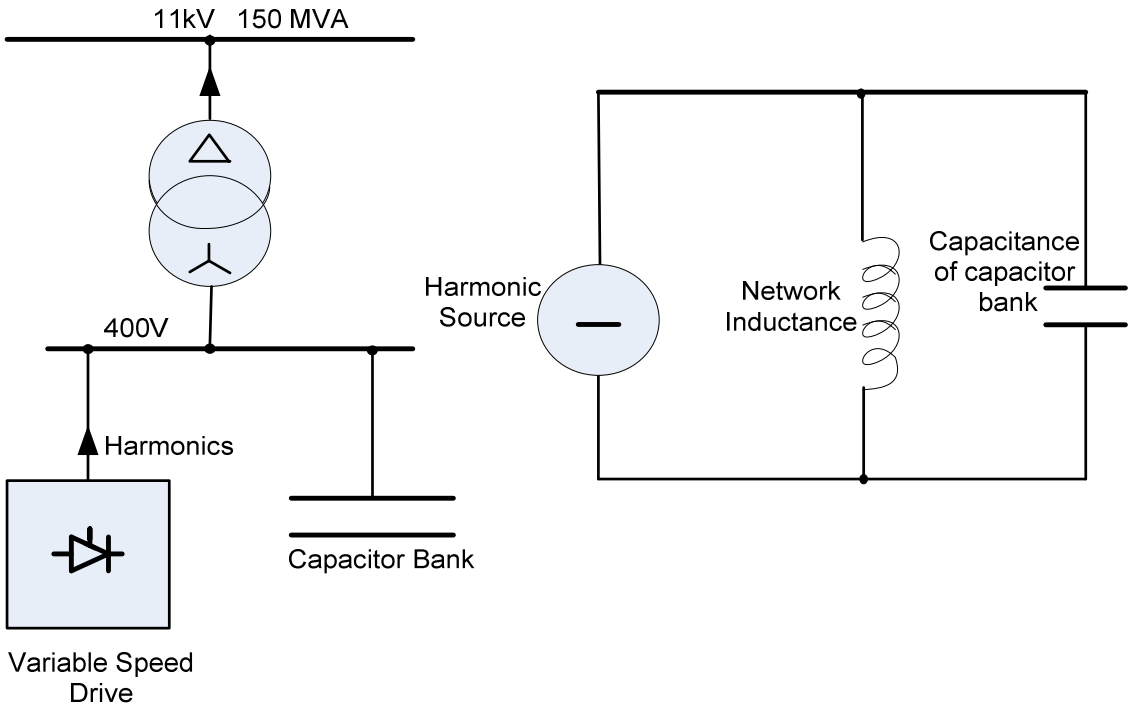

Fig. 5.3: (a) Parallel resonance circuit (b) Equivalent circuit

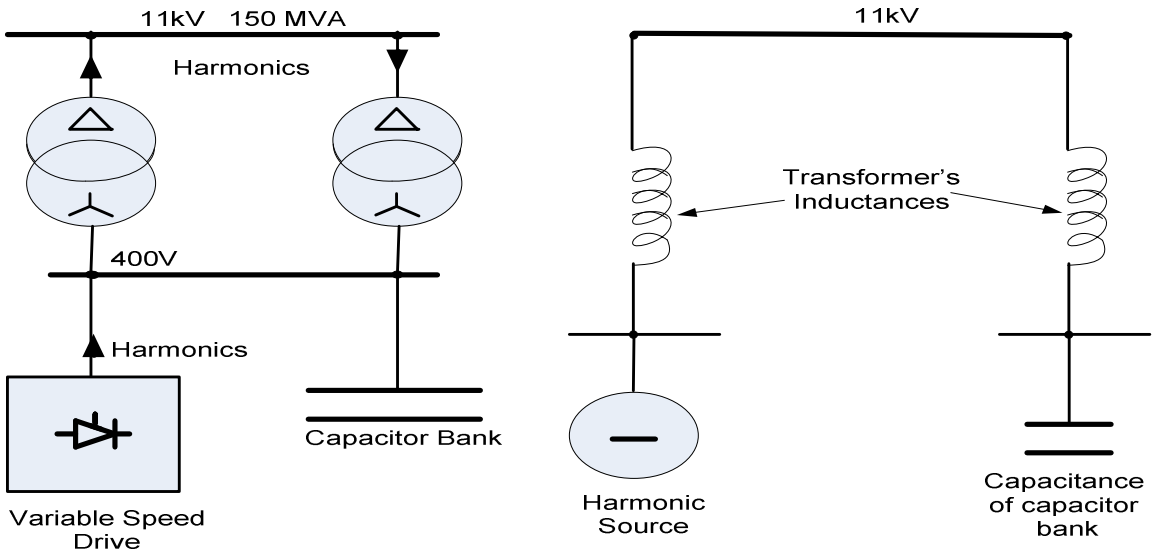

Fig. 5.4: (a) Series resonance circuit (b) Equivalent circuit

5.3.3 Problems of Harmonic Generation from Compensation Devices

Thyristors and diode rectifiers inject harmonics in utility and industrial networks which contribute significantly to deterioration of the power quality in networks [44]. In this paper, the theoretically computed and the measured AC-side values of the 5^{th} order harmonic currents in real network are 28% and 20%, respectively. Also, there was an increase in 5^{th} order harmonic current at reduced loading while the absolute values of the harmonic currents are higher under high load situation. The main effect of the harmonic currents and voltages in rotating machinery is increased heating caused by iron and copper losses emanating at harmonic frequency. The attendant consequences are reduced torque and machine efficiency. With this situation, actual generator outputs may vary significantly with design and operational values. To guide against inaccurate power system status computation, there is need to utilize indexes which give actual status of the system.

Another point is that harmonic filters are designed using the computed values and have no feature to automatically accommodate deviations. The work done in [44] showed that these theoretical design values do not in most cases correspond to actual power system operating harmonics which vary according to loading, fault level, and changing system parameter characterization. There is therefore the need to utilize independent system monitoring indexes.

5.3.4 Compensation Devices Not Suitable for Faulty Operating Conditions

Most compensation devices like the SVC and STATCOM for load bus application and the TCSC, TCR, and static synchronous series compensator (SSSC) for transmission line application are designed to operate under specified limits. These correspond to their normal conditions. However, during faulty conditions in the network, these devices give unreliable results. Due to the fast varying loading and near limit operating conditions of power systems presently, there is need to incorporate additional status monitoring scheme to be able to determine some of these abnormal situations and what will be the impact on the overall network when the safe bypass switches incorporated to protect these devices operate.

5.3.5 Effect of Reactive Power Compensation Not Localized

Generally, the present day power systems are composed of interconnected complex transmission lines, transformers, network compensators, and varied types of load and generator buses spanning regional and international barriers. To ensure that the

realization of the two basic objective of power system compensation, namely, increasing the power transfer capability of transmission systems and keeping power flow over designated routes [30], thyristor switches are utilized to control the combined reactive impedance of both the capacitor and reactor banks. This presents a variable reactive admittance to the transmission network and hence changes the characteristics of the system impedance. With this the overall system admittance matrix is affected and so do the entire network loop flows.

The absorption or injection of voltages at a given bus or transmission line in a large network by an SVC and the change of transmission angle by a phase-shifter at a node have proportionate impact on all portions of the network, thereby effecting its status. With privatization and competition, different ISOs and RTOs feel very uncomfortable to share their system operational conditions with adjoining competitors for economic and strategic reasons. So the only way to guarantee the stability of their local network is to incorporate mechanisms that will enable them to have a fairly good knowledge of both their local system and that of the entire network.

5.3.6 Ensuring Optimal Utilization of Emerging FACTS Devices

In an effort to reduce the cost of FACTS devices and address some of the present power system challenging problems, new FACTS devices have been developed in compact and modular forms. Some of the devices are been packaged in movable vehicular structures for relocation to sites of urgent need. With the upgrade to the voltage stability index and other power system status indicators, there will be easier determination of points that require reactive compensation or voltage support.

5.4 Modeling of Long Transmission System BVS Index

In an earlier effort to estimate the voltage stability of a power system, used a two machine transmission line structure was used to develop a short line voltage stability indicator (L-index) [23]

$$L = \max_{j \in \alpha_L} \{L_j\} = \max_{j \in \alpha_L} \left| 1 - \frac{\sum_{i \in \alpha_G} F_{jk} V_k}{V_j} \right| \tag{1}$$

where

$$F_{jk} = -[Y_{jk}][Y_{jj}]^{-1} \tag{2}$$

The L-index was validated when it was compared with the voltage ratio index to determine the strength of each of the buses in IEEE 14 bus network [24]. However, the authors went further in [26] to develop an algorithm which made it possible to consider the effect on longer transmission line distances in the voltage stability of a given network.

In view of the long distance bulk wheeling of power between different ISOs and RTOs due to seasonal and hourly difference in power generation and peak load demand as well as reduced cost in remote generations, it became necessary to further consider the effect of transmission line distances on the voltage stability index models [25]. Therefore, a complex long transmission line structure as presented in Fig. (5.5) is now used to development of a new Ls-index.

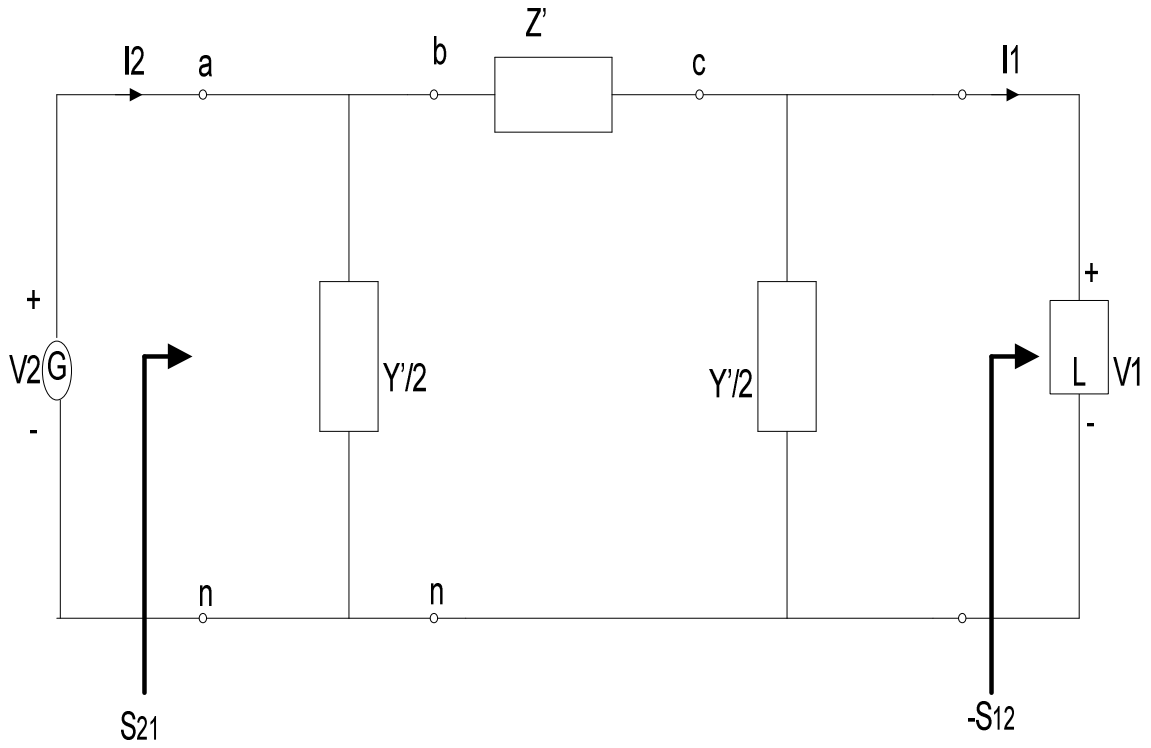

Fig. 5.5: Transmission Line Complex Pi-Model [25]

The line parameters are defined hereunder.

Modified total line series impedance, $Z' = Z_c \sinh \gamma l = Z \dfrac{\sinh \gamma l}{\gamma l}$

Modified total line-neutral admittance, $\dfrac{Y'}{2} = yl = \dfrac{Y}{2} \dfrac{\tanh(\gamma l / 2)}{\gamma l / 2}$

The characteristic impedance, $Z_c = \sqrt{\dfrac{z}{y}}$

Propagation constant, $\gamma = \sqrt{yz}$

For typical power lines, $\frac{\sinh \gamma}{\gamma l} \approx 1$ and when detailed line data are not known, the modified total series impedance and line-neutral admittance are taking approximately equal to the total line series line impedance and line-neutral admittance respectively.

5.4.1 Single-node Model

With the above definitions and from Fig. (5.1), the sending end and receiving end complex power are given from [25] as

$$S_2 = S_{21} = \frac{Y'^*}{2}|V_2|^2 + \frac{|V_2|^2}{Z'^*} - \frac{V_2 V_1}{Z'^*} \tag{3}$$

The receiving end complex power becomes

$$S_1 = S_{12} = \frac{Y'^*}{2}|V_1|^2 + \frac{|V_1|^2}{Z'^*} - \frac{V_1 V_2}{Z'^*} \tag{4}$$

Equation (4) represents the complex power at node 1 (load bus) whose voltage is of interest. The basic equations developed in the derivation of medium and long transmission line voltage stability index (Ls-index) using similar approach adopted in [26] are presented hereafter.

$$\frac{S_1}{V_1} = \frac{Y'^*}{2}\frac{|V_1|^2 V_1^*}{V_1 V_1^*} + \frac{|V_1|^2 V_1^*}{Z'^* V_1 V_1^*} - \frac{V_2}{Z'^*} \tag{5}$$

$$\frac{S_1}{V_1} = V_1^*\left(\frac{Y'^*}{2} + \frac{1}{Z'^*}\right) - \frac{V_2}{Z'^*} \tag{6}$$

Letting $M_{11} = \frac{Y'^*}{2} + \frac{1}{Z'^*}$ and $M_{12} = \frac{1}{Z'^*}$ in equation, we get

$$\frac{S_1}{M_{11}} = V_1^* V_1 - \frac{M_{12}V_2}{M_{11}} V_1 = a_1 + jb_1 \tag{7}$$

Letting $V_{01} = -\frac{M_{12}}{M_{11}} V_2$, Equation (7) gives

$$|V_1|^2 + V_{01}V_1^* = \frac{S_1}{M_{11}} = a_1 + jb_1 \tag{8}$$

Defining $V_{01} = x_0 + jy_0$ and $V_1 = x_1 + jy_1$

Equation (8) gives

$$|V_1|^2 - a_1 + x_0x_1 - y_0y_1 = j(b_1 - x_0y_1 - y_0x_1) \tag{9}$$

$$x_0x_1 - y_0y_1 = a_1 - |V_1|^2 \tag{10}$$

$$x_0y_1 + y_0x_1 = b_1 \tag{11}$$

$$x_0^2x_1^2 + y_0^2y_1^2 - 2x_0x_1y_0y_1 = a_1^2 - 2a_1|V_1|^2 + |V_1|^4 \tag{12}$$

$$x_0^2y_1^2 + y_0^2x_1^2 + 2x_0x_1y_0y_1 = b_1^2 \tag{13}$$

Adding Equations (12) and (13) gives

$$x_0^2x_1^2 + y_0^2y_1^2 + x_0^2y_1^2 + y_0^2x_1^2 = a_1^2 + b_1^2 - 2a_1|V_1|^2 + |V_1|^4 \tag{14}$$

$$\left(x_1^2 + y_1^2\right)\left(x_0^2 + y_0^2\right) = a_1^2 + b_1^2 - 2a_1|V_1|^2 + |V_1|^4 \tag{15}$$

$$|V_1|^2|V_{01}|^2 = a_1^2 + b_1^2 - 2a_1|V_1|^2 + |V_1|^4 \tag{16}$$

$$|V_1|^2 = \frac{(2a_1 + |V_{01}|^2) \pm \sqrt{(2a_1 + |V_{01}|^2)^2 - 4(a_1^2 + b_1^2)}}{2} \tag{17}$$

$$|V_1| = \sqrt{\frac{|V_{01}|^2}{2} + a_1^2 \pm \sqrt{\left(\frac{|V_{01}^4|}{4} + a_1|V_{01}|^2 - b_1^2\right)}} \tag{18}$$

From [23], it was deduced that the stability limit of the two-node system which we are considering here lies at the border line satisfying the discriminant of Equation (18) given as

$$\sqrt{\left(\frac{\left|V_{01}^{4}\right|}{4}+a_1\left|V_{01}\right|^{2}-b_1^{2}\right)}=0 \tag{19}$$

With the aid of complex transformation, Equation (19) gives

$$\left|1+\frac{V_{01}}{V_1}\right|=1 \tag{20}$$

Equation (19) is used to define an index for computation of closeness of load buses to voltage stability limit given as

$$L_1=\left|1+\frac{V_{01}}{V_1}\right| \tag{21}$$

5.4.2 Multi-Node System Voltage Stability Index

Since a typical power system involves a large number of load buses, the above two machine model has to be extended to cover such a large system. To achieve this, the hybrid (H) matrix scheme has been severally adopted. H-matrix is represented as [23]

$$\begin{bmatrix} V^{L} \\ I^{G} \end{bmatrix}=\begin{bmatrix} Z^{LL} & F^{LG} \\ K^{GL} & Y^{GG} \end{bmatrix}\begin{bmatrix} I^{L} \\ V^{G} \end{bmatrix} \tag{22}$$

where

$$H=\begin{bmatrix} Z^{LL} & F^{LG} \\ K^{GL} & Y^{GG} \end{bmatrix} \tag{23}$$

$H_{11} = \sum_{k \in \alpha_L} Z_{jk}$ represents the aggregate impedance connecting other load buses to load bus of focus. $H_{12} = \sum_{k \in \alpha_G} \frac{Y_{jk}}{Y_{jj}}$ is a dimensionless ratio of the net-admittance to the sum of the admittance linking the generator buses to the load bus of interest. With this hybrid matrix, we get the load bus voltage as

$$V_j = \sum_{k \in \alpha_L} Z_{jk} I_k + \sum_{k \in \alpha_G} \frac{Y_{jk}}{Y_{jj}} V_k \tag{24}$$

Defining $V_{0j} = -\sum_{k \in \alpha_G} \frac{Y_{jk}}{Y_{jj}} V_k$, the present derivation is given by

$$V_{0j} = -\sum_{k \in \alpha_G} \frac{M_{jk}}{M_{jj}} V_k \tag{25}$$

$$\left|V_j\right|^2 + V_{0j} V_j^* = \frac{S_j^*}{Y_j} \tag{26}$$

Therefore, for a given load bus j in a multi-system, its proximity to collapse could be computed similar to that for two machine model as

$$L_j = \left| 1 + \frac{V_{0j}}{V_j} \right| \tag{27}$$

Hence, a new generalized index for computation of proximity to voltage collapse for load buses in medium and long lines which are the predominant cases in power pooling could be written as

$$L_{sys} = \sum_{l \in \alpha_L} \max \left| 1 - \frac{\sum_{k \in \alpha_G} \frac{M_{lk}}{M_{ll}} V_k}{V_l} \right| \tag{28}$$

5.4.3 Modification of the Original L-Index

To further make the computation of the bus voltage collapse index L-index, consideration of the fact that the net contribution resistance to the impedance of the medium and long transmission lines to the self-admittance of each bus is negligible when compared with that of the reactance. Therefore, the hybrid term of $F_{ji} = -\left[Y_{jj}\right]^{-1} Y_{ji}$ was reduced to $F_{ji}^{1} = -\left[B_{jj}\right]^{-1} Y_{ji}$. When this was substituted in the formulation for the L-index, we now obtain

$$L_S = \max_{j \in \alpha_L} \left\{ L_j \right\} = \max_{j \in \alpha_L} \left| 1 - \frac{\sum_{i \in \alpha_G} F_{ji}^{1} V_k}{V_l} \right| \tag{29}$$

5.5 Inclusion of Shunt Devices in Newton-Raphson's Load Flow Model Newton's Power Flow Model

The basic real and reactive power flow equations for a transmission line between buses 'p' and 'q' as

$$P_p = \sum_{q=1}^{N} \left| V_p \right\| V_q \left| \left(G_{pq} \cos \theta_{pq} + \mathbf{B}_{pq} \sin \theta_{pq} \right) \right. \tag{30}$$

$$Q_p = \sum_{q=1}^{N} \left| V_p \right\| V_q \left| \left(G_{pq} \sin \theta_{pq} - \mathbf{B}_{pq} \cos_{pq} \right) \right. \tag{31}$$

For p=1, 2, 3 . . . N,

The Newton power flow equation in polar coordinate is written as

$$\begin{bmatrix} \frac{\partial P_p}{\partial \theta_p} & \frac{\partial P_p}{\partial V_p} \\ \frac{\partial Q_p}{\partial \theta_p} & \frac{\partial Q_p}{\partial V_p} \end{bmatrix} \begin{bmatrix} \Delta\theta_p \\ \Delta V_p \end{bmatrix} = -\begin{bmatrix} \Delta P_p \\ \Delta Q_p \end{bmatrix} \tag{32}$$

5.5.1 Multi-STATCOM Structure in Newton Power Flow

When a STATCOM is connected to a bus as shown in Figures (5.6) and (5.7), the equations representing real and reactive the power exchange between the bus and STATCOM are given by

$$P_{sh} = V_p{}^2 G_{sh} - V_p V_{sh} \left(G_{sh} \cos\left(\theta_p - \theta_{sh}\right) - B_{sh} \sin\left(\theta_p - \theta_{sh}\right)\right) \tag{33}$$

$$Q_{sh} = -V_p{}^2 G_{sh} - V_p V_{sh} \left(G_{sh} \sin\left(\theta_p - \theta_{sh}\right) - B_{sh} \cos\left(\theta_p - \theta_{sh}\right)\right) \tag{34}$$

Because STATCOM is primarily utilized for reactive power compensation or bus voltage enhancement, a major consideration is to ensure that the net active power exchange is made close to zeros as much as possible to ensure maximum reactive power flow. Hence, active power exchange (PE) becomes a control given as

$$PE = V_p{}^2 G_{sh} - V_p V_{sh} \left(G_{sh} \cos\left(\theta_p - \theta_{sh}\right) - B_{sh} \sin\left(\theta_p - \theta_{sh}\right)\right) = 0 \tag{35}$$

Equation (35) is one of the two equations required for the inclusion of STATCOM in the power flow model of Newton's equation.

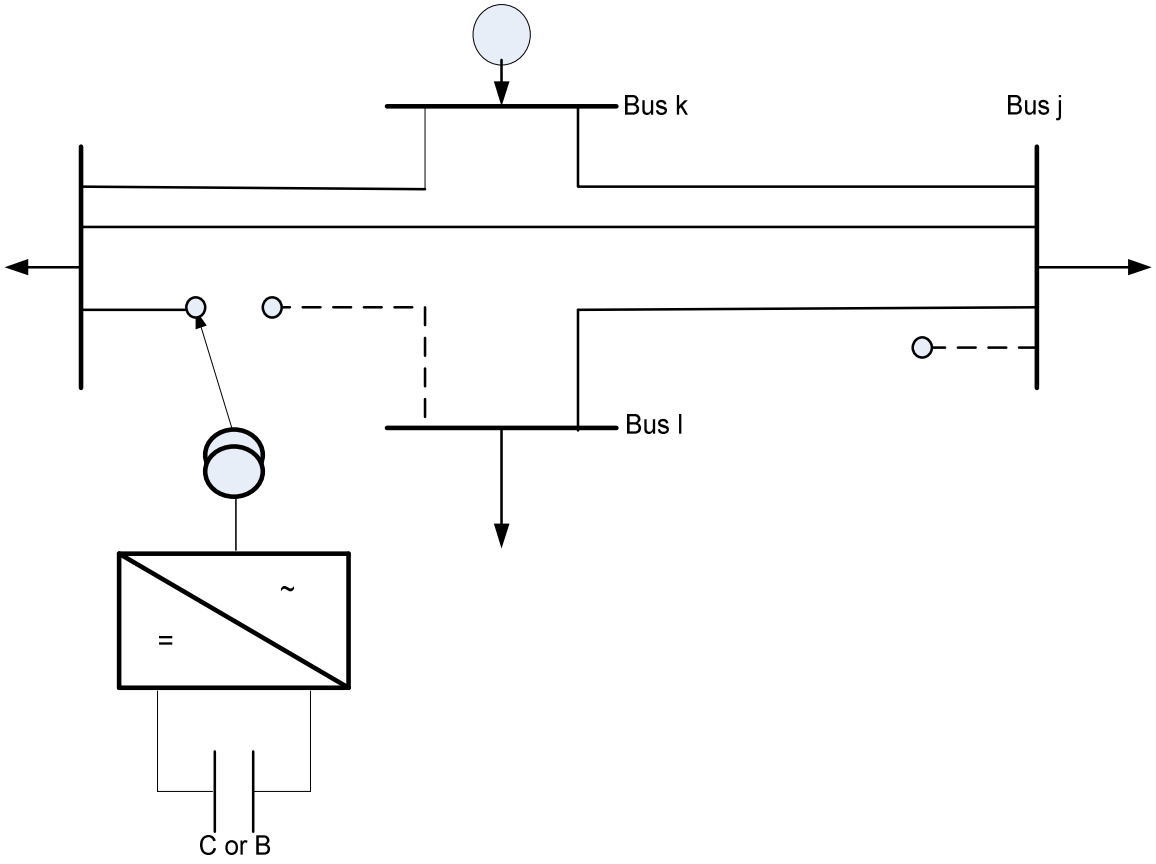

Fig. 5.6: Multi-STATCOM in power system network

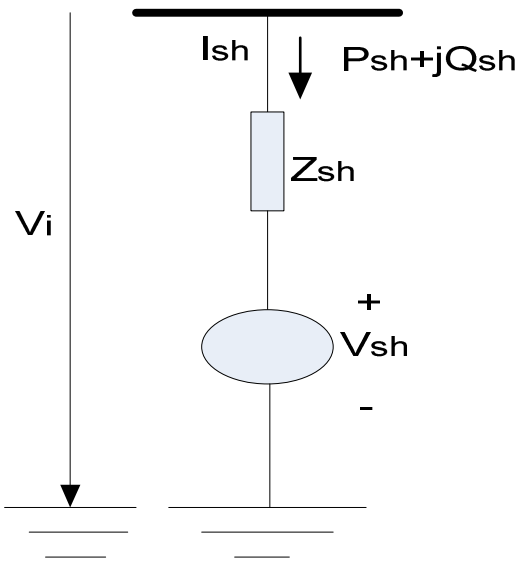

Fig. 5.7: STATCOM equivalent circuit

5.5.2 Utilizing STATCOM Power System Control Functions

The second important equation is selected from one of the STATCOM control functions F(x) given in Equations (36) to (42).

(a) Control of reactive power injection to connected bus given by

$$Q_{sh} - Q_{sh}^{spec} = 0 \tag{36}$$

where Q_{sh} is as stated in Equation (34).

(b) Control of load bus voltage magnitude

$$V_p - V_p^{spec} = 0 \tag{37}$$

(c) Control of equivalent STATCOM injected voltage magnitude

$$V_{sh} - V_{sh}^{spec} = 0 \tag{38}$$

(d) Control of STATCOM reactive impedance

$$X_{pq} - X_{pq}^{spec} = 0 \tag{39}$$

(e) Control of leading or lagging current magnitude

The capacitive (leading current) control mode is given by

$$\mathrm{Re}\left(I_{sh}^{spec} \angle \left(\theta_{sh} + 90^0\right)\right) = \mathrm{Re}\left(\left(V_p - V_{sh}\right) / Z_{sh}\right)$$

$$\Rightarrow \mathrm{Im}\left(I_{sh}^{spec} \angle \left(\theta_{sh}^{spec} + 90^0\right)\right) = \mathrm{Im}\left(\left(V_p - V_{sh}\right) / Z_{sh}\right) \tag{40}$$

Inductive (lagging current) control mode is represented as

$$\mathrm{Re}\left(I_{sh}^{spec} \angle \left(\theta_{sh} - 90^0\right)\right) = \mathrm{Re}\left(\left(V_p - V_{sh}\right) / Z_{sh}\right)$$

$$\Rightarrow \mathrm{Im}\left(I_{sh}^{spec} \angle \left(\theta_{sh}^{spec} - 90^0\right)\right) = \mathrm{Im}\left(\left(V_p - V_{sh}\right) / Z_{sh}\right) \tag{41}$$

(f) Control of local load bus apparent power

$$S_{pq} - S_{pq}^{spec} = 0 \tag{42}$$

The control functions of the STATCOM of Equations (36)–(42) are combined to get the generalized control function denoted as

$$\Delta E(x) = E(x) - E(x)^{spec} \tag{43}$$

where $x = \lfloor \theta_p, V_p, \theta_{sh}, V_{sh} \rfloor$

5.5.3 Derivation of the STATCOM Jacobian Matrix

In the formulation of the Jacobian matrix of the STATCOM, the equations used are the active power net-zeros exchange of Equation (35) and the STATCOM reactive power given in Equation (36). Adding the partial derivatives of these two equations into the Newton's Jacobian matrix of Equation (32), we obtained the generalized multi-STATCOM Jacobian as indicated in Equation (44).

$$[J] = \begin{bmatrix} \frac{\partial P_p}{\partial \theta_p} & \frac{\partial P_p}{\partial V_p} & \frac{\partial P_p}{\partial \theta_{sh}} & \frac{\partial P_p}{\partial V_{sh}} \\ \frac{\partial Q_p}{\partial \theta_p} & \frac{\partial Q_p}{\partial V_p} & \frac{\partial Q_p}{\partial \theta_{sh}} & \frac{\partial Q_p}{\partial V_{sh}} \\ \frac{\partial PE}{\partial \theta_p} & \frac{\partial PE}{\partial V_p} & \frac{\partial PE}{\partial \theta_{sh}} & \frac{\partial PE}{\partial V_{sh}} \\ \frac{\partial E}{\partial \theta_p} & \frac{\partial E}{\partial V_p} & \frac{\partial E}{\partial \theta_{shq}} & \frac{\partial E}{\partial V_{sh}} \end{bmatrix} \tag{44}$$

where

$$[J] = \begin{bmatrix} J1 & J2 & J3 & J4 \\ J5 & J6 & J7 & J8 \\ J9 & J10 & J11 & J12 \\ J13 & J14 & J15 & J16 \end{bmatrix}$$

The unique arrangement of the multi-STATCOM Jacobian matrix above to ensure a complete load flow program for implementation of a power system network having more than one STATCOM interconnected is illustrated by the expansion of the Jacobian of (44) as

$$\left[J_{\exp}\right]=\begin{bmatrix} \frac{\partial P_1}{\partial \theta_1} & \cdots & \frac{\partial P_1}{\partial \theta_{N-1}} & \frac{\partial P_1}{\partial V_1} & \cdots & \frac{\partial P_1}{\partial V_{N-1}} & \frac{\partial P_1}{\partial \theta_{sh}} & \frac{\partial P_1}{\partial V_{sh}} \\ \vdots & \cdots & \vdots & \vdots & \cdots & \vdots & \vdots & \vdots \\ \frac{\partial P_{N-1}}{\partial \theta_1} & \cdots & \frac{\partial P_{N-1}}{\partial \theta_{N-1}} & \frac{\partial P_{N-1}}{\partial V_1} & \cdots & \frac{\partial P_{N-1}}{\partial V_{N-1}} & \frac{\partial P_{N-1}}{\partial \theta_{sh}} & \frac{\partial P_{N-1}}{\partial V_{sh}} \\ \frac{\partial Q_1}{\partial \theta_1} & \cdots & \frac{\partial Q_{N-1}}{\partial \theta_{N-1}} & \frac{\partial Q_1}{\partial V_1} & \cdots & \frac{\partial Q_1}{\partial V_{N-1}} & \frac{\partial Q_1}{\partial \theta_{sh}} & \frac{\partial Q_1}{\partial V_{sh}} \\ \vdots & \cdots & \vdots & \vdots & \cdots & \vdots & \vdots & \vdots \\ \frac{\partial Q_{N-1}}{\partial \theta_1} & \cdots & \frac{\partial Q_{N-1}}{\partial \theta_{N-1}} & \frac{\partial Q_{N-1}}{\partial V_1} & \cdots & \frac{\partial P_{N-1}}{\partial V_{N-1}} & \frac{\partial Q_{N-1}}{\partial \theta_{sh}} & \frac{\partial Q_{N-1}}{\partial V_{sh}} \\ \frac{\partial PE}{\partial \theta_1} & \cdots & \frac{\partial PE}{\partial \theta_{N-1}} & \frac{\partial PE}{\partial V_1} & \cdots & \frac{\partial PE}{\partial V_{N-1}} & \frac{\partial PE}{\partial \theta_{sh}} & \frac{\partial PE}{\partial V_{sh}} \\ \frac{\partial E}{\partial \theta_1} & \cdots & \frac{\partial E}{\partial \theta_{N-1}} & \frac{\partial E}{\partial V_1} & \cdots & \frac{\partial E}{\partial V_{N-1}} & \frac{\partial E}{\partial \theta_{sh}} & \frac{\partial E}{\partial V_{sh}} \end{bmatrix} \tag{45}$$

The generalized dimension for each of these Jacobian matrices where the slack bus is removed for the full Newton Raphson's model and the system has N buses is as follows J1=J2=J5=J6 has size of [(N-1) x (N-1)]; J3=J4=J7=J8 has size of [(N-1) x 1]; J9=J10=J13=J14 has size of [1 x (N-1)] and J11=J12=J15=J16 has size of [1 x 1], respectively. This arrangement gives the over all dimension of $\left[J\right]$ to be [2N x 2N] and the number of known and unknown variables are 2N as well.

However, to make the appropriate use of the multi-STATCOM connection and consider situations where more than one STATCOM are installed in networks, each of the J

terms in Equation (45) should be made to vary according to the number of buses in the network. To speed up computation and save storage space, the program was developed to avoid computations involving zeros and the each result stored in sparse form. With this arrangement of the Jacobian, the Newton power flow equation in polar coordinate now becomes

$$[J]\begin{bmatrix} \Delta\theta_1 \\ \cdot \\ \cdot \\ \Delta\theta_{N-1} \\ \Delta V_1 \\ \cdot \\ \cdot \\ \Delta V_{N-1} \\ \Delta\theta_{sh} \\ \Delta V_{sh} \end{bmatrix} = -\begin{bmatrix} \Delta P_1 \\ \cdot \\ \cdot \\ \Delta P_{N-1} \\ \Delta Q_1 \\ \cdot \\ \cdot \\ \Delta Q_{N-1} \\ \Delta PE \\ \Delta E \end{bmatrix} \tag{46}$$

$$\begin{bmatrix} \Delta\theta_1 \\ \cdot \\ \cdot \\ \Delta\theta_2 \\ \Delta V_1 \\ \cdot \\ \cdot \\ \Delta V_{N-1} \\ \Delta\theta_{sh} \\ \Delta V_{sh} \end{bmatrix} = -([J])^{-1}\begin{bmatrix} \Delta P_1 \\ \cdot \\ \cdot \\ \Delta P_{N-1} \\ \Delta Q_1 \\ \cdot \\ \cdot \\ \Delta Q_N \\ \Delta PE \\ \Delta E \end{bmatrix} \tag{47}$$

In the above derivation, the known quantities are

$$P_p = P_p^{gen} - P_p^{load} \tag{48}$$

$$Q_p = Q_p^{gen} - Q_p^{load} \tag{49}$$

$$P_p^{cal}(x) = \sum_q^N V_p V_q (G_{pq} \cos(\theta_p - \theta_q) + B_{pq} \sin(\theta_p - \theta_q)) \quad (50)$$

$$Q_p^{cal}(x) = \sum_q^N V_p V_q (G_{pq} \sin(\theta_p - \theta_q) - B_{pq} \cos(\theta_p - \theta_q)) \quad (51)$$

$$\Delta P_p = P_p - P_p^{cal}(x) \quad (52)$$

$$\Delta Q_p = Q_p - Q_p^{cal}(x) \quad (53)$$

$$\Delta E = E(x) - E(x)^{spec} \quad (54)$$

$$\Delta PE = PE(x) - PE^{spec} \quad (55)$$

The Jacobian entries are given by

$$J1 = \frac{\partial P_p}{\partial \theta_p} = V_p V_q (G_{pq} \sin\theta_{pq} - B_{pq} \cos\theta_{pq}) \quad (56)$$

$$J2 = \frac{\partial P}{\partial V_p} V_p = V_p V_q (G_{pq} \cos\theta_{pq} - B_{pq} \sin\theta_{pq}) \quad (57)$$

$$J3 = \frac{\partial P_p}{\partial \theta_{sh}} = V_p V_{sh} (G_{sh} \sin(\theta_p - \theta_{sh}) - B_{sh} \cos(\theta_p - \theta_{sh})) \quad (58)$$

$$J4 = \frac{\partial P_p}{\partial V_{sh}} V_{sh} = V_p V_{sh} (G_{sh} \cos(\theta_p - \theta_{sh}) - B_{sh} \sin(\theta_p - \theta_{sh})) \quad (59)$$

$$J5 = \frac{\partial Q_p}{\partial \theta_p} = -V_p V_q (G_{pq} \cos\theta_{pq} - B_{pq} \sin\theta_{pq}) \quad (60)$$

$$J6 = \frac{\partial Q_p}{\partial V_p} V_p = V_p V_q (G_{pq} \sin\theta_{pq} - B_{pq} \cos\theta_{pq}) \quad (61)$$

$$J7 = \frac{\partial Q_p}{\partial \theta_{sh}} = -V_p V_{sh} (G_{sh} \cos(\theta_p - \theta_{sh}) - B_{sh} \sin(\theta_p - \theta_{sh})) \quad (62)$$

$$J8 = \frac{\partial Q_p}{\partial V_{sh}} V_{sh} = V_p V_{sh}(G_{sh}\sin(\theta_p - \theta_{sh}) - B_{sh}\cos(\theta_p - \theta_{sh})) \quad (63)$$

From the active power exchange equation we obtain the $J9 - J12$ terms as

$$J9 = \frac{\partial PE(x)}{\partial \theta_p} = V_p V_{sh}(G_{sh}\sin(\theta_p - \theta_{sh}) - B_{sh}\cos(\theta_p - \theta_{sh})) \quad (64)$$

$$J11 = \frac{\partial PE(x)}{\partial \theta_{sh}} = -V_p V_{sh}(G_{sh}\sin(\theta_p - \theta_{sh}) + B_{sh}\cos(\theta_p - \theta_{sh})) \quad (65)$$

$$J12 = \frac{\partial PE(x)}{\partial V_{sh}} V_{sh} = -2V_{sh}^2 G_{sh} - V_p V_{sh}(G_{sh}\cos(\theta_p - \theta_{sh}) - B_{sh}\sin(\theta_p - \theta_{sh})) \quad (66)$$

Utilizing the STATCOM reactive power equation as the control function we obtain the $J13 - J16$ terms by taking the partials of Equation (67).

$$E(x) = -V_p^2 B_{sh} - V_p V_{sh}(G_{sh}\sin(\theta_p - \theta_{sh}) - B_{sh}\cos(\theta_p - \theta_{sh})) \quad (67)$$

$$J13 = \frac{\partial E(x)}{\partial \theta_p} = -V_p V_{sh}(G_{sh}\cos(\theta_p - \theta_{sh}) + B_{sh}\sin(\theta_p - \theta_{sh})) \quad (68)$$

$$J14 = \frac{\partial E(x)}{\partial V_p} V_p = -2V_p^2 - V_p V_{sh}(G_{sh}\sin(\theta_p - \theta_{sh}) - B_{sh}\cos(\theta_p - \theta_{sh})) \quad (69)$$

$$J15 = \frac{\partial E(x)}{\partial \theta_{sh}} = V_p V_{sh}(G_{sh}\cos(\theta_p - \theta_{sh}) + B_{sh}\sin(\theta_p - \theta_{sh})) \quad (70)$$

$$J16 = \frac{\partial E(x)}{\partial V_{sh}} V_{sh} = -V_p V_{sh}(G_{sh}\sin(\theta_p - \theta_{sh}) - B_{sh}\cos(\theta_p - \theta_{sh})) \quad (71)$$

In the matrix form, this can be written as (72)

$$\begin{bmatrix} \theta_1^{t+1} \\ . \\ . \\ \theta_{N-1}^{t+1} \\ V_1^{t+1} \\ . \\ . \\ V_{N-1}^{t+1} \\ \theta_{sh}^{t+1} \\ V_{sh}^{t+1} \end{bmatrix} = \begin{bmatrix} \theta_1^{t} \\ . \\ . \\ \theta_{N}^{t} \\ V_{N-1}^{t} \\ . \\ . \\ V_{N-1}^{t} \\ \theta_{sh}^{t} \\ V_{sh}^{t} \end{bmatrix} + \begin{bmatrix} \Delta\theta_1^{t} \\ . \\ . \\ \Delta\theta_{N-1}^{t} \\ V_1^{t} \\ . \\ . \\ V_{N-1}^{t} \\ \Delta\theta_{sh}^{t} \\ \Delta V_{sh}^{t} \end{bmatrix} \tag{72}$$

This was then checked for limits; if violated reset the limits violated and run the load flow until convergence was achieved.

In running the program, the row and column entries relating to the slack bus were deleted since its voltage was already known.

5.6 Scheme Implementation Algorithm

The implementation process involved development of the power system Newton-Raphson's load flow model equations with both the load bus voltage stability indexes. Then an associated MATLAB-based program was developed and simulated to determine the stability status of the required load bus or the transmission line. A summarized operational algorithm is shown in Fig. (5.8).

A decision was made based on the computed status from index value whether there is any bus or line within the zone of interest that requires compensation. If there is, then appropriate shunt device was incorporated into the N-R load flow model. The next step

involved check for the settings of the FACTS devices. At this point the system asks if the operator requires dynamic simulation or a rerun of the load flow steady state simulation.

If the dynamic simulation is required, the program shifts the routine to the dynamic module and displays the result for the dynamic results and then goes back to read system input data if not prompted to stop. Also, the steady state load flow and setting of the FACTS values continue thereby ensuring that the power system runs in optimal conditions. The simulation stops when prompted.

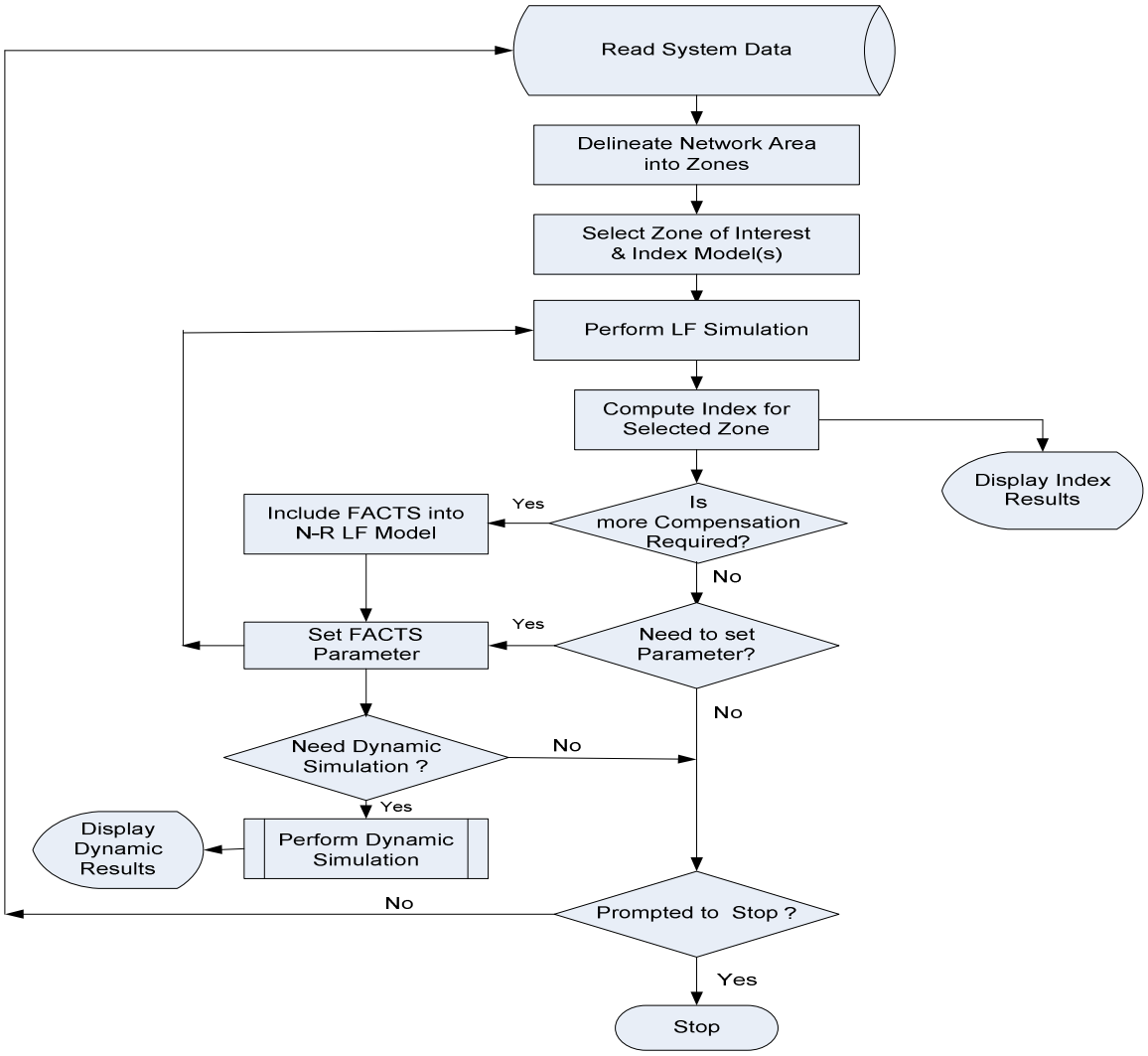

Fig. 5.8: Voltage stability index FACTS scheme implementation algorithm

A decision is made based on the computed status from index value whether there is any bus or line within the zone of interest that requires compensation. If there is, then appropriate FACTS device (shunt or series) is incorporated into the N-R load flow model.

The next step involves check for the settings of the FACTS devices. At this point the system asks if the operator requires dynamic simulation or a rerun of the load flow steady state simulation. If the dynamic simulation is required, the program shifts the routine to the dynamic module and displays the result for the dynamic results and then goes back to read system input data if not prompted to stop. Also, the steady state load flow and setting of the FACTS values continue thereby ensuring that the power system runs in optimal conditions. The simulation stops when prompted.

5.7 Results and Discussions

The bus voltage stability status obtained from the steady state MATLAB power flow program using Newton Raphson's approach for the entire IEEE 300 bus system is depicted in Fig. (5.9). An index value of '1' indicates that the bus is definitely unstable while a value of '0' indicates extreme stability. The weakest bus is denoted as "FlashPoint" and it is prone to initiate system outage. The corresponding bus number and its operating status are indicated at the top of the plot.

To increase the efficiency of the computation scheme and show the dynamism of the developed model to adequately provide wide area monitoring of any network size, the entire network was grouped into five zones. Each of the zones had a span comprising 60 buses and the zones were arranged sequentially from 'A' through 'E'.

The results obtained are classified under normal system, 10% overloaded with base STATCOM setting and overloaded with increased STATCOM magnitude.

5.7.1 Normal System Loading

The results obtained for the five zones under base loading are depicted in Figures (5.10) through (5.14). Provision was also made to accommodate further zonings or special interest re-arrangement of the network. This feature is ably captured in the result displayed in Fig. (5.20) where only part of zone "B" ranging from bus 100 to bus 120 is shown.

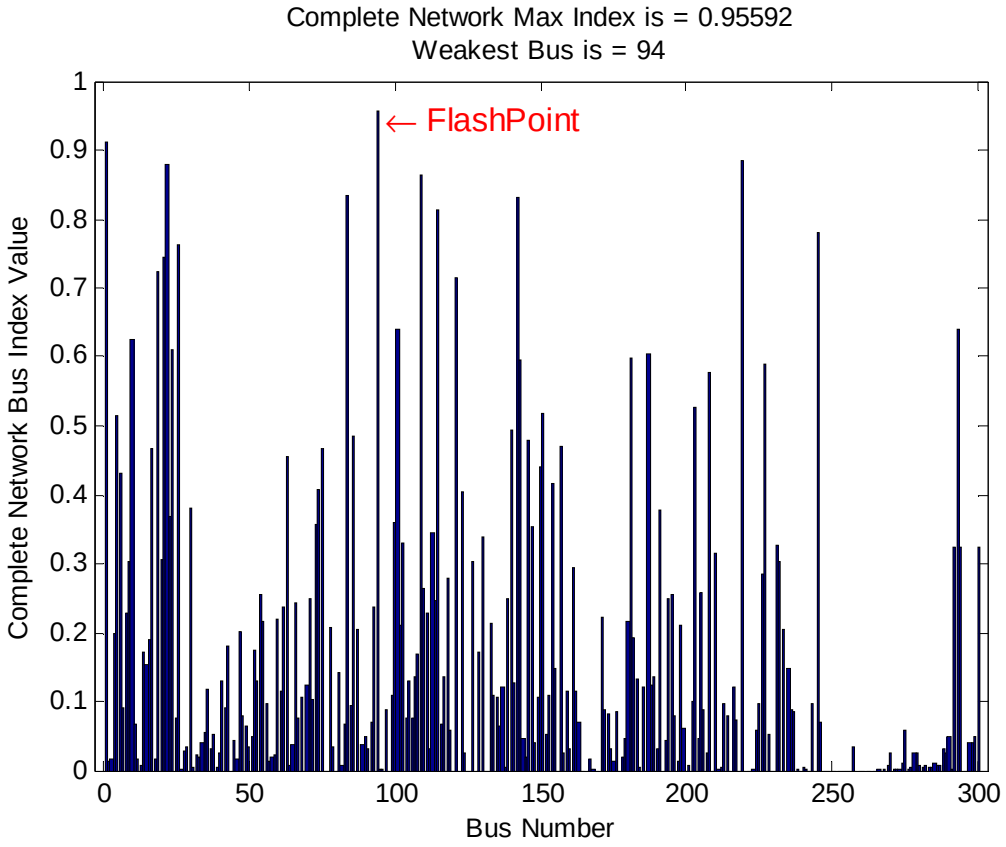

Fig. 5.9: Bus voltage stability index for IEEE 300 Bus

As in the result for the entire network, the developed scheme also shows the weakest load bus, its index values and gives a “FlashPoint” for each zone or off-zone selected. The scheme has the capability of ensuring that the compensation is directed at the actual weakest bus in case the operator was not able to give the correct value. It picks up the weakest bus for the entire network. The data acquisition component of the program has subroutines that automatically change the status of a bus from generator bus to load bus and vice versa depending on the net loading value and takes care of the double lines in the network. The buses with zero index values are either generator buses or close to the generators.

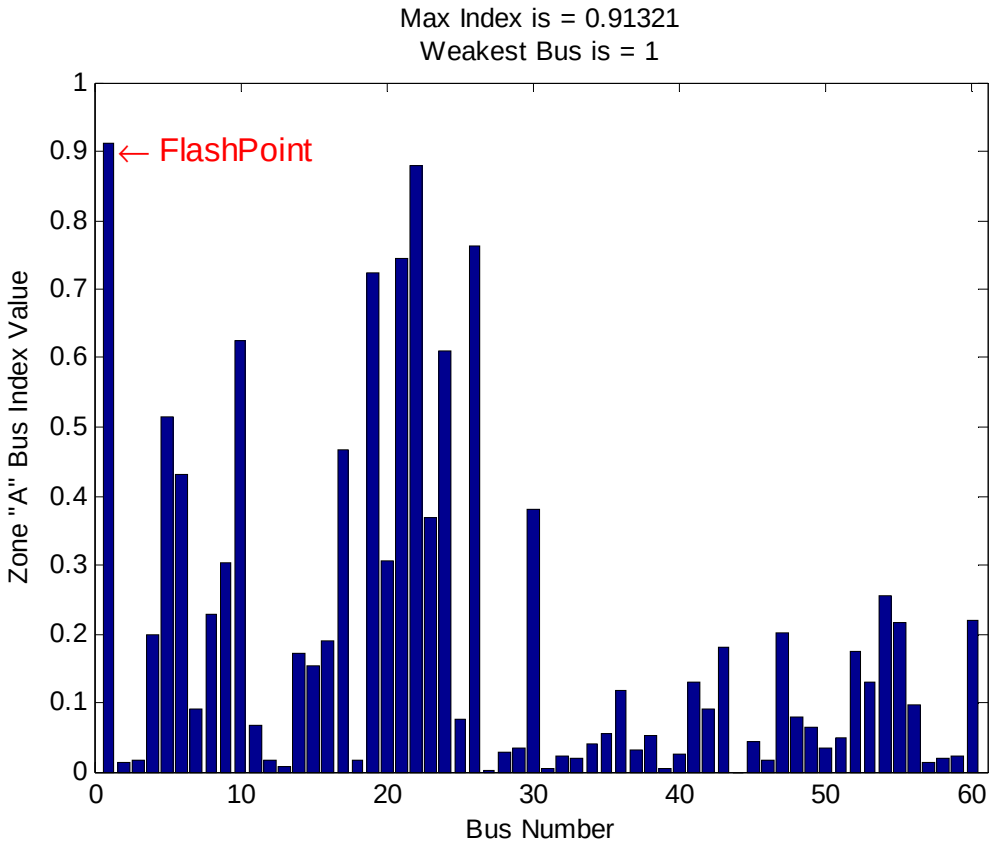

Fig. 5.10: Bus voltage stability index for IEEE 300 Bus (Zone A)

As expected, the load buses close to the generator buses gave very stable values. The buses with zero indexes are those whose net generations are greater than their current load demand, while those close to zero are very stable.

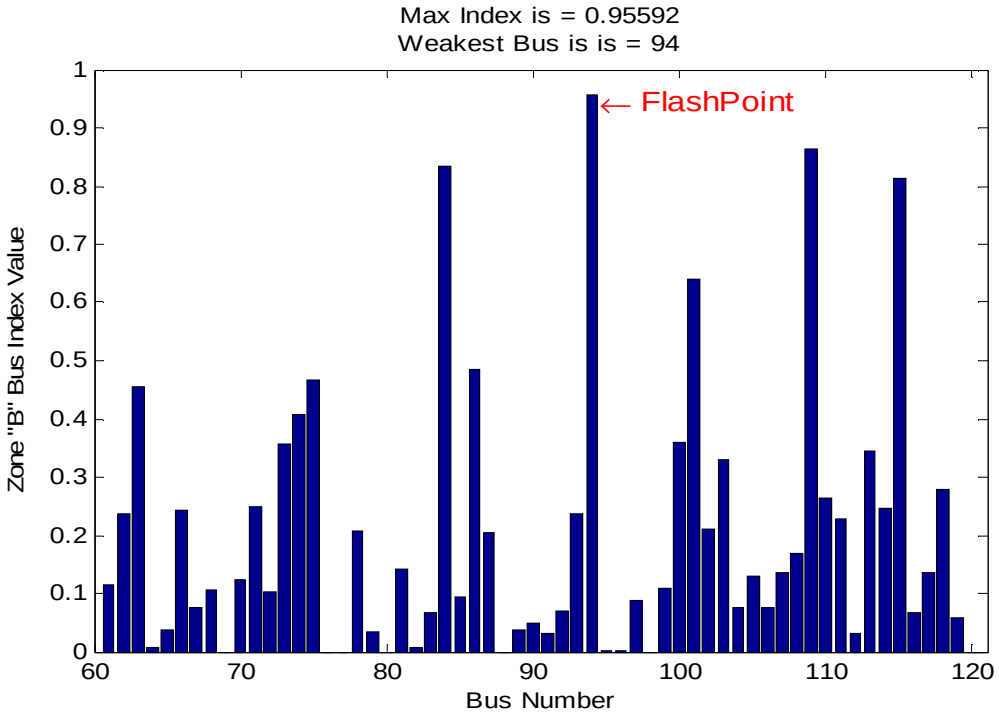

Fig. 5.11: Bus voltage stability index for IEEE 300 Bus (Zone B)

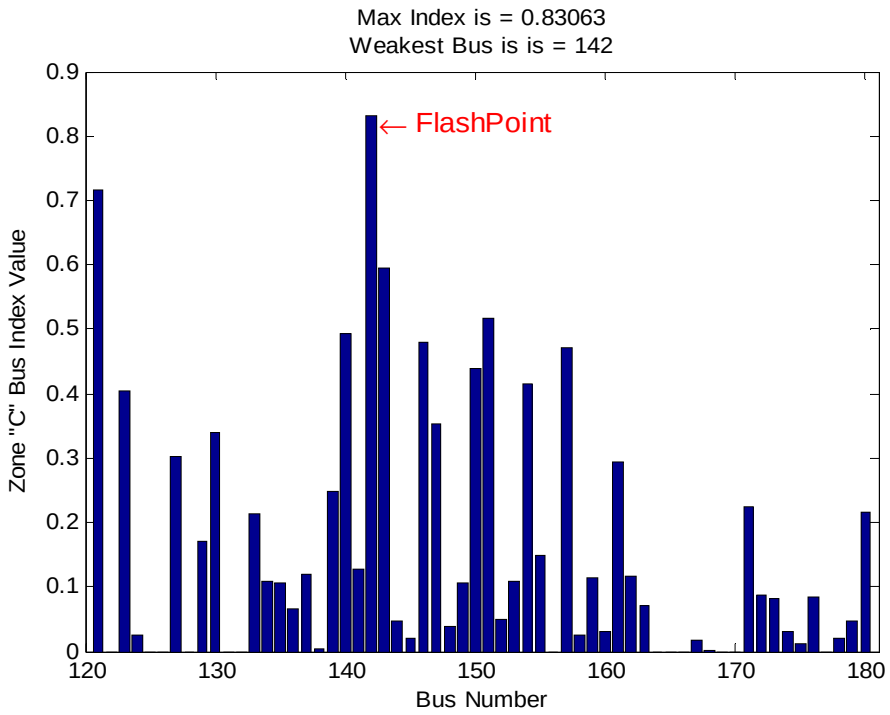

Fig. 5.12: Bus voltage stability index for IEEE 300 Bus (Zone C)

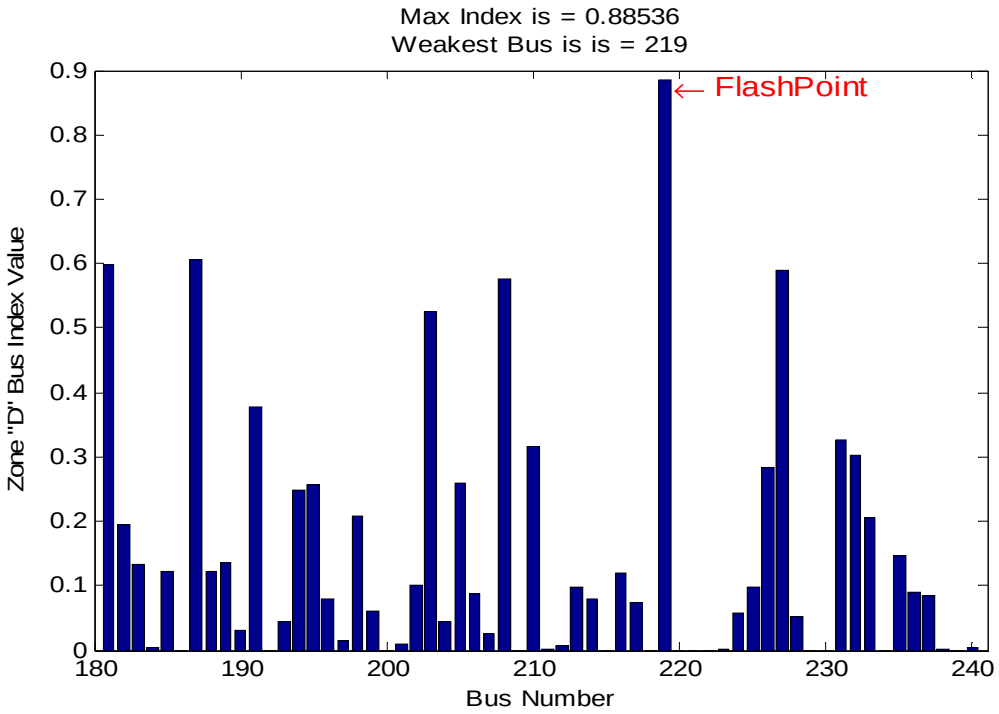

Fig. 5.13: Bus voltage stability index for IEEE 300 Bus (Zone D)

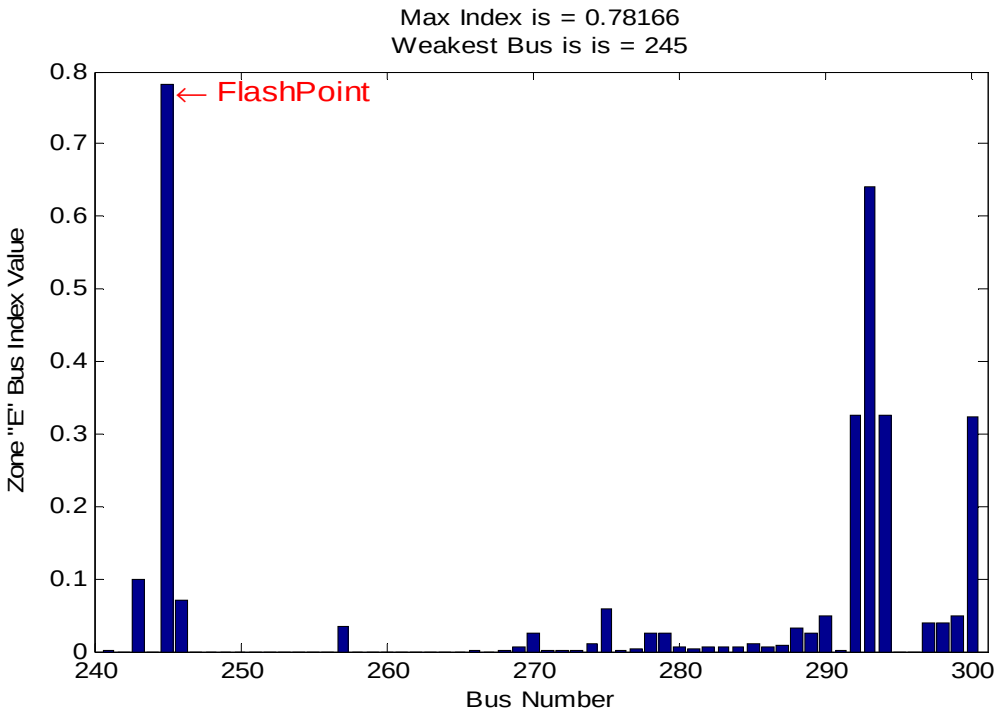

Fig. 5.14: Bus voltage stability index for IEEE 300 Bus (Zone E)

Based on the preliminary results displayed under the current loading arrangement, the buses that required immediate compensation and their zones are displayed in Table (5.2)

Based on Table (5.2) and the work done by the authors in [24, 28], only buses 1 and 94 may be compensated as their indexes are pretty close to the stability margin which each controlling authority may set according to the level of system security desired. The program was able to appropriately compute the statuses of buses when the selection did not march with zonal specifications (Fig. 5.15).

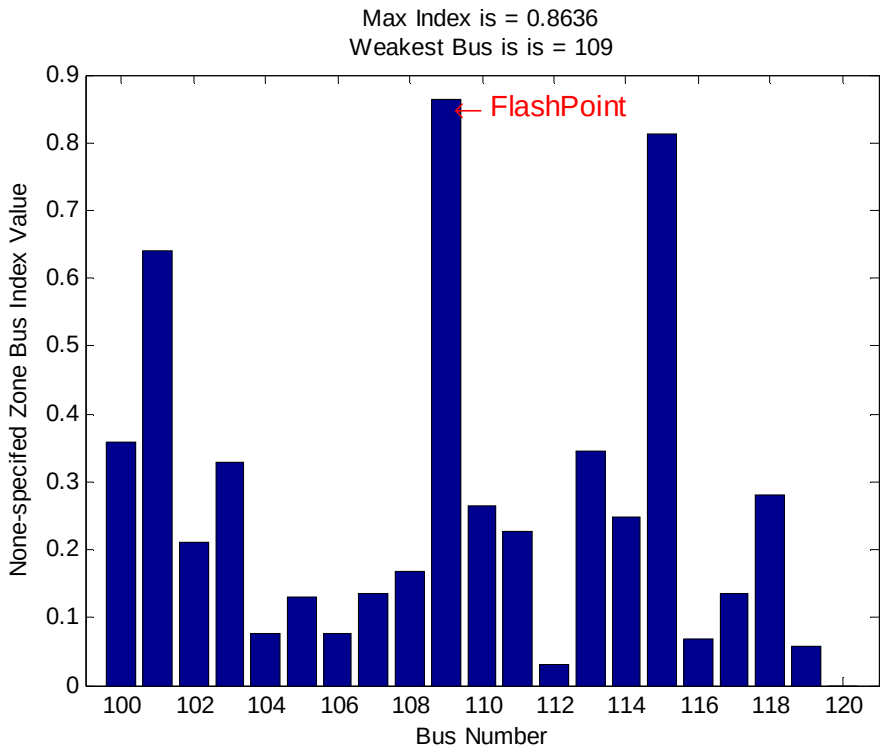

Fig. 5.15: Bus voltage stability index for IEEE 300 Bus (off Zone part of B)

Table 5.2: Instability of IEEE 300 bus system by zone

Focus Area	Bus No	Max Index	Bus Range
Entire N/W	94	0.95592	1 to 300
Zone A	1	0.91021	1 to 60
Zone B	94	0.95592	61 to 120
Zone C	142	0.83063	121 to 180
Zone D	219	0.88536	181 to 240
Zone E	241	0.78166	241 to 300
Off-Zone "B"	109	0.8636	100 to 120

5.7.2 STATCOM with 10% Increased Loading

With a STATCOM placed in buses 1 and 94, respectively, and 10% increased system loading, a new set of voltage stability indexes were computed for the entire system as presented in Fig (5.16).

The summary of the status of all the zones with the 10% increased loading and installation of STATCOM in buses 1 and 94 are as indicated in Table (5.3). The indexes of buses 1 and 94 dropped to very stable values, while bus 174 became the new weakest bus for the entire system. So the effect of placing STATCOM at buses 1 and 94 and increased loading were felt by the entire system. Other zonal stability values presented subsequently further confirmed these findings.

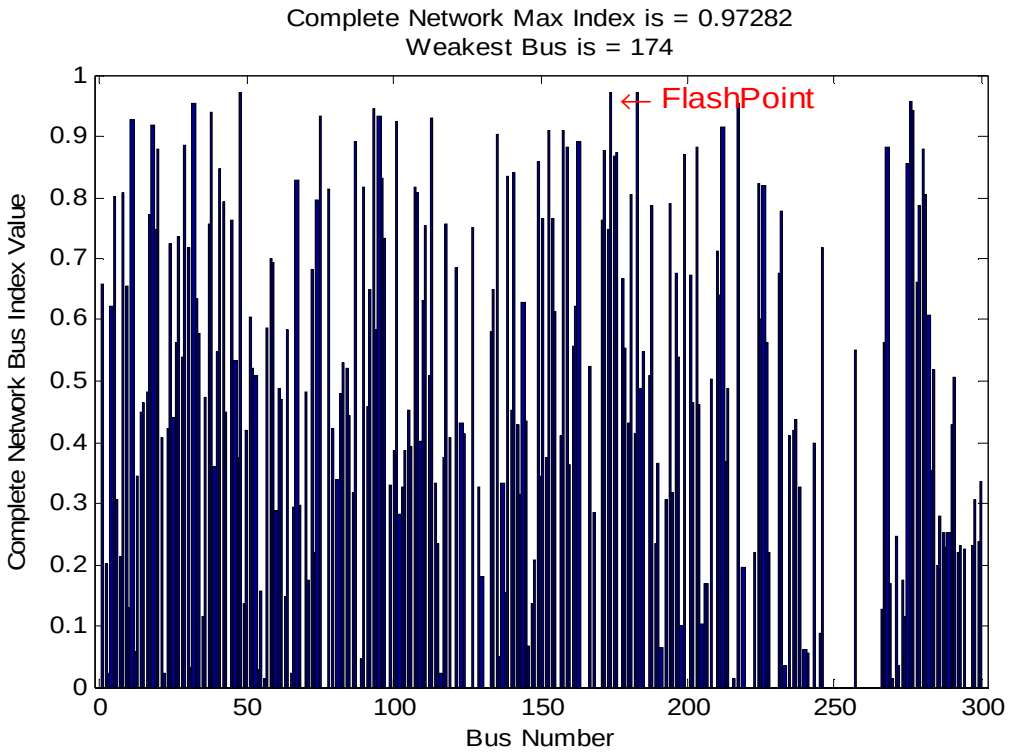

Fig. 5.16: Bus voltage stability index for IEEE 300 Bus with STATCOM and 10% increased loading.

Table 5.3: Instability of IEEE 300 bus system by zone with STATCOM and 10% increased loading

Focus Area	Bus No	Max Index	Bus Range
Entire N/W	174	0.97282	1 to 300
Zone A	48	0.97135	1 to 60
Zone B	93	0.94593	61 to 120
Zone C	174	0.97282	121 to 180
Zone D	183	0.97111	181 to 240
Zone E	276	0.95703	241 to 300

In this simulation for Figures (16) to (18), an optimal voltage stability limit of 0.97 was chosen. Zones 'B' and 'E' had maximum index of 0.94593 and 0.95703, respectively. The status indicator continues to flash that these two zones do not need any further compensation. Further simulation performed with STATCOM installed on buses 48, 174, and 183 of zones 'A', 'C', and 'D', respectively, indicated a fairly improved stability levels of not just the load buses where installed but had much more effect on the adjoining buses and on the entire network.

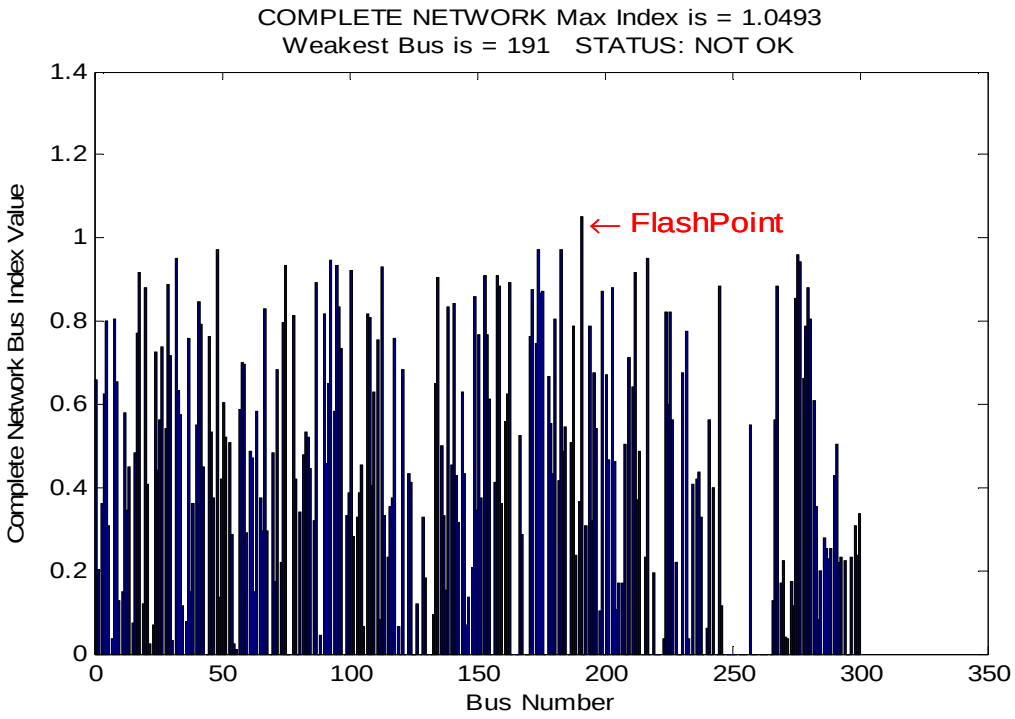

Fig. 5.17: Bus voltage stability index for IEEE 300 Bus with 20% increased loading

The results for 20% increased loading of the IEEE 300 bus system with STATCOM still placed at buses 1 and 94, and other condition remaining the same are shown in Fig. (5.17). The zonal instability status is summarized as in Table (5.4). In this condition, the weakest bus in the whole network shifted from bus 174 of zone three to bus 191 of zone four. The index value of bus 191 is now greater than one which indicated collapse condition if this condition is to hold.

Table 5.4: Instability of IEEE 300 bus system by zone with 20% increased loading

Focus Area	Bus No	Max Index	Bus Range
Entire N/W	191	1.0493	1 to 300
Zone A	48	0.9735	1 to 60
Zone B	93	0.9569	61 to 120
Zone C	174	0.97328	121 to 180
Zone D	191	1.0493	181 to 240
Zone E	276	0.96703	241 to 300

In the last step, a third STATCOM is now introduced at load bus 191 with same loading condition. The complete system status is as indicated in Fig. 18. Though the placement of STATCOM at bus 191 reduced the index value below one, with the desired maximum voltage stability limit still kept at 0.97, the status monitoring system still indicated that bus 191 is still not ok and requires further compensation.

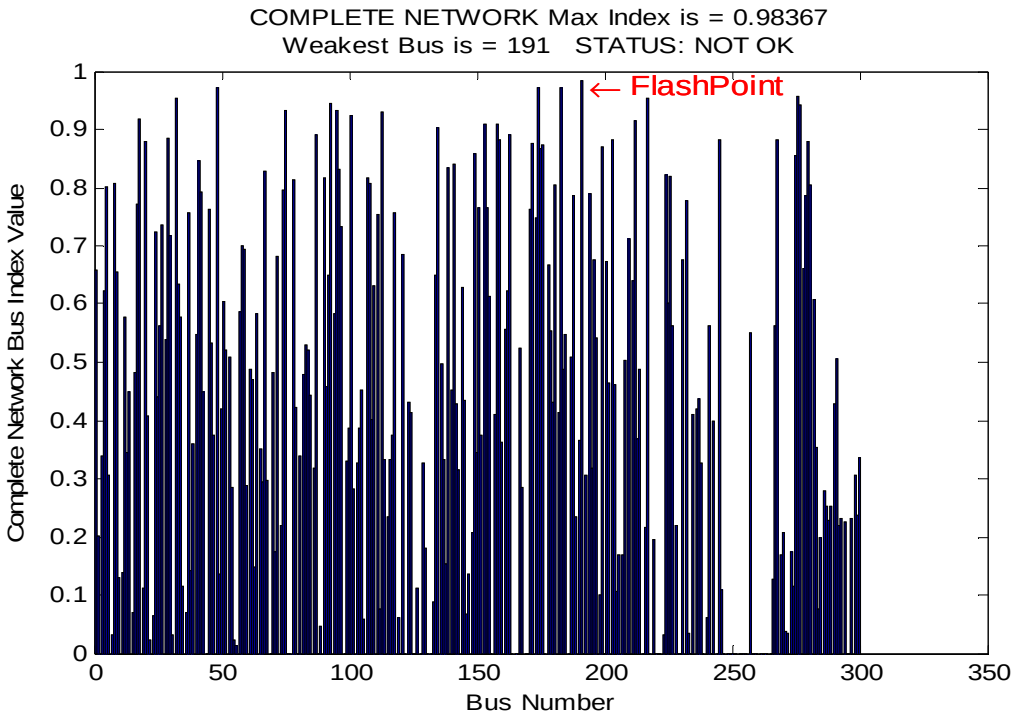

Fig. 5.18 Bus voltage stability index for IEEE 300 Bus with 20% increased loading and STATCOM on Bus 191.

5.7.3 STATCOM Magnitude Increased

The magnitude of the STATCOM (i.e. level of compensation) is further increased by 10% and the final system condition is as displayed in Fig. (5.24). The weakest bus in the entire system now shifts to bus 158. Bus 191 status is now ok indicating that it had been compensated effectively.

However, the level of compensation in practice will depend on availability and cost considerations among other factors. It was observed during simulation that the time for the display of complete system status is 1.8minutes while that of zonal displayed averaged 0.4 minutes. However, zone E which has the fewest number of load buses had the lowest simulation time of 0.25 minutes. This zone also showed greater stability.

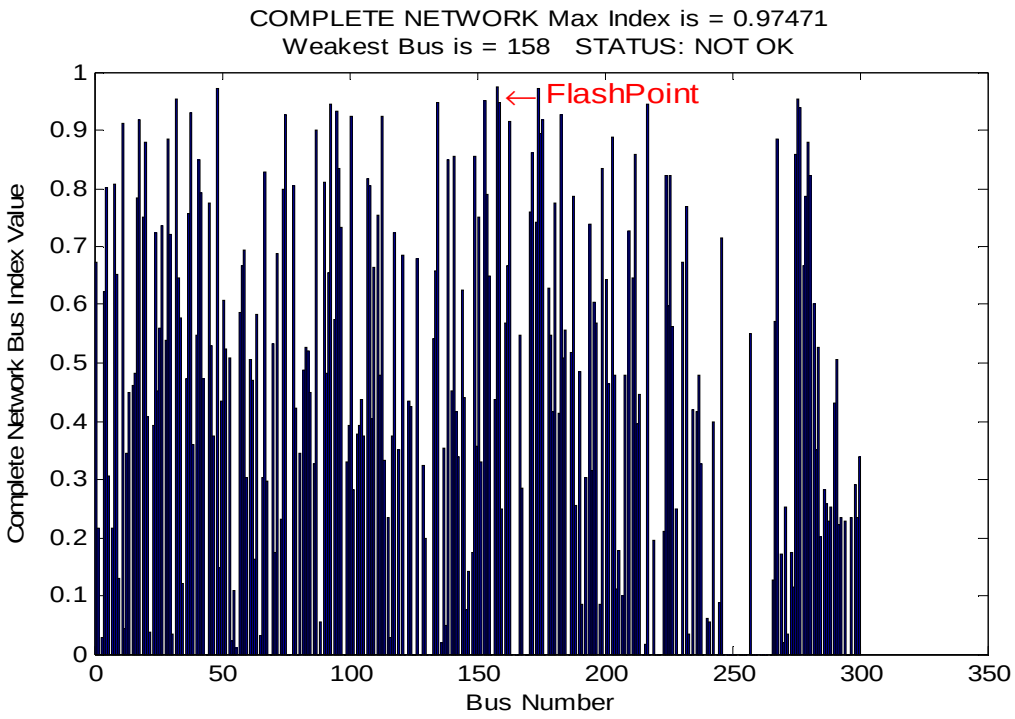

Fig. 5.19 Bus voltage stability index for IEEE 300 Bus with 20% increased loading and increased STATCOM magnitude on Bus 191.

5.8 Conclusion

A BVS-index based shunt compensation scheme and its accompanying algorithm have been developed and applied to rank the load buses of the IEEE 300 bus system and/or any other network according to their vulnerability to outages. The scheme applied in this work had been validated with its earlier applications to the IEEE 14 and 30 bus systems. It was observed that by splitting the entire network into five zones the simulation speed increased thereby indicating the practical applicability of the developed scheme. Results obtained agreed with similar work done previously as referenced.

The proposed scheme may reduce problems faced by network operators in regulating interconnection of FACTS devices and will give Utility owners, Regional Transmitting Organizations (RTOs), and Independent System Operators (ISOs) the tool to monitor not just the performances of their networks, but also those of their adjoining systems. Apart from system monitoring, it will also enhance proper system planning and control. The scheme can easily be adapted to dynamic operation and also indicate the effect of applied compensation in all parts of the network.

Further research work will be required to implement this scheme in a parallel computer simulation system where each program segment will be performed by different processors with a master controller co-coordinating the over all decision making process of the VSC. The simulation should also be performed under diverse power system operating conditions to reaffirm its robustness.

5.9 References

[1] P. Kundur, J. Paserba, V. Ajjarapu, G. Anderson, A. Bose, C. Canizares, N. Hatziargyriou, D. Hill, A. Stankovic, C. Taylor, T. Van Cutsem and V. Vittal, "Definition and classification of power system stability," IEEE Transaction on Power Systems, vol. 19, pp. 1387-1401, May 2004.

[2] P. Kundur, Power System Stability and Control. New York: McGraw-Hill, 1994.

[3] L. Philipson and H. L. Willis, "Understanding Electric Utilities and De-Regulation," Marcel Dekker, Inc. NY 10016, pp. 2, 1998.

[4] X. P. Zhang, C. Rehtanz and B. Pal, Flexible AC Transmission Systems: Modeling and Control, Springer-Verlag Berlin Heidelberg Germany, pp 2-3, 2006.

[5] S. Panda and R. N. Patel, "Improving power system transient stability with an off-centre location of shunt FACTS devices," Journal of Electrical Engineering, vol. 57, no. 6, pp. 365-368, 2006.

[6] Y. Shimazaki, "Model analysis of microgrid cogeneration system zero emission industrial park," UPE7 – The 7th International Conference on Urban Planning and Environment, Bangkok, Thailand, 2007.

.

[7] N. Panagis, A. E. Kiprakis, W. A. Robin, and G.P. Harrison, "Centralized and distributed voltage control: Impact on distributed generation penetration," IEEE Trans. on Power Systems, vol. 22, no. 1, 2007.

[8] J. A. Silva, H.B. Funmilayo and K. L. Butler-Purry, "Impact of distributed generation on the IEEE 34 node radial test feeder with overcurrent protection," Proceedings of the 2007 39th North American Power Symposium, New Mexico State University, Las Cruces, new Mexico. pp. 49, 2007.

[9] L.M. Cipcigan, P. C. Taylor and P. Trichakis, "The impact of small scale wind generation on low voltage distribution systems voltage," International Conf. on Clean Electrical Power, Italy, pp. 9, 2007.

[10] D. E. Feero, D. C. Dawson and J. Stevens, "Protection issues of the microgrid concept, CERTS," Transmission Reliability Program, Office of Power technologies, Assistant Secretary for Energy Efficiency and Renewable Energy, U.S. DOE, pp. 4-9, 2002.

[11] R. Firestone and C. Marnay, "Energy manager design for microgrids," Consultant Report by CERTS for the California Energy Commission, pp. 1, 2005.

[12] J. A. Pecas Lopes, C. L. Moreira and F.O. Resende, "Microgrids black start and islanded operation," 15th PSCC, Liege, session 27, paper 4, page 2. 2005.

[13] C. Billy, G. Heydt, P. Langness, A. Laughter, B. Mann, M. Rice and L. Winslow, "Sustainable electric power options with attention to native American communities," Proc. of the 39th North American Power Symposium, New Mexico State University. pp 177, 2007.

[14] C. L. Moreira and J. A. Pecas Lopes, "Microgrids dynamic security assessment," International Conference on clean Electrical Power, Capri Italy, , May 21st-23rd, pp. 26, 2007.

[15] J. A. Pecas Lopes, C. L. Moreira and A. G. Madureira, "Defining control strategies for microgrids islanded operation," IEEE Trans. on Power Systems, vol. 21, no. 2, pp. 916-924, 2006.

[16] United States-Canada Power System Outage Task Force, Interim Report: Causes of the August 14th Blackout in the United States and Canada (Nov. 2003) (Interim Report).

[17] U.S.-Canada Task Force on 14 August 2003 Blackout [2003], "The August 14 blackout compared with previous major North America outages," Final Report on the August 14th 2003 Blackouts in the United States and Canada, pp. 103-106.

[18] "Storms knock out power to over 600,000 customers in U.S. Northeastern Coast," U.S. DOE Energy Assurance Daily, Wednesday, July 19, 2006.

[19] "Biggest blackout in U.S. history," CBS News, pp. 1-3, August 15, 2003.

[20] M. Amin, "Powering the 21st century, we can – and must – modernize the grid," IEEE-U.S.A. Today's Engineer online at http:www.todaysengineer.org/2006/Apr/backscatter.asp.

[21] R. Siegel, "Massive power outages cripples Los Angeles," NPR October 14, 2006.

[22] M. Amin, "North America's Electricity Infrastructure: Are we ready for more storms?" IEEE Security & Privacy, published by the IEEE Computer Society, pp. 19-25, 2003.

[23] P. Kessel and H. Glavitsch, "Estimating the voltage stability of a power system," IEEE Trans. on Power Del., vol. 1. PWRD-1, no. 3. 1986.

[24] C. Reis and F. P. Maciel Barbosa, "A comparison of voltage stability indices," IEEE Melecon Benalmadena Spain, 2006.

[25] A. R. Bergen and V. Vittal, Power System Analysis 2nd Edition Prentice-Hall Inc. Upper Saddle River, New Jersey 07458, 2000, pp 101 and 112, 2000.

[26] D. O. Dike, S. M. Mahajan and G. Radman, "Development of versatile voltage stability index algorithm, IEEE Electrical Power Conference 2007, Montreal QC, Canada, 2007.

[27] D. O. Dike and S. M. Mahajan, "L-index based microgrid interconnected power system," Accepted for publication in the proceedings of IEEE PES General Meeting, July 20 -24, 2008, Pittsburg, PA.

[28] D. X. Zhang, B. Pal and C. Rehtanz, "Flexible AC transmission systems: modeling and control," Springer-Verlag Berlin Heidelberg, Germany, 2006.

[29] D-VAR Solutions – Dynamic VAR Support for a More Reliable Grid, 2007, American Superconductor, Inc.

[30] Y. H. Song and A. T. Johns, "Flexible ac transmission systems (FACTS)," The Institute of Electrical Engineers, London, United Kingdom, 1999.

[31] J. Rodríguez, J. Lai and F. Z. Peng, "Multilevel Inverters: A survey of topologies, controls and applications," IEEE Trans. Ind. Electronics, vol. 49, no. 4, pp. 724-738., 2002.

[32] E. Babaei, S. Hosseini and G. B. Gharehpetian, "A new topology for multilevel current source converters," ECTI Trans. Electrical Eng., Electronics and Communications, vol. 4, no. pp. 2-12, 2006.

[33] M. E. Ortúzar, R. E. Carmi, J. W. Dixon and L. Morán "Voltage-source active power filter based on multilevel converter and ultracapacitor dc link," IEEE Trans. Ind. Electronics, vol. 53, no. 2, pp 477-485, 2006.

[34] J. Rodríguez, S. Bernet, B. Wu, J. O. Pontt and S. Kouro, "Multilevel voltage-source converter topologies for industrial medium –voltage drives," IEEE Trans. Ind. Electronics, vol. 54, no. 6, pp. 2930-2945, 2007.

[35] S. B. Monge, S. Somavilla, J. Bordonau and D. Boroyevuch, "Capacitor voltage balance for neutral-point-clamped converter using virtual space vector concepts with optimized special performance," IEEE Transactions on Power Electronics, vol. 22, no. 4, pp. 1128-1134, 2007.

[36] P. Purkait and R. S. Sriramakavacham, “A new generalized space vector modulation algorithm for neutral-point-clamped multilevel converters,” Progress in Electromagnetics Research Symposium, Cambridge, USA, pp.330-335, 2006.

[37] A. Bendre and G. Venkataramanan, “Neutral current ripple minimization in a three-level rectifier,” IEEE Transaction on Industrial Applications, vol. 42, no. 2, pp. 582-590, March 2006.

[38] S. Panda, “Improving power system transient stability with an off-centre location of shunt FACTS devices,” Journal of Electrical Engineering, vol. 57, no. 6, 2006, pp. 365-368.

[39] C. Hochgraf and R. H. Lasseter, “STATCOM controls for operation with unbalanced voltages,” IEEE Transaction on Power Delivery, vol. 13, no. 2, April 1998.

[40] P.T. Nguyen and T. K. Saha, “Dynamic voltage restorer against balanced and unbalanced voltage sags: modeling and simulation,” IEEE PES General Meeting Proceedings, 6-10 June 2004, vol. 1, pp. 639-644.

[41] G. Wolf, “Utilities apply new technologies to solve age-old transmission grid problems,” Transmission & Distribution World, November 2007.

[42] “Dynamic reactive power compensation,” American Superconductor D-VAR Data Sheet, 2008.

[43] “Dynamic Voltage Restorer,” ABB Automation Power Electronic Systems, January 2001.

[44] M. Tuomainen, “Harmonics and reactive power compensation in practice,” Nokian Capacity.

CHAPTER 6

PAPER 5: OPTIMAL AVAILABLE TRANSFER CAPABILITY COMPUTATION SCHEME USING LVS-INDEX MODEL[†]

D. O. Dike and S. M. Mahajan

Department of Electrical and Computer Engineering

Tennessee Technological University, Cookeville, TN 38505, USA

ABSTRACT— A simplified available transfer capability (ATC) computation and improved management scheme for power transfer is presented. The scheme selects appropriate line voltage stability (LVS) index model to compute the proximity to collapse of a chosen transmission line using successive incremental loading of the line. The ATC is then computed as the amount of additional line loading before the stability index reaches its pre-fixed limit. The improved management comes with the incorporation of a series compensator at the determined weak lines to improve their extra power wheeling capability. This entails applying the LVS index model to multi-series FACTS-incorporated Newton-Raphson's (N-R) power flow model to monitor and regulate its performance. The results obtained when this scheme was simulated with the IEEE 300 bus system with zoning and under varying operating conditions, showed the system's capability to provide simplified and reliable system ATC computation and thereby enabling the proper monitoring of the series compensated transmission lines' operating statuses.

[†] Submitted to IEEE Transaction on Power Delivery

6.1 Introduction

With deregulation of most of the generation and distribution sectors of the power industry in many countries, there has been tremendous increase in the number of operating entities and resources in these two areas, while there is no commensurate growth in the transmission sector [1]. The restructuring and the restrictions imposed to the construction of new transmission lines by environmental and the citizenry resistance to location of new lines across their neighborhood has severely reduced the quantity and quality of transmitted electrical power to meet demand and increased congestion condition [2]. Therefore, the transmission lines are increasingly overloaded due to unplanned wheeling of power during emergencies, peak load periods, seasonal variation of power utilization trends and most importantly for economic reasons and lack of pre-determination of the capabilities of each transmission line [3].

"A key concept in the restructuring of the electric power industry is the ability to accurately and rapidly quantify the capabilities of the transmission system [4]." ATC is defined as "a measure of the transfer capability remaining in the physical transmission network for further commercial activity over and above committed uses," [5-7]. When power systems were isolated, it was easier to compute ATC, but with deregulation which has actually encouraged looped and large scale power systems interconnection, such machine localized ATC computation arrangements are no longer reliable [4].

To ensure uninterrupted access to transmission facilities, FERC issued open access transmission orders (Order Nos. 888 and 888-A) mandating utilities to provide transmission services to all eligible entities and to construct new facilities or operate off-cost generation to provide requested transmission services when capacity is not available

[8]. Therefore, with these orders and the fact that the computation of ATC is very crucial to the transmission system security and market forecasting, developing simpler, quicker, and faster schemes for its actualization becomes very necessary [9].

A review of line voltage stability index models and simulations performed by the authors in [10, 11] revealed that there exists a proportional ratio relationship between the actual power transmitted over a given transmission line and the system predetermined maximum transmittable power across the same transmission line. Consequently, the concept of LVS-index is now being extended to the computation of ATC. This effort is further justified by the work carried out in [12, 13] which considered ATC as load dependent, while other methods of ATC computation utilized system wide multi-parameters [2-9]. However, the thermal stability constraint which is a local phenomenon determining the available transfer capacity (often confused with available transfer capability which is a generalized concept encompassing all stabilities) is accommodated by leaving out some margin in the maximum index limits.

In view of the need to increase the amount of power transferable to reduce the gap between supply and demand of quality electrical power, Flexible AC Transmission Systems (FACTS) have been applied to provide reactive supports, reduce the effective transmission line impedance, protect and enhance grid controllability [14-21]. To this end, the scheme developed in this work had been extended to permit the inclusion of series compensated FACTS device to the N-R load flow model at the predetermined weak lines. This part is justified by the reports of North American Task Forces and Committees as contained in [22, 23] which categorized the precipitating events or causes of the August 14th 2003 North American blackout:(i) “inadequate situational awareness”

on the part of FirstEnergy; (ii) FirstEnergy's failure to "manage adequately tree growth in its transmission right-of-way"; and (iii) failure of the interconnected grid's reliability organizations to provide effective diagnostic support."

The series compensation devices are required to improve the transmission line controllability, reduce losses by decreasing the effective line reactance and increase line stability all geared towards enhancing the amount of power transmittable to meet growing demand. In this wise, the paper is focusing on transmission line improvement to meet the power demand in areas where there is not enough generation, and to smoothen the trading of electrical power which is the hallmark of deregulation and commercialization of power industries worldwide.

6.2 Review of Series Compensation Devices

FACTS application in power system may be classified under three major application groupings – shunt, series, and combined devices. Shunt devices in use today are shunt static VAR compensator (SVC) and static synchronous shunt compensator (STATCOM). Series devices include thyristor controlled series capacitor (TCSC) and a voltage source inverter based static synchronous series compensator (SSSC). A combination of shunt-series converters forms unified power flow controller (UPFC), two or more series – series connected converters gives interline power flow controller (IPFC) and a shunt-series-series composite of three or more converters gives the generalized unified power flow controller (GUPFC) [20, 21]. There are other emerging forms of FACTS devices aimed at addressing recent power system problems and reduce cost.

These include the various brands of Dynamic VAR system (D-VAR) been championed by the American Superconductor team [24].

Despite the robustness of these combined FACTS devices, their high cost has prevented practical applications. Power system operators utilize mostly the simpler and cost effective FACTS devices and ordinary forms of series and shunt compensator which use capacitor and inductor banks. Much of the series compensation reported in Table (6.1) comprised of thyristor switched capacitor (TSC) and thyristor switched reactors (TSR) which are installed on a fully insulated platform together with over-voltage protection circuits.

This is to ensure that the main capacitor bank is able to withstand the throughput fault current. Primary over-voltage protection involves nonlinear metal-oxide varistor having park gap and fast bypass switch, while the secondary protection is handled with a ground mounted electronics acting on signals from optical current transducers [24].

For improvement in active power transfer across the power transmission grid, frequency regulation and transient stability sustainability and operational control, the TCSC and SSSC had proved very reliable, and are hereafter discussed as main series compensators.

Table 6.1: Estimated number & capacity of FACTS devices installed worldwide [28].

Type of Device	Number	Total Installed Power (MVA)
SVC	600	90,000
STATCOM	15	1,200
Series Compensation	700	350,000
TCSC	10	2,000
HVDC B2B	41	14,000
HVDC VSC B2B	8	900
UPFC	3	250

6.2.1 TCSC Application in Transmission Lines

TCSC is modeled as series impedance consisting of thyristor-controlled reactors (TCRs) in parallel with capacitor bank, and a metal-oxide varistor (MOV) connected across each capacitor bank to prevent over-voltages (Fig. (6.1)). The bank capacitors are mounted on fully insulated platforms on the ground and the thyristor valves are high powered with maximum total blocking voltage. All TCSC power equipment including the thyristor controlling main capacitor actions is located on an isolated steel platform.

The primary roles of TCSC are to

(i) Increase power system damping when large systems are interconnected;

(ii) Overcome the problem of sub-synchronous resonance, and provide mechanism for controlling line power flow which facilitates increased line loading; and

(iii) Rapid adjustment of line power flow in response to various contingencies.

TCSC operational limits are determined by the thermal limits and firing angle of its thyristor. The degree of insulation and protection provided determines its cost.

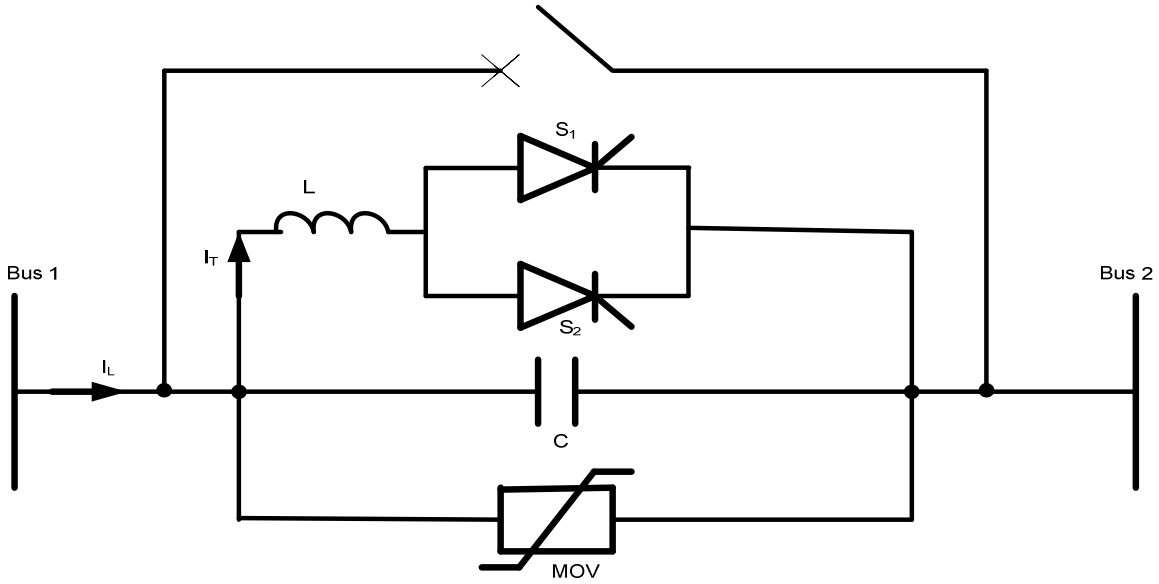

Fig. 6.1: Single-line single-phase diagram of TCSC interconnection

Above its operational limits, the bypass switch provided acts to save the equipment. Therefore, an independent transmission line stability monitoring index is required to know the exact status of the interconnected power system during TCSC operation, at the point of bypass and when it is not operating.

6.2.2 Application of SSSC in Transmission Lines

SSSC is connected in series to the transmission line (Fig. (6.2)) as a voltage source, and has the same structure as STATCOM. Its main function is transmission line power regulation. This is achieved by direct control of the line current or indirectly by injecting series voltage to reduce the effective transmission line impedance and hence decreasing the reactive power consumed by the line inductive elements. By so doing, it improves the transferable active power. However, because the line current flows through SSSC, it requires very expensive protection to safeguard the sensitive semiconductor control devices. This makes SSSC very expensive and not any appreciable number of it has been installed for practical transmission power utilization.

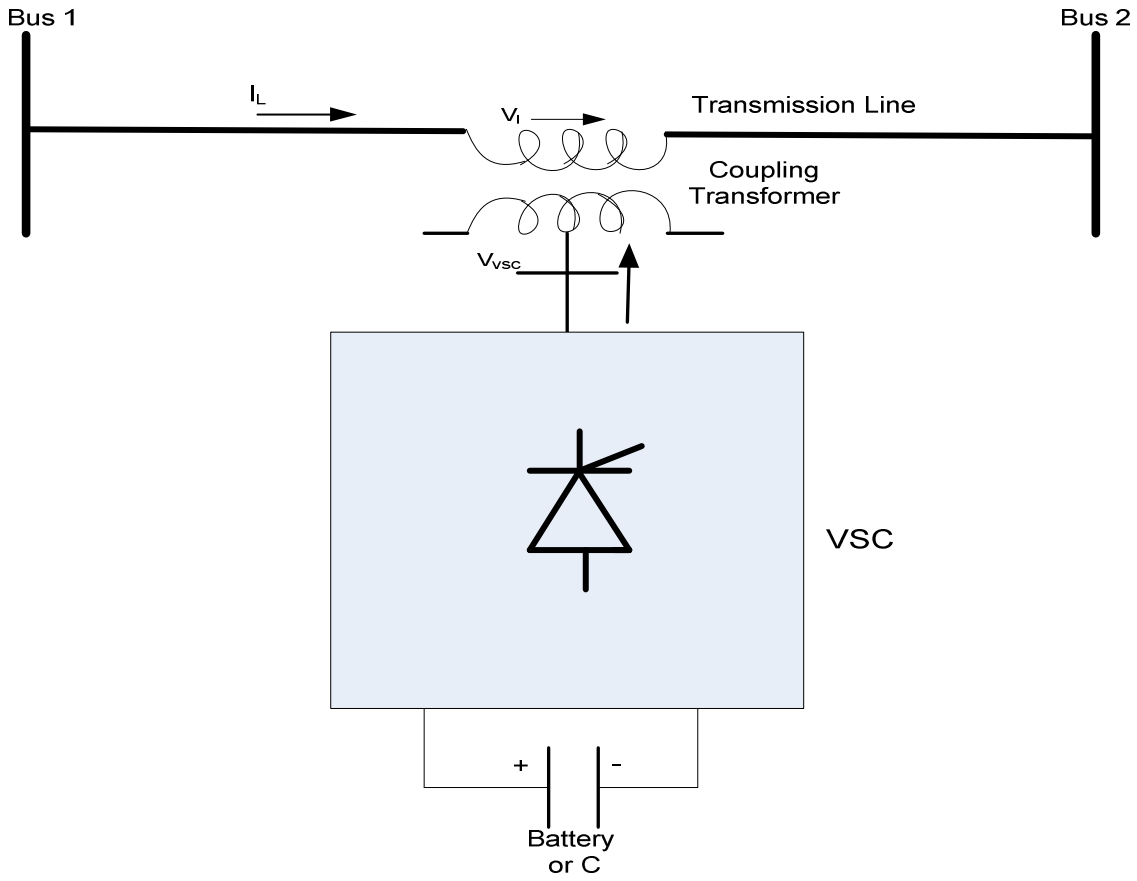

Fig. 6.2: SSSC interconnection to a power transmission line

6.3 ATC Computational Methods

ATC is the maximum amount of additional MW transfer possible between two parts of the power system. This implies that there should be no overloads during the transfer and under contingencies as the transfer is increased. Some of the methods adopted towards computing ATC include the following:

(i) Linear Methods [25]: The following linear schemes for ATC computation were outlined – Single Linear Step ATC Computation and Iterated Linear Step fall into the fast methods.

These methods were arrived at by using the fast decoupled load flow method to compute at the DC Power Flow involving just the real part. The slow linear methods include bus voltage and angle sensitivities to a Transfer, Power Transfer Distribution Factors, Line Outage Distribution Factors, Line closure distribution factors, and Iterated Linear with full AC Load Flow with OPF makes the slower group.

(ii) A simplified method of transfer capability calculation working top-down from the purpose of transfer capability by discussing definitions and meanings of its various components, explaining how each is computed and then deducting the known quantities to get the unknowns was adopted in [3, 5] with certain assumptions.

Same approach was adopted by several other authors [4, 6-9] to arrive at general formulae for computing ATC from related terms given as

$$ATC = TTC - CBM - TRM - ETC$$

where

TTC=Total Transfer Capability.

CRM=Capacity Benefit Margin.

TRM=Transmission Reliability Margin.

ETC=Existing Transmission Commitment.

(iii) Hybrid Evolution Algorithm was used as a means of computing TTC and its enhancement in [6]. However, in all the methods utilized, the simple logic required was manipulation of the basic equations involved in power flow. In view of this and the fact that ATC is mostly transmission line based, the authors came to the view of applying the concept of live voltage stability (LVS) index since it will take into account the six basic

principles of ATC as enunciated by Federal Energy Regulatory Commission (FERC) which are stated hereafter [4].

That ATC calculation should

(a) Give a reasonable and reliable indication of transfer capabilities.

(b) Recognize time-variant conditions, simultaneous transfers, and parallel flows.

(c) Recognize the dependence sources and sinks.

(d) Reflect regional coordination to include the interconnected network.

(e) Conform to NERC and other organizational system reliability criteria and guides.

(f) Accommodate reasonable uncertainties in system conditions and provide flexibility.

These facts were considered and certain assumptions made in the present effort to extend the LVS index to ATC computation.

6.4 Modeling of LVS-Index for ATC Computation

Some of the available line voltage stability index models include VCP, VCQ, LQP, Lmn and FVSI [17, 18]. Definitions of these indexes are presented below

$$VCP = \frac{P_r}{P_{r(\max)}} \tag{2}$$

where in Equation (1), $P_{r\ (max)}$ is the maximum rating of line 'r' at the given operating conditions specified for a given transmission line and P_r is the active power transferred along transmission line r given as

$$P_r = \left[\left(V_s \cos\delta - V_r \right) \frac{R}{R^2 + X^2} + V_s \sin(\delta) \frac{R}{R^2 + X^2} \right] V_r \tag{3}$$

$$VCQ = \frac{Q_r}{Q_{r(\max)}} \tag{4}$$

where

$$Q_r = \left[\left(V_s \cos\delta - V_r \right) \frac{R}{R^2 + X^2} - V_s \sin(\delta) \frac{R}{R^2 + X^2} \right] V_r \tag{5}$$

$$L_{mn} = \frac{4XQ_j}{\left[V_i (\theta - \delta) \right]^2} \tag{6}$$

$$LQP_{ij} = 4 \left(\frac{X_{ij}^2}{V_i^4} P_i^2 + \frac{X_{ij}}{V_i^2} Q_j \right) \tag{7}$$

$$FVSI_{ij} = \frac{4Z^2 Q_j}{V_i^2 X_{ij}} \tag{8}$$

The range of values for all the index models outlined in Equations (1) through (6) is equal to $0 \le (LVS - index) \le 1$. Consideration of each of these LVS shows that each of these models has a unique computation need and are developed to address specific power system operation condition and/or problem.

Based on the review of ATC computation schemes, it was decided to use active power transfer ratio model of Equation (1). To compensate for the other probabilistic factors which were not part of the LVS-index model, the upper limit of the index was set to 0.98 considering the simulation results the authors have obtained in previous applications of the LVS-index [10, 11]. By so doing, a margin of 0.02 was allocated to cater for contingencies. With this arrangement, TTC=0.98.

$$=> ATC = TTC - (LVS - index) \quad (9)$$

Therefore, the LVS-index accounts for the summation of all other components of transfer capability, and the relationship is as stated in Equation (10).

$$=> (LVS - index) = CBM + TRM + ETC \quad (10)$$

An alternative approach was to continue increasing the amount of power transferred until the LVS index attained the stated critical value. The amount of power transferred before the LVS index reached its critical value gives the available transfer capability under the operating condition. The alternative computation method serves as a means of validating the result obtained using Equations (1)-(3) and (9)-(10) for the active power and (1), (4), (5), and (9)-(10) for the reactive power, respectively.

The next section considers the application of series compensator to improve the available transfer capability of weak lines.

6.5 Inclusion of Series Compensation Devices in Newton-Raphson's Load Flow Model

6.5.1 A. Newton's Power Flow Model

The basic real and reactive power flow equations for a transmission line between buses 'i' and 'j' as shown in Fig. (4) are presented in Equations (3) and (4), respectively.

$$P_i = \sum_{j=1}^{N} V_i V_j \left(g_{ij} Cos\theta_{ij} + b_{ij} Sin\theta_{ij} \right) \quad (11)$$

$$Q_i = \sum_{j=1}^{N} V_i V_j \left(g_{ij} Sin\theta_{ij} - b_{ij} Cos\theta_{ij} \right) \quad (12)$$

For p=1, 2, 3 . . . N,

The Newton power flow equation in polar coordinate is written as

$$\begin{bmatrix} \frac{\partial P_i}{\partial \theta_j} & \frac{\partial P_i}{\partial V_j} \\ \frac{\partial Q_i}{\partial \theta_j} & \frac{\partial Q_i}{\partial V_j} \end{bmatrix} \begin{bmatrix} \Delta\theta_i \\ \Delta V_i \end{bmatrix} = -\begin{bmatrix} \Delta P_i \\ \Delta Q_i \end{bmatrix} \tag{13}$$

6.5.2 Multi-SSSC Structure in Newton Power Flow

When a series compensator such as SSSC is connected to a transmission line as in Figure (3) and the equivalent representation is on Figure (4), the real and reactive power Equations of (11) and (12) changes to Equations (14) through (17) for the respective active and reactive power flows across the given line: The resulting real and reactive power equations become

$$P_{ij} = V_i^2 g_{ii} - V_i V_j (g_{ij} \cos(\theta_i - \theta_j) + b_{ij} \sin(\theta_i - \theta_j)) - V_i V_{se} (g_{ij} \cos(\theta_i - \theta_{se}) + b_{ij} \sin(\theta_i - \theta_{se})) \tag{14}$$

$$Q_{ij} = -V_i^2 B_{ii} - V_i V_j (g_{ij} \sin(\theta_i - \theta_j) - B_{ij} \cos(\theta_i - \theta_j)) - V_i V_{se} (G_{ij} \sin(\theta_i - \theta_{se}) - B_{ij} \cos(\theta_i - \theta_{se})) \tag{15}$$

$$P_{ji} = V_j^2 g_{jj} - V_j V_i (g_{ij} \cos(\theta_j - \theta_i) + b_{ij} \sin(\theta_j - \theta_i)) + V_j V_{se} (g_{ij} \cos(\theta_j - \theta_{se}) + b_{ij} \sin(\theta_j - \theta_{se})) \tag{16}$$

$$Q_{ji} = -V_j^2 b_{jj} - V_j V_i (g_{ij} \sin(\theta_j - \theta_i) - b_{ij} \cos(\theta_j - \theta_i)) + V_j V_{se} (g_{ij} \sin(\theta_j - \theta_{se}) - b_{ij} \cos(\theta_i - \theta_{se})) \tag{17}$$

Equations (14) through (17) replace the real and reactive power flow Equations (11) and (12).

The system variables used in preceding equation are

$$\underline{V}_i = V_i\angle\theta_i,\ \underline{V}_j = V_j\angle\theta_j \qquad \underline{V}_{se} = V_{se}\angle\theta_{se} \text{ and } g_{ij} + jb_{ij} = \frac{1}{Z_{se}}$$

As in STATCOM, the operating constraint of the SSSC is that the net active power exchange through the DC link is zeros, as given in Equation (10).

$$\begin{aligned} PE &= -V_i V_{se}\,(g_{ij}\cos(\theta_i - \theta_{se}) - b_{ij}\sin(\theta_i - \theta_{se})) + \\ & V_j V_{se}\,(g_{ij}\cos(\theta_j - \theta_{se}) - b_{ij}\sin(\theta_j - \theta_{se})) = 0 \end{aligned} \tag{18}$$

where $PE = \mathrm{Re}(V_{se} I_{se}^{*}) = 0$

Equation (18) serves as the first equation to be used for inclusion of the series FACTS device into the N-R model.

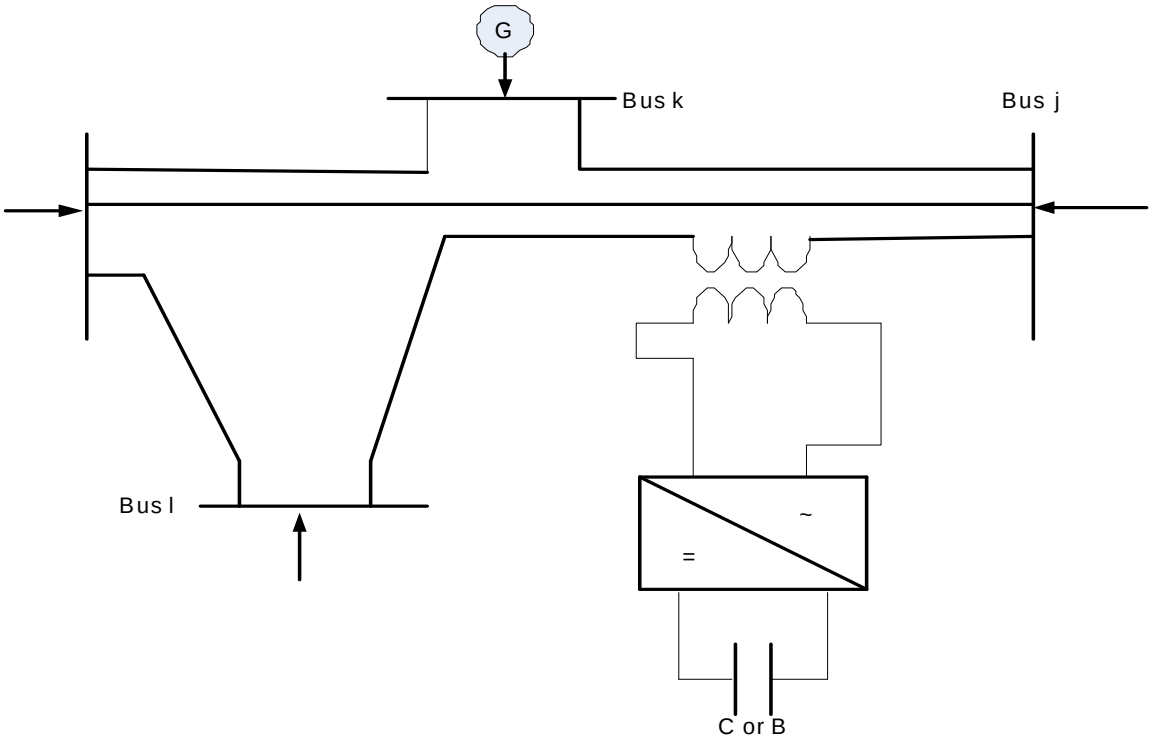

Fig. 6.3: Inclusion of SSSC in power system network

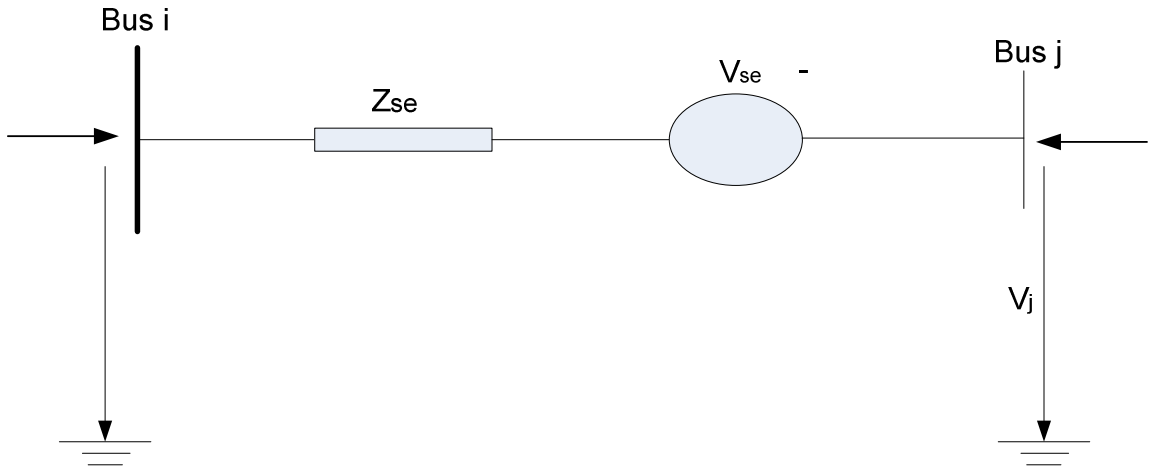

Fig. 6.4: SSSC equivalent circuit

6.5.3 Multi-Control Function of the SSSC

SSSC has one degree of freedom due to the single constraint equation of the DC active power transfer just like the STATCOM. However, it has only four control functions with only one in use at any given time. These control functions are

(i) Active power flow control $\Rightarrow P_{ji} - P_{ji}^{spec} = 0$ (19)

(ii) Reactive power flow control $\Rightarrow Q_{ji} - Q_{ji}^{spec} = 0$ (20)

(iii) Bus voltage magnitude control $\Rightarrow V_i - V_i^{spec} = 0$ (21)

(iv) Reactance control $X_{comp} - X_{comp}^{spec} = 0$ (22)

Any one of these four control modes can be chosen and included in the Newton's power flow model as the second additional equation. The generalized control function is represented as

$$\Delta E(x) = E(x) - E^{spec} = 0 \quad (23)$$

where $x = \left[\theta_i, V_i, \theta_j, V_j, \theta_{se}, V_{se}\right]$

6.5.4 Application of SSSC to N-R Load Flow Model

Power mismatches for SSSC are represented by Equations (24) to (27) showing real and reactive power leaving bus i and k as the case may be.

$$\Delta P_i = P_{gi} - P_{di} - P_i = 0 \tag{24}$$

$$\Delta Q_i = Q_{gi} - Q_{di} - Q_i = 0 \tag{25}$$

$$\Delta P_j = P_{gj} - P_{dj} - P_j = 0 \tag{26}$$

$$\Delta Q_j = Q_{gj} - Q_{dj} - Q_j = 0 \tag{27}$$

Since SSSC has only one degree of freedom, it may be used to control only one of

(iii) Active power flow on the transmission line

(iv) Reactive power flow on the transmission line

(v) The reactance of the transmission line

(vi) The bus voltage

To accommodate SSSC into the N-R model, two new equations are needed; namely active power balance Equation (18) and any one of the generalized control function Equations (24) to (27). The reactive power flow constraint was chosen for this work to give the control function as

$$E(x) = -V_j^2 b_{jj} - V_j V_i (g_{ji} Sin(\theta_j - \theta_i) - b_{ji} \cos(\theta_j - \theta_i) + V_j V_{se} (g_{ji} Sin(\theta_j - \theta_{se}) - b_{ji} \cos(\theta_j - \theta_{se}) \tag{28}$$

The two additional equations took care of the two extra variables introduced by SSSC (i.e. SSSC voltage angle and magnitude. The new Jacobian is now given by Equation (29).

$$[J]=\begin{bmatrix} \frac{\partial P_i}{\partial \theta_j} & \frac{\partial P_i}{\partial V_j} & \frac{\partial P_i}{\partial \theta_{se}} & \frac{\partial P_i}{\partial V_{se}} \\ \frac{\partial Q_i}{\partial \theta_j} & \frac{\partial Q_i}{\partial V_j} & \frac{\partial Q_i}{\partial \theta_{se}} & \frac{\partial Q_i}{\partial V_{se}} \\ \frac{\partial PE}{\partial \theta_j} & \frac{\partial PE}{\partial V_j} & \frac{\partial PE}{\partial \theta_{se}} & \frac{\partial PE}{\partial V_{se}} \\ \frac{\partial E}{\partial \theta_j} & \frac{\partial E}{\partial V_j} & \frac{\partial E}{\partial \theta_{se}} & \frac{\partial E}{\partial V_{se}} \end{bmatrix} \tag{29}$$

where $1 \le i \le N$ and $1 \le j \le N$, N is the maximum number of buses in the system, and i may or may not be equal to j. This arrangement gives sixteen entries as denoted in Equation (30).

$$\text{where } [J]=\begin{bmatrix} J1 & J2 & J3 & J4 \\ J5 & J6 & J7 & J8 \\ J9 & J10 & J11 & J12 \\ J13 & J14 & J15 & J16 \end{bmatrix} \tag{30}$$

The generalized dimension for each of these Jacobian matrices where the slack bus is removed for the full Newton Raphson's model and the system has N buses is as follows: J1=J2=J5=J6 has size of [(N-1) x (N-1)]; J3=J4=J7=J8 has size of [(N-1) x 1]; J9=J10=J13=J14 has size of [1 x (N-1)] and J11=J12=J15=J16 has size of [1 x 1], respectively. This arrangement gives the over all dimension of $[J]$ to be [2N x 2N] and the number of known and unknown variables are 2N as well.

However, to make appropriate use of the multi-SSSC connection and consider situations where more than one device may be installed in networks, each of the J terms in Equation (30) should be made to vary according to the number of buses in the network.

To speed up computation and save storage space, the program was developed to avoid computations involving zeros and the each result stored in sparse form. With this arrangement of the Jacobian, the Newton power flow equation in polar coordinate now becomes

$$[J]\begin{bmatrix} \Delta\theta_1 \\ \cdot \\ \cdot \\ \Delta\theta_{N-1} \\ \Delta V_1 \\ \cdot \\ \cdot \\ \Delta V_{N-1} \\ \Delta\theta_{sh} \\ \Delta V_{sh} \end{bmatrix} = -\begin{bmatrix} \Delta P_1 \\ \cdot \\ \cdot \\ \Delta P_{N-1} \\ \Delta Q_1 \\ \cdot \\ \cdot \\ \Delta Q_{N-1} \\ \Delta PE \\ \Delta E \end{bmatrix} \tag{31}$$

$$\begin{bmatrix} \Delta\theta_1 \\ \cdot \\ \cdot \\ \Delta\theta_2 \\ \Delta V_1 \\ \cdot \\ \cdot \\ \Delta V_{N-1} \\ \Delta\theta_{sh} \\ \Delta V_{sh} \end{bmatrix} = -([J])^{-1}\begin{bmatrix} \Delta P_1 \\ \cdot \\ \cdot \\ \Delta P_{N-1} \\ \Delta Q_1 \\ \cdot \\ \cdot \\ \Delta Q_N \\ \Delta PE \\ \Delta E \end{bmatrix} \tag{32}$$

The Jacobian entries are given by

$$J1 = \frac{\partial P_i}{\partial \theta_j} = V_i V_j (b_{ij} \sin\theta_{ij} - g_{ij} \cos\theta_{ij}) \tag{33}$$

$$J2 = \frac{\partial P_i}{\partial V_j} V_j = V_i V_j (g_{ij} \cos\theta_{ij} + b_{ij} \sin\theta_{ij}) \tag{34}$$

$$J3 = \frac{\partial P_i}{\partial \theta_{se}} = -V_i V_{se} (g_{se} \sin(\theta_i - \theta_{se}) - b_{se} \cos(\theta_i - \theta_{se})) \tag{35}$$

$$J4 = \frac{\partial P_i}{\partial V_{se}} V_{se} = -V_i V_{se} (g_{se} \cos(\theta_i - \theta_{se}) + b_{se} \sin(\theta_i - \theta_{se})) \tag{36}$$

$$J5 = \frac{\partial Q_i}{\partial \theta_j} = -V_i V_j (g_{ij} \cos\theta_{ij} - b_{ij} \sin\theta_{ij}) \tag{37}$$

$$J6 = \frac{\partial Q_i}{\partial V_j} V_j = V_i V_j (g_{ij} \sin\theta_{ij} - b_{ij} \cos\theta_{ij}) \tag{38}$$

$$J7 = \frac{\partial Q_i}{\partial \theta_{se}} = -V_i V_{se} (g_{se} \cos(\theta_i - \theta_{se}) - b_{se} \sin(\theta_i - \theta_{se})) \tag{39}$$

$$J8 = \frac{\partial Q_i}{\partial V_{se}} V_{se} = V_i V_{se} (G_{se} \sin(\theta_i - \theta_{se}) - B_{se} \cos(\theta_p - \theta_{se})) \tag{40}$$

From the active power exchange equation, the $J9 - J12$ terms were obtained as

$$J9 = \frac{\partial PE(x)}{\partial \theta_j} = V_j V_{se} (g_{se} \sin(\theta_j - \theta_{se}) - b_{se} \cos(\theta_j - \theta_{se})) \tag{41}$$

$$J10 = \frac{\partial PE(x)}{\partial V_j} V_j = -V_j V_{se} (g_{se} \cos(\theta_j - \theta_{se}) - b_{se} \sin(\theta_j - \theta_{se})) \tag{42}$$

$$J11 = \frac{\partial PE(x)}{\partial \theta_{se}} = -V_i V_{se} (g_{se} \sin(\theta_i - \theta_{se}) + b_{se} \cos(\theta_i - \theta_{se})) + V_j V_{se} (g_{se} \sin(\theta_j - \theta_{se}) + b_{se} \cos(\theta_j - \theta_{se})) \tag{43}$$

$$J12 = \frac{\partial PE(x)}{\partial V_{se}} V_{se} = -V_i V_{se} (g_{se} \cos(\theta_i - \theta_{se}) - b_{se} (\theta_i - \theta_{se})) + V_j V_{se} (g_{se} \cos(\theta_j - \theta_{se}) - b_{se} \sin(\theta_j - \theta_{se})) \tag{44}$$

The $J13 - J16$ terms were obtained by taking the partials of Equation (45).

$$E(x) = -V_p^2 B_{sh} - V_p V_{sh} (g_{sh} \sin(\theta_p - \theta_{sh}) - b_{sh} \cos(\theta_p - \theta_{sh})) \tag{45}$$

$$J13 = \frac{\partial E(x)}{\partial \theta_p} = -V_p V_{sh} (g_{sh} \cos(\theta_p - \theta_{sh}) + b_{sh} \sin(\theta_p - \theta_{sh})) \tag{46}$$

$$J14 = \frac{\partial E(x)}{\partial V_p} V_p = -2V_p^2 - V_p V_{sh} (g_{sh} \sin(\theta_p - \theta_{sh}) - b_{sh} \cos(\theta_p - \theta_{sh})) \tag{47}$$

$$J15 = \frac{\partial E(x)}{\partial \theta_{se}} = -V_i V_{se}(g_{se}\cos(\theta_i - \theta_{se}) + b_{se}\sin(\theta_i - \theta_{se})) \quad (48)$$

$$J16 = \frac{\partial E(x)}{\partial V_{se}} V_{se} = V_i V_{se}(g_{se}\sin(\theta_i - \theta_{se}) - g_{se}\cos(\theta_i - \theta_{se})) \quad (49)$$

The updating is done using Equation (50)

$$\begin{bmatrix} \theta_1^{t+1} \\ . \\ . \\ \theta_{N-1}^{t+1} \\ V_1^{t+1} \\ . \\ . \\ V_{N-1}^{t+1} \\ \theta_{se}^{t+1} \\ V_{se}^{t+1} \end{bmatrix} = \begin{bmatrix} \theta_1^t \\ . \\ . \\ \theta_N^t \\ V_{N-1}^t \\ . \\ . \\ V_{N-1}^t \\ \theta_{se}^t \\ V_{se}^t \end{bmatrix} + \begin{bmatrix} \Delta\theta_1^t \\ . \\ . \\ \Delta\theta_{N-1}^t \\ V_1^t \\ . \\ . \\ V_{N-1}^t \\ \Delta\theta_{se}^t \\ \Delta V_{se}^t \end{bmatrix} \quad (50)$$

Then check for limits; if violated set to limits violated and run the load flow until convergence is achieved. In running the program, the row and column entries relating to the slack bus are deleted since its voltage is known and fixed already.

6.6 Scheme Implementation Algorithm

The implementation process involves development of the power system Newton-Raphson's load flow model equations with LVS-index incorporated. . Then an associated MATLAB-based program was developed and simulated to determine the stability status of the various transmission lines in the system. Weak lines could be detected with the result obtained here. Also, the ATC is computed for the various transmission lines.

A decision was made based on the computed index and ATC values whether there was any line within the zone of interest that requires compensation to make it transfer the required amount of power. If there was, then appropriate series device is incorporated into the N-R load flow model. The program is rerun to find the effect of introduction of the series FACTS devices since it could have a wide area effect on the rest of the network. At this point the system asks if the operator requires dynamic simulation or a rerun of the load flow steady state simulation. If the dynamic simulation is required, the program shifts the routine to the dynamic module and displays the result for the dynamic results and then goes back to read system input data if not prompted to stop. Also, the steady state load flow and setting of the FACTS values continue thereby ensuring that the power system runs in optimal conditions. The program stops when prompted.

The entire procedure has been articulated in Fig. (6.5).

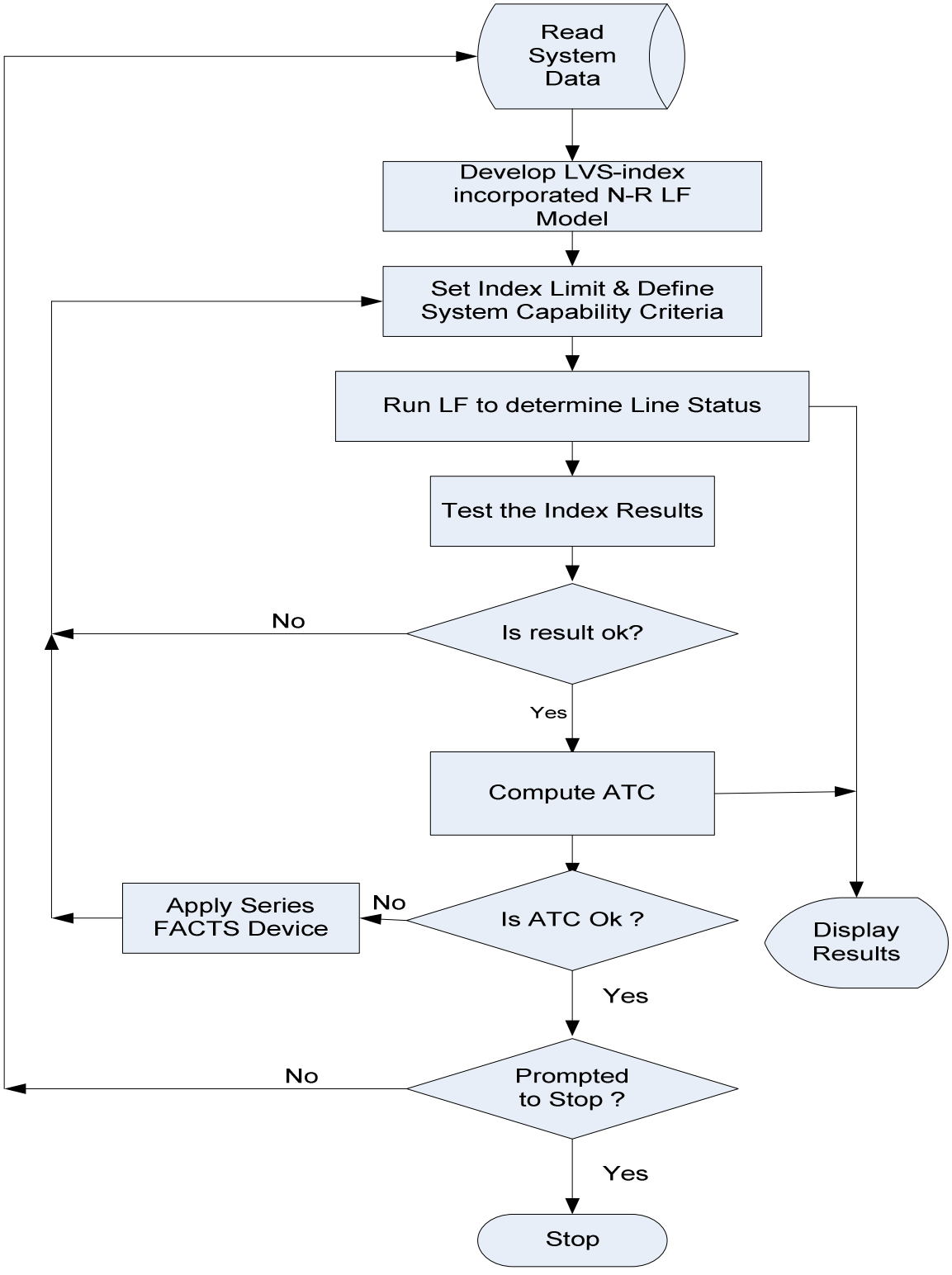

Fig. 6.5: LVS-index based optimal ATC computation algorithm

6.7 Results and Discussion

The IEEE 300 bus system was utilized in the demonstration of ATC computation using LVS index. This network has two sets of separate double lines to give a total of 411 lines. However, the network was simplified by developing a program which combined each of the double lines to form single lines, leaving the final number of lines to 409. Out of the 300 buses, 56 were selected as generator buses by the program based on the difference between the generated and consumed power. This leaves 244 buses as load buses. With this feature, the program can automatically convert a bus from generator to load or from load bus to generator depending on the operating status. The slack bus was also selected as the generator bus with the maximum net generation.

To improve the efficiency of the model, the scheme as shown in Fig. (6.5) has capability of dividing a large network into line zones and/or computing the ATC of selected lines from a given network. To illustrate this approach, the IEEE 300 network had been grouped into six zones, ‘A’ through ‘F’ composed of 70 lines each, apart from the last zone which was less than 70 lines. VCP values close to ‘0’ are stable while those close to ‘1’ are highly unstable, while lines with ATC values close to ‘1’ are ideal for bulk-wheeling of power and ATC values tending to ‘0’ implies that such lines could need to have some of its power redirected through alternative lines .

Two loading case scenarios were simulated – normal loading and 20% overloading.

6.7.1 Normal System Loading

The results obtained in the case of normal loading are depicted in Figures (6.6) to (6.11). In Figures (6.6) and (6.11) the VCP and its corresponding ATC for zones 'A' and 'F', respectively have been shown to capture the inverse proportionality of the system ATC and VCP at the base system condition as indicated in Appendices 'E' and 'F'. Figures (6.7) through (6.10) showed the ATC results for lines in zones 'B' through 'E'. This is done to clearly display the computed values.

The important of such zoning may be clearer if one considers that in present day electricity industry emphasizes the procurement of power from the cheapest sources putting every factor into consideration. In this way, an Independent System Operator (ISO) may be interested in determining the freest line to send power to firms under its jurisdiction. Therefore, it will check which lines have enough capability to bulk-wheel its power to each of the companies it is serving. This will enable the determination of where to buy and sale safe, quality, and cheap power.

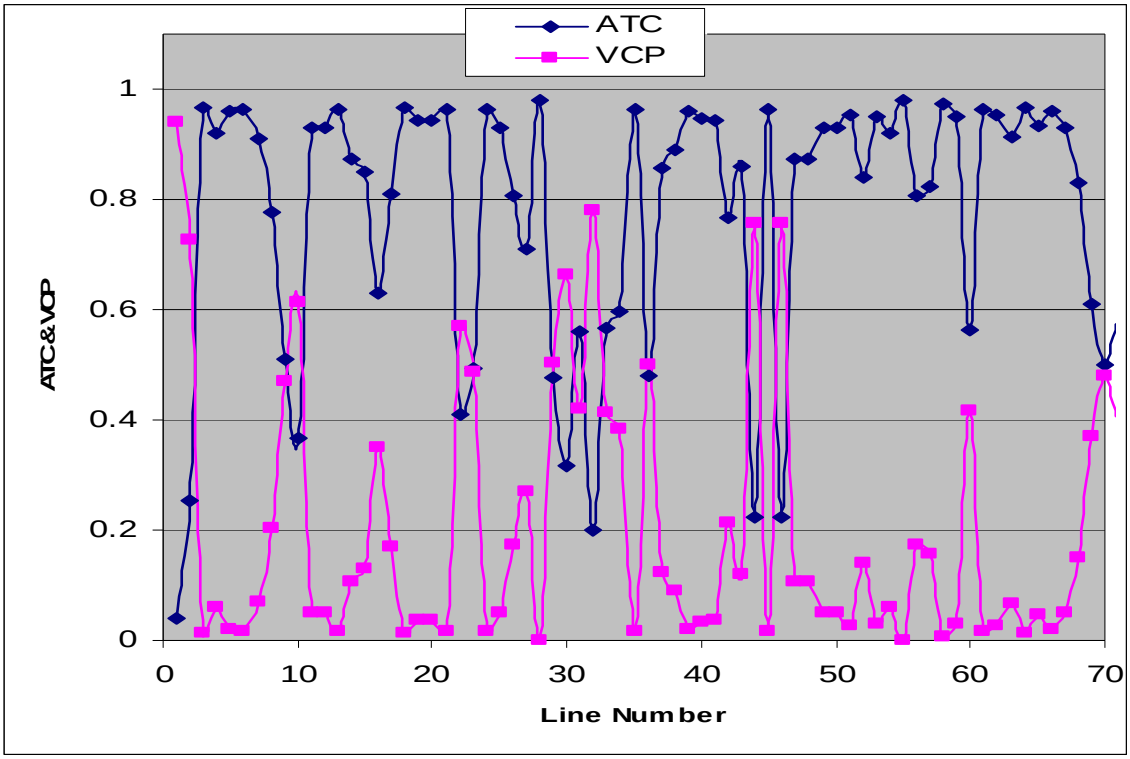

Fig. 6.6: Plot of VCP and ATC for Lines 1 to 72 using VCP model (Zone A)

In the plots, lines linking generator buses to load buses showed lower ATC values while lines connecting generator bus showed high ATC values. The lines connecting two load buses showed moderate ATC values. This clearly depicted the facts that there exist a great exchange of power between generator buses and load buses and that some load buses which are connected directly to generator buses (primary load buses) got larger supply of power than other load buses not directly connected to generator buses (secondary load buses). The primary load buses then serve as somewhat generator buses to supply the secondary load buses.

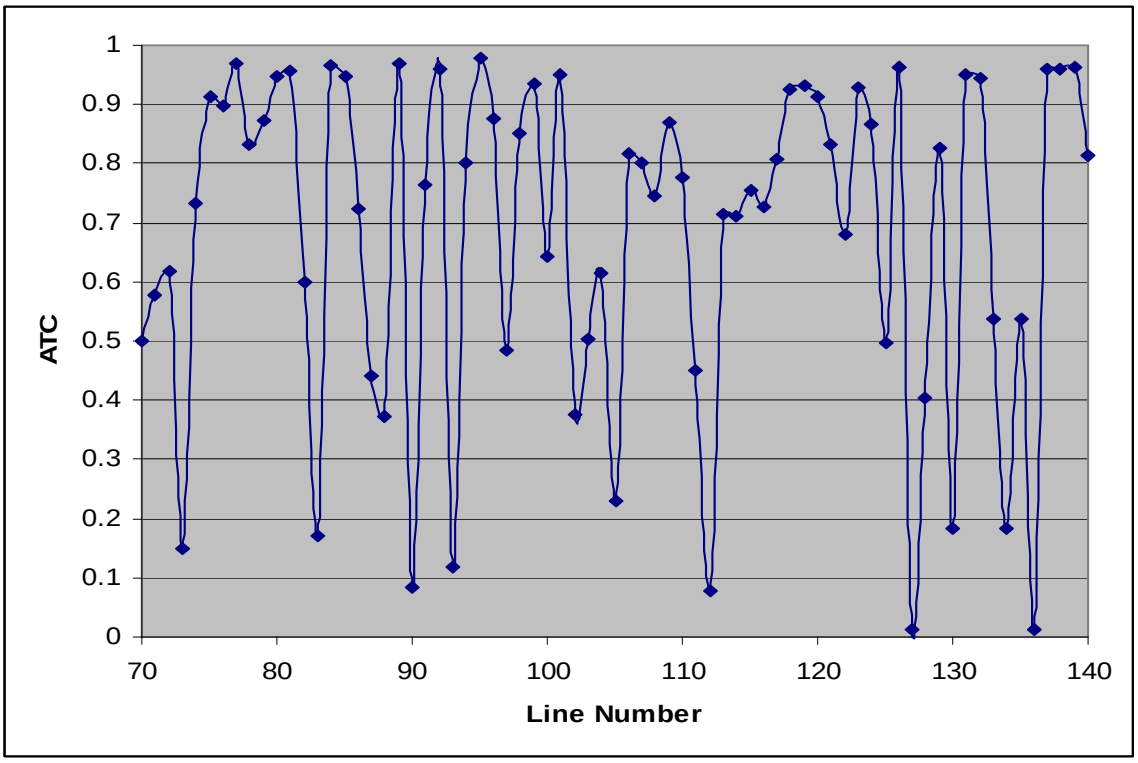

Fig. 6.7: Plot of ATC for Lines 70 to 140 using VCP model (Zone B)

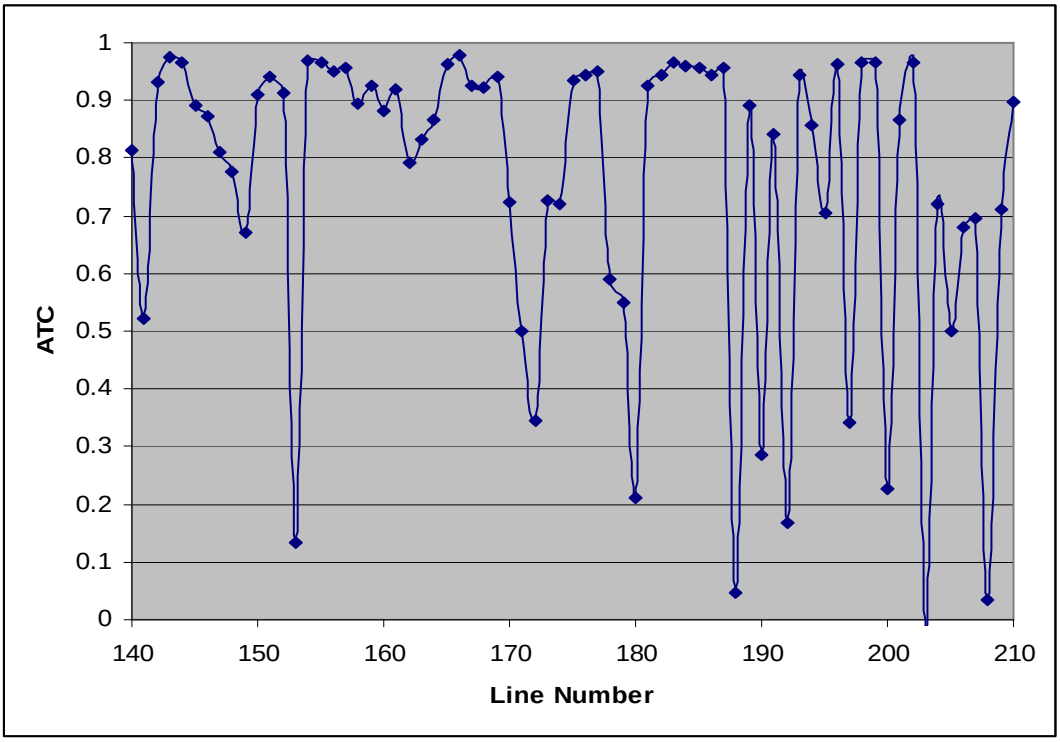

Fig. 6.8: Plot of ATC for Lines 140 to 210 using VCP model (Zone C).

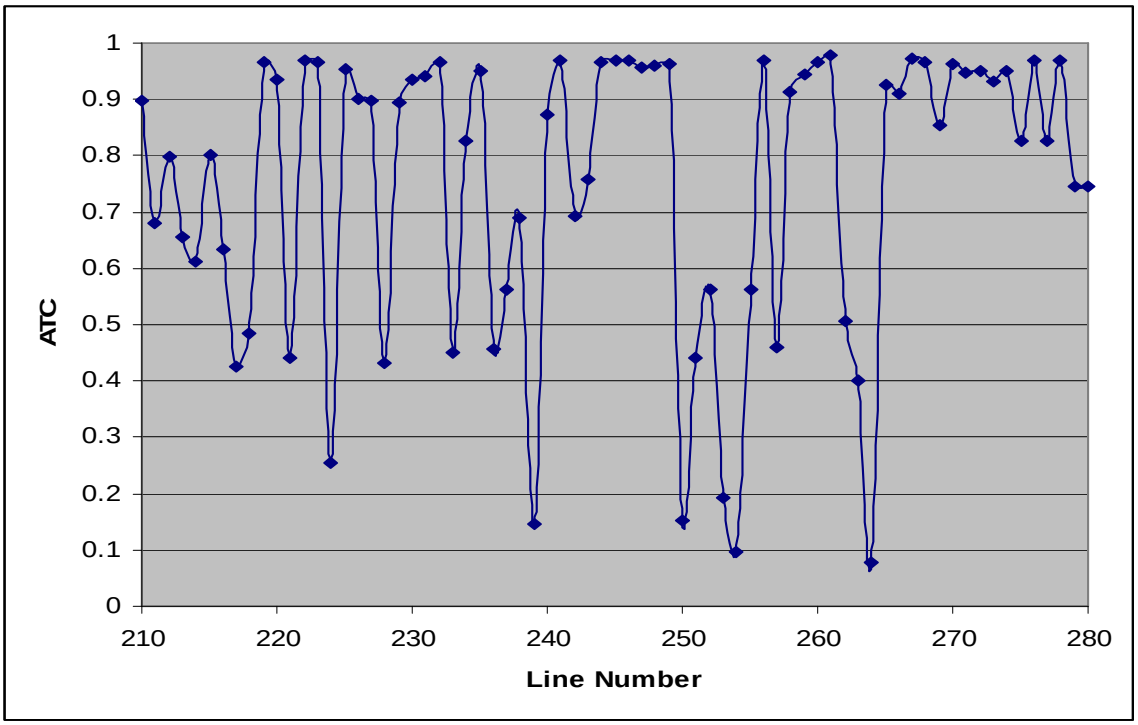

Fig. 6.9: Plot of ATC for Lines 210 to 280 using VCP model (Zone D).

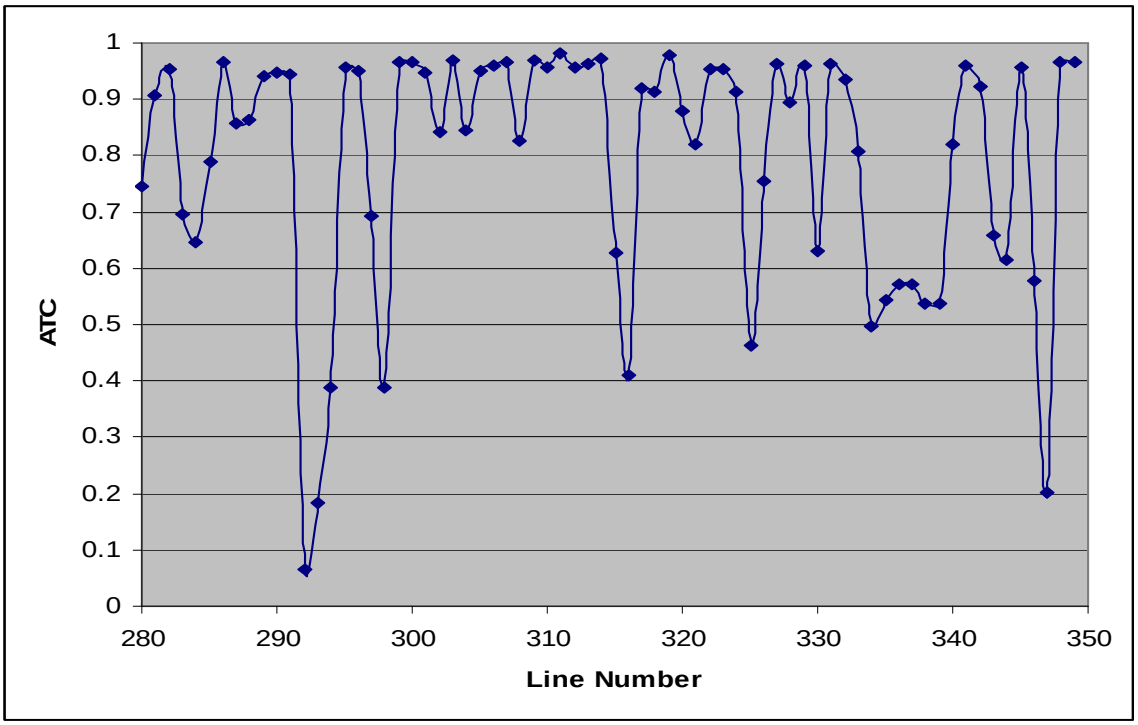

Fig. 6.10: Plot of ATC for Lines 280 to 350 using VCP model (Zone E).

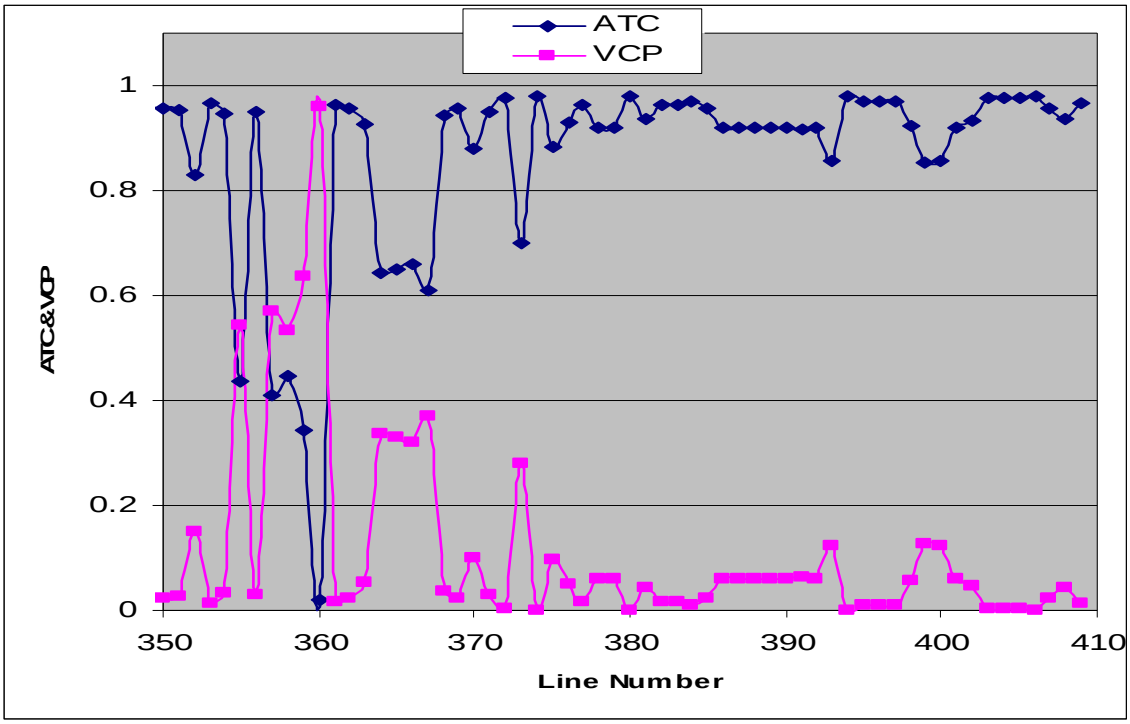

Fig. 6.11: Plot of ATC &VCP for Lines 350 to 409 (Zone F).

There was a somewhat reduced exchange between generator buses. It was very visible from Fig. (6.11) that lines 370 to 409 showed consistently high ATC values. This was traceable to the fact that the IEEE 300 bus system had more generators connected to these lines and therefore less power is transferred along them.

6.7.2 20 Percent Increased System Loading

The results obtained when the entire system active power loading was increased by 20% is displayed in Figures (6.12) and (6.13) for only zones 'A' and 'F' which were found to have significant variation in the ACP and ATC values under normal loading conditions.

It was noticed that at 20% increased active power load demand, the VCP of line one in Fig. (6.12) and line 360 in Fig. (6.13) were above the threshold value of 1.0 for stable condition. Accordingly, their corresponding ATC values became negative.

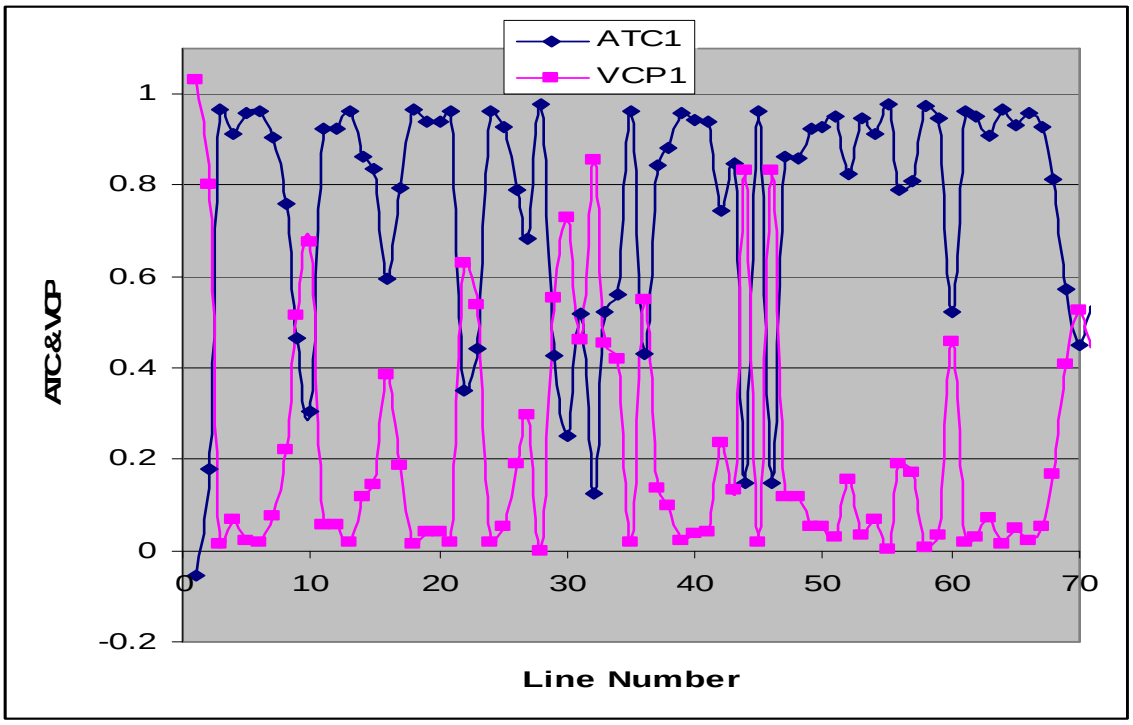

Fig. 6.12: Plot of ATC &VCP for Lines 1 to 70 (Zone A) with 20% increased loading.

The consequence of this observation was that these lines could not accommodate 20% increased loading of the entire system. If such loading condition was to be executed in practice, such other adjoining lines (line 3 - 8 in Fig. (6.12) and many close lines in Fig. (6.13)) if connected to same buses could be used as alternative route to wheel the extra power required to meet the increased loading condition.

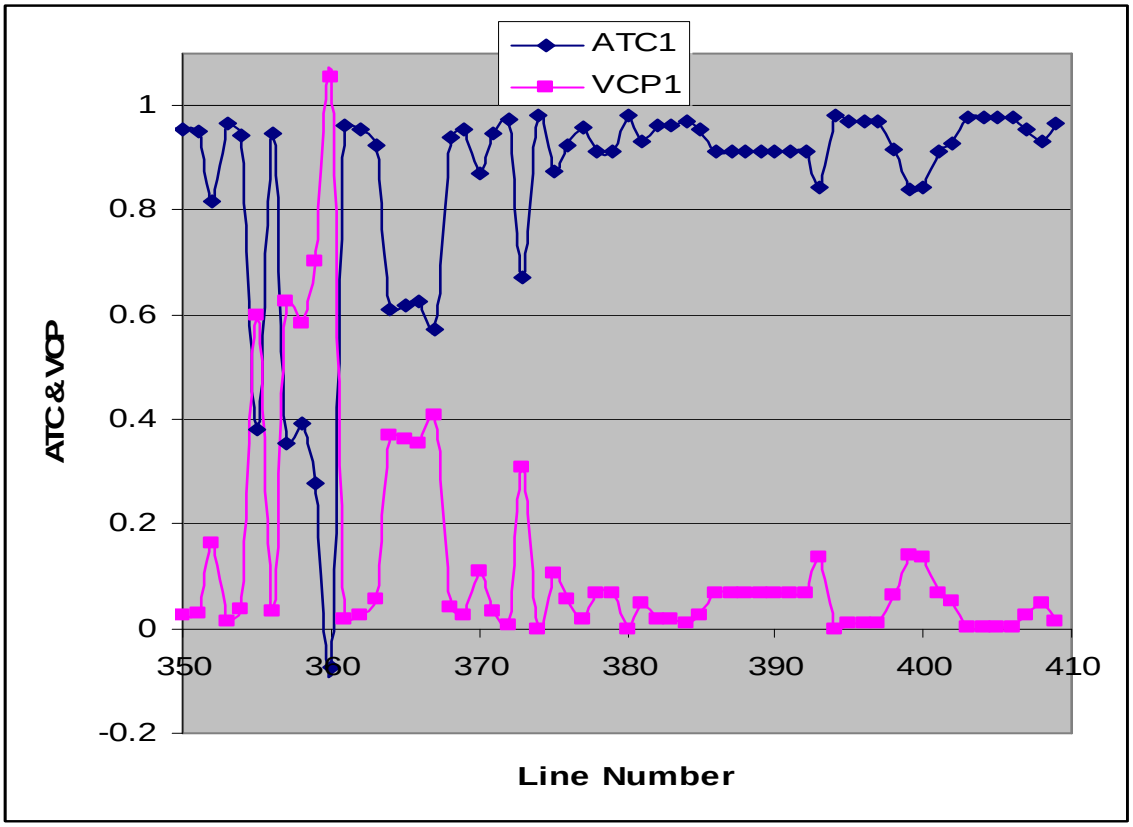

Fig. 6.13: Plot of ATC &VCP for Lines 350 to 410 (Zone F) with 20% increased loading

6.8 Conclusion

The concept of line voltage stability index has been effectively applied to determine the transmission line available transfer capability of the IEEE 300 bus system. Results obtained and analyzed with the placement of generators and loading of the test system showed that the concept was able to give a good picture of the commitment of the lines.

The effect of increased loading on the ATC computation was demonstrated in the second part of this work. With this method, it was possible to determine lines vulnerable

to collapse under increased loading as well as alternate lines which may be used to wheel power to meet increasing demand safely.

This is the first step in a series of application and verification of the concept. Further evaluation of this idea could be targeted at successive loading of selected lines to determine what amount of additional power can be transferred across them before the allocated total transfer capability is reached using the line voltage stability index. Thereafter, the selected weak lines will be compensated and the system wide effect of this compensation on the line voltage stability index values and the available transfer capability could be evaluated.

As a future work, the series compensation component of the developed algorithm could be implemented. It may also be interesting to utilize other line voltage stability index models to see the effect of reactive power flow on the available transfer capability of the entire system. Some assumptions which considered Line Voltage Stability (LVS) index to be equal to the sum of the Capacity Benefit Margin (CBM), Transmission Reliability Margin (TRM), and Existing Transmission Commitment (ETC) were made. This may need further evaluation.

6.9 References

[1] L. Philipson and H. L. Willis [1998], "Understanding Electric Utilities and De-Regulation," Marcel Dekker, Inc. NY 10016, pp. 2.

[2] P. Marannino, P. Bresesti, A. Garavaglia, F. Zanellini and R. Vailati, "Assessing the transmission transfer capability sensitivity to power system parameters," 14th PSCC, Sevilla, 24-28 June 2002.

[3] "Electric power transfer capability Concepts, applications, sensitivity, uncertainty," Power Systems Engineering Research Center, 2001.

[4] P. W. Sauer, "Technical challenges of computing available transfer capability (ATC) in electric power systems," Proceedings, 30th Annual Hawaii International Conference on System Sciences, April, 7-10, 1997.

[5] Available transfer capability definitions and determination, A framework for determining available transfer capabilities of the interconnected transmission networks for commercially viable electricity market, North America Electric reliability Council, June 1996.

[6] P. Jirapong, "Total transfer enhancement using hybrid evolution algorithm," CMU. J. Sci. vol. 6(2), pp 301 – 311, 2007.

[7] FRCC ATC calculation and coordination procedures, Florida Reliability Coordinating Council, Approved by the Planning Committee April 4, 2006.

[8] S. H. Goh, "Evaluating power transfer capability for deregulated power systems," A Ph.D. Dissertation submitted to the School of Information Technology and Electrical Engineering, The University of Queensland, St. Lucia, 4072, April 2008.

[9] K. N. Rao, J. Amarnath and K. A. Kumar, "Voltage constrained available transfer capability enhancement with FACTS devices," ARPN Journal of Engineering and Applied Sciences, Vol. 2, No. 6, December 2007.

[10] C. Reis and F. P. Maciel Barbosa, "A comparison of voltage stability indices," IEEE Melecon Benalmadena Spain, 2006.

[11] D. O. Dike, S. M. Mahajan and G. Radman [2007], "Development of versatile voltage stability index algorithm," IEEE Electrical Power Conference 2007, Montreal QC, Canada.

[12] L. Zhao and A. Abur, "Two-layer multi-area total transfer capability computation," Bulk Power System Dynamics and Control – VI, pp 499-503, August 22-27, 2004, Cortina d'Ampezzo, Italy.

[13] R. Gnanadass, P. Venkatesh, T. G. Palanievelu and N. P. Padhy, "Assessment of available and economic transfer capability for practical power systems with capacity benefit and transmission reliability margins," IE(I) Journal-EL, Vol. 87, June 2006.

[14] X. P. Zhang, C. Rehtanz and B. Pal, Flexible AC Transmission Systems: Modeling and Control, Springer-Verlag Berlin Heidelberg Germany, pp 2-3, 2006.

[15] Y. H. Song and A. T. Johns, Flexible ac transmission systems (FACTS), The Institute of Electrical Engineers, London, United Kingdom, 1999.

[16] D. N. Nkwetta, V. V. Thong and R. Belmans, "Protection of transmission lines using series compensation capacitors in Cameroon-Southern interconnected system," 3rd IEEE Benelux Young Researchers Symposium in Electrical Power Engineering, 27-28 April 2006, Ghent, Belgium, pp. 1-5.

[17] V. Venkatasubramanian and C. W. Taylor, "Improving Pacific Intertie stability using Slatt thyristor controlled series compensator," IEEE PES 2000 WM Panel Session, Singapore.

[18] S. Panda and R. N. Patel, "Improving power system transient stability with an off-centre location of shunt FACTS devices," Journal of Electrical Engineering, vol. 57, no. 6, pp. 365-368, 2006. of Power technologies, Assistant Secretary for Energy Efficiency and Renewable Energy, U.S. DOE, pp. 4-9, 2002.

[19] W. Ongsakul and P. Jirapong, "Optimal placement of multi-type FACTS devices for total transfer capability enhancement using improved evolution programming," Asian Institute of Technology, P. O. Box 4, Klong Luang, Pathumthani 12120, Thailand, email: ongsakul@ait.ac.th.

[20] D. X. Zhang, B. Pal and C. Rehtanz, "Flexible AC transmission systems: modeling and control," Springer-Verlag Berlin Heidelberg, Germany, 2006.

[21] Y. H. Song and A. T. Johns, Flexible ac transmission systems (FACTS), The Institute of Electrical Engineers, London, United Kingdom, 1999.

[22] United States-Canada Power System Outage Task Force, Interim Report: Causes of the August 14th Blackout in the United States and Canada (Nov. 2003) (Interim Report).

[23] U.S.-Canada Task Force on 14 August 2003 Blackout, "The August 14 blackout compared with previous major North America outages," Final Report on the August 14th 2003 Blackouts in the United States and Canada, pp. 103-106, 2003.

[24] D-VAR Solutions – Dynamic VAR Support for a More Reliable Grid, 2007, American Superconductor, Inc. River, New Jersey, 2000, pp.112.

[25] J. Webber, “Efficient available transfer capability analysis using linear methods,” PSERC Internet Seminar, November 7, 2000.

CHAPTER 7

CONCLUSION

7.1 General

Various available voltage stability indices and reactive power compensation schemes were reviewed and their weakness in view of the increasing cases of large scale system outages was identified. To improve the performance of compensation schemes, a set of factors and criteria that need to be considered in their application to solving current and evolving problems associated with a restructured and weak grid have been developed.

In view of the perceived weaknesses of the present index models and compensation schemes, new models were developed for the application of voltage stability index to long distance bulk power wheeling which was not the case before restructuring. This new index model developed was simulated with the IEEE 14 and 30 bus systems (Data in Appendices ‘A’ through ‘D’). The results obtained were compared with those simulated using the same systems and under the same conditions with earlier developed index models. In addition, schemes that may determine which reactive power compensation method may be suitable given a set of operation guidelines from the client or utility were presented.

The developed model was also applied successfully to the IEEE 14 bus system (Appendices ‘A’ and ‘B’) where microgrid was connected. It proved to be useful in

improving the operational modes of the microgrid interconnected system and led to restoration of stability to load buses that were tending towards voltage collapse. These models and schemes have been published and presented in the IEEE conferences and seen as a viable option towards addressing the continued power system outages.

Additional models to utilize these indices to obtain enhanced reactive power compensation using FACTS were done with microgrids. These will reveal the effect of FACTS inclusion in power system which has been reported to introduce disturbances in the form of harmonics which is prevalent in power electronic devices.

7.2 Contributions of the Dissertation

The following were accomplished in this dissertation:

7.2.1 A novel voltage stability index model using the complex transmission line pi-structure was developed.

This new model considered the effect of long and medium length transmission lines covering more than 150 miles, the current distances between various RTOs and ISOs in North America in the performance of power systems. However, existing voltage stability index models which were developed using the two-machine model which were found to be suitable for short transmission lines only. The model was simulated and compared with existing models, and the result published in IEEE EPC conference in Montreal QC, Canada, October 25 - 26, 2007.

7.2.2 The application of L-index Model to Develop Improved Microgrid System

A novel microgrid with improved operational modes was another novel contribution of this dissertation. The results obtained in this work showed that using this concept may provide unique opportunities in load shedding, seamless interconnection of distributed energy resources to power grids and smooth transition from grid to islanded operation of the microgrid. Results were presented in the IEEE PES General Meeting in Pittsburg, July 20 – 24, 2008.

7.2.3 L-index Application to Converter Modulation

The work applied the L-index obtained from the steady state MATLAB ® load flow program to successfully provide a system-based modulation index to obtain a generalized modulation signal. This signal was effectively transferred to the MATLAB Simulink model and compared with carrier based triangular signals (T1 and T2) to generate multi-level converter switching functions. This gave rise to the L-index modulated multi-level Voltage Source Inverter (VSI) scheme which was the first attempt to utilize online computed power system status as a control parameter for the VSI. This was considered a unique contribution in this work in view of the key role VSI is currently playing in FACTS technology and various other energy DC-AC and AC-DC power conversion systems utilized variously in industries and other power application areas.

7.2.4 Newton-Raphson's Load Flow Model was extended to include Multiple FACTS Applications.

The shunt devices were successfully applied to determine the condition of IEEE 300 bus system with zoning. The data utilized for this simulation is as indicated in appendices 'E' and 'F'.

7.2.5 Developed Criteria for the Optimal Utilization of Index models

This will help system operators to determine which index should be used in given conditions was also developed.

7.2.6 Developed Operational Algorithms for Different Reactive Power Compensation Approaches

These algorithms made it possible to perform simulations of the IEEE 14, 30 and 300 bus systems using MATLAB ® program.

7.2.7 Line Voltage Stability (LVS) index was successfully used to determine the Available Transfer Capability

The ATC of IEEE 300 bus system under both normal and increased loading conditions was computed. The scheme though simplified was able to show clearly lines that are overloaded and provided alternate transmission lines through which power may be transferred without violating set standards.

7.2.8 Developed an Interactive Demo Using MATLAB GUI Platform

This demo was demonstrated with the IEEE 300, 30 and 14 bus systems for the Bus Voltage Stability Index regulated shunt compensation scheme and the ATC computation.

The MATLAB dynamic Simulink models and MATLAB program developed are included in this dissertation as Appendices 'G' and 'H'.

7.3 Future Work

Suggested further research work may be targeted to address one of these issues:

(I) Optimization of the Developed Models using Genetic Algorithm**.**

This will predict some unforeseen power system conditions which were not addressed in this dissertation.

(II) Develop Improved System Security by Utilizing LVS Index-based ATC Computation

The application of the concept of line voltage stability index model to compute available transfer capacity is a novel idea which may open up diverse research interest considering the current problems being experienced by utilities, independent system operators, regional transmission organizations and various governmental agencies in appropriate determining the most secured way of bulk wheeling of power.

(III) Develop a Composite Reactive Power Support Philosophy.

Further application of the concepts developed in this work may lead to the evolvement of a novel reactive power support system which will improve the present situation.

(IV) Performing a Small Signal Analysis to Determine System Stability

If a new compensation device is developed, there is need to performance a small signal analysis of this structure to check its robustness and develop practical stability criteria for its operation.

(V) Develop a New Model for Line Voltage Stability Index Complex Pi-model.

(VI) Reactive Power Quantification Using the Concept of Voltage Stability Index

This will help to pay appropriate compensation to reactive power suppliers, which will lead to increase in the number of participant and thereby pulling of resources.

7.4 Summary

This research effort has created a renewed awakening of mind as to the need to provide an appropriate index for computation of power system status and develop selection criteria that could serve as a base of generalized power system index model. From the practical perspective, we have shown that the various voltage stability index models could be applied to a variety of current power system problems.

The concept of voltage stability index has been successfully applied to various sectors of power system related to reactive power compensation, power transfer, monitoring and determination of the status of FACTS and microgrid interconnected

networks. The final decision of the authors to utilize line voltage stability index has created new research foci that will evolve renewed interest in the emerging power system restructured market. It is believed that with innovative research in the application of voltage stability index, fresh hopes for the effective determination and quantification of reactive power supplied and consumed by various entities. Such an achievement could lead to better pricing for reactive power in the future which will propel various players in the power industry to venture into the now almost abandoned reactive power supply.

The results obtained in this dissertation compared favorably with other results from similar research efforts. It is believed that this dissertation could make significant contributions towards technology enhancement through improved system performance.

APPENDIX

APPENDIX A

Bus Data for IEEE 14 Bus System

Bus Number	Flat V (p.u)	P load (p.u)	P gen. (p.u)	Q gen (p.u)	Q load (p.u)	Flat Bus Angle
1	1	0	2.3239	-0.16888	0	0
2	1	0.217	0.4	0.42396	0.127	0
3	1	0.942	0	0.23394	0.19	0
4	1	0.478	0	0.2	0.0129	0
5	1	0.076	0	0	0.0016	0
6	1	0.112	0	0.1224	0.075	0
7	1	0	0	0	0	0
8	1	0	0	0.17357	0	0
9	1	0.295	0	0	0.0166	0
10	1	0.09	0	0.08	0.058	0
11	1	0.035	0	0	0.018	0
12	1	0	0	0	0.31	0
13	1	0.135	0	0	0.058	0
14	1	0.149	0	0.2	0.0412	0

Source: http://www.ee.washington.edu/research/pstca/

APPENDIX B

Line Data for IEEE 14 Bus System

Line No	frombus	tobus	R(p.u.)	X1(p.u.)	Bh(p.u.)	a to 1
1	1	2	0.01938	0.05917	0.0528	1
2	1	5	0.05811	0.22304	0.0492	1
3	2	3	0.04699	0.19797	0.0438	1
4	2	4	0.05811	0.17632	0.0374	1
5	2	5	0.05695	0.17388	0.034	1
6	3	4	0.06701	0.17103	0.0346	1
7	4	5	0.01335	0.04211	0.0128	1
8	4	7	0	0.20912	0	0.978
9	4	9	0	0.55618	0	0.969
10	5	6	0	0.25202	0	0.932
11	6	11	0.09498	0.1989	0	1
12	6	12	0.12291	0.25581	0	1
13	6	13	0.06615	0.193087	0	1
14	7	8	0	0.17615	0	1
15	7	9	0	0.11001	0	1
16	9	10	0.1686	0	0	1
17	9	14	0.12711	0.27038	0	1
18	10	11	0.08205	0.67	0	1
19	12	13	0.22092	0.29988	0	1
20	13	14	0.17093	0.39802	0	1

Source: http://www.ee.washington.edu/research/pstca/

APPENDIX C

Bus Data for IEEE 30 Bus System

Bus No	V(p.u)	Pg (p.u)	Qg (p.u)	Pl (p.u)	Ql(p.u)	Bus Angle
1	1	0	0	0	0	0
2	1	0.6097	0	0.217	0.127	0
3	1	0	0	0.024	0.012	0
4	1	0	0	0.076	0.016	0
5	1	0	0	0	0	0
6	1	0	0	0	0	0
7	1	0	0	0.228	0.109	0
8	1	0	0	0.3	0.3	0
9	1	0	0	0	0	0
10	1	0	0	0.058	0.02	0
11	1	0	0	0	0	0
12	1	0	0	0.112	0.075	0
13	1	0.37	0	0	0	0
14	1	0	0	0.062	0.016	0
15	1	0	0	0.082	0.025	0
16	1	0	0	0.035	0.018	0
17	1	0	0	0.09	0.058	0
18	1	0	0	0.032	0.009	0
19	1	0	0	0.095	0.034	0
20	1	0	0	0.022	0.007	0
21	1	0	0	0.175	0.112	0
22	1	0.2159	0	0	0	0
23	1	0.192	0	0.032	0.016	0
24	1	0	0	0.087	0.067	0
25	1	0	0	0	0	0
26	1	0	0	0.035	0.023	0
27	1	0.2691	0	0	0	0
28	1	0	0	0	0	0
29	1	0	0	0.024	0.009	0
30	1	0	0	0.106	0.19	0

Source: http://www.ee.washington.edu/research/pstca/

APPENDIX D

Line Data for IEEE 30 Bus System

Line No.	Fbus	Tbus	R (p.u)	X (p.u)	Line Susc a to 1	
1	1	2	0.0192	0.0575	0.0132	1
2	1	3	0.0452	0.1852	0.0102	1
3	2	4	0.057	0.1737	0.0092	1
4	2	5	0.0472	0.1983	0.01045	1
5	2	6	0.0581	0.1763	0.00935	1
6	3	4	0.0132	0.0379	0.0021	1
7	4	6	0.0119	0.0414	0.00225	1
8	4	12	0	0.256	0	1
9	5	7	0.046	0.116	0.0051	1
10	6	7	0.0267	0.082	0.00425	1
11	6	8	0.012	0.042	0.00225	1
12	6	9	0	0.208	0	1
13	6	10	0	0.556	0	1
14	6	28	0.0169	0.0599	0.00325	1
15	8	28	0.0636	0.2	0.0107	1
16	9	10	0	0.11	0	1
17	9	11	0	0.208	0	1
18	10	17	0.0324	0.0845	0	1
19	10	20	0.0936	0.209	0	1
20	10	21	0.0348	0.0749	0	1
21	10	22	0.0727	0.1499	0	1
22	12	13	0	0.14	0	1
23	12	14	0.1231	0.2559	0	1
24	12	15	0.0662	0.1304	0	1
25	12	16	0.0945	0.1987	0	1
26	14	15	0.221	0.1997	0	1
27	15	18	0.107	0.2185	0	1
28	15	23	0.1	0.202	0	1
29	16	17	0.0824	0.1932	0	1
30	18	19	0.0639	0.1292	0	1
32	19	20	0.034	0.068	0	1
33	21	22	0.0116	0.0236	0	1
34	22	24	0.115	0.179	0	1
35	23	24	0.132	0.27	0	1
35	24	25	0.1885	0.3292	0	1
36	25	26	0.2544	0.38	0	1
37	25	27	0.1093	0.2087	0	1
38	27	29	0.2198	0.4153	0	1
39	27	30	0.3202	0.6027	0	1
40	28	27	0	0.396	0	1

Source: http://www.ee.washington.edu/research/pstca/

APPENDIX E

Bus Data for IEEE 300 Bus System

Bus No. Modified	Bus No. Actual	Flat Bus V (p.u)	Pl (p.u)	Pg (p.u)	Qg (p.u)	Ql (p.u)	Flat Bus V_angle
1	1	1	0.9	0	0.4	0.29	0
2	2	1	0.56	0	0	0.15	0
3	3	1	0.2	0	0	0	0
4	4	1	0	0	0	0	0
5	5	1	3.53	0	0	1.3	0
6	6	1	1.2	0	0	0.41	0
7	7	1	0	0	0	0	0
8	8	1	0.58	-0.05	0	0.14	0
9	9	1	0.96	0	0	0.43	0
10	10	1	1.48	-0.05	0	0.33	0
11	11	1	0.83	0	0	0.21	0
12	12	1	0	0	0	0	0
13	13	1	0.58	0	0	0.1	0
14	14	1	1.6	0	0	0.6	0
15	15	1	1.267	0	0	0.23	0
16	16	1	0	0	0	0	0
17	17	1	5.61	0	0	0	0
18	19	1	0	0	1	0	0
19	20	1	5.95	-0.1	0	0.2	0
20	21	1	0.77	0	0	0.01	0
21	22	1	0.81	0	0	0.23	0
22	23	1	0.21	0	0	0.07	0
23	24	1	0	0	0	0	0
24	25	1	0.45	0	0	0.12	0
25	26	1	0.28	0	0	0.09	0
26	27	1	0.69	0	0	0.13	0
27	33	1	0.55	0	0	0.06	0
28	34	1	0	0	0	0.5	0
29	35	1	0	0	0	0.5	0
30	36	1	0	0	0	0	0
31	37	1	0.85	0	0	0.32	0
32	38	1	1.55	0	0	0.18	0
33	39	1	0	0	0	0	0
34	40	1	0.46	0	0	-0.21	0
35	41	1	0.86	0	0	0	0
36	42	1	0	0	0	0	0
37	43	1	0.39	0	0	0.09	0
38	44	1	1.95	0	0	0.29	0
39	45	1	0	0	0	0	0
40	46	1	0	0	0	0	0
41	47	1	0.58	0	0	0.118	0
42	48	1	0.41	0	0	0.19	0
43	49	1	0.92	0	0	0.26	0
44	5051	1	-0.005	0	0	0.05	0
45	52	1	0.61	0	0	0.28	0
46	53	1	0.69	0	0	0.03	0
47	54	1	0.1	0	0	0.01	0
48	55	1	0.22	0	0	0.1	0
49	57	1	0.98	0	0	0.2	0
50	58	1	0.14	0	0	0.01	0

51	59	1	2.18	0	0	1.06	0
52	60	1	0	0	0	0	0
53	61	1	2.27	0	0	1.1	0
54	62	1	0	0	0	0	0
55	63	1	0.7	0	0	0.3	0
56	64	1	0	0	0	0	0
57	69	1	0	0	0	0	0
58	70	1	0.56	0	0	0.2	0
59	71	1	1.16	0	0	0.38	0
60	72	1	0.57	0	0	0.19	0
61	73	1	2.24	0	0	0.71	0
62	74	1	0	0	0	0	0
63	76	1	2.08	0	0	1.07	0
64	77	1	0.74	0	0	0.28	0
65	78	1	0	0	0	0	0
66	79	1	0.48	0	0	0.14	0
67	80	1	0.28	0	0	0.07	0
68	81	1	0	0	0	0	0
69	84	1	0.37	3.75	0	0.13	0
70	85	1	0	0	0	0	0
71	86	1	0	0	0	0	0
72	87	1	0	0	0	0	0
73	88	1	0	0	0	0	0
74	89	1	0.442	0	0	0	0
75	90	1	0.66	0	0	0	0
76	91	1	0.174	1.55	0	0	0
77	92	1	0.158	2.9	0	0	0
78	94	1	0.603	0	0	0	0
79	97	1	0.399	0	0	0	0
80	98	1	0.667	0.68	0	0	0
81	99	1	0.835	0	0	0	0
82	100	1	0	0	0	0	0
83	102	1	0.778	0	0	0	0
84	103	1	0.32	0	0	0	0
85	104	1	0.086	0	0	0	0
86	105	1	0.496	0	0	0	0
87	107	1	0.046	0	0	0	0
88	108	1	1.121	1.17	0	0	0
89	109	1	0.307	0	0	0	0
90	110	1	0.63	0	0	0	0
91	112	1	0.196	0	0	0	0
92	113	1	0.262	0	0	0	0
93	114	1	0.182	0	0	0	0
94	115	1	0	0	0	0	0
95	116	1	0	0	0	0	0
96	117	1	0	0	0	0	0
97	118	1	0.141	0	0	6.5	0
98	119	1	0	19.3	0	0	0
99	120	1	7.77	0	0	2.15	0
100	121	1	5.35	0	0	0.55	0

101	122	1	2.291	0	0	0.118	0
102	123	1	0.78	0	0	0.014	0
103	124	1	2.76	2.4	0	0.593	0
104	125	1	5.148	0	0	0.827	0
105	126	1	0.579	0	0	0.051	0
106	127	1	3.808	0	0	0.37	0
107	128	1	0	0	0	0	0
108	129	1	0	0	0	0	0
109	130	1	0	0	0	0	0
110	131	1	0	0	0	0	0
111	132	1	0	0	0	0	0
112	133	1	0	0	0	0	0
113	134	1	0	0	0	0	0
114	135	1	1.692	0	0	0.416	0
115	136	1	0.552	0	0	0.182	0
116	137	1	2.736	0	0	0.998	0
117	138	1	8.267	-1.92	0	1.352	0
118	139	1	5.95	0	0	0.833	0
119	140	1	3.877	0	0	1.147	0
120	141	1	1.45	2.81	0	0.58	0
121	142	1	0.565	0	0	0.245	0
122	143	1	0.895	6.96	0	0.355	0
123	144	1	0	0	0	0	0
124	145	1	0.24	0	0	0.14	0
125	146	1	0	0.84	0	0	0
126	147	1	0	2.17	0	0	0
127	148	1	0.63	0	0	0.25	0
128	149	1	0	1.03	0	0	0
129	150	1	0	0	0	0	0
130	151	1	0	0	0	0	0
131	152	1	0.17	3.72	0	0.09	0
132	153	1	0	2.16	0	0	0
133	154	1	0.7	0	0	0.05	0
134	155	1	2	0	0	0.5	0
135	156	1	0.75	0	0	0.5	0
136	157	1	1.235	0	0	-0.243	0
137	158	1	0	0	0	0	0
138	159	1	0.33	0	0	0.16	0
139	160	1	0	0	0	0	0
140	161	1	0.35	0	0	0.15	0
141	162	1	0.85	0	0	0.24	0
142	163	1	0	0	0	0.004	0
143	164	1	0	0	0	0	0
144	165	1	0	0	0	0	0
145	166	1	0	0	0	0	0
146	167	1	2.999	0	0	0.957	0
147	168	1	0	0	0	0	0
148	169	1	0	0	0	0	0
149	170	1	4.818	2.05	0	2.05	0
150	171	1	7.636	0	0	2.911	0

151	172	1	0.265	0	0	0	0
152	173	1	1.635	0	0	0.43	0
153	174	1	0	0	0	0	0
154	175	1	1.76	0	0	0.83	0
155	176	1	0.05	0	0	0.04	0
156	177	1	0.28	2.28	0	0.12	0
157	178	1	4.274	0.84	0	1.73	0
158	179	1	0.74	0	0	0.29	0
159	180	1	0.695	0	0	0.493	0
160	181	1	0.734	0	0	0	0
161	182	1	2.407	0	0	0.89	0
162	183	1	0.4	0	0	0.04	0
163	184	1	1.368	0	0	0.166	0
164	185	1	0	2	0	0	0
165	186	1	0.598	12	0	0.243	0
166	187	1	0.598	12	0	0.243	0
167	188	1	1.82	0	0	0.436	0
168	189	1	0.07	0	0	0.02	0
169	190	1	0	4.75	0	0	0
170	191	1	4.89	19.73	0	0.53	0
171	192	1	8	0	0	0.72	0
172	193	1	0	0	0	0	0
173	194	1	0	0	0	0	0
174	195	1	0	0	0	0	0
175	196	1	0.1	0	0	0.03	0
176	197	1	0.43	0	0	0.14	0
177	198	1	0.64	4.24	0	0.21	0
178	199	1	0.35	0	0	0.12	0
179	200	1	0.27	0	0	0.12	0
180	201	1	0.41	0	0	0.14	0
181	202	1	0.38	0	0	0.13	0
182	203	1	0.42	0	0	0.14	0
183	204	1	0.72	0	0	0.24	0
184	205	1	0	0	0	-0.05	0
185	206	1	0.12	0	0	0.02	0
186	207	1	-0.21	0	0	-0.14	0
187	208	1	0.07	0	0	0.02	0
188	209	1	0.38	0	0	0.13	0
189	210	1	0	0	0	0	0
190	211	1	0.96	0	0	0.07	0
191	212	1	0	0	0	0	0
192	213	1	0	2.72	0	0	0
193	214	1	0.22	0	0	0.16	0
194	215	1	0.47	0	0	0.26	0
195	216	1	1.76	0	0	1.05	0
196	217	1	1	0	0	0.75	0
197	218	1	1.31	0	0	0.96	0
198	219	1	0	0	0	0	0
199	220	1	2.85	1	0	1	0
200	221	1	1.71	4.5	0	0.7	0

201	222	1	3.28	2.5	0	1.88	0
202	223	1	4.28	0	0	2.32	0
203	224	1	1.73	0	0	0.99	0
204	225	1	4.1	0	0	0.4	0
205	226	1	0	0	0	0	0
206	227	1	5.38	3.03	0	3.69	0
207	228	1	2.23	0	0	1.48	0
208	229	1	0.96	0	0	0.46	0
209	230	1	0	3.45	0	0	0
210	231	1	1.59	0	0	1.07	0
211	232	1	4.48	0	0	1.43	0
212	233	1	4.04	3	0	2.12	0
213	234	1	5.72	0	0	2.44	0
214	235	1	2.69	0	0	1.57	0
215	236	1	0	6	0	0	0
216	237	1	0	0	0	0	0
217	238	1	2.55	2.5	0	1.49	0
218	239	1	0	5.5	0	0	0
219	240	1	0	0	0	0	0
220	241	1	0	5.75	0	0	0
221	242	1	0	1.7	0	0	0
222	243	1	0.08	0.84	0	0.03	0
223	244	1	0	0	0	0	0
224	245	1	0.61	0	0	0.3	0
225	246	1	0.77	0	0	0.33	0
226	247	1	0.61	0	0	0.3	0
227	248	1	0.29	0	0	0.14	0
228	249	1	0.29	0	0	0.14	0
229	250	1	-0.23	0	0	-0.17	0
230	281	1	-0.331	0	0	-0.29	0
231	319	1	1.158	0	0	-0.24	0
232	320	1	0.024	0	0	-0.12	0
233	322	1	0.024	0	0	-0.039	0
234	323	1	-0.149	0	0	0.265	0
235	324	1	0.247	0	0	-0.012	0
236	526	1	1.453	0	0	-0.34	0
237	528	1	0.281	0	0	-0.205	0
238	531	1	0.14	0	0	0.025	0
239	552	1	-0.111	0	0	-0.014	0
240	562	1	0.505	0	0	0.174	0
241	609	1	0.296	0	0	0.006	0
242	664	1	-1.137	0	0	0.767	0
243	1190	1	1	0	0	0.2917	0
244	1200	1	-1	0	0	0.3417	0
245	1201	1	0	0	0	0	0
246	2040	1	0	0	0	0	0
247	7001	1	0	4.67	0	0	0
248	7002	1	0	6.23	0	0	0
249	7003	1	0	12.1	0	0	0
250	7011	1	0	2.34	0	0	0

251	7012	1	0	3.72	0	0	0
252	7017	1	0	3.3	0	0	0
253	7023	1	0	1.85	0	0	0
254	7024	1	0	4.1	0	0	0
255	7039	1	0	5	0	0	0
256	7044	1	0	0.37	0	0	0
257	7049	1	0	0	0	0	0
258	7055	1	0	0.45	0	0	0
259	7057	1	0	1.65	0	0	0
260	7061	1	0	4	0	0	0
261	7062	1	0	4	0	0	0
262	7071	1	0	1.16	0	0	0
263	7130	1	0	12.92	0	0	0
264	7139	1	0	7	0	0	0
265	7166	1	0	5.53	0	0	0
266	9001	1	0	0	0	0	0
267	9002	1	0	-0.042	0	0	0
268	9003	1	0.0271	0	0	0.0094	0
269	9004	1	0.86	0	0	0.0028	0
270	9005	1	0	0	0	0	0
271	9006	1	0	0	0	0	0
272	9007	1	0	0	0	0	0
273	9012	1	0	0	0	0	0
274	9021	1	0.0475	0	0	0.0156	0
275	9022	1	0.0153	0	0	0.0053	0
276	9023	1	0	0	0	0	0
277	9024	1	0.0135	0	0	0.0047	0
278	9025	1	0.0045	0	0	0.0016	0
279	9026	1	0.0045	0	0	0.0016	0
280	9031	1	0.0184	0	0	0.0064	0
281	9032	1	0.0139	0	0	0.0048	0
282	9033	1	0.0189	0	0	0.0065	0
283	9034	1	0.0155	0	0	0.0054	0
284	9035	1	0.0166	0	0	0.0058	0
285	9036	1	0.0303	0	0	0.01	0
286	9037	1	0.0186	0	0	0.0064	0
287	9038	1	0.0258	0	0	0.0089	0
288	9041	1	0.0101	0	0	0.0035	0
289	9042	1	0.0081	0	0	0.0028	0
290	9043	1	0.016	0	0	0.0052	0
291	9044	1	0	0	0	0	0
292	9051	1	0	-0.3581	0	0	0
293	9052	1	0.3	0	0	0.23	0
294	9053	1	0	-0.2648	0	0	0
295	9054	1	0	0.5	0	0	0
296	9055	1	0	0.08	0	0	0
297	9071	1	0.0102	0	0	0.0035	0
298	9072	1	0.0102	0	0	0.0035	0
299	9121	1	0.038	0	0	0.0125	0
300	9533	1	0.0119	0	0	0.0041	0

Source: http://www.ee.washington.edu/research/pstca/

APPENDIX F

Line Data for IEEE 300 Bus System

Line No	From bus Modified	From bus Actual	To bus Modified	To bus Actual	R (p.u)	X (p.u)	Tap ratio a	Bh(p.u)
1	1	1	3	3	0	0.052	0.947	0
2	1	1	5	5	0.001	0.006	0	0
3	1	1	247	7001	0	0.01953	1	0
4	2	2	3	3	0	0.052	0	0
5	2	2	6	6	0.001	0.009	0	0
6	2	2	8	8	0.006	0.027	0	0.054
7	2	2	248	7002	0.001	0.014	1	0
8	3	3	4	4	0	0.005	0	0
9	3	3	7	7	0	0.003	0	0
10	3	3	18	19	0.008	0.069	0	0.139
11	3	3	129	150	0.001	0.007	0	0
12	3	3	249	7003	0	0.01054	1	0
13	4	4	16	16	0.002	0.019	0	1.127
14	5	5	7	7	0	0.039	0.948	0
15	5	5	9	9	0.006	0.029	0	0.018
16	6	6	7	7	0	0.039	0.959	0
17	7	7	12	12	0.001	0.009	0	0.07
18	7	7	110	131	0.001	0.007	0	0.018
19	8	8	11	11	0.013	0.0595	0	0.033
20	8	8	14	14	0.013	0.042	0	0.042
21	9	9	11	11	0.006	0.027	0	0.013
22	10	10	11	11	0	0.089	1.046	0
23	10	10	12	12	0	0.053	0.985	0
24	11	11	13	13	0.008	0.034	0	0.018
25	11	11	250	7011	0	0.01923	1	0
26	12	12	20	21	0.002	0.015	0	0.118
27	12	12	251	7012	0	0.0312	1	0
28	13	13	19	20	0.006	0.034	0	0.016
29	14	14	15	15	0.014	0.042	0	0.097
30	15	15	16	16	0.001	0.038	0.971	0
31	15	15	17	17	0.0194	0.0311	0.9561	0
32	15	15	30	37	0.065	0.248	0	0.121
33	15	15	74	89	0.099	0.248	0	0.035
34	15	15	75	90	0.096	0.363	0	0.048
35	16	16	36	42	0.002	0.022	0	1.28
36	17	17	252	7017	0	0.01654	0.942	0
37	18	19	20	21	0.0022	0.018	0	0.036
38	18	19	72	87	0.013	0.08	0	0.151
39	19	20	20	21	0	0.014	0.952	0
40	19	20	21	22	0.016	0.033	0	0.015
41	19	20	26	27	0.069	0.186	0	0.098
42	20	21	23	24	0.004	0.034	0	0.28
43	21	22	22	23	0.052	0.111	0	0.05
44	22	23	23	24	0	0.064	0.943	0
45	22	23	24	25	0.019	0.039	0	0.018
46	22	23	253	7023	0	0.023	1	0
47	23	24	231	319	0.007	0.068	0	0.134
48	23	24	254	7024	0	0.02889	1	0
49	24	25	25	26	0.036	0.071	0	0.034
50	25	26	26	27	0.045	0.12	0	0.065

51	25	26	232	320	0.043	0.13	0	0.014
52	27	33	28	34	0	0.063	0	0
53	27	33	32	38	0.0025	0.012	0	0.013
54	27	33	34	40	0.006	0.029	0	0.02
55	27	33	35	41	0.007	0.043	0	0.026
56	28	34	36	42	0.001	0.008	0	0.042
57	29	35	30	36	0	0.047	1.01	0
58	29	35	60	72	0.012	0.06	0	0.008
59	29	35	63	76	0.006	0.014	0	0.002
60	29	35	64	77	0.01	0.029	0	0.003
61	30	36	73	88	0.004	0.027	0	0.043
62	31	37	32	38	0.008	0.047	0	0.008
63	31	37	34	40	0.022	0.064	0	0.007
64	31	37	35	41	0.01	0.036	0	0.02
65	31	37	43	49	0.017	0.08	0	0.048
66	31	37	74	89	0.102	0.254	0	0.033
67	31	37	75	90	0.047	0.127	0	0.016
68	31	37	266	9001	0.00006	0.00046	1.0082	0
69	32	38	35	41	0.008	0.037	0	0.02
70	32	38	37	43	0.032	0.087	0	0.04
71	33	39	36	42	0.0006	0.0064	0	0.404
72	33	39	255	7039	0	0.03159	0.965	0
73	34	40	42	48	0.026	0.154	0	0.022
74	35	41	36	42	0	0.029	0	0
75	35	41	43	49	0.065	0.191	0	0.02
76	35	41	44	51	0.031	0.089	0	0.036
77	36	42	40	46	0.002	0.014	0	0.806
78	37	43	38	44	0.026	0.072	0	0.035
79	37	43	42	48	0.095	0.262	0	0.032
80	37	43	46	53	0.013	0.039	0	0.016
81	38	44	39	45	0	0.02	1.008	0
82	38	44	41	47	0.027	0.084	0	0.039
83	38	44	47	54	0.028	0.084	0	0.037
84	38	44	256	7044	0	0.18181	0.942	0
85	39	45	40	46	0	0.021	1	0
86	39	45	52	60	0.007	0.041	0	0.312
87	39	45	62	74	0.009	0.054	0	0.411
88	40	46	68	81	0.005	0.042	0	0.69
89	41	47	61	73	0.052	0.145	0	0.073
90	41	47	92	113	0.043	0.118	0	0.013
91	42	48	87	107	0.025	0.062	0	0.007
92	43	49	44	51	0.031	0.094	0	0.043
93	43	49	257	7049	0	0.0124	1	0
94	44	51	45	52	0.037	0.109	0	0.049
95	45	52	48	55	0.027	0.08	0	0.036
96	46	53	47	54	0.025	0.073	0	0.035
97	47	54	48	55	0.035	0.103	0	0.047
98	48	55	49	57	0.065	0.169	0	0.082
99	48	55	258	7055	0	0.19607	0.942	0
100	49	57	50	58	0.046	0.08	0	0.036

101	49	57	55	63	0.159	0.537	0	0.071
102	49	57	259	7057	0	0.05347	0.95	0
103	50	58	51	59	0.009	0.026	0	0.005
104	51	59	53	61	0.002	0.013	0	0.015
105	52	60	54	62	0.009	0.065	0	0.485
106	53	61	54	62	0	0.059	0	0.975
107	53	61	260	7061	0	0.0238	1	0
108	54	62	56	64	0.016	0.105	0	0.203
109	54	62	123	144	0.001	0.007	0	0.013
110	54	62	261	7062	0	0.03214	0.95	0
111	55	63	56	64	0	0.038	1.017	0
112	55	63	236	526	0.0265	0.172	0	0.026
113	57	69	66	79	0.051	0.157	0	0.023
114	57	69	180	201	0	0.098	1.1	0
115	57	69	190	211	0.051	0.232	0	0.028
116	58	70	59	71	0.032	0.1	0	0.062
117	58	70	237	528	0.02	0.1234	0	0.028
118	59	71	60	72	0.036	0.131	0	0.068
119	59	71	61	73	0.034	0.099	0	0.047
120	59	71	262	7071	0	0.06896	0.9565	0
121	60	72	64	77	0.018	0.087	0	0.011
122	60	72	238	531	0.0256	0.193	0	0
123	61	73	62	74	0	0.0244	1	0
124	61	73	63	76	0.021	0.057	0	0.03
125	61	73	66	79	0.018	0.052	0	0.018
126	62	74	73	88	0.004	0.027	0	0.05
127	62	74	240	562	0.0286	0.2013	0	0.379
128	63	76	64	77	0.016	0.043	0	0.004
129	64	77	65	78	0.001	0.006	0	0.007
130	64	77	67	80	0.014	0.07	0	0.038
131	64	77	239	552	0.0891	0.2676	0	0.029
132	64	77	241	609	0.0782	0.2127	0	0.022
133	65	78	66	79	0.006	0.022	0	0.011
134	65	78	69	84	0	0.036	0	0
135	66	79	190	211	0.099	0.375	0	0.051
136	67	80	190	211	0.022	0.107	0	0.058
137	68	81	73	88	0	0.02	1	0
138	68	81	173	194	0.0035	0.033	0	0.53
139	68	81	174	195	0.0035	0.033	0	0.53
140	70	85	71	86	0.008	0.064	0	0.128
141	70	85	81	99	0	0.048	1	0
142	71	86	72	87	0.012	0.093	0	0.183
143	71	86	83	102	0	0.048	1	0
144	71	86	234	323	0.006	0.048	0	0.092
145	72	87	78	94	0	0.046	1.015	0
146	74	89	76	91	0.047	0.119	0	0.014
147	75	90	77	92	0.32	0.174	0	0.024
148	76	91	78	94	0.1	0.235	0	0.031
149	76	91	79	97	0.022	0.077	0	0.039
150	77	92	84	103	0.019	0.144	0	0.017

151	77	92	86	105	0.017	0.092	0	0.012
152	78	94	79	97	0.278	0.427	0	0.043
153	79	97	82	100	0.022	0.053	0	0.007
154	79	97	83	102	0.038	0.092	0	0.012
155	79	97	84	103	0.048	0.122	0	0.015
156	80	98	82	100	0.024	0.064	0	0.007
157	80	98	83	102	0.034	0.121	0	0.015
158	81	99	87	107	0.053	0.135	0	0.017
159	81	99	88	108	0.002	0.004	0	0.002
160	81	99	89	109	0.045	0.354	0	0.044
161	81	99	90	110	0.05	0.174	0	0.022
162	82	100	83	102	0.016	0.038	0	0.004
163	83	102	85	104	0.043	0.064	0	0.027
164	84	103	86	105	0.19	0.062	0	0.008
165	85	104	88	108	0.076	0.13	0	0.044
166	85	104	233	322	0.044	0.124	0	0.015
167	86	105	87	107	0.012	0.088	0	0.011
168	86	105	90	110	0.157	0.4	0	0.047
169	88	108	235	324	0.074	0.208	0	0.026
170	89	109	90	110	0.07	0.184	0	0.021
171	89	109	92	113	0.1	0.274	0	0.031
172	89	109	93	114	0.109	0.393	0	0.036
173	90	110	91	112	0.142	0.404	0	0.05
174	91	112	93	114	0.017	0.042	0	0.006
175	93	114	186	207	0	0.149	0.967	0
176	94	115	100	121	0	0.028	1.05	0
177	94	115	101	122	0.0036	0.0199	0	0.004
178	95	116	99	120	0.002	0.1049	0	0.001
179	95	116	103	124	0.0052	0.0174	1.01	0
180	96	117	97	118	0.0001	0.0018	0	0.017
181	96	117	138	159	0	0.016	1.0506	0
182	97	118	98	119	0	0.0271	0	0
183	97	118	100	121	0.0022	0.2915	0	0
184	97	118	245	1201	0	0.6163	0	0
185	98	119	99	120	0	0.0339	0	0
186	98	119	100	121	0	0.0582	0	0
187	98	119	243	1190	0.001	0.023	1.0223	0
188	99	120	244	1200	0	0.023	0.9284	0
189	99	120	245	1201	0	-0.3697	0	0
190	101	122	102	123	0.0808	0.2344	0	0.029
191	101	122	104	125	0.0965	0.3669	0.054	0
192	101	122	136	157	0.0005	0.0195	1	0
193	102	123	103	124	0.036	0.1076	0	0.117
194	102	123	104	125	0.0476	0.1414	0	0.149
195	103	124	139	160	0.0012	0.0396	0.975	0
196	104	125	105	126	0.0006	0.0197	0	0
197	105	126	106	127	0.0059	0.0405	0	0.25
198	105	126	108	129	0.0115	0.1106	0	0.185
199	105	126	111	132	0.0198	0.1688	0	0.321
200	105	126	136	157	0.005	0.05	0	0.33

201	105	126	137	158	0.0077	0.0538	0	0.335
202	105	126	148	169	0.0165	0.1157	0	0.1157
203	106	127	107	128	0.0059	0.0577	0	0.095
204	106	127	113	134	0.0049	0.0336	0	0.208
205	106	127	147	168	0.0059	0.0577	0	0.095
206	107	128	109	130	0.0078	0.0773	0	0.126
207	107	128	112	133	0.0026	0.0193	0	0.03
208	108	129	109	130	0.0076	0.0752	0	0.122
209	108	129	112	133	0.0021	0.0186	0	0.03
210	109	130	110	131	0	0.018	1.0522	0
211	109	130	111	132	0.0016	0.0164	0	0.026
212	109	130	129	150	0	0.014	1.0522	0
213	109	130	130	151	0.0017	0.0165	0	0.026
214	109	130	146	167	0.0079	0.0793	0	0.127
215	109	130	147	168	0.0078	0.0784	0	0.125
216	109	130	263	7130	0	0.0193	1	0
217	111	132	149	170	0.001	0.0402	1.05	0
218	112	133	147	168	0.0026	0.0193	0	0.03
219	112	133	148	169	0.0021	0.0186	0	0.03
220	112	133	150	171	0.0002	0.0101	0	0
221	113	134	113	135	0.0043	0.0293	0	0.18
222	113	134	163	184	0.0039	0.0381	0	0.258
223	114	135	115	136	0.0091	0.0623	0	0.385
224	115	136	116	137	0.0125	0.089	0	0.54
225	115	136	131	152	0.0056	0.039	0	0.953
226	116	137	119	140	0.0015	0.0114	0	0.284
227	116	137	142	163	0.0013	0.0384	0.98	-0.057
228	116	137	160	181	0.0005	0.0034	0	0.021
229	116	137	165	186	0.0007	0.0151	0	0.126
230	116	137	167	188	0.0005	0.0034	0	0.021
231	117	138	160	181	0.0004	0.0202	0	0
232	117	138	167	188	0.0004	0.0202	0	0
233	118	139	151	172	0.0562	0.2248	0	0.081
234	118	139	161	182	0.0003	0.0131	1.03	0
235	118	139	264	7139	0	0.0167	1	0
236	119	140	120	141	0.012	0.0836	0	0.123
237	119	140	121	142	0.0152	0.1132	0	0.684
238	119	140	124	145	0.0468	0.3369	0	0.519
239	119	140	125	146	0.043	0.3031	0	0.463
240	119	140	126	147	0.0489	0.3492	0	0.538
241	119	140	161	182	0.0013	0.0089	0	0.119
242	120	141	125	146	0.0291	0.2267	0	0.342
243	120	141	153	174	0.0024	0.0603	0.975	0
244	121	142	122	143	0.006	0.057	0	0.767
245	121	142	154	175	0.0024	0.0498	1	-0.087
246	122	143	123	144	0	0.0833	1.035	0
247	122	143	124	145	0.0075	0.0773	0	0.119
248	122	143	127	148	0.0013	0.0371	0.9565	0
249	122	143	128	149	0.0127	0.0909	0	0.135
250	124	145	125	146	0.0085	0.0588	0	0.087

251	124	145	128	149	0.0218	0.1511	0	0.223
252	124	145	159	180	0.0005	0.0182	1	0
253	125	146	126	147	0.0073	0.0504	0	0.074
254	127	148	157	178	0.0523	0.1526	0	0.074
255	127	148	158	179	0.1371	0.3919	0	0.076
256	130	151	149	170	0.001	0.0392	1.05	0
257	131	152	132	153	0.0137	0.0957	0	0.14
258	132	153	140	161	0.0055	0.0288	0	0.19
259	132	153	162	183	0.0027	0.0639	1.073	0
260	133	154	135	156	0.1746	0.3161	0	0.04
261	133	154	162	183	0.0804	0.3054	0	0.045
262	134	155	135	156	0.008	0.0256	1.05	0
263	134	155	140	161	0.011	0.0568	0	0.388
264	134	155	143	164	0.0009	0.0231	0.956	-0.033
265	136	157	138	159	0.0008	0.0098	0	0.069
266	137	158	138	159	0.0029	0.0285	0	0.19
267	137	158	139	160	0.0066	0.0448	0	0.277
268	141	162	143	164	0.0024	0.0326	0	0.236
269	141	162	144	165	0.0018	0.0245	0	1.662
270	142	163	143	164	0.0044	0.0514	0	3.597
271	144	165	145	166	0.002	0.0123	0	0
272	145	166	265	7166	0	0.0154	1	0
273	146	167	148	169	0.0018	0.0178	0	0.029
274	151	172	152	173	0.0669	0.4843	0	0.063
275	151	172	153	174	0.0558	0.221	0	0.031
276	152	173	153	174	0.0807	0.3331	0	0.049
277	152	173	154	175	0.0739	0.3071	0	0.043
278	152	173	155	176	0.1799	0.5017	0	0.069
279	154	175	155	176	0.0904	0.3626	0	0.048
280	154	175	158	179	0.077	0.3092	0	0.054
281	155	176	156	177	0.0251	0.0829	0	0.047
282	156	177	157	178	0.0222	0.0847	0	0.05
283	157	178	158	179	0.0498	0.1855	0	0.029
284	157	178	159	180	0.0061	0.029	0	0.084
285	160	181	166	187	0.0004	0.0083	0	0.115
286	163	184	164	185	0.0025	0.0245	0	0.164
287	165	186	167	188	0.0007	0.0086	0	0.115
288	166	187	167	188	0.0007	0.0086	0	0.115
289	168	189	187	208	0.033	0.095	0	0
290	168	189	188	209	0.046	0.069	0	0
291	168	189	189	210	0	0.252	1.03	0
292	169	190	210	231	0.0004	0.0022	0	602
293	169	190	219	240	0	0.0275	0	0
294	169	190	208	229	0	0.0626	0	1.364
295	170	191	171	192	0.003	0.048	0	0
296	170	191	204	225	0.001	0.061	0	0
297	171	192	204	225	0.002	0.009	0	0
298	172	193	175	196	0	0.237	1.03	0
299	172	193	183	205	0.045	0.063	0	0
300	172	193	187	208	0.048	0.127	0	0

301	173	194	198	219	0.0031	0.0286	0	0.5
302	173	194	242	664	0.0024	0.035	0	0.36
303	174	195	191	212	0.0008	0.036	0	0
304	174	195	198	219	0.0031	0.0286	0	0.5
305	175	196	176	197	0.014	0.04	0	0.004
306	175	196	189	210	0.03	0.081	0	0.01
307	175	196	246	2040	0.0001	0.02	1	0
308	176	197	177	198	0.01	0.06	0	0.009
309	176	197	190	211	0.015	0.04	0	0.006
310	177	198	181	202	0.332	0.688	0	0
311	177	198	182	203	0.009	0.046	0	0.025
312	177	198	188	209	0.026	0.211	1.03	0
313	177	198	189	210	0.02	0.073	0	0.008
314	177	198	190	211	0.034	0.109	0	0.032
315	178	199	179	200	0.076	0.135	0	0.009
316	178	199	189	210	0.04	0.102	0	0.005
317	179	200	189	210	0.081	0.128	0	0.014
318	179	200	227	248	0	0.098	1	0
319	180	201	183	204	0.124	0.183	0	0
320	181	202	190	211	0	0.128	1.01	0
321	182	203	190	211	0.01	0.059	0	0.008
322	183	204	184	205	0.046	0.068	0	0
323	183	204	246	2040	0.02	0.204	1.05	-0.012
324	184	205	185	206	0.302	0.446	0	0
325	184	205	190	211	0.01	0.059	0	0.008
326	185	206	186	207	0.073	0.093	0	0
327	185	206	187	208	0.24	0.421	0	0
328	190	211	191	212	0.003	0.0122	1	0
329	191	212	194	215	0.0139	0.0778	0	0.086
330	192	213	193	214	0.0025	0.038	0	0
331	193	214	194	215	0.0017	0.0185	0	0.02
332	193	214	221	242	0.0015	0.0108	0	0.002
333	194	215	195	216	0.0045	0.0249	0	0.026
334	195	216	196	217	0.004	0.0497	0	0.018
335	196	217	197	218	0	0.045	0	0
336	196	217	198	219	0.0005	0.0177	0	0.02
337	196	217	199	220	0.0027	0.0395	0	0.832
338	197	218	198	219	0.001	0.035	0.97	-0.01
339	197	218	199	220	0.0037	0.0484	0	0.43
340	198	219	216	237	0.003	0.0018	0	5.2
341	199	220	200	221	0.001	0.0295	0	0.503
342	199	220	217	238	0.0016	0.0046	0	0.402
343	200	221	202	223	0.0003	0.0013	0	1
344	201	222	216	237	0.0014	0.0514	0	0.33
345	202	223	203	224	0.0012	0.0195	1	-0.364
346	203	224	204	225	0.01	0.064	0	0.48
347	203	224	205	226	0.0019	0.0081	0	0.86
348	205	226	210	231	0.0005	0.0212	0	0
349	206	227	210	231	0.0009	0.0472	1	0.186
350	207	228	208	229	0.0019	0.0087	0	1.28

351	207	228	210	231	0.0026	0.0917	0	0
352	207	228	213	234	0.0013	0.0288	0	0.81
353	208	229	209	230	0.001	0.0332	1.02	0
354	210	231	211	232	0.0002	0.0069	0	1.364
355	210	231	216	237	0.0001	0.0006	0	3.57
356	211	232	212	233	0.0017	0.0485	0	0
357	213	234	214	235	0.0002	0.0259	0	0.144
358	213	234	215	236	0.0005	0.016	1.07	0
359	213	234	216	237	0.0006	0.0272	0	0
360	214	235	217	238	0.0002	0.0006	0	0.8
361	216	237	220	241	0.0005	0.0154	1	0
362	217	238	218	239	0.0005	0.016	1.02	0
363	219	240	230	281	0.0003	0.0043	0	0.009
364	221	242	224	245	0.0082	0.0851	0	0
365	221	242	226	247	0.0112	0.0723	0	0
366	222	243	223	244	0.0127	0.0355	0	0
367	222	243	224	245	0.0326	0.1804	0	0
368	223	244	225	246	0.0195	0.0551	0	0
369	224	245	225	246	0.0157	0.0732	0	0
370	224	245	226	247	0.036	0.2119	0	0
371	225	246	226	247	0.0268	0.1285	0	0
372	226	247	227	248	0.0428	0.1215	0	0
373	227	248	228	249	0.0351	0.1004	0	0
374	228	249	229	250	0.0616	0.1857	0	0
375	266	9001	270	9005	0.0008	0.00348	0	0
376	266	9001	271	9006	0.02439	0.43682	0.9668	0
377	266	9001	273	9012	0.03624	0.64898	0.9796	0
378	267	9002	273	9012	0.07622	0.43286	0	0
379	267	9002	273	9012	0.07622	0.43286	0	0
380	267	9002	274	9021	0.0537	0.07026	0	0
381	267	9002	277	9024	0.50748	3.2202	1	0
382	268	9003	271	9006	0.11118	0.49332	0	0
383	268	9003	271	9006	0.11118	0.49332	0	0
384	268	9003	272	9007	0.0558	0.24666	0	0
385	268	9003	280	9031	0.73633	4.6724	1	0
386	268	9003	281	9032	0.76978	4.8846	1	0
387	268	9003	282	9033	0.75732	4.8056	1	0
388	268	9003	283	9034	0.13006	1.3912	1	0
389	268	9003	284	9035	0.54484	3.4572	1	0
390	268	9003	285	9036	0.15426	1.6729	1	0
391	268	9003	286	9037	0.3849	2.5712	1	0
392	268	9003	287	9038	0.4412	2.9668	1	0
393	268	9003	291	9044	0.07378	0.06352	0	0
394	269	9004	288	9041	0.36614	2.456	1	0
395	269	9004	289	9042	1.0593	5.4536	1	0
396	269	9004	290	9043	0.1567	1.6994	1	0
397	269	9004	291	9044	0.03832	0.02894	0	0
398	270	9005	292	9051	0.01578	0.37486	1.0435	0
399	270	9005	293	9052	0.01578	0.37486	0.9391	0
400	270	9005	294	9053	0.01602	0.38046	1.0435	0

401	270	9005	295	9054	0	0.152	1.0435	0
402	270	9005	296	9055	0	0.8	1.0435	0
403	271	9006	272	9007	0.05558	0.24666	0	0
404	272	9007	297	9071	0.4412	2.9668	1	0
405	272	9007	298	9072	0.30792	2.057	1	0
406	273	9012	299	9121	0.23552	0.99036	0	0
407	274	9021	275	9022	0.44364	2.8152	1	0
408	274	9021	276	9023	1.1068	0.95278	0	0
409	276	9023	278	9025	0.66688	3.944	1	0
410	276	9023	279	9026	0.6113	3.6152	1	0
411	294	9053	300	9533	0	0.75	0.9583	0

Source: http://www.ee.washington.edu/research/pstca/

APPENDIX G

Simulink Dynamic Model for Voltage Source Converter

Appendix G1

Main Voltage Source Converter Model

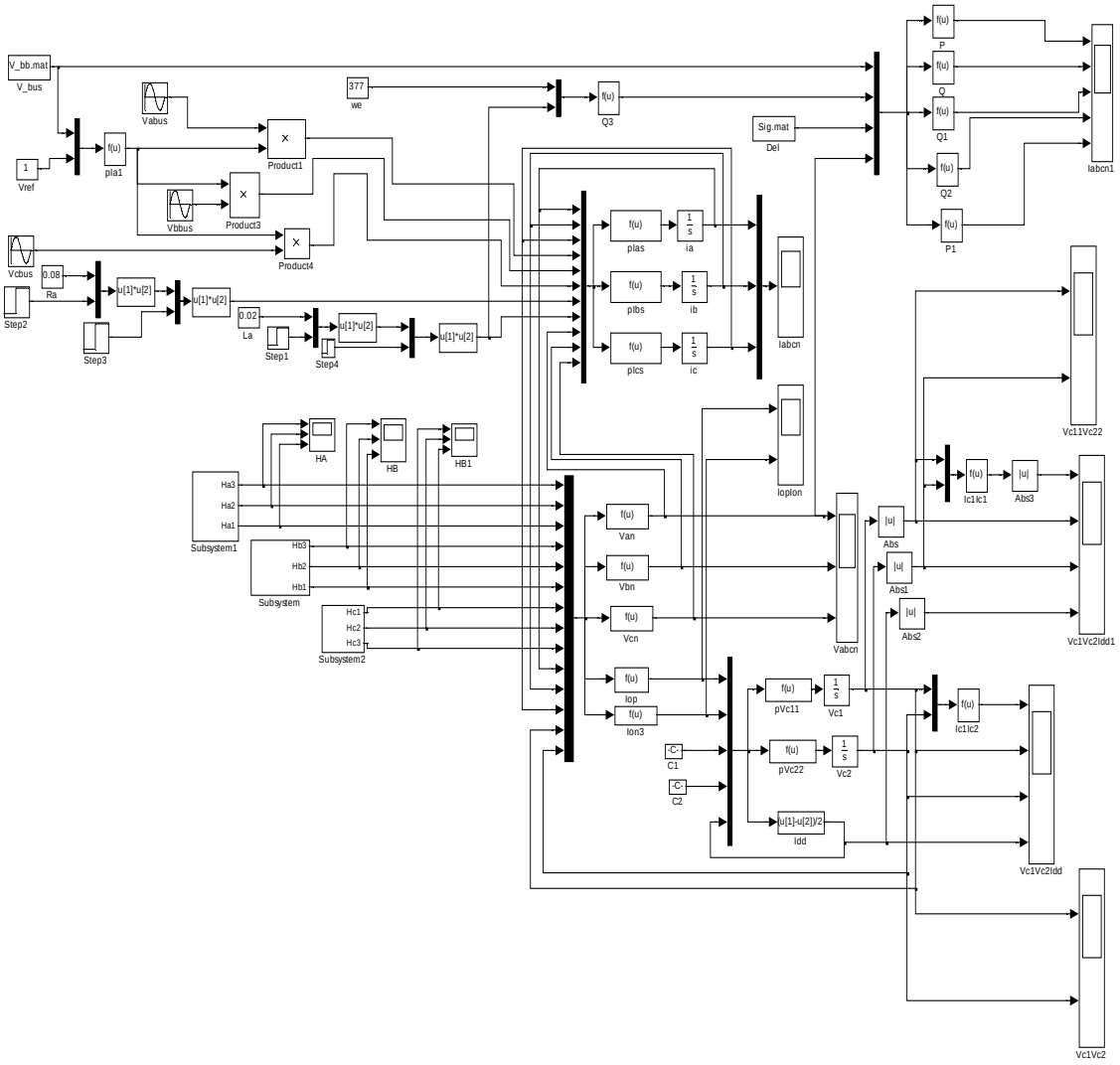
V_bb.mat
V_bus
Vabus
377
we
Q3
Sig.mat
Del
P
Q
Q1
Q2
P1
labcn1
1
Vref
pla1
Product1
Vbbus
Product3
Product4
Vcbus
0.08
Ra
Step2
Step3
u[1]*u[2]
0.02
La
Step1
Step4
pias
pibs
pics
ia
ib
ic
labcn
loplon
Vc11Vc22
HA
HB
HB1
Ha3
Ha2
Ha1
Subsystem1
Hb3
Hb2
Hb1
Subsystem
Hc1
Hc2
Hc3
Subsystem2
Van
Vbn
Vcn
Vabcn
Ic1Ic1
Abs3
Abs
Abs1
Abs2
Vc1Vc2Idd1
Iop
Ion3
pVc11
Vc1
pVc22
Vc2
C1
C2
Idd
Ic1Ic2
Vc1Vc2Idd
Vc1Vc2

Appendix G2

Switching Pulse Generation Model (Phase ‘A’)

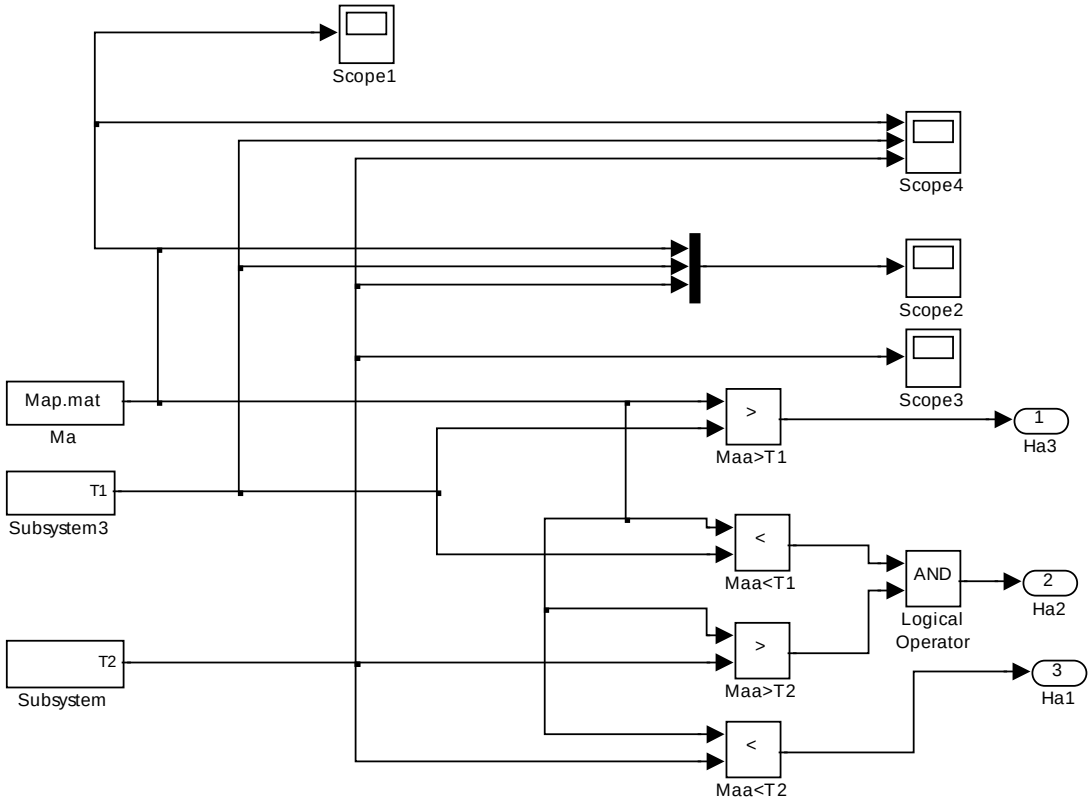
Scope1
Scope4
Scope2
Scope3
Map.mat
Ma
T1
Subsystem3
T2
Subsystem
>
Maa>T1
<
Maa<T1
>
Maa>T2
<
Maa<T2
AND
Logical
Operator
1
Ha3
2
Ha2
3
Ha1

APPENDIX H

Generalized MATLAB ® Program Code

```
clc
clear all
format long
%==========================================
% Gloabl Variable Declaration
www=1;
ST=0;
st=0;
FlashPoint=10000;
Da_index=zeros(N,1);
Db_index=zeros(N,1);
D2_1=zeros(N,1);
D2_2=zeros(N,1);
while www<4 %While No. 1
    if ST~=FlashPoint % if No 1
%========================================
% SUBROUTINE TO Input Bus Data Line Numbers
disp('Get the Input File Bus Data Lines Ready')
disp('Pls Enter the Bus Data Input File Title')
b0=input('b0:','s');
disp('Enter Bus Number File Data Line')
b1 =input('b1:');
disp('Enter Bus Flat Voltage File Data Line')
b2 =input('b2:');
disp('Enter Real Power Demand File Data Line')
b3 =input('b3:');
disp('Enter Real Power Generated File Data Line')
b4 =input('b4:');
```

```
disp('Enter Reactive Power Generated File Data Line')
b5 =input('b5:');
disp('Enter Reactive Power Demand File Data Line')
b6 =input('b6:');
disp('Enter Bus Voltage Angle File Data Line')
b7 =input('b7:')
disp('Enter Compensation Angle File Data Line')
b8 =input('b8:')
disp('Enter Compensation Voltage  File Data Line')
b9 =input('b9:')
%=========================================================
% SUBROUTINE TO Read Bus Data from Excel Fine
[BusNum,V_1,Pl,Pg,Qg1,Ql_1,Sig] = BDAT(b0,b1,b2,b3,b4,b5,b6,b7);
 N=max(BusNum);
 %============================================================
 % SUBROUTINE TO Compute the Real and Reactive Power Partials
 t=0;
ww=0; [Gen_bus,Load_bus,P_1,Q_1]=BUSTYPE(Qg1,Ql_1,Pg,Pl,N);
 [MM,slack_bus] = max(P_1);
tSysbus=t+ww;
GS=length(Gen_bus);
 %============================================================
 %SUBROUTINE TO Input Transmission Data Line Numbers
disp('Fine, Now Get the Input File for Transmission Data Lines Ready')
disp('Pls Enter the Line Data Input File Title')
Lt=input('Lt:','s');
disp('Enter Line Number File Data Line')
L1 =input('L1:');
disp('Enter From Bus File Data Line')
```

```
L2 =input('L2:');
disp('Enter To Bus File Data Line')
L3 =input('L3:');
disp('Enter Line Resistance File Data Line')
L4 =input('L4:');
disp('Enter Line Reactance File Data Line')
L5 =input('L5:');
disp('Enter Transformer Tap File Data Line')
L6 =input('L6:');
disp('Enter Shunt Reactance File Data Line')
L7 =input('L7:');
%================================================================
% SUBROUTINE TO Read Transmission Line Data from Excel File
 [Ld,LineNum,Fbus,Tbus,R,X,a,Bh] = LDAT(Lt,L1,L2,L3,L4,L5,L6,L7);
  sze=length(LineNum);
 %================================================================
 % SUBROUTINE TO Compute Transmission Line NET RESISTANCE AND %
 % INDUCTANCES
      [Rt,Xt,Bht,at,LineNum,Fb,Tb,LN]=yL(R,X,Bh,a,sze,Fbus,Tbus);
       M=max(LN);
  %=====================================================================
  % SUBROUTINE TO PRIMITIVE ADMITTANCE FOR EACH LINE &  PHASE ANGLES
    [y1,del]=y1del(Rt,Xt,Bht,at,M);
 %================================================================
 % SUBROUTINE TO Compute Y Bus Matrix
 [Y_1]=YBUS(y1,at,Bht,M,Tb,Fb);
%=====================================================================
% SUBROUTINE TO Compute the Real and Reactive Component of Y Bus
 N=max(BusNum);
```

```
[G_1,B_1]=GB(Y_1,N);
  %============================================================
  %SUBROUTINE TO Compute the Bus Angle

        [th]=theta(B_1,G_1,N);
%=================================================
 % SUBROUTINE TO Compute the Bus Impedance Matrix
         [Z_1]=ZBUS(Y_1,N);
%====================================================================
  % SUBROUTINE TO Compute the INJECTED REAL AND REACTIVE POWER
Va_1=zeros(N);
t=2;
w_w=zeros(N);
%E=1;

[P1,Q1,Sig,deP,deQ]=Pupdate(N,M,GS,slack_bus,V_1,G_1,B_1,Sig,P_1,Gen_bu
s,Q_1);
 %====================================================================
 % SUBROUTINE TO Compute the Bus VOLTAGE ANGLE AND MAGNITUDE
[Sig,V_1]=Pupdate2(N,slack_bus,V_1,G_1,Q_1,B_1,Sig,Gen_bus,deP,deQ);

%====================================================================
% % COMPUTATION OF LINE STABILITY INDEX VCP
deSig=zeros(N-1,1);
deV=zeros(N-GS,1);
Line=zeros(M,1);
Linec=zeros(M,1);
Lined=zeros(M,1);
```

```
Prmax=zeros(M,1);
Pr=zeros(M,1);
VCP=zeros(M,1);
v=1;;
A6=0;
A7=0;
    for j=1:M % xxx ============


     if Fbus(j)~=A6
        A6=Fbus(j);
        for k=1:M,
          if Fbus(k)==A6
            A7=Tbus(k);
            if  Sig(A6)-Sig(A7)~=0
              sig(v)=Sig(A6)-Sig(A7);
              Linec(v)=Linec(v)+1;
              A6=Fbus(j);
              A7=Tbus(k);
              Pr(v)=Pr(v)+(V_1(A6)*V_1(A7)*B_1(A6,A7)*sin(sig(v))) ;
              Prmax(v)=V_1(A6)*V_1(A7)/Xt(A6);
              if Prmax(v)~=0
                 VCP(v)=abs(Pr(v)/Prmax(v));
              end
            end
               v=v+1;
          end
       end
    end
```

```
 end % for xxx ends here



%=====================================================================
% COMPUTATION OF LINE STABILITY INDEX  VCQ
Qrmax=zeros(M,1);
Qr=zeros(M,1);
VCQ=zeros(M,1);
A4=0;
A5=0;
u=0;
for j=1:M  %  xx
   if Fbus(j)~=A4;
       A4=Fbus(j);
    for k=1:M;
     if Fbus(k)==A4
          A5=Tbus(k);
          u=u+1;
          sig(u)=Sig(A4)-Sig(A5);
          Lined(j)=u;
          Qr(u)=Qr(u)-(V_1(A4)*V_1(A5)*B_1(A4,A5)*cos(sig(u)));
       if Xt==0
          Xt=1;
       end
       if Xt(j)~=0
          Qrmax(u)=Qrmax(u)-(V_1(A4)*V_1(A5)/Xt(j));
       end
```

```
        if Qrmax(u)~=0
           VCQ(u)=abs(Qr(u)/Qrmax(u));
        end
        if VCQ(u)>1 && VCQ(u)<2
          VCQ(u)=abs(1-VCQ(u));
        else
           VCQ(u)=abs(VCQ(u));
        end
      end
    end
  end
end % for xx ends here
%=========================================================================
% COMPUTATION OF LINE STABILITY INDEX LQP
r=1;
w=0;
A3=0;
A4=0;
u=0;
Linea=0;
  for k=1:M,
     if A3~=Fbus(k)
         A3=Fbus(k);
       for l=1:M
         if Fbus(l)==A3
           A4=Tbus(l);
           u=u+1;
           Xt(A3)=Xt(k);
           LQP(u)=abs(4*(Xt(u)/V_1(A3)^2)*((Xt(u)*P_1(A3)^2/V_1(A3)^2)+
```

```
                Q_1(A4)));
          Linea(u)=u;
        end
     end
   end
end
%-----------------------------------------------------------------------
% COMPUTATION OF LINE STABILITY INDEX F_vsi1
r=1;
w=0;
A3=0;
A4=0;
u=0;
Line=0;
t=2;
for t=RP
  for k=1:M,
      if A3~=Fbus(k)
        A3=Fbus(k);
        for l=1:M
          if Fbus(l)==A3
            A4=Tbus(l);
            u=u+1;
            w=w+1;
            F_vsi1(u)=abs((4*Z_1(A3,A4)^2*Q_1(A4))/(V_1(A3)^2*Xt(u)));
            Line(u)=u;
         end
       end
    end
```

```
  end
end
%=====================================================================
% COMPUTATION OF LINE STABILITY INDEX Lmn
X=0;
Linea=0;
 u=0;
 for t=RP
    for k=1:M,
          A3=Fbus(k);
               for l=1:M
                 if Fbus(l)==A3
                    A4=Tbus(l);
                     if k==l
                      u=u+1;
                      sig(u)=Sig(A3)-Sig(A4);
                      Lmn(u)=abs(4*Xt(A3)*Q_1(A4)/(V_1(A3)*sind(del(u)-
                             sig(u)))^2);
                       Linea(u)=u;
                     else
                       Xt(A3)=0;
                     end
                 end
             end
   end
 end
%=====================================================================
% COMPUTATION OF BUS VOLTAGE STABILITY INDEX L-INDEX
 D2_1=zeros(N);
```

```
Da=0;
Do_1=0;
D2_1=zeros(N,1);
d_1=zeros(N-GS,1);
d_2=zeros(N,1);
D_1=zeros(N,N);
Da=0;
    for j=1:N
        for k=1:N
             if Y_1(k,k)~=0
              D_1(j,k)=-inv(Y_1(k,k))*Y_1(j,k);
              D_2(j,k)=-B_1(k,k);
             end
        end
    end
      D1=D_1;
     D2=D_2\B_1';
     p=0;
     L=zeros(N,1);
      La=zeros(N,1);
      for h=1:N;
           if h ~=Gen_bus
               k=h-p;
             for l=1:N;
                 if Y_1(k,l)~=0;
                    d_1(k)=d_1(k)-D1(k,l)*V_1(l)/V_1(k);
                 end
                 if B_1(k,l)~=0;
                    d_2(k)=d_2(k)-D2(k,l)*V_1(l)/V_1(k);
```

```
                end
            end
                L(h)=1-abs(d_1(k));
                La(h)=abs(1-abs(d_2(k)));
        else
             La(h)=La(h);
             L(h)=L(h);
             p=p+1;
         end
    end
 %=====================================================================
COMPUTATION OF BUS VOLTAGE STABILITY INDEX RATIO
V_0=ones(N,1);
 p=0
 for h=1:N,
     A(j)=V_1(j)/V_0(j);
 end
%=====================================================================
 disp('Enter Desired Stability Limit ');
 DSI =input('dsi:');
disp('Enter Start Bus ');
sb =input('sb:'); disp('Enter End Bus ');
eb =input('eb:');
r=1;
for i=sb:eb
    if BusNum(i)~=Gen_bus
      LoadBus(r)=i;
      r=r+1;
    end
```

```
end
disp('Load buses to select are ');
sparse(LoadBus)'
disp('Enter Bus of Interest');
sss=1;
bd =input('bd:');
uu = 1;
uu = 1;
while uu == 1
   if (bd<sb || bd>eb)
       disp('Please Enter Correct Load Bus');
       bd =input('bd:');
       if bd~=Load_bus
           disp('Please Enter Correct Load Bus');
           bd =input('bd:');
       end
       uu = 1;
   else
       uu = 2;
   end
end
  b=0;
    Max_index=0;
     for k=sb:eb
       b=b+1;
       BNum(b)=k;
      Lga(b)= L(k);
       if Lga(b)>=Max_index;
       Max_index=Lga(b);
```

```
        FlashPoint=k;
       else
        Max_index=Max_index;
        FlashPoint=FlashPoint;
        end
      end
   Ldd=L(bd);
      if Max_index>=Ldd
       Ldd=Max_index;
       bd=FlashPoint;
       ST=FlashPoint
      else
       Ldd=Ldd;
       bd=bd;
      end
else   % for if No 1 and start of STATCOM INCLUSION

 if Ldd>=DSI
     STATUS=1;
%=========================================================================
%INITIALIZATION OF STATCOM PARAMETERS
tot=0;
SS=10;
while tot<2; % BEGIN OF CONVERGENCE CHECK
Gsh=0.15;
Bsh=0.13;
PE_spec=0.003;
F_spec=0.003;
```

```
PE_cal=zeros(N-1,1);F_cal=zeros(N-1,1);
dPE=zeros(N-1,1);
dF=zeros(N-1,1);
J1=zeros(N-1,N-1);J2=zeros(N-1,N-1);J3=zeros(N-1,1);J4=zeros(N-
1,1);J5=zeros(N-1,N-1);J6=zeros(N-1,N-1);
J7=zeros(N-1,1);J8=zeros(N-1,1);
J9=zeros(1,N-1);J10=zeros(1,N-
1);J11=zeros(1,1);J12=zeros(1,1);J13=zeros(1,N-1);J14=zeros(1,N-
1);J15=zeros(1,1);J16=zeros(1,1);
NR=0;
%=====================================================================
    % COMPUTE STATCOM TERMS
 st=st+1;
 if st==1
     Vsh=1.04;
     Sigsh=0.04;
     V_1=ones(N,1);
     sig=zeros(N,1);
    PE_spec=0.005;
 end
 j=0;
p=0;
pp=0;
for h=1:N
 if h~=slack_bus
  j=h-p;
  pp=0;
  for hh=1:N,
     if hh~=slack_bus
```

```
        k=hh-pp;
        J1(j,k)=V_1(j)*V_1(k)*(G_1(j,k)*sind(sig(j)-sig(k))-
             B_1(j,k)*cosd(sig(j)-sig(k)));
        J2(j,k)=V_1(j)*V_1(k)*(G_1(j,k)*cosd(sig(j)-
             sig(k))+B_1(j,k)*sind(sig(j)-sig(k)));
        J5(j,k)=-V_1(j)*V_1(k)*(G_1(j,k)*cosd(sig(j)-
              sig(k))+B_1(j,k)*sind(sig(j)-sig(k)));
        J6(j,k)=V_1(j)*V_1(k)*(G_1(j,k)*sind(sig(j)-sig(k))-
             B_1(j,k)*cosd(sig(j)-sig(k)));
      else
       pp=1;
      end
     end
   else
    p=1;
   end
end
p=0;
for h=1:N,
  if h~=slack_bus
    j=h-p;
  if j==ST;
    J3(j)=V_1(j)*Vsh*(Gsh*sind(sig(j)-Sigsh)-Bsh*cosd(sig(j)-Sigsh));
    J4(j)=V_1(j)*Vsh*(Gsh*cosd(sig(j)-Sigsh)+Bsh*sind(sig(j)-Sigsh));
    J7(j)=-V_1(j)*Vsh*(Gsh*cosd(sig(j)-Sigsh)+Bsh*sind(sig(j)-Sigsh));
   J8(j)=V_1(j)*Vsh*(Gsh*sind(sig(j)-Sigsh)-Bsh*cosd(sig(j)-Sigsh));
   J9(j)=-V_1(j)*Vsh*(Gsh*cosd(sig(j)-Sigsh)+Bsh*sind(sig(j)-Sigsh));
   J10(j)=-2*V_1(j)^2*Bsh+V_1(j)*Vsh*(Gsh*sind(sig(j)-Sigsh)-
          Bsh*cosd(sig(j)-Sigsh));
```

```
  J13(j)=V_1(j)*Vsh*(Gsh*sind(sig(j)-Sigsh)-Bsh*cosd(sig(j)-Sigsh));
  J14(j)=-V_1(j)*Vsh*(Gsh*cosd(sig(j)-Sigsh)-Bsh*sind(sig(j)-Sigsh)) ;
  J11=-V_1(j)*Vsh*(Gsh*cosd(sig(j)-Sigsh)+Bsh*sind(sig(j)-Sigsh));
  J12=-V_1(j)*Vsh*(Gsh*sind(sig(j)-Sigsh)+Bsh*cosd(sig(j)-Sigsh));
  J15=-V_1(j)*Vsh*(Gsh*sind(sig(j)-Sigsh)+Bsh*cosd(sig(j)-Sigsh));
  J16=2*Vsh^2*Gsh-V_1(j)*Vsh*(Gsh*cosd(sig(j)-Sigsh)-Bsh*sind(sig(j)-
      Sigsh));
  PE_cal(j)=PE_cal(j)+Vsh^2*Gsh-V_1(j)*Vsh*(Gsh*cosd(sig(j)-Sigsh)-
            Bsh*sind(sig(j)-Sigsh));
  dPE(j)=PE_cal(j)-PE_spec;
  F_cal(j)=F_cal(j)-V_1(j)^2*Bsh-V_1(j)*Vsh*(Gsh*sind(sig(j)-Sigsh)-
          Bsh*cosd(sig(j)-Sigsh));
  dF(j)=F_cal(j)-F_spec;
  end
  else
   p=1;
  end
end
%=====================================================================
P_cal=zeros(N-1,1);
 p=0;
for h=1:N
  if h~=slack_bus
   j=h-p;
   for k=1:N,
    if B_1(j,k)~=0
      Sig(k)=sig(j)-sig(k);
      P_cal(j)=P_cal(j)+dd*(V_1(j)*V_1(k)*(G_1(j,k)*cosd(Sig(k))+
      B_1(j,k)*sind(Sig(k))));
```

```
    end
  end
 deP(j)=P_1(j)-P_cal(j);
 P1(j)=P_cal(j);
 else
 p=1;
 end
end
%=====================================================================
% % COMPUTE INJECTED REACTIVE POWER
 p=0;
 Q_cal=zeros(N-1,1);
for h=1:N
  if h~=Gen_bus
     j=h-p;
   for k=1:N,
     if B_1(j,k)~=0
      if  Sig(j)-Sig(k)~=90
          Q_cal(j)=Q_cal(j)+dd*(V_1(j)*V_1(k)*(G_1(j,k)*sind(sig(j)-
                   sig(k))-B_1(j,k)*cosd(sig(j)-Sig(k))));
         end;
      end
   end
      deQ(j)=Q_1(j)-Q_cal(j);
      Q1(j)=Q_cal(j);
      Q_cal(j)=0;
   else
     p=p+1;
   end
```

```
end

%=====================================================================
p=0;
   DQ=zeros(N-1,1);
   pp=0;
   j=1;
   k=0;
    for h=1:N,
        if h~=slack_bus
         j=h-p;
           if j~=Gen_bus
             k=k+1;
            DQ(j)=deQ(k);
            dV(j)=deV(k);
           else
               DQ(j)=0;
             dV(j)=0;
           end
        else
          p=1;
        end
     end
  NR==1;
   pp=0;
   p=0;
   for j=1:N-1,
       if dPE(j)~=0
           DPE=dPE(j
```

```
    end
end
for h=1:N-1,
    if dF(h)~=0
        j=h-p;
        DF=dF(j);
    else
        pp=pp+1;
    end
end
AAA = {J1, J2,J3,J4;J5,J6,J7,J8;J9,J10,J11,J12;J13,J14,J15,J16};
JJ = cell2mat(AAA);
RR = [deP;DQ;DPE;DF];
VVV=-ee*JJ\RR;
NN=2*(N-1);
deSig=VVV(1:N-1);
deV_1=VVV(N:NN);
deSigsh=VVV(NN+2);
deVsh=VVV(2*N);
Sigsh=Sigsh+deSigsh;
Vsh=Vsh+deVsh;
p=0;
for h=1:N
  if h~=Gen_bus
     i=h-p ;
     V_1(h)=V_1(h)+deV_1(i);
  else
     V_1(h)=V_1(h);
     p=p+1;
```

```
      end
   end
   p=0;
   for h=1:N
       if h~=slack_bus
           i=h-p ;
           sig(h)=sig(h)+deSig(i);
       else;
           sig(h)=sig(h);
           p=1;
       end
   end

%=========================================================================
   % COMPUTATION OF INDEXEX WITH COMPENSATION INCLUDED

   r=1;
w=0;
A3=0;
A4=0;
u=0;
Linea=0;
for k=1:M,
  if A3~=Fbus(k)
    A3=Fbus(k);
    for l=1:M
      if Fbus(l)==A3
         A4=Tbus(l);
```

```
          u=u+1;
          V_1(A3);
          Xt(A3)=Xt(k);
          LQP(u)=abs(4*(Xt(u)/V_1(A3)^2)*((Xt(u)*P_1(A3)^2/V_1(A3)^2)
                 +Q_1(A4)));
          Linea(u)=u;
        end
      end
    end
end
     %=================================================================
   r=1;
w=0;
A3=0;
A4=0;
u=0;
Line=0;
t=2;
for t=RP
   for k=1:M,
    if A3~=Fbus(k)
      A3=Fbus(k);
      for l=1:M
        if Fbus(l)==A3
          A4=Tbus(l);
          u=u+1;
          w=w+1;
         if (V_1(A3)^2*Xt(u))~=0;
           F_vsi1(u)=abs((4*Z_1(A3,A4)^2*Q_1(A4))/(V_1(A3)^2*Xt(u)));
```

```
        end
           Line(u)=u;
      end
    end
   end
 end
end
%=====================================================================
X=0;
Linea=0;
 u=0;
for t=RP
  for k=1:M,
   A3=Fbus(k);
   for l=1:M
     if Fbus(l)==A3
        A4=Tbus(l);
       if k==l
          u=u+1;
          sig(u)=Sig(A3)-Sig(A4);
          Lmn(u)=abs(4*Xt(A3)*Q_1(A4)/(V_1(A3)*sind(del(u)-sig(u)))^2);
          Linea(u)=u;
       else
        Xt(A3)=0;
       end
      end
    end
  end
end
```

```
 Da=0;
Do_1=0;
D2_1=zeros(N,1);
d_1=zeros(N-GS,1);
d_2=zeros(N,1);
D_1=zeros(N,N);
for j=1:N
   for k=1:N
     if Y_1(k,k)~=0
        D_1(j,k)=-inv(Y_1(k,k))*Y_1(j,k);
     end
   end
 end
 D1=D_1;
 p=0;
 L=zeros(N,1);
 La=zeros(N,1);
 for h=1:N;
   if h ~=Gen_bus
     k=h-p;
    for l=1:N;
     if Y_1(k,l)~=0;
       d_1(k)=d_1(k)-D1(k,l)*V_1(l)/V_1(k);
     end
    end
    L(h)=1-abs(d_1(k
  else
   L(h)=L(h);
   p=p+1;
```

```
   end
 end

%=====================================================================
   % CHECK FOR CONVERGENCE OF ACTIVE POWER EXCHANGE

   ss=abs(dPE);
   SS=max(ss);
   tot=tot+1;
  end %  WHILE FOR CONVERGENCE CHECK

 else
    STATUS=2;
 end
if STATUS==1
    disp('STATUS IS NOT OK, Compensation Required ')
    fstatus = 'STATUS: NOT OK';
else
    disp('STATUS Ok, No Compensation Required Now !')
    fstatus = 'STATUS: OK';
end
  %=====================================================================
   Da_index= Da';
   Z_bus=abs(Z_1);
   F_vsi=abs(F_vsi1);
    Da_index= Da';
disp (['Maximum Index is ' num2str(Max_index)])
pp=Ldd-0.01;
```

```
   if sb==1 & eb==300
      figure(1)
      bar(BNum,Lga)
      xlabel('Bus Number')

%=====================================================
ylabel('Complete Network Bus Index Value')
text(FlashPoint,pp,'\leftarrow flashPoint','FontSize',12,'Color','red')
title ({['COMPLETE NETWORK Max Index is = ' num2str(Max_index)
];['Weakest Bus is = ' num2str(FlashPoint) '    ' fstatus ]})
hold on
 elseif sb==1 & eb==60
  figure(2)
  bar(BNum,Lga)
  xlabel('Bus Number')
%=====================================================
      ylabel('Zone "A" Bus Index Value')
      text(FlashPoint,pp,' \leftarrow
FlashPoint','FontSize',12,'Color','red')
      title ({['Zone "A" Max Index is = ' num2str(Max_index) ];['Weakest
Bus is = ' num2str(FlashPoint) '    ' fstatus ]})
     hold on
   elseif sb==61 & eb==120
     figure(3)
     bar(BNum,Lga)
     xlabel('Bus Number')
     ylabel('Zone "B" Bus Index Value')
```

```
     text(FlashPoint,pp,' \leftarrow
FlashPoint','FontSize',12,'Color','red')
     title ({['Max Index is = ' num2str(Max_index) ];['Weakest Bus is is
= ' num2str(FlashPoint) ]})
     hold on
   elseif sb==121 & eb==180
      figure(4)
      bar(BNum,Lga)
      xlabel('Bus Number')
      ylabel('Zone "C" Bus Index Value')
      text(FlashPoint,pp,' \leftarrow
FlashPoint','FontSize',12,'Color','red')
      title ({['Max Index is = ' num2str(Max_index) ];['Weakest Bus is
is = ' num2str(FlashPoint) ]})
      hold on
   elseif sb==181 & eb==240
     figure (5)
     bar(BNum,Lga)
     xlabel('Bus Number')
     ylabel('Zone "D" Bus Index Value')
     text(FlashPoint,pp,' \leftarrow
FlashPoint','FontSize',12,'Color','red')
     title ({['Max Index is = ' num2str(Max_index) ];['Weakest Bus is is
= ' num2str(FlashPoint) ]})
     hold on
   elseif sb==241 & eb==300
     figure (6)
     bar(BNum,Lga)
     xlabel('Bus Number')
```

```
      ylabel('Zone "E" Bus Index Value')
      text(FlashPoint,pp,' \leftarrow
FlashPoint','FontSize',12,'Color','red')
      title ({['Max Index is = ' num2str(Max_index) ];['Weakest Bus is is
= ' num2str(FlashPoint) ]})
      hold on
   elseif sb==151
      figure (7)
      bar(BNum,Lga)
      xlabel('Bus Number')
      ylabel('Zone "F" Bus Index Value')
      text(FlashPoint,pp,' \leftarrow
FlashPoint','FontSize',12,'Color','red')
      title ({['Max Index is = ' num2str(Max_index) ];['Weakest Bus is is
= ' num2str(FlashPoint) ]})
      hold on
   elseif sb==181
      figure (8)
      bar(BNum,Lga)
      xlabel('Bus Number')
      ylabel('Zone "G" L-indx')
      text(FlashPoint,pp,' \leftarrow
FlashPoint','FontSize',12,'Color','red')
      title ({['Max Index is = ' num2str(Max_index) ];['Weakest Bus is is
= ' num2str(FlashPoint) ]})
      hold on
   elseif sb==211
      figure (9)
      bar(BNum,Lga)
```

```
  xlabel('Bus Number')
  ylabel('Zone "H" Bus Index Value')
  text(FlashPoint,pp,' \leftarrow
  FlashPoint','FontSize',12,'Color','red')

  title ({['Max Index is = ' num2str(Max_index) ];['Weakest Bus is
   is = ' num2str(FlashPoint) ]})
  hold on
 elseif sb==241
  figure (10)
  bar(BNum,Lga)
  xlabel('Bus Number')
  ylabel('Zone "I" Bus Index Value')
  text(FlashPoint,pp,' \leftarrow
   FlashPoint','FontSize',12,'Color','red')
  title ({['Max Index is = ' num2str(Max_index) ];['Weakest Bus is
  is = ' num2str(FlashPoint) ]})
  hold on
elseif sb==271
  figure (11)
  bar(BNum,Lga)
  xlabel('Bus Number')
  ylabel('Zone "J" Bus Index Value')
  text(FlashPoint,pp,' \leftarrow
  FlashPoint','FontSize',12,'Color','red')
  title ({['Max Index is = ' num2str(Max_index) ];['Weakest Bus is
  is = ' num2str(FlashPoint) ]})
else
```

```
      disp('Starting bus outside present Zone order')
      figure (12)
      bar(BNum,Lga)
      xlabel('Bus Number')
      ylabel('None-specifed Zone Bus Index Value')
      text(FlashPoint,pp,' \leftarrow
      FlashPoint','FontSize',12,'Color','red')
      title ({['Max Index is = ' num2str(Max_index) ];['Weakest Bus is
      is = ' num2str(FlashPoint) ]})

end%=================================================================
   del=60*pi/180;
for i=1:1:10800;
thrad(i)=i*8*pi/180;
t(i)=thrad(i)/377;
va(i)=Ld*cos(thrad(i));
vb(i)=Ld*cos(thrad(i)-2*pi/3);
vc(i)=Ld*cos(thrad(i)+2*pi/3);
vd(i)=-(va(i)+vb(i)+vc(i))/3;
v=[va(i) vb(i) vc(i) vd(i)];
vmax(i)=max(v);
vmin(i)=min(v);
X=cos(3*(377*t(i)+del));
   if X<0
      alph=1;
  elseif X>0
      alph=0;
   else
     alph=0.5;
```

```
      alp(i)=alph;
      Map(i)=1-2*alph+va(i)-(vmax(i)*(1-alph))-(vmin(i)*alph);
      Mbp(i)=1-2*alph+vb(i)-(vmax(i)*(1-alph))-(vmin(i)*alph);
      Mcp(i)=1-2*alph+vc(i)-(vmax(i)*(1-alph))-(vmin(i)*alph);
      Vno(i)=alph*vmin(i)-(1-alph)*vmax(i);
      Mdp(i)=-2*Vno(i)/360;
    end
figure(13)
title('Modulating Signals');
subplot(3,1,1);plot(t,Map,'r');xlabel('t');ylabel('Map');
subplot(3,1,2);plot(t,Mbp,'b');xlabel('t');ylabel('Mbp');
subplot(3,1,3);plot(t,Mcp,'g');xlabel('t');ylabel('Mcp');
Ma=[t;Map];Mb=[t;Mbp];Mc=[t;Mcp];Md=[t;Mdp];dd=[1;Ld];Delta=[1;Sig];
save Map Ma;
save Mbp Mb;
save Mcp Mc;
save Mdp Md;
save Ld dd;
save Sig Delta;
 end % end for if No 1
www=www+1;
end % end for while No 1.
  b=0;
       for k=sb:eb
           b=b+1;
          BNum(b)=k;
          Lga(b)= L(k);
         if Lga(b)>=Max_index;
            Max_index=Lga(b);
```

```
            FlashPoint=k;
          else
            Max_index=Max_index;
            FlashPoint=FlashPoint;
          end
        end
         Ld=L(bd);
        if Max_index>=Ld
          Ld=Max_index;
          bd=FlashPoint;
          ST=FlashPoint
        else
          Ld=Ld;
          bd=bd;
        end


disp('Final Bus Voltage Value is ')
disp (['FLASHPOINT IS AT ' num2str(FlashPoint)])
```

VITA

Damian Obioma Dike was born in Enyiogugu, Aboh Mbaise Local Government Area of Imo State, Nigeria, in 1963. He had his early elementary education at St. Mary's LA School Umusu Waterside and Community School Olokwu both in Owerri West Local Government Area, Imo State, and completed his primary education at Community School Umuelem Enyiogugu in 1976. He passed out of Enyiogugu Secondary School in 1982, and proceeded to obtain a Bachelor of Engineering Degree in Electrical and Electronics and Master of Sciences Degree in Electrical Engineering from the Federal University of Technology, Owerri, Imo State, Nigeria, in 1995 and 2004 respectively. He entered Tennessee Technological University Cookeville in 2005, and is a candidate for the Doctor of Philosophy Degree in Engineering.